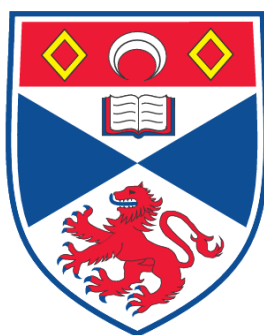


**POLYHEDRAL OLIGOMERIC SILSESQUIOXANES IN CATALYSIS
AND PHOTOLUMINESCENCE APPLICATIONS**

Nicolas R. Vautravers

**A Thesis Submitted for the Degree of PhD
at the
University of St. Andrews**

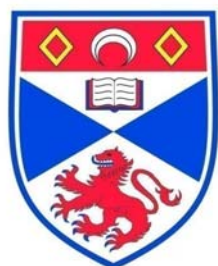


2009

**Full metadata for this item is available in the St Andrews
Digital Research Repository
at:
<https://research-repository.st-andrews.ac.uk/>**

**Please use this identifier to cite or link to this item:
<http://hdl.handle.net/10023/729>**

This item is protected by original copyright



University
of
St Andrews

Polyhedral Oligomeric Silsesquioxanes in catalysis and photoluminescence applications

Nicolas R. Vautravers

Thesis for the degree of
DOCTOR OF PHILOSOPHY

November 2008

Declaration

I, **Nicolas Romain Vautravers**, hereby certify that this thesis, which is approximately 40000 words in length, has been written by me, that it is the record of my work carried out by me and that it has not been submitted in any previous application for a higher degree.

Date _____ signature of candidate _____

I was admitted as a research student in September 2005 and as a candidate for the degree of Doctor of Philosophy in November 2006; the higher study for which this is a record was carried out in the University of St Andrews between 2005 and 2008.

Date _____ signature of candidate _____

I hereby certify that the candidate has fulfilled the conditions of the Resolution and Regulations appropriate for the degree of Doctor of Philosophy in the University of St Andrews and that the candidate is qualified to submit this thesis in application for that degree.

Date _____ signature of supervisor _____

In submitting this thesis to the University of St Andrews we understand that we are giving permission for it to be made available for use in accordance with the regulations of the University Library for the time being in force, subject to any copyright vested in the work not being affected thereby. We also understand that the title and the abstract will be published, and that a copy of the work may be made and supplied to any bona fide library or research worker, that my thesis will be electronically accessible for personal or research use unless exempt by award of an embargo as requested below, and that the library has the right to migrate my thesis into new electronic forms as required to ensure continued access to the thesis. We have obtained any third-party copyright permissions that may be required in order to allow such access and migration, or have requested the appropriate embargo below.

The following is an agreed request by candidate and supervisor regarding the electronic publication of this thesis:

Access to Printed copy and electronic publication of thesis through the University of St Andrews.

Date

signature of candidate

signature of supervisor

Acknowledgements

In completing this thesis, I am very much indebted to many people for their help and encouragement.

First of all, I thank Professor David Cole-Hamilton for his invaluable help and enthusiasm all along the development of this project. Beyond the clever chemist he is, an outstanding character resides. Thanks are also due to Professor Paul Kamer for helpful discussions and to IDECAT for giving me the opportunity (funding) to carry out my project.

Several people have provided technical and practical assistance during the course of this project. I would like particularly to thank for their help and advice Peter Pogorzelec (lab), Melanja Smith and Tomas Lebl (NMR), Catherine Botting and Alex Houston (MALDI-TOF), Alex Slawin (Crystallography), Pascal André (Molecular dynamic studies and photoluminescence measurements), Sylvia Williamson (microanalyses), Caroline Horsburgh (Mass spectrometry) and Graeme Smith (Methoxycarbonylation of ethene with monodentate phosphines).

Many thanks also go to all the people I met in the laboratory during these years for their help and friendship: Simon, Cheng, Lukas, Mark, Jenny, Jacorien, Inĕ, Loïc, Lynzi, Gong, Jan, Ben, Bert, Gregorio, Gavin, Diego, Vincent, etc.

Thanks to my family and all my friends (Jurgen, Paul, Dirk, Gary and all the others) for encouraging and helping me along the years.

Last but not least, Nelly deserves a special attention as being part of me.

Abstract

Cubic Polyhedral Oligomeric Silsesquioxanes (POSS) of general formula $\text{Si}_8\text{O}_{12}\text{R}_8$ (R = alkenyl, alkoxy, aryl, hydrogen...) have found applications in various fields ranging from biology to chemistry. Besides the advantage of presenting the characteristic dendritic globular shape at low generation, these three-dimensional molecules, easily modified by organic or inorganic reactions, quickly exhibit multiple end groups at their periphery, thus featuring attractive properties in catalysis and photoluminescence applications.

Various dendritic POSS containing diphenylphosphine moieties at their periphery have been used in the methoxycarbonylation of ethene. Those with a $-\text{CH}_2\text{CH}_2-$ spacer between the silicon and the phosphorus atoms (**G0-8ethylPPh₂** and **G1-16ethylPPh₂**) only produce methyl propanoate whilst a similar dendrimer with a $-\text{CH}_2-$ spacer between Si and P (**G1-16methylPPh₂**) gives only copolymer. The effect of the molecular architecture is discussed in comparison with the selectivities observed when using small molecule analogues. A wide range of non dendritic monodentate phosphines has also been studied in this reaction showing that low steric bulk and high electron density favours polyketone formation.

The poorly active, monodentate SemiEsphos phosphine has been turned into an active ligand for rhodium catalysed vinyl acetate hydroformylation by attachment to the periphery of a Polyhedral Oligomeric Silsesquioxane. Whilst some of these dendritic ligands have shown activity, others precipitated upon mixing with the rhodium precursor. Modelling studies correlating the experimental facts have shown that the former are more compact and rigid in comparison to the latter, which are more flexible and hence more prone to monodentate binding to rhodium and cross-linking.

Grubbs cross metathesis has been used to functionalize octavinylsilsesquioxane with fluorescent vinylbiphenyl modified chromophores to design new hybrid organic-inorganic nanomaterials. Those macromolecules have been characterized by NMR, microanalyses, MALDI-TOF mass spectrometry and photoluminescence. This last method was shown to be an interesting tool in the analysis of the purity of the cube derivatives. Reduction of the peripheral 4'-vinylbiphenyl-3,5-dicarbaldehyde groups on a Polyhedral Oligomeric Silsesquioxane (POSS) with NaBH_4 or LiAlH_4 activates the fluorescence of this macromolecule by turning the aldehydic functions into primary alcohols providing novel optical sensors for reducing environments.

Abbreviations

Ac	Acetate
Acac	Acetylacetone
Ar	Aryl
b	Branched
Binap	2,2'-bis(diphenylphosphino)-1,1'-binaphthyl
Binaphos	(2-(diphenylphosphino)-1,1'-binaphthalen-2'-yl)-(1,1'-binaphthalene-2,2'-diyl)phosphite
ⁿBu	<i>n</i> -Butyl
^tBu	<i>tert</i> -Butyl
bpy	bipyridine
Chiraphite	1,3-Di-methyl-1,3-propanediyl]bis(oxy)]bis[4,8-bis(t-butyl)-2,10-dimethoxy- bibenzo[d,f][1,3,2]dioxaphosphepin
CI	Chemical ionisation
COD	Cyclooctadiene
CVD	Chemical vapour deposition
COSY	Correlation spectroscopy
Cy	Cyclohexyl
DCM	Dichloromethane
DMF	Dimethylformamide
DMSO	Dimethyl sulfoxide
DNA	Deoxyribonucleic acid
E1	Unimolecular elimination
ESPHOS	(2 <i>R</i> , 5 <i>S</i>)-(1,2-phenylene)bis(-3-phenyl-1,3-diaza-2-phosphabicyclo[3.3.0] ^{1,5} octane)
Et	Ethyl
<i>Ee</i>	Enantiomeric excess
ESI	Electrospray ionisation
Exc	Excitation
GC	Gas chromatography
HMQC	Heteronuclear multiple quantum coherence
HRMS	High resolution mass spectrometry
Hz	Hertz
Ind	Indenyl
<i>J</i>	Coupling constant
Kelliphite	6,6'-[(1,1'-Biphenyl-2,2'-diyl)bis(oxy)]bis[4,8-di-tbutyl-1,2,10,11-tetramethyl]dibenzo[d,f][1,3,2]dioxaphosphepin
l	Linear
MALDI-TOF	Matrix assisted laser desorption ionisation-Time of flight
Me	Methyl
MeP	Methyl propanoate
MRI	Magnetic resonance imaging
MSA	Methanesulphonic acid
NMR	Nuclear magnetic resonance
Oct	Octyl
OLED	Organic light emitting diode
PA	Photon absorption
PAMAM	Polyamidoamine
pH	Potential hydrogen

Ph	Phenyl
PK	Polyketone
PL	Photoluminescence
PLE	Photoluminescence excitation
PLQY	Photoluminescence quantum yield
POSS	Polyhedral oligomeric silsesquioxane
PPI	Polypropyleneimine
ppm	Parts per million
ppy	Phenyl pyridine
Pr	Propyl
ⁱPr	<i>iso</i> -Propyl
Rg	Radius of gyration
ROMP	Ring opening metathesis polymerisation
Salen	2,2'-Ethylenebis(salicylimine)
SemiEsphos	(2R, 5S)-2-(2-methoxyphenyl)-3-phenyl-1,3-diaza-2-phosphabicyclo[3.3.0] ^{1,5} octane
TADDOL	trans- α,α' -(Dimethyl-1,3-dioxolane-4,5-diyl)bis(diphenylmethanol)
THF	Tetrahydrofuran
TMEDA	Tetramethylethylenediamine
TOF	Turnover frequency
TON	Turnover number
tpy	Terpyridine
UV	Ultraviolet

Outline

I.	ABOUT DENDRIMERS AND SILSESQUIOXANES.....	1
I. 1	THE CHEMISTRY OF DENDRIMERS.....	1
I. 1. 1	<i>The dendritic structure and its properties</i>	<i>1</i>
I. 1. 2	<i>The construction of dendrimers.....</i>	<i>2</i>
I. 1. 3	<i>Applications of dendrimers.....</i>	<i>5</i>
I. 2	THE CHEMISTRY OF SILSESQUIOXANES.....	6
I. 3	DENDRIMERS IN CATALYSIS	10
I. 3. 1	<i>The three different types of dendritic catalysts</i>	<i>10</i>
I. 3. 1. 1	Catalysis at the dendrimer's core.....	11
I. 3. 1. 2	Catalysis within a dendrimer's interior.....	16
I. 3. 1. 3	Catalysis at the periphery of dendrimers	20
I. 4	REFERENCES	26
II.	DIPHENYLPHOSPHINE BASED LIGANDS IN THE PALLADIUM CATALYZED ETHENE METHOXYCARBONYLATION.....	33
II. 1	INTRODUCTION.....	33
II. 2	NON DENDRITIC MONODENTATE LIGANDS IN THE METHOXYCARBONYLATION OF ETHENE	36
II. 2. 1	<i>Triaryls phosphines.....</i>	<i>37</i>
II. 2. 2	<i>Mixed alkyl aryl and trialkyl phosphines</i>	<i>38</i>
II. 2. 3	<i>Oligoketone formation.....</i>	<i>42</i>
II. 2. 4	<i>Studies of model complexes</i>	<i>43</i>
II. 2. 5	<i>Conclusions.....</i>	<i>45</i>
II. 3	POLYHEDRAL OLIGOMERIC SILSESQUIOXANE DENDRITIC LIGANDS IN THE METHOXYCARBONYLATION OF ETHENE	45
II. 3. 1	<i>Generation 0 Polyhedral Oligomeric Silsesquioxane decorated diphenylphosphines.....</i>	<i>46</i>
II. 3. 2	<i>Generation 1 Polyhedral Oligomeric Silsesquioxane decorated diphenylphosphines.....</i>	<i>48</i>
II. 3. 3	<i>Conclusions.....</i>	<i>54</i>
II. 4	REFERENCES	55

III. DIAZAPHOSPHOLIDINE TERMINATED POLYHEDRAL OLIGOMERIC SILSESQUIOXANES CORED DENDRIMERS IN ASYMMETRIC HYDROFORMYLATION	57
III. 1 INTRODUCTION.....	57
III. 2 SYNTHETIC APPROACHES TO THE BINDING OF SEMIESPHOS ONTO POLYHEDRAL OLIGOMERIC SILSESQUIOXANE CORED DENDRIMERS	61
<i>III. 2. 1 The SemiEsphos oxide route.....</i>	<i>61</i>
<i>III. 2. 2 The SemiEsphos borane protected route.....</i>	<i>64</i>
<i>III. 2. 3 The unprotected SemiEsphos route.....</i>	<i>64</i>
III. 3 SEMIESPHOS DECORATED POLYHEDRAL OLIGOMERIC SILSESQUIOXANE CORED DENDRIMERS IN VINYL ACETATE AND STYRENE HYDROFORMYLATION	70
<i>III. 3. 1 Vinyl acetate hydroformylation.....</i>	<i>70</i>
<i>III. 3. 2 Styrene hydroformylation.....</i>	<i>73</i>
<i>III. 3. 3 Molecular Dynamics Studies.....</i>	<i>74</i>
III. 3. 3. 1 “Branch extensions”	76
III. 3. 3. 2 “Intradendron PP distances”	78
III. 3. 3. 3 “Interdendron PP distances”	79
<i>III. 3. 4 Conclusions.....</i>	<i>81</i>
III. 4 REFERENCES.....	83
IV. POLYHEDRAL OLIGOMERIC SILSESQUIOXANE CORED DENDRIMERS IN PHOTOLUMINESCENCE APPLICATIONS.....	86
IV. 1 INTRODUCTION.....	86
<i>IV. 1. 1 Dendrimers as gas sensors</i>	<i>86</i>
<i>IV. 1. 2 Dendrimers as ion sensors.....</i>	<i>88</i>
<i>IV. 1. 3 Dendrimers as organic compound sensors</i>	<i>91</i>
IV. 2 SENSING REDUCING AGENTS THROUGH FLUORESCENCE ACTIVATION OF A POLYHEDRAL OLIGOMERIC SILSESQUIOXANE	93
<i>IV. 2. 1 Synthesis of a dialdehyde functionalized Polyhedral Oligomeric Silsesquioxane and its reduced alcoholic form.....</i>	<i>94</i>
<i>IV. 2. 2 Molecular dynamics investigations of both macromolecules S1 and S2</i>	<i>96</i>
<i>IV. 2. 3 Photoluminescence spectral characteristics of monomers M7 and M8 and macromolecules S1 and S2.....</i>	<i>99</i>
<i>IV. 2. 4 Reducing agents titration with S1</i>	<i>101</i>
<i>IV. 2. 5 Conclusion.....</i>	<i>102</i>

IV. 3	SYNTHESIS AND CHARACTERIZATION OF PHOTOLUMINESCENT VINYLBIIPHENYL DECORATED POLYHEDRAL OLIGOMERIC SILSESQUIOXANES	103
IV. 3. 1	<i>Synthesis and photoluminescent properties of vinylbiphenyl monomers</i>	<i>104</i>
IV. 3. 2	<i>Synthesis and photoluminescent properties of vinylbiphenyl functionalized Polyhedral Oligomeric Silsesquioxanes.....</i>	<i>106</i>
IV. 3. 3	<i>Photoluminescent properties of homometathesis side products.....</i>	<i>109</i>
IV. 4	REFERENCES	115
V.	EXPERIMENTAL	119
V. 1	GENERAL.....	119
V. 2	PHOTOPHYSICAL MEASUREMENTS.....	120
V. 3	MOLECULAR DYNAMICS: PROTOCOLE AND MODELLING ANALYSIS	121
V. 4	PROCEDURE FOR ALKENE HYDROFORMYLATION	122
V. 5	PROCEDURE FOR ETHENE METHOXYCARBONYLATION.....	122
V. 6	SEMIESPPOS TERMINATED POLYHEDRAL OLIGOMERIC SILSESQUIOXANES.....	123
V. 6. 1	<i>SemiEspPos modified dendrons.....</i>	<i>123</i>
V. 6. 2	<i>SemiEspPos terminated Polyhedral Oligomeric Silsesquioxane building blocks</i>	<i>125</i>
V. 6. 3	<i>SemiEspPos terminated Polyhedral Oligomeric Silsesquioxanes.....</i>	<i>127</i>
V. 7	PHOTOLUMINESCENT POLYHEDRAL OLIGOMERIC SILSESQUIOXANE CORED DENDRIMERS AND ASSOCIATED DENDRONS	135
V. 8	REFERENCES	147
VI.	CONCLUSIONS AND FUTURE WORK	148
VI. 1	CONCLUSIONS	148
VI. 2	FUTURE WORK.....	149
VI. 2. 1	<i>Catalysis.....</i>	<i>149</i>
VI. 2. 2	<i>Photoluminescence.....</i>	<i>150</i>
VI. 3	REFERENCES	151
	ANNEXE I.....	152
	ANNEXE II.....	163

I. About dendrimers and silsesquioxanes

I. About dendrimers and silsesquioxanes

I. 1 The chemistry of dendrimers

At the end of 1970s, considerable attention was devoted to the construction of large and substrate-selective ligands in host-guest ^{1, 2} and supramolecular chemistry.³ The first successful synthesis of such a molecule (a dendrimer) was reported by Vögtle in 1978.⁴ Over the next few years, research groups led by Tomalia,⁵ Denkewalter ⁶ and Newkome ⁷ made this class of new polymers of considerable interest. Prompted by the pioneering work of these groups, research into dendrimers took off rapidly as exemplified by the huge number of papers and patents that followed and their current commercial availability. A deeper insight into their general properties and applications will be described in the following sections to illustrate this high degree of interest in dendrimer chemistry.

I. 1. 1 The dendritic structure and its properties

A dendrimer, (from the Greek “dendron” ~ tree and “meros” ~ part), is a tree-like, hyperbranched and symmetrical structure that is found widely in nature (e.g. tree branching, lightning patterns, snow flakes...). These monodisperse, nanoscaled macromolecules are composed of three distinct domains (Figure 1.1): i) a central core, which is either a single atom or a molecule, ii) branches radiating from the core, constituted of repeated branching units and iii) surface groups, generally located on the exterior of the dendrimer.

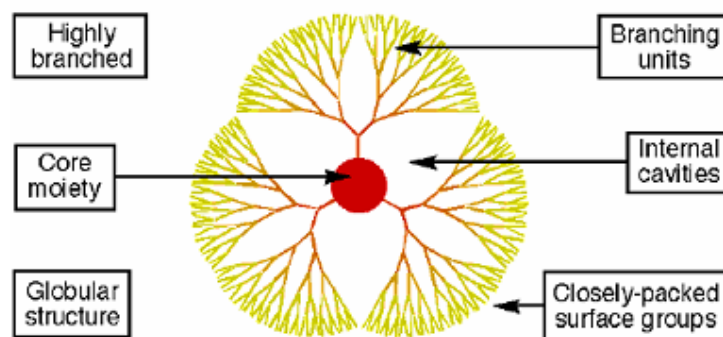


Figure 1.1 The dendritic structure ⁸

Dendrimers, also known as fractal polymers, cascade molecules or arborols, can be described as multi-layer compounds in which each new layer creates a new generation (G_n) that doubles the number of end groups and approximately doubles the molecular weight of the previous generation (Figure 1.2). The core molecule without surrounding dendrons is referred to as the zero generation. Each successive branching unit along the dendrimer forms the next generation.

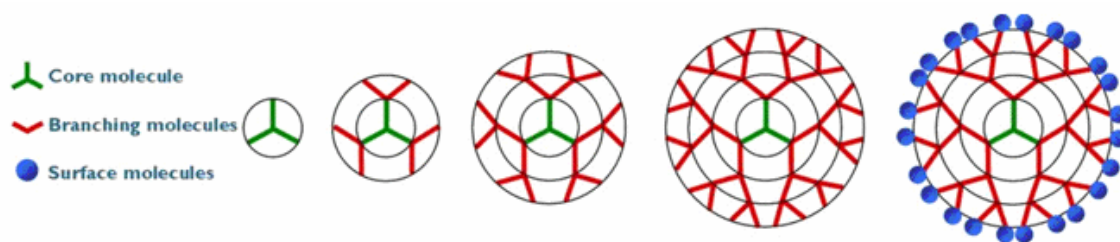
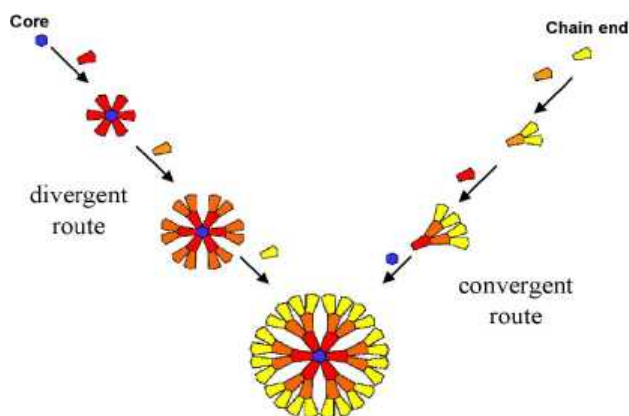


Figure 1.2 Successive generation of a dendrimer ⁹

Dendrimers are characterised by the presence of a large number of closely packed functional surface groups. The pseudo-globular to globular 3D structures, which many of them adopt, resemble biomolecules such as proteins and exhibit similar characteristics including low intrinsic viscosity, high solubility and high reactivity (from the presence of many chain ends). However, one has to remember that some of the surface groups are in reality back-folded i.e. pointing towards the inner core. This particular organisation of the molecule is mainly controlled by steric factors within dendrons. Indeed, the structural properties of the arms and branching units, as well as the size of the dendrons and the interaction between end-groups and the surrounding medium also influence the spatial shape of the dendritic molecule.⁸ For higher generation dendrimers, solubility characteristics depend predominantly on the properties of the surface groups. It thus becomes possible to tune the structure, size, shape and solubility of these dendrimers to give persistent, controllable dimensions (1-100 nm) and topologies with specific functionalities in predetermined positions.

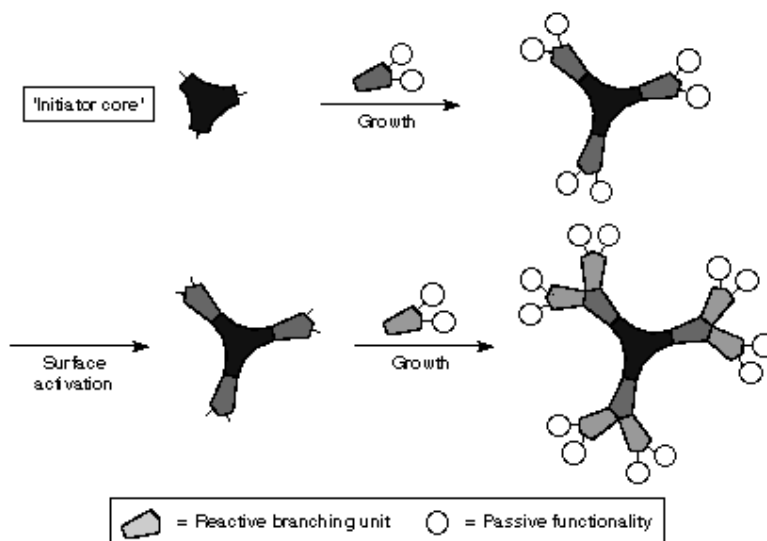
I. 1. 2 The construction of dendrimers

Dendrimers are produced in an iterative sequence of reaction steps by either a convergent or divergent approach (Scheme 1.1).



Scheme 1.1 Iterative dendrimer synthesis ¹⁰

In the divergent approach (Scheme 1.2), pioneered by Tomalia ⁵ and Newkome ⁷ in 1985, the synthesis starts from the core moiety to the periphery of the dendrimer. A series of coupling and deprotection/activation reactions characterize this process. Its major drawback is the inherent difficult purification of the higher generation dendrimers that is often necessary owing to low yield preparations even in the presence of a large excess of reagents.



Scheme 1.2 Divergent approach in dendrimer synthesis ¹¹

Moreover, as the dendrimer grows larger, the end groups on the surface become more and more closely packed and eventually, because of steric hindrance, the dendrimer reaches its upper generation limit. This is known as the “de Gennes dense packing” ¹² after Pierre-Gilles de Gennes or “starburst effect” after Tomalia.¹³

The paradigm of this divergent approach is PolyAmidoAmine (PAMAM) developed by Tomalia in 1985 (Figure 1.3).⁵

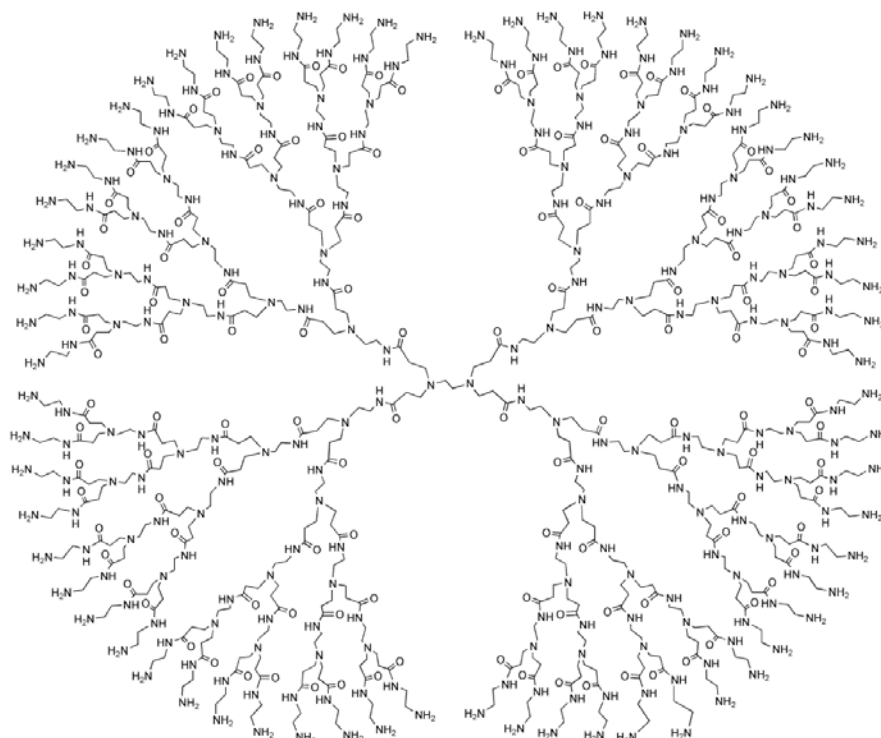
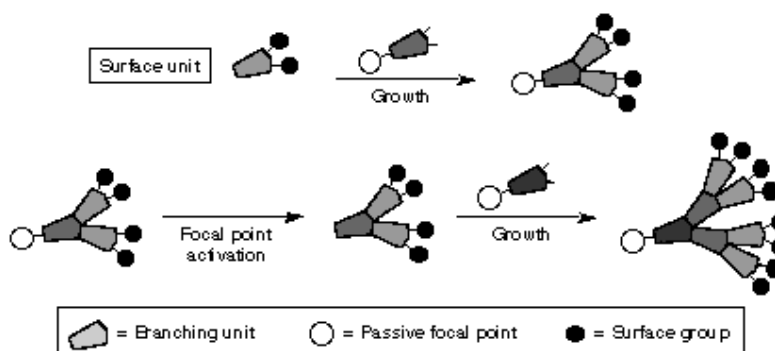


Figure 1.3 A PolyAmidoAmine (PAMAM) dendrimer (reproduced from ¹⁴)

Hawker and Fréchet developed the convergent methodology, in 1990, which assembles the macromolecule from the outside to finish at the core (Scheme 1.3 and Figure 1.4).¹⁵



Scheme 1.3 Convergent approach in dendrimer synthesis ¹¹

In this case, the reactive species remains at the focal point of the growing molecule; its building only involves two or three active groups and thus limits undesired or incomplete reactions. However, steric hindrance at the reactive point prevents the preparation of high generations of dendrimers because the final macromolecule is synthesized by coupling two or more wedges, which themselves are highly sterically demanding.

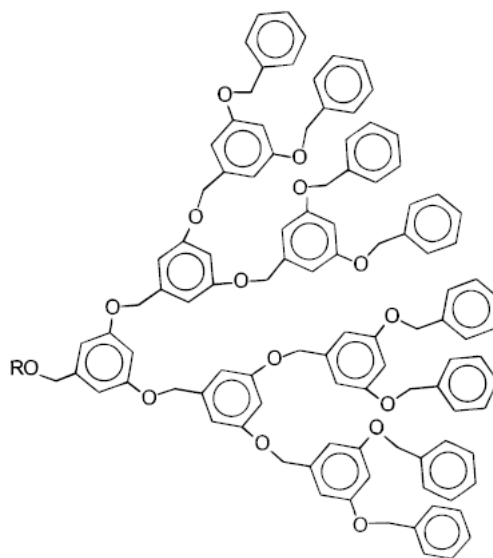


Figure 1.4 A polyether Fréchet type dendron (reproduced from ¹⁶)

A major problem inherent to dendrimer synthesis, and common to the two approaches, lies in the fact that the quantity of defects potentially increases with each successive dendritic layer. Thus, to reduce the number of synthetic steps and obtain a high yield of dendrimer, several methods have been investigated but alternative synthetic methods are still needed.¹⁷

I. 1. 3 Applications of dendrimers

A large number of applications can be envisaged for dendrimers and many interesting papers in the scientific literature and popular press have accounted for their great potential. The steric crowding of the branches at a dendrimer's surface forces it to adopt a globular shape. Depending on the degree of backfolding of the terminal groups, cavities inside the dendrimer can also be created, offering the potential for applications such as drug delivery systems^{18, 19} or molecular recognition.²⁰⁻²³ Moreover, their nanometric size, combined with their multiple surface groups, make them interesting candidates for catalyst supports,²⁴⁻²⁶ light emitting materials,^{27, 28} membranes components,²⁹ MRI contrast agents,³⁰ gene transfection vectors³¹ and DNA intercalation compounds.³²

Currently, more than 50 different families of dendrimers have been specifically developed for the ever increasing number of applications in a diverse range of fields. Whilst

Polyamidoamines (PAMAM),⁵ polypropylene imines (PPI),³³ polybenzyl ethers (Fréchet-type),¹⁵ polyaliphatic esters,³⁴ polycarbosilanes,³⁵ polyphenylene,³⁶ polyphosphorus³⁷ and polyester amides (Newkome-type)⁷ are among the most common. Polyhedral Oligomeric Silsesquioxane (POSS) have recently emerged as a new class of dendrimers featuring appealing properties and applications, which will be described in the following section.

1.2 The chemistry of silsesquioxanes

The term silsesquioxane is derived from the Greek word “sesqui” meaning one and a half, and refers in this case to the 3 to 2 stoichiometry between oxygen and silicon in the POSS cube.³⁸ Silsesquioxanes, with the general formula $\text{RSiO}_{3/2}$, are three-dimensional oligomeric, organo-silicon compounds³⁹ which possess a wide range of different shapes (random, ladder, cage, etc). Their mixed organic-inorganic structures are of interest as aluminosilicates,^{40, 41} microporous materials,^{42, 43} sol-gel precursors⁴⁴ and silica-reinforced composites⁴⁵ or as pre-ceramic coatings that can be pyrolysed to silicon carbide⁴⁶ and nitrided glass.⁴⁷

The following discussion will predominantly focus on Polyhedral Oligomeric Silsesquioxanes of general formula $\text{Si}_8\text{O}_{12}\text{R}_8$ (T_8R_8) with a cubic structure (Figure 1.5),⁴⁸ although a variety of other structures of polyhedral silsesquioxanes $(\text{RSiO}_{3/2})_n$ with $n = 6, 8, 10, 12$ are detailed in the literature.⁴⁹ (R = alkenyl, alkoxy, aryl, hydrogen, etc.) The silicon atoms, bound to a pendant R group, are situated at each corner of the cube bridged by oxygen.

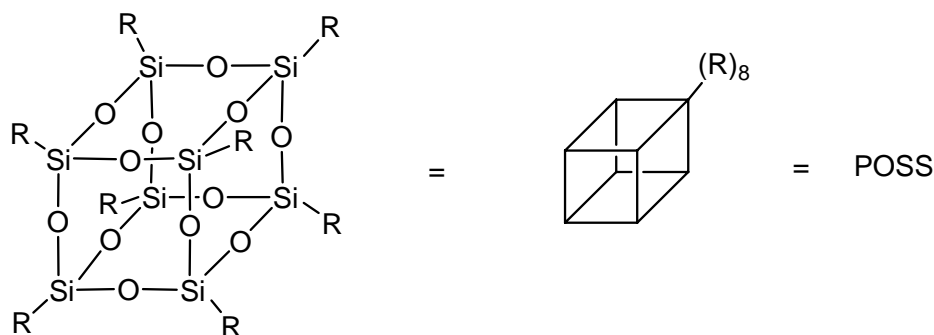


Figure 1.5 POSS molecule based on a cubic structure

Recent advances have seen many POSS species prepared by either cross metathesis,^{50, 51, 52} hydrosilylation⁵²⁻⁵⁴ or hydrolysis of RSiY_3 .⁵⁵ In the latter case, solvent, pH, temperature and

the nature of the side chain are some of the many parameters that can influence the structure of POSS systems.

The incompletely condensed cage, in which one of the silicon groups is missing, has attracted a great deal of attention in the field of metallasilsesquioxanes. (Figure 1.6)

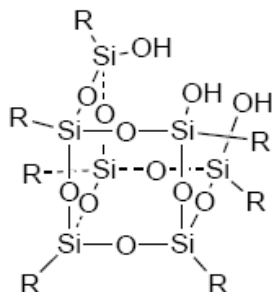
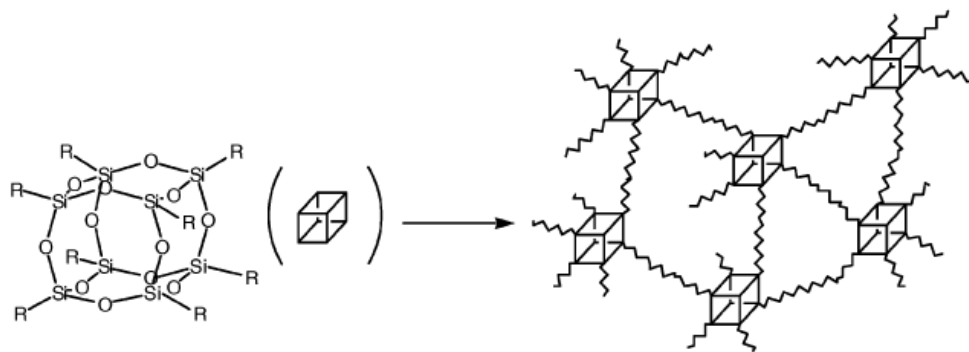


Figure 1.6 An open cage POSS molecule

Here, the mono-functionalisation of one corner of the cube may provide insights into the chemistry of silica-supported transition metal catalysts that are for instance, widely used in alkene polymerisation.⁵⁶ Although many studies have devoted their attention to open-cage cubic POSS molecules, in which one of the corners was either directly substituted with a metal⁵⁶⁻⁶² or indirectly, through phosphines coordination,^{63, 64} an extensive discussion on this class of compounds is beyond the scope of this report and it will not be discussed further.

Dendritic macromolecules based on closed polyhedral oligomeric silsesquioxane (POSS) cores have been mainly used in materials chemistry applications ranging from models of silica surfaces⁶⁵ and zeolites⁶⁶ to organic-inorganic hybrid polymers.⁶⁷ A standard method of preparation of these latter nanomaterials is the substitution of one or more of the POSS corner groups by a functional moiety capable of undergoing polymerization, followed by its incorporation into organic polymers (Scheme 1.4).⁶⁸⁻⁷⁰



Scheme 1.4 Nanocomposite materials from cubic silsesquioxanes ⁷¹

These new materials exhibit greatly enhanced thermal stability,⁷² mechanical⁷³ and electrical properties⁷⁴ while providing higher brightness and photo-luminescence efficiency to conjugated polymers.⁷⁵ Similarly, higher photoluminescence efficiency was reported for polyfluorenes grown at the eight corners of the silicon oxide cube,⁷⁶ and chromophore-substituted octa-vinyl silsesquioxane has recently started to be developed for OLED applications.^{77, 78} POSS have also been shown to be useful when employed as additives to alter the chemical and physical properties of a variety of materials used in e.g. paints, coatings, resins, elastomers and advanced plastics.⁷⁹⁻⁸¹ Their ability to produce water-soluble micelles,⁸² nanocomposite foams,⁸³ liquid crystals^{84, 85} and CVD coatings⁸⁶ is also well documented.

Completely condensed POSS molecules have also been proposed as catalytic supports because the characteristic dendritic globular shape they possess at low generation enables the quick exhibition of multiple end groups which may be quite attractive in catalysis. However, little work has been published so far in this field. What there is will be discussed further in the following section and next chapter.

Feher *et al.* reported the synthesis of an octadiphenylphosphine POSS cored molecule (Figure 1.7, (a)) but no catalytic activity was observed in hydroformylation or alkene isomerisation.⁸⁷ The same group functionalized the POSS core with pendant amino/phosphine groups to create new ranges of dendritic molecules (Figure 1.7, (b)).^{88, 89}

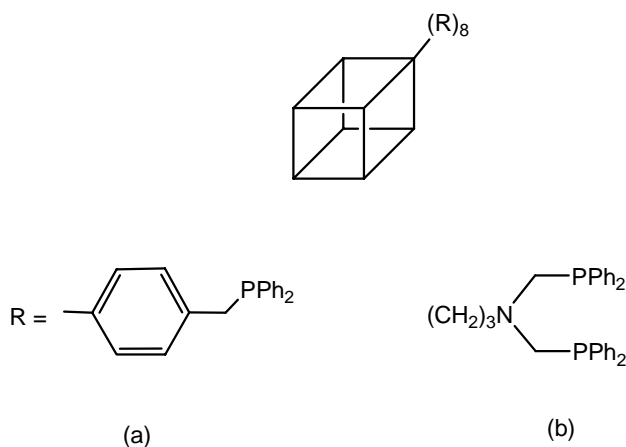


Figure 1.7 Schematic representation of dendritic POSS substituted by (a) benzyldiphenylphosphine group, (b) aminomethyldiphenylphosphine group

Miscellaneous functionalizations of POSS molecules with ferrocene or Ru^{II} based chromophores have respectively featured interesting electrochemical properties⁹⁰ as well as attractive redox- and photo-active attributes, respectively (Figure 1.8).⁹¹

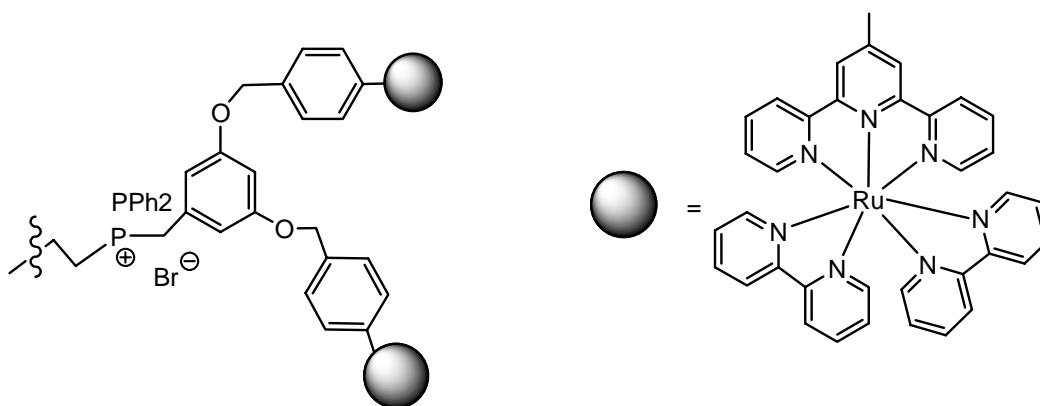


Figure 1.8 POSS core substituted by redox-active and photoactive $[\text{Ru}(\text{bpy})_2(\text{tpy})]^{2+}$ groups

Despite the relative ease of tailoring Polyhedral Oligomeric Silsesquioxane cubes by organic or inorganic reactions, their chemistry and properties seem far from being fully exploited, especially in the field of catalysis where a number of dendrimers have already been shown to be more active and selective than their small molecules analogues.

1.3 Dendrimers in catalysis

1.3.1 The three different types of dendritic catalysts

In recent years, several groups have investigated the incorporation or complexation of transition metal fragments within dendritic architectures to yield a variety of metallodendritic species.⁹² Among them, dendrimer-supported catalysts⁹³ combine the main advantages of both homogeneous and heterogeneous catalysts.⁹⁴ On the one hand, they present excellent solubility in common organic solvents, a good activity resulting from the high availability of the catalytic centres and a well-defined structure that enables deep characterisations and better mechanistic understanding. On the other hand, their persistent shape and large size permit their separation from the reaction products and solvents by ultrafiltration using suitable membranes.⁹⁵⁻¹⁰¹ Thus, they offer a neat solution to the separation problem, which has dogged the commercialisation of otherwise very attractive homogeneous catalytic systems.⁹⁴

Different dendritic structures afford the distribution of catalytic units in the core, along the branches of the interior or at the periphery of the macromolecule (Figure 1.9).

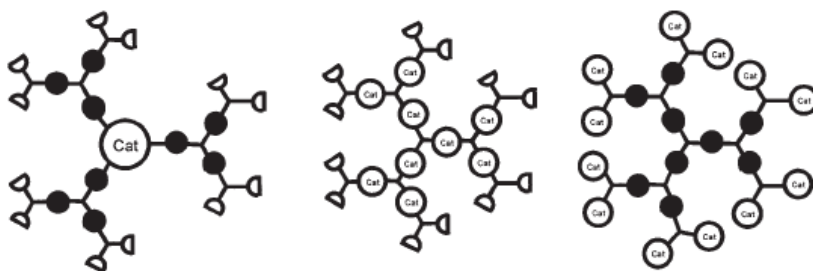


Figure 1.9 Type of dendritic catalysts¹⁰²

Although excellent examples of heterogenised dendritic catalytic systems have been reported in the literature,¹⁰³⁻¹⁰⁶ emphasis herein will be placed on dendrimers as homogeneous catalysts, particularly those exhibiting so-called “dendritic effects”, which arise from the immobilisation of a catalyst onto a dendritic support.

I. 3. 1. 1 Catalysis at the dendrimer's core

Placing the catalytic site at the core of a dendrimer allows the creation of a microenvironment, which resembles in many ways the active sites of natural enzymes.

Brunner *et al.* first prepared a so-called “dendrzyme” in 1994, by growing chiral dendritic branches around a metal (Figure 1.10) to catalyze the cyclopropanation of styrene with ethyldiazoacetate. Unfortunately, enantioselectivities were found to be rather low,^{107, 108} possibly because of the lack of secondary structure within dendrimers employed.

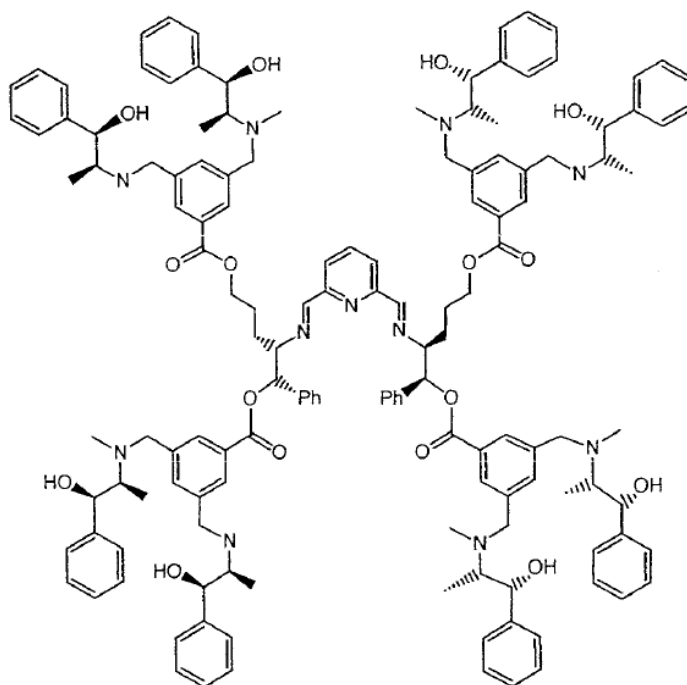
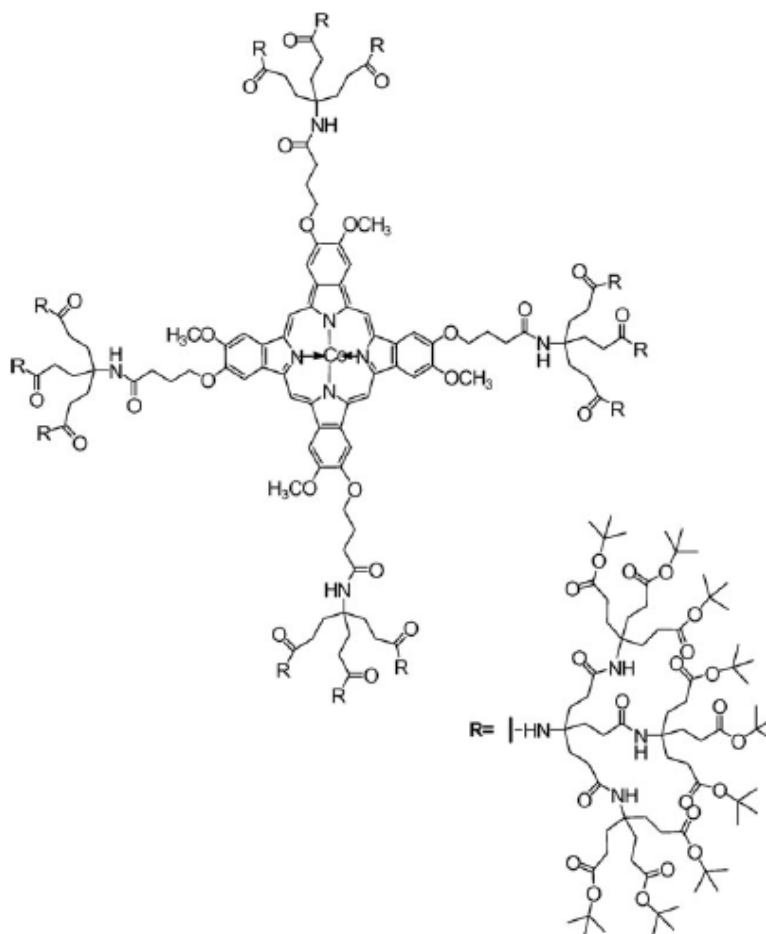


Figure 1.10 Example of Brunner's “dendrzyme” (reproduced from ⁹³)

However, the steric bulk of Fréchet-type dendrons around BINAP has been shown positively to affect the stereoselectivity of the asymmetric hydrogenation of a modified acrylic acid (92.6% compared to 89.9% obtained for the parent BINAP).¹⁰⁹ Similarly, Seebach and co-workers reported significantly higher enantioselectivities than those obtained by the parent molecules in protonation reactions catalyzed by TADDOL dendritic complexes.¹¹⁰

In addition to the enhancement of stereoselectivity offered by the dendrimer over its small molecule analogue, dramatic increases in the regioselectivity, stability and/or activity of the

Studies on oxidation catalysts or oxygen carriers have related the excellent stability and longer lifetimes of porphyrin or phthalocyanine cored dendritic catalysts due to the efficient shielding of the higher generation dendrimers.^{8, 112} An example of this effect is the cobalt phthalocyanine complex represented in Figure 1.11, which shows enhanced stability by encapsulation of the active centre within the dendritic structure.



A similar concept is found in the chemistry of PolyOxoMetalate cored dendrimers, where the dendritic structure increases the stability of these non-covalently linked clusters in various oxidation reactions (Figure 1.12).¹¹⁴ While the dendrimer catalysts are easily recovered and

recycled without a discernable loss of activity, the small molecule analogues have shown unsatisfactory results.

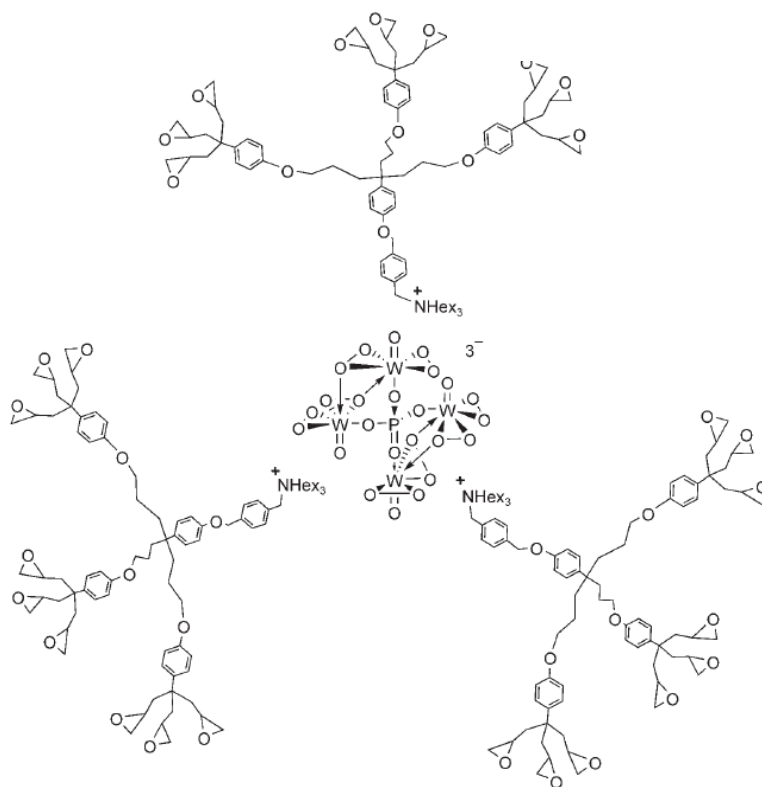


Figure 1.12 PolyOxoMetalates cored dendrimer ¹¹⁴

Dendritic rhodium(I) complexes bearing N-heterocyclic carbenes have been used in the hydrosilylation of ketones under mild conditions, although these reactions are usually limited by factors such as catalyst stability and activity.¹¹⁵ The observed positive dendrimer effect, resulting in an increase in the yield of the reaction, was attributed to the folding of the dendrimer around the active site leading to a greater stability and higher turnover as a consequence.

This protective effect of the dendritic architecture can also be correlated to the ability of dendrimers to select appropriate substrates and reject others, which could be referred to some sort of shape or size selectivity analogous to the behaviour of enzymatic systems. Chow and co-workers demonstrated this concept in the dendrimer catalyzed Diels-Alder reaction between cyclopentadiene and a 1 : 1 mixture of dienophiles of different sizes.¹¹⁶ For all dendrimers investigated (generation 0 to generation 3), the smaller dienophile always reacted

much faster than the larger dienophiles thereby highlighting the aptitude of the dendrimers to offer some degree of steric selectivity during catalysis.

While the previous example invoked one single dendritic ligand in the catalytic reaction, it is also common for several ligands to be present at the active metal centre. Indeed, several catalytic species with different activities may be present in solution. For instance, nickel complexes bearing P,O ligands, such as *o*-diphenylphosphinophenols, tend to dimerize forming inactive bis(P,O)nickel complexes. Suppression of dimerisation, through the “site-isolation” of *o*-diphenylphosphinophenol within a carbosilane platform (Figure 1.13), allows the dendritic ligand to outperform the parent molecule in the oligomerisation of ethylene.¹¹⁷

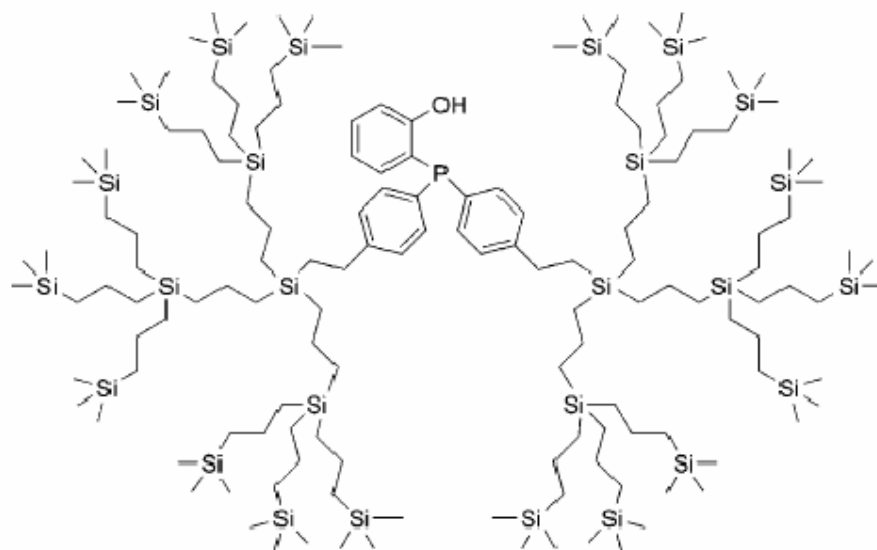
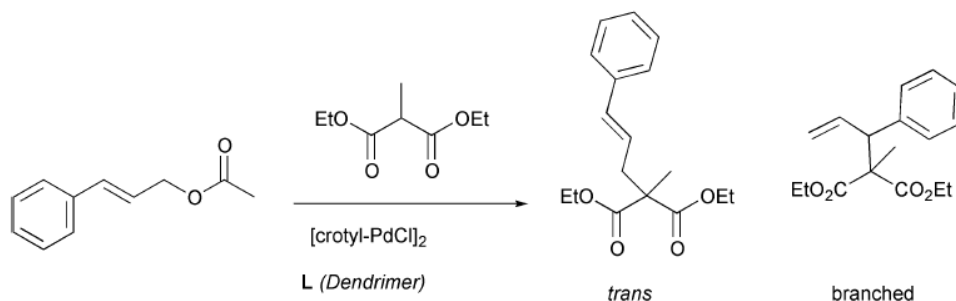


Figure 1.13 Van Leeuwen's core functionalized P, O ligand¹¹⁷

Although it has been shown that the dendritic encapsulation of a reactive species may offer advantages in terms of activity, selectivity and/or stability of a catalyst, in general slower rates of reaction with increasing dendrimer generation are observed.

The example of the Henry reaction (aldol-type addition of nitro-ethane to benzaldehyde) catalyzed by a tertiary amine located at the core of poly-L-lysine or a Fréchet-type dendrimer, led the groups of Cossio and Lopez to conclude that steric hindrance from increasing generations and branching multiplicity was responsible for slower rates and a low syn/anti stereoselective ratio compared to the small molecule analogues.¹¹⁸

Van Leeuwen and co-workers drew the same conclusions concerning the palladium catalyzed allylic amination of 3-phenylallyl acetate with diethyl 2-methylmalonate using ferrocenyl phosphorus cored carbosilane dendrimers (Scheme 1.5).¹¹⁹



Scheme 1.5 Allylic alkylation of 3-phenylallyl acetate with diethyl 2-methylmalonate catalyzed by dendritic palladium complexes (reproduced from ¹⁴)

Seebach and co-workers also attributed their decreasing yield from generation 3 to 4, in the titanium-TADDOLate (Figure 1.14) catalyzed addition of diethylzinc to benzaldehyde, to steric problems associated with mass transport limitations and substrate access to the catalytic site.¹²⁰

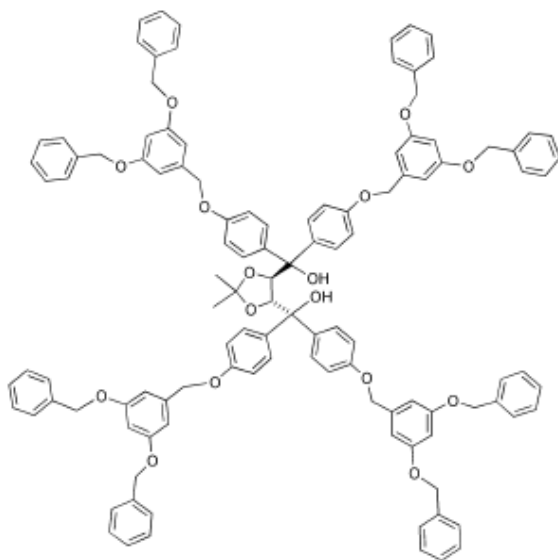


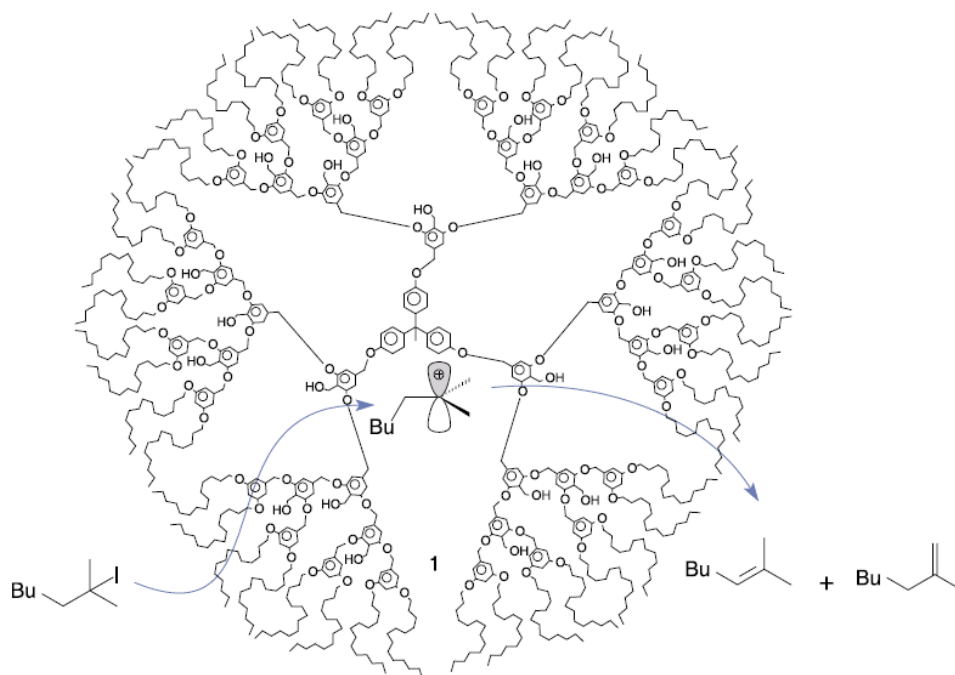
Figure 1.14 Seebach's TADDOL cored catalytic dendrimer (reproduced from ¹⁴)

However, taking full advantage of the cavity inside a dendrimer could be a driving force for substrate penetration of crowded surfaces and further reactions inside the dendrimer.

I. 3. 1. 2 Catalysis within a dendrimer's interior

An elegant way to circumvent the problem of steric crowding and mass transport limitations described in the previous section is to use dendrimer voids as a substrate concentrator and/or stabilizer of transition states or charged intermediates.

Piotti *et al.* applied this principle in the E1 elimination of hydrogen iodide from iodoalkane in cyclohexane, using a dendrimer with a polar core (Scheme 1.6).¹²¹

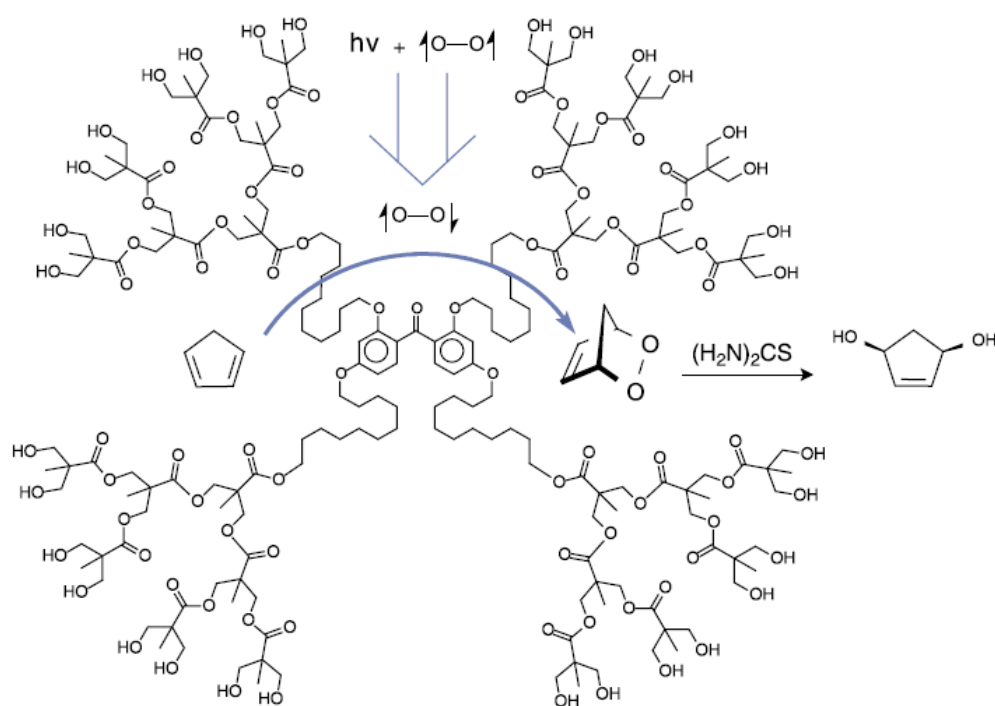


Scheme 1.6 Elimination reaction of tertiary alkyl halides in cyclohexane within the interior of a polar-cored dendrimer (reproduced from ¹²²)

The charged transition state is stabilized inside the dendrimer, which allows the reaction to proceed catalytically whereas no product was detected without dendrimer. The authors attributed this result to a “concentrator effect” whereby the polarity gradient intrinsic to the dendrimer drives the relatively polar substrate into the macromolecule’s core. Subsequently, the substrate accumulates in a polar nanoenvironment that is more suitable for the E1 elimination than the external apolar medium. In addition, the non-polar alkene product has more affinity for the hydrophobic surrounding medium thereby achieving the so-called “catalytic pump”.

The concepts of concentrator effect, the accumulation of substrates near a catalytically active site, and catalytic pump, for the prevention of product inhibition, have been broadly applied with different amphiphilic dendrimers.

Several research groups have used the hydrophobic interior of dendrimers to concentrate hydrophobic reagents and release hydrophilic products.¹²³ For instance, the hydrophobic core of the aliphatic polyester dendrimer represented in Scheme 1.7 and equipped with a benzophenone photosensitizer, catalyzes the [4+2] cycloaddition of singlet oxygen to cyclopentadiene in a polar solvent.⁸

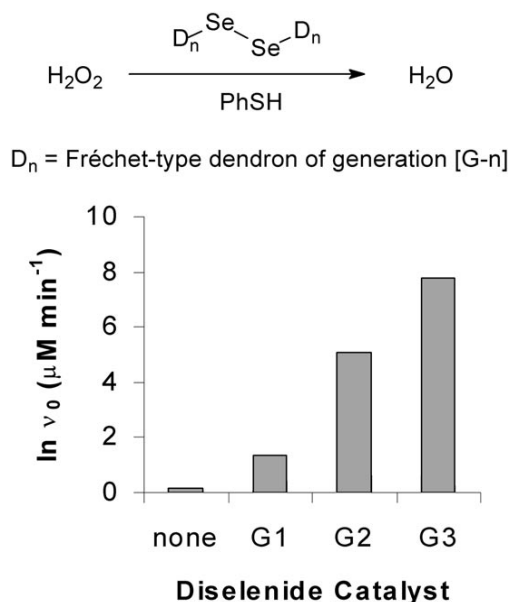


Scheme 1.7 [4+2] cycloaddition of singlet oxygen to cyclopentadiene in a polar solvent (reproduced from ¹²²)

The hydrophobic, dendritic microenvironment allows the binding of the non-polar cyclopentadiene but not of the diol product, which is thus “pumped out” of the dendrimer. Since the product has a greater affinity for the surrounding polar medium, vacant sites for incoming cyclopentadiene are generated and a high turnover can be achieved.

In addition to the amphiphilic nature of the nanoenvironment generated by the dendrimer, the globular dendritic architecture also functions to bind molecules, another important factor for achieving efficient catalysis. This ability to bind substrates is exhibited by enzymes in which

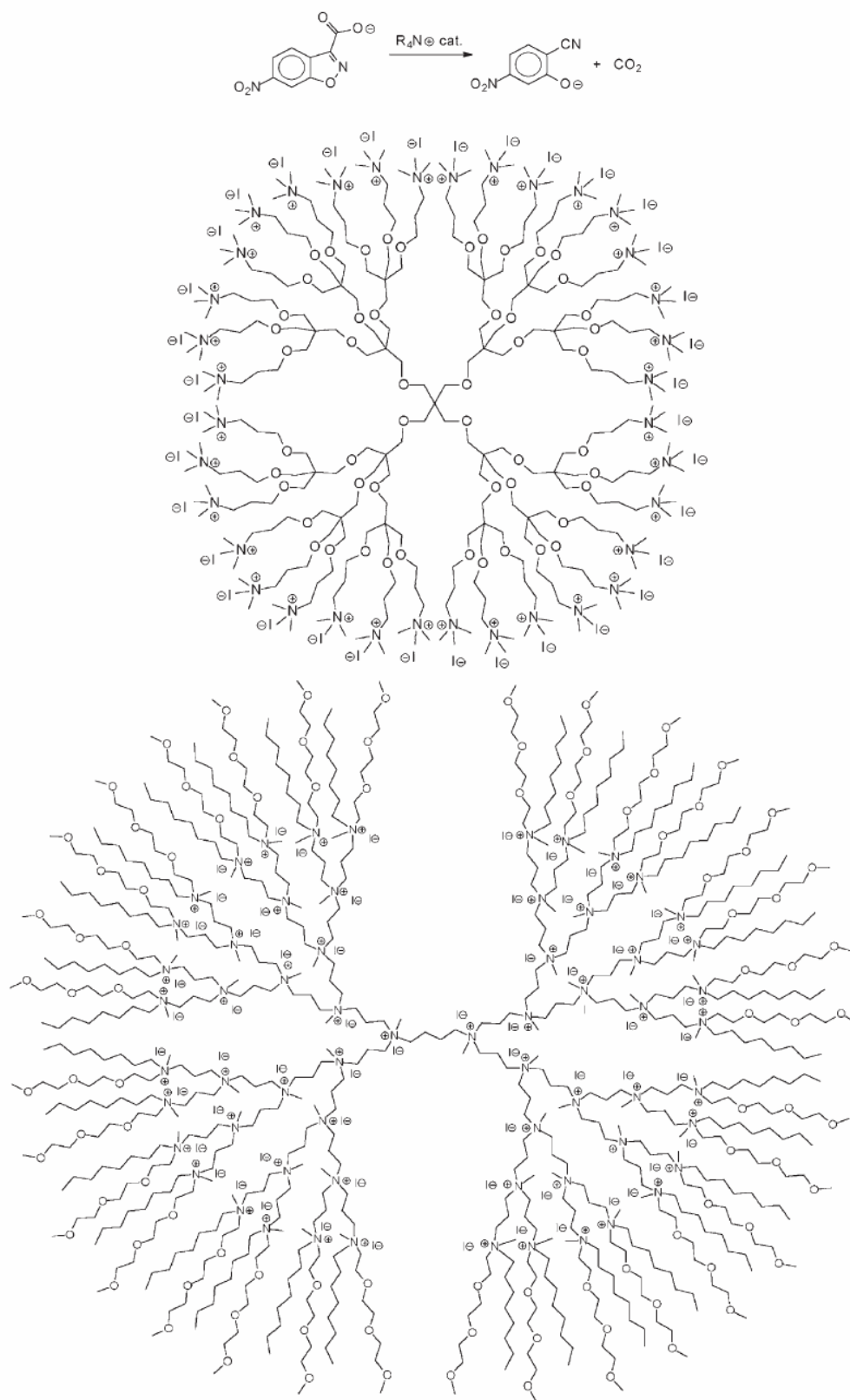
substrate binding features prominently in determining the substrate selectivity.¹²² A nice example of this phenomenon has been reported by Zhang *et al.* who studied diselenide-cored Fréchet-type dendrimers for the reduction of hydrogen peroxide.¹²⁴ Substrate binding was enhanced on passing from dendrimer generations G1 to G3, which caused a concomitant increase in the initial rate (v_0) of the reaction (Scheme 1.8).



Scheme 1.8 Hydrogen peroxide reduction by dendritic diselenides (reproduced from ¹¹¹)

A totally different approach that benefits from the interior cavities of dendrimers is to entrap and stabilize metallic nanoparticles for further catalytic reactions. The research groups of Tomalia,¹²⁵ Crooks¹²⁶ and Torigoe¹²⁷ pioneered this work but an extensive discussion of their results is beyond the scope of this report.

Before investigating the catalysis at the periphery of dendrimers in more detail, the effect of placing catalytic groups on the macromolecule on the outcome of a reaction will be described. The effect of dendritic quaternary ammonium salts on the decarboxylation of 6-nitrobenzoxazole-3-carboxylate was studied using either internal or peripheral modified dendrimers (Scheme 1.9).^{128, 129}



Scheme 1.9 Decarboxylation of 6-nitrobenzisoxazole-3-carboxylate using either internal or peripheral modified dendrimers (reproduced from ¹¹¹)

The internally decorated dendritic catalysts showed improved rates over their peripheral analogues, probably because of the enhancement of hydrophobicity necessary to destabilize the carboxylate for subsequent reaction.

This study clearly illustrates the importance of the placement of the catalytic groups within the dendritic framework.

I. 3. 1. 3 Catalysis at the periphery of dendrimers

Using the surface of dendrimers to locate catalysts offers a high loading of active sites that are available for reactions. The dendritic support can also give rise to proximity interactions that lead to cooperative effects or steric crowding at the periphery, that are either beneficial or detrimental in nature.

In 1994, the groups of Van Koten and Van Leeuwen reported the first carbosilane based dendrimer decorated at its periphery by pincer-Ni(II) catalysts (Figure 1.15).¹³⁰

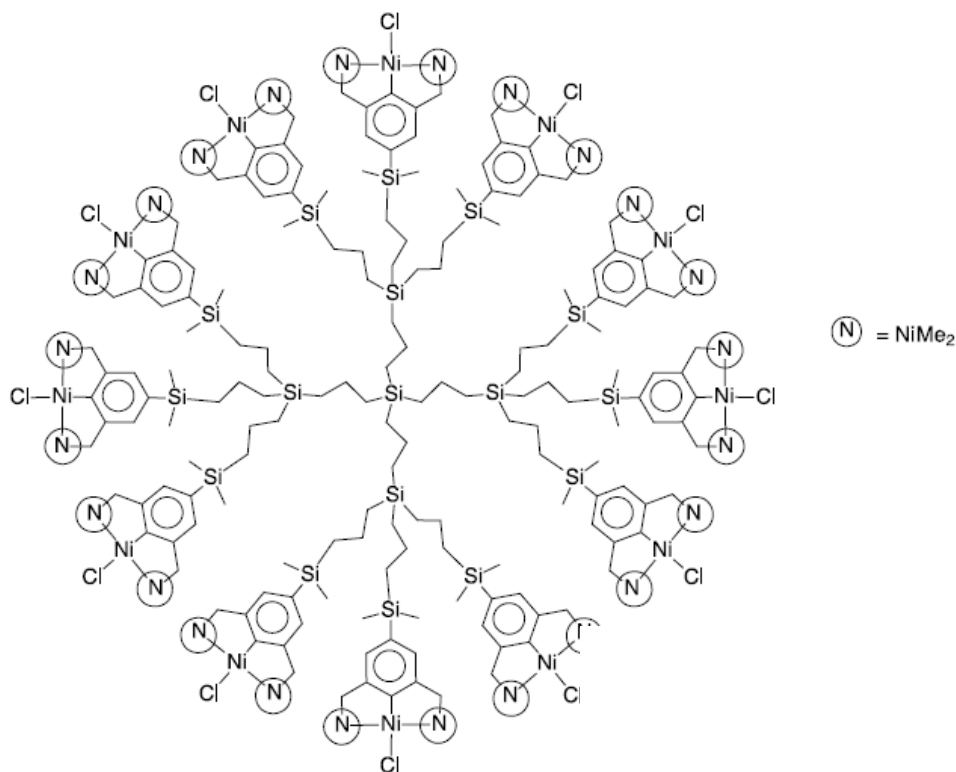


Figure 1.15 Dendritic [NiCl(NCN)] polycarbosilane complex (reproduced from ¹²²)

Unfavourable interactions between nickel sites were responsible responsible for a decrease in the catalytic activity of this system in the Kharasch addition of tetrachloromethane to methylmethacrylate (Figure 1.16).

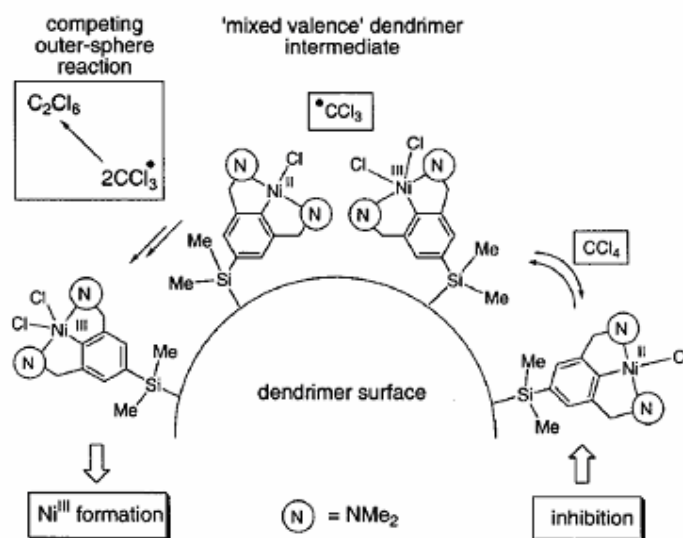
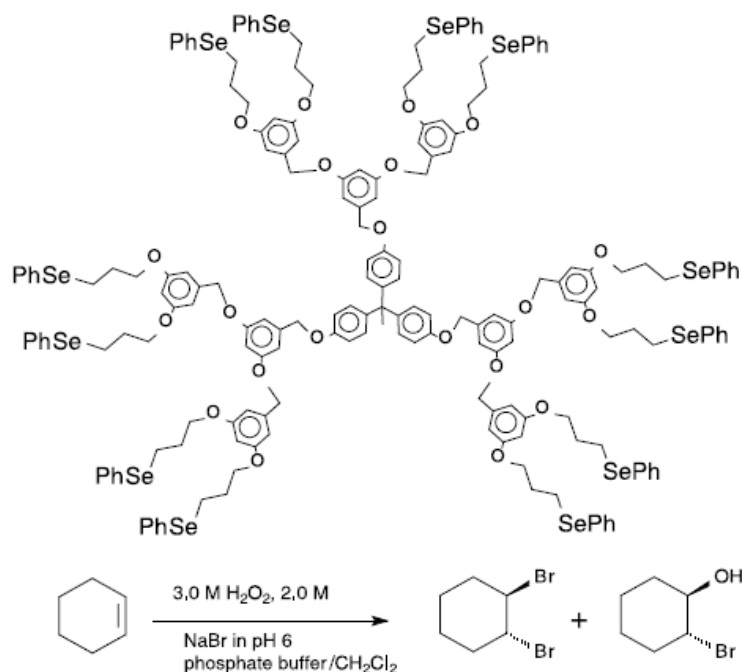


Figure 1.16 Possible negative cooperative effects between adjacent nickel moieties leading to deactivation of catalytic sites¹³¹

The decrease of catalytic activity as a consequence of “surface congestion” in peripherally modified dendrimers has precedents in the literature.^{132, 133} Astruc and co-workers, for instance, demonstrated that increasing steric bulk around the active metal centres leads to a negative dendritic effect in Pd(II) catalyzed Sonogashira carbon-carbon coupling.¹³⁴

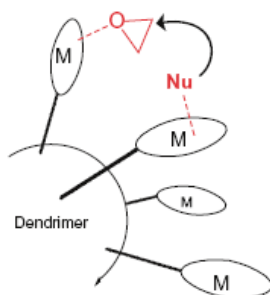
However, other dendritic systems have proven to be much better performing than their isolated small analogues.¹³⁵⁻¹³⁸ One of these strongest positive dendritic effects was reported in 2003 by Detty and co-workers who studied the oxidation of bromine and subsequent bromination of cyclohexene (Scheme 1.10).¹³⁹ The increase in generation of this selenium terminated polyaryl ether dendrimer led to the formation of more reactive catalysts responsible for a high turnover number ($> 60\,000\text{ mol}^{-1}$) as a consequence of enhanced interactions between selenium species at the surface of the macromolecule.



Scheme 1.10 Selenium terminated poly(benzyl ether) dendrimer in the oxidation of bromine and subsequent bromination reaction of cyclohexene. (reproduced from ¹²²)

Similarly, the specific and unique ionic interaction, between the active, cationic zirconocene $[(\text{Ind})_2\text{ZrMe}]^+$ and the crowded anionic surface of a carbosilane modified dendrimer, was found to be the origin of the positive dendritic effect observed in the polymerisation of ethylene.¹⁴⁰

A Co(salen) terminated PAMAM (Poly(amidoamine)) dendrimer, created by Jacobsen and co-workers, also shows significant rate enhancement in the hydrolytic resolution of terminal epoxides.¹⁴¹ This was attributed to positive cooperative effects between two metallic species, each activating either the epoxide or the nucleophile (Scheme 1.11).



Scheme 1.11 Illustration of positive cooperative effect between metal Co(salen) sites in the ring opening of an epoxide (reproduced from ¹²²)

Astruc and co-workers reported another interesting positive dendritic effect that was observed during the initiation of the ROMP of norbornene with dendritic ruthenium-benzylidene complexes (Figure 1.17).¹³³

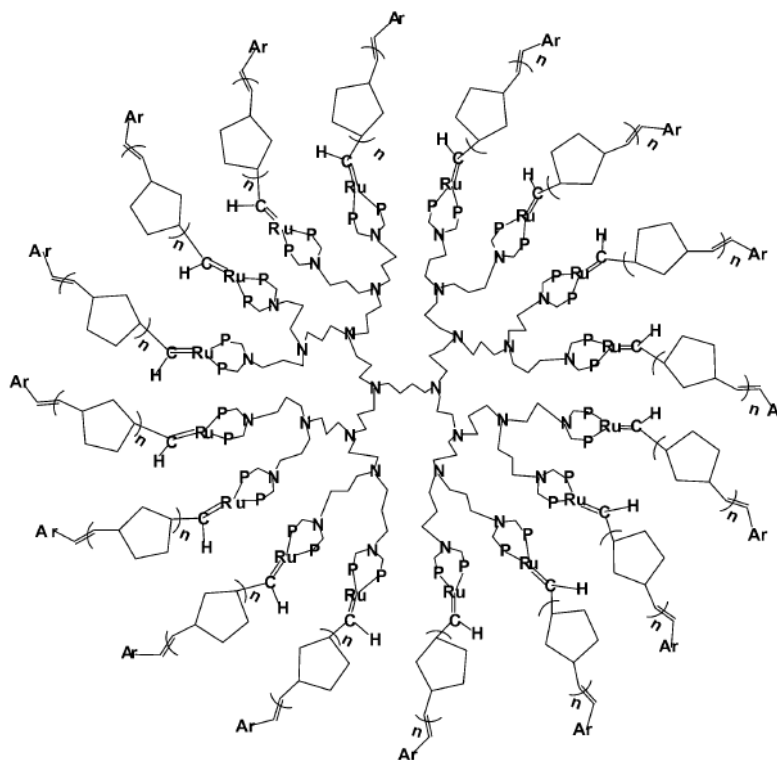


Figure 1.17 Astruc's dendritic star polynorbornene¹³²

This effect was rationalized in terms of labilization of a ruthenium-phosphorus bond at each Ru centre within the dendrimer, which is known to play an important role for the Grubbs' catalyst.¹⁴²

Ropartz *et al.* demonstrated that a POSS cored dendrimer with 16 terminal diphenylphosphines gives much higher selectivity to the desired linear product (linear: branched ratio (l:b) = 13.9) in the hydroformylation of oct-1-ene when compared to its small molecule analogues (l:b typically 2-5) (Figure 1.18).¹⁴³

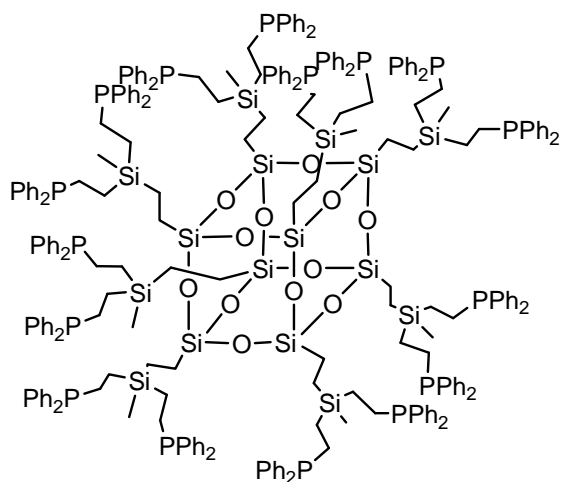


Figure 1.18 Diphenylphosphine terminated POSS cored dendrimer

This dramatic enhancement in linear selectivity appears to be caused by steric interactions on the surface of the dendrimer that force the binding groups into the desired equatorial equatorial configuration.¹⁴⁴ It is known that such a geometry around the rhodium centre leads to increased linear selectivity for hydroformylation reactions.¹⁴⁵

Supramolecular dendrimers (Figure 1.19), in which the catalyst is anchored at the periphery of the dendritic support via Coulombic interactions, have also been synthesised independently by a number of research groups,^{99, 146-148} although similar activity was observed in comparison to their small molecule analogues. However, this new concept has great potential since ligand modifications with the binding motifs provide a straightforward alternative to the complex synthesis of sophisticated dendrimers.

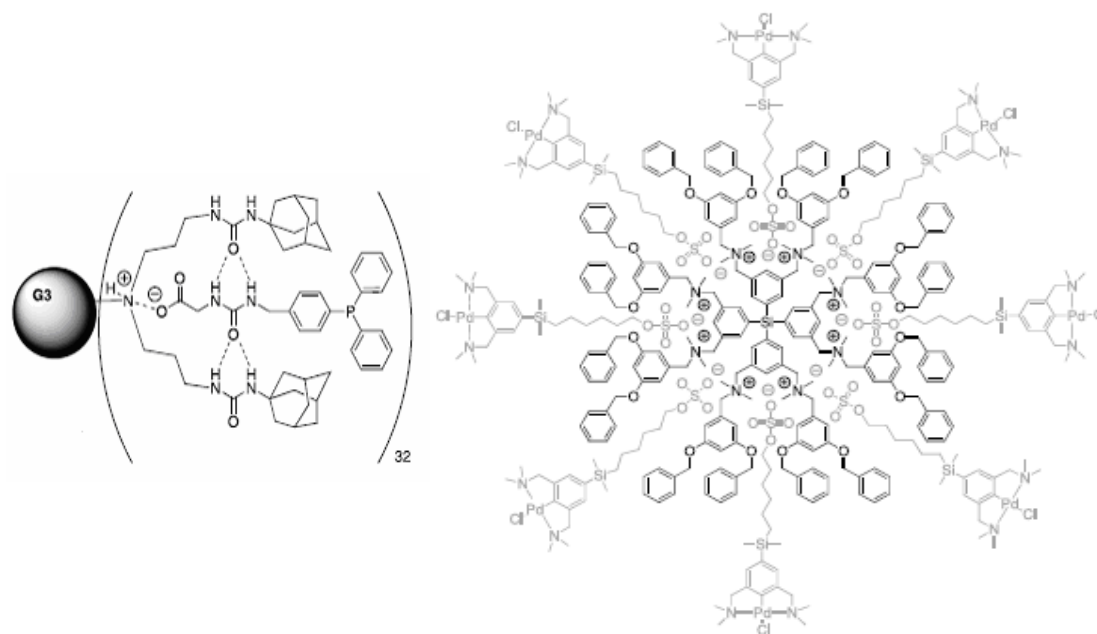


Figure 1.19 (left) Phosphine ligand assembled to the periphery of a urea adamantyl functionalized poly(propyleneimine) dendrimer (right) Octa-cationic core-shell together with eight anionic Pd(II) guest molecules¹⁴⁹

In conclusion, it has been observed that whilst the stability and lifetime of a dendritic-cored catalyst is often enhanced upon growing generations, its activity often decreases because of mass transport problems and difficult access to the core. However, these limitations can be circumvented by the concentration of reagents and/or stabilization of transition states or charged intermediates within a dendrimer. Additionally, while a positive dendritic effect may occur as a consequence of cooperativity between dendrons or catalytic sites at the periphery of a dendrimer, surface congestion can also lead to deactivation and a negative dendritic effect.

The application of dendrimers based on the POSS core in catalysis could profit from the cooperative effect between dendrons as well as the “constructive” steric interactions between end groups that give rise to positive dendritic effects. Emphasis will be placed on such applications, throughout the major part of the work reported further in this thesis.

I. 4 References

1. D. J. Cram and J. M. Cram, *Science*, 1974, **183**, 803.
2. C. J. Pedersen, *Angew. Chem.*, 1988, **100**, 1053.
3. J.-M. Lehn, *Angew. Chem.*, 1988, **100**, 91.
4. E. Buhleier, W. Wehner and F. Vogtle, *Synthesis*, 1978, 155.
5. D. A. Tomalia, H. Baker, J. Dewald, M. Hall, G. Kallos, S. Martin, J. Roeck, J. Ryder and P. Smith, *Polym. J.*, 1985, **17**, 117.
6. R. G. Denkewalter, J. Kolc and W. J. Lukasavage, *US Pat.*, 4 289 872, 1981.
7. G. R. Newkome, Z. Yao, G. R. Baker and V. K. Gupta, *J. Org. Chem.*, 1985, **50**, 2003.
8. S. Hecht and J. M. J. Fréchet, *Angew. Chem. Int. Ed.*, 2001, **40**, 74.
9. www.starpharma.com/images/technology_001.gif.
10. www.polychem.mat.ethz.ch/research/spherical_dendrimers/dendrimers_synthesis.jpg.
11. www.ninger.com/dendrimer/two.htm.
12. P. G. de Gennes and H. J. Hervet, *J. Phys. Lett.*, 1983, **44**, 351.
13. D. A. Tomalia, *Adv. Mat.*, 1994, **6**, 529.
14. L. J. Twyman, A. S. H. King and I. K. Martin, *Chem. Soc. Rev.*, 2002, **31**, 69.
15. C. J. Hawker and J. M. J. Fréchet, *J. Chem. Soc., Chem. Commun.*, 1990, 1010.
16. A. W. Bosman, H. M. Janssen and E. W. Meijer, *Chem. Rev.*, 1999, **99**, 1665.
17. K. Inoue, *Prog. Polym. Sci.*, 2000, **25**, 453.
18. M. Goldberg, R. Langer and X. Jia, *J. Biomat. Sci.-Polym. E.*, 2007, **18**, 241.
19. H. S. Parekh, *Curr. Pharm. Design*, 2007, **13**, 2837.
20. C. Valerio, J.-L. Fillaut, J. Ruiz, J. Guittard, J.-C. Blais and D. Astruc, *J. Am. Chem. Soc.*, 1997, **119**, 2588.
21. F. Zeng and S. C. Zimmerman, *Chem. Rev.*, 1997, **97**, 1681.
22. R. P. Brinas, T. Troxler, R. M. Hochstrasser and S. A. Vinogradov, *J. Am. Chem. Soc.*, 2005, **127**, 11851.
23. J. Leclaire, R. Dagiral, S. Fery-Forgues, Y. Coppel, B. Donnadieu, A.-M. Caminade and J.-P. Majoral, *J. Am. Chem. Soc.*, 2005, **127**, 15762.
24. R. Andres, E. de Jesus and J. C. Flores, *New J. Chem.*, 2007, **31**, 1161.
25. L. H. Gade, *Dendrimer Catalysis*, Springer GmbH edn., Berlin, Germany, 2006.
26. C. Omelas, J. R. Aranzaes, L. Salmon and D. Astruc, *Chem. Eur. J.*, 2008, **14**, 50.
27. P. L. Burn, S.-C. Lo and I. D. W. Samuel, *Adv. Mater.*, 2007, **19**, 1675.
28. S.-C. Lo and P. L. Burn, *Chem. Rev.*, 2007, **107**, 1097.

29. T. Aoki and T. Kaneko, *Polym. J.*, 2005, **37**, 717.
30. S. Langereis, A. Dirksen, T. M. Hackeng, M. H. P. van Genderen and E. W. Meijer, *New J. Chem.*, 2007, **31**, 1152.
31. M. Guillot-Nieckowski, S. Eisler and F. Diederich, *New J. Chem.*, 2007, **31**, 1111.
32. B. Felber and F. Diederich, *Helv. Chim. Acta*, 2005, **88**, 120.
33. E. M. M. de Brabander-van den Berg and E. W. Meijer, *Angew. Chem.*, 1993, **32**, 1308.
34. H. Ihre, O. L. Padilla de Jesus and J. M. J. Fréchet, *J. Am. Chem. Soc.*, 2001, **123**, 5908.
35. R. van Heerbeek, P. C. J. Kamer, P. W. N. M. van Leeuwen and J. N. H. Reek, *Org. Biomol. Chem.*, 2006, **4**, 211.
36. D. Liu, S. de Feyter, M. Cotlet, A. Stefan, U.-M. Wiesler, A. Herrmann, D. Grebel-Koehler, J. Qu, K. Mullen and F. D. de Schryver, *Macromolecules*, 2003, **36**, 5918.
37. A.-M. Caminade, M. Slany, N. Launay, M. L. Lartigue and J.-P. Majoral, *Phosphorus, Sulfur and Silicon*, 1996, **109**, 517.
38. J.-P. Majoral and A.-M. Caminade, *Chem. Rev.*, 1999, **99**, 845.
39. A. Tsuchida, C. Bolln, F. G. Sernetz, H. Frey and R. Mulhaupt, *Macromolecules*, 1997, **30**, 2818.
40. F. J. Feher and K. J. Weller, *Organometallics*, 1990, **9**, 2638.
41. F. J. Feher, K. J. Weller and J. W. Ziller, *J. Am. Chem. Soc.*, 1992, **114**, 9686.
42. P. Agaskar, *J. Chem. Soc., Chem. Commun.*, 1992, 1024.
43. S. Lee, S. Makan, M. M. B. Holl and F. R. MacFeely, *J. Am. Chem. Soc.*, 1994, **116**, 11819.
44. D. A. Loy and K. J. Shea, *Chem. Rev.*, 1995, **95**, 1431.
45. R. A. Mantz, P. F. Jones, K. P. Chaffe, J. D. Lichtenhan, J. W. Gilman and I. M. K. Ismail, *Chem. Mater.*, 1996, **8**, 1250.
46. G. T. Burns, R. B. Taylor, Y. R. Xu, A. Zangril and G. A. Zank, *Chem. Mater.*, 1992, **4**, 1313.
47. K. Kamiya, M. Okya and T. Yoko, *J. Noncryst. Solids*, 1986, **83**, 208.
48. M. G. Voronkov and V. L. Lavrent'yev, *Top. Curr. Chem.*, 1982, **102**, 199.
49. R. H. Baney, M. Itoh, A. Sakakibara and T. Suzuki, *Chem. Rev.*, 1995, **95**, 1409.
50. Y. Itami, B. Marciniak and M. Kubicki, *Chem. Eur. J.*, 2004, **10**, 1239.
51. M. Y. Lo, C. Zhen, M. Lauters, G. E. Jabbour and A. Sellinger, *J. Am. Chem. Soc.*, 2007, **129**, 5808.

52. G. Cheng, N. R. Vautravers and D. J. Cole-Hamilton, *Org. Biomol. Chem*, DOI: 10.1039/B812140K.
53. J. D. Froehlich, R. Young, T. Nakamura, Y. Ohmori, S. Li and A. Mochizuki, *Chem. Mater.*, 2007, **19**, 4991.
54. K. Wada, N. Watanabe, K. Yamada, T. Kondo and T.-A. Mitsudo, *Chem. Commun.*, 2005, 95.
55. A. R. Bassindale, Z. Liu, I. A. MacKinnon, P. G. Taylor, Y. Yang, M. E. Light, P. N. Horton and M. B. Hursthouse, *J. Chem. Soc., Dalton Trans.*, 2003, 2945.
56. R. Duchateau, H. C. L. Abbenhuis, R. A. van Santen, A. Meetsma, S. K.-H. Thiele and M. F. H. van Tol, *Organometallics*, 1998, **17**, 5663.
57. F. J. Feher and R. L. Blanski, *J. Am. Chem. Soc.*, 1992, **114**, 5886.
58. S. Krijnen, H. C. L. Abbenhuis, R. W. J. M. Hanssen, J. H. C. van Hooff and R. A. van Santen, *Angew. Chem. Int. Ed.*, 1998, **37**, 356.
59. T. Maschmeyer, M. C. Klunduk, C. M. Martin, D. S. Shephard, J. M. Thomas and B. F. G. Jonhson, *Chem. Commun.*, 1997, 1847.
60. K. Wada, M. Nakashita, A. Yamamoto and T. Mitsudo, *Chem. Commun.*, 1998, 133.
61. M. Crocker, R. H. M. Herold, A. G. Orpen and M. T. A. Overgaag, *J. Chem. Soc., Dalton. Trans.*, 1999, 3791.
62. F. J. Feher and T. A. Budzichowski, *Polyhedron*, 1995, **14**, 3239.
63. V. Ruffieux, G. Schmid, P. Braunstein and J. Rose, *Chem. Eur. J.*, 1997, **3**, 900.
64. G. Schmid, R. Pugin, J.-O. Malm and J.-O. Bovin, *Eur. J. Inorg. Chem.*, 1998, 813.
65. J. Dobler, M. Pritzsche and J. Sauer, *J. Am. Chem. Soc.*, 2005, **127**, 10861.
66. A. R. Bassindale, D. J. Parker, M. Pourny, P. G. Taylor, P. N. Horton and M. B. Hursthouse, *Organometallics*, 2004, **23**, 4400.
67. J. Choi, J. Harcup, A. F. Yee, Q. Zhu and R. M. Laine, *J. Am. Chem. Soc.*, 2001, **123**, 11420.
68. J. Choi, S. G. Kim and R. M. Laine, *Macromolecules*, 2004, **37**, 99.
69. K. Liang, G. Li, H. Toghiani, J. H. Koo and C. U. Pittman, *Chem. Mater.*, 2006, **18**, 301.
70. L. Zheng, S. Hong, G. Cardoen, E. Burgaz, S. P. Guido and E. B. Coughlin, *Macromolecules*, 2004, **37**, 8606.
71. J. Choi, A. F. Yee and R. M. Laine, *Macromolecules*, 2003, **36**, 5666.
72. H. Y. Xu, S. W. Kuo, J. Y. Lee and F. C. Chang, *Polymer*, 2002, **43**, 5117.

73. S. A. Pellice, D. P. Fasce and R. J. J. Williams, *J. Polym. Sci., Part B: Polym. Phys.*, 2003, **41**, 1451.
74. K. Su, D. R. Bujalski, K. Eguchi, G. V. Gordon, S. Hu and D.-L. Ou, *J. Mater. Chem.*, 2005, **15**, 4115.
75. T. T. Lin, C. B. He and Y. Xiao, *J. Phys. Chem. B*, 2003, **107**, 13788, and references therein.
76. W. J. Lin, W. C. Chen, W. C. Wu, Y. H. Niu and A. K. Y. Jen, *Macromolecules*, 2004, **37**, 2335-2341.
77. M. Y. Lo, K. Ueno, H. Tanabe and A. Sellinger, *Chem. Rec.*, 2006, **6**, 157.
78. S.-C. Lo, C. Zhen, M. Lauters, G. E. Jabbour and A. Sellinger, *J. Am. Chem. Soc.*, 2007, **129**, 5808.
79. T. C. Ionescu, F. Qi, C. McCabe, A. Striolo, J. Kieffer and P. T. Cummings, *J. Phys. Chem. B*, 2006, **110**, 2502.
80. A. Lee and J. D. Lichtenhan, *J. Appl. Polym. Sci.*, 1999, **73**, 1993.
81. J. J. Schwab and J. D. Lichtenhan, *Appl. Organomet. Chem.*, 1998, **12**, 707.
82. K.-M. Kim, D.-K. Keum and Y. Chujo, *Macromolecules*, 2003, **36**, 867.
83. C.-M. Leu, Y.-T. Chang and K.-H. Wei, *Chem. Mater.*, 2003, **15**, 3721.
84. C. Zhang, T. J. Bunning and R. M. Laine, *Chem. Mater.*, 2001, **13**, 3653.
85. K.-M. Kim and Y. Chujo, *J. Polym. Sci. Part A: Polym. Chem.*, 2001, **39**, 4035.
86. M. D. Nyman, S. B. Desu and C. H. Peng, *Chem. Mater.*, 1993, **5**, 1636.
87. F. J. Feher, J. J. Schwab, S. H. Phillips, A. Eklund and E. Martinez, *Organometallics*, 1995, **14**, 4452.
88. F. J. Feher and K. D. Wyndham, *J. Chem. Soc., Chem. Commun.*, 1998, 323.
89. F. J. Feher, K. D. Wyndham, D. Soulivong and F. Nguyen, *J. Chem. Soc., Dalton Trans.*, 1999, 1491.
90. M. Moran, C. M. Casado, I. Cuadrado and J. Losada, *Organometallics*, 1993, **12**, 4327.
91. H. J. Murfee, T. P. S. Thoms, J. Greaves and B. Hong, *Inorg. Chem.*, 2000, **39**, 5209.
92. G. R. Newkome, C. He and C. N. Moorefield, *Chem. Rev.*, 1999, **99**, 1689.
93. D. Astruc and F. Chardac, *Chem. Rev.*, 2001, **101**, 2991.
94. D. J. Cole-Hamilton, *Science*, 2003, **299**, 1702.
95. H. P. Dijkstra, C. A. Kruithof, N. Ronde, R. van de Coevering, D. J. Ramon, D. Vogt, G. P. M. van Klink and G. van Koten, *J. Org. Chem.*, 2003, **68**, 675.

96. N. J. Ronde and D. Vogt, in *Catalyst Separation, Recovery and Recycling; Chemistry and Process Design*, eds. D. J. Cole-Hamilton and R. P. Tooze, Dordrecht, The Netherlands, Springer edn., 2005.
97. N. Brinkmann, D. Giebel, G. Lohmer, M. T. Reetz and U. Kragl, *J. Catal.*, 1999, **183**, 163.
98. R. van Heerbeek, P. C. J. Kamer, P. W. N. M. van Leeuwen and J. N. H. Reek, *Chem. Rev.*, 2002, **102**, 3717.
99. D. de Groot, B. F. M. de Waal, J. N. H. Reek, A. P. H. J. Schenning, P. C. J. Kamer, E. W. Meijer and P. W. N. M. van Leeuwen, *J. Am. Chem. Soc.*, 2001, **123**, 8453.
100. N. J. Hovestad, E. B. Eggeling, H. J. Heidbuchel, J. T. B. H. Jastrzebski, U. Kragl, W. Keim, D. Vogt and G. van Koten, *Angew. Chem. Int. Ed.*, 1999, **38**, 1655.
101. A. V. Gaikwad, V. Boffa, J. E. ten Elshof and G. Rothenberg, *Angew. Chem. Int. Ed.*, 2008, **47**, 5407.
102. A. Dahan and M. Portnoy, *J. Polym. Sci. Part A: Polym. Chem.*, 2005, **43**, 235.
103. J. P. K. Reynhardt and H. Alper, *J. Org. Chem.*, 2003, **68**, 8353.
104. A. Dahan and M. Portnoy, *Chem. Commun.*, 2002, 2700.
105. A. Dahan and M. Portnoy, *Org. Lett.*, 2003, **5**, 1197.
106. P. Li and S. Kawi, *Catal. Today*, 2008, **131**, 61.
107. H. Brunner and S. Altmann, *Chem. Ber.*, 1994, **127**, 2285.
108. H. Brunner, *J. Organomet. Chem.*, 1995, **500**, 39.
109. Q.-H. Fan, Y.-M. Chen, X.-M. Chen, D.-Z. Jiang, F. Xi and A. S. C. Chan, *Chem. Commun.*, 2000, 789.
110. T. Butz, P. Murer and D. Seebach, *Polym. Mater. Sci. Eng.*, 1997, **77**, 132.
111. B. Helms and J. M. J. Fréchet, *Adv. Synth. Catal.*, 2006, **348**, 1125.
112. M. Kimura, Y. Sugihara, T. Muto, K. Hanabusa, H. Shirai and N. Kobayashi, *Chem. Eur. J.*, 1999, **5**, 3495.
113. D.-H. Hwang, C. D. Shreiner, C. N. Moorefield and G. R. Newkome, *New J. Chem.*, 2007, **31**, 1192.
114. S. Nlate, L. Plault and D. Astruc, *Chem. Eur. J.*, 2006, **12**, 903.
115. T. Fujihara, Y. Obora, M. Tokunaga, H. Sato and Y. Tsuji, *Chem. Commun.*, 2005, 4526.
116. C. C. Mak and H.-F. Chow, *J. Org. Chem.*, 1997, **62**, 5116.
117. C. Muller, L. J. Ackerman, J. N. H. Reek, P. C. J. Kamer and P. W. N. M. van Leeuwen, *J. Am. Chem. Soc.*, 2004, **126**, 14960.

118. A. Zubia, F. P. Cossio, I. Morao, M. Rieumont and X. Lopez, *J. Am. Chem. Soc.*, 2004, **126**, 5243.
119. G. E. Oosterom, R. J. van Haaren, J. N. H. Reek, P. C. J. Kamer and P. W. N. M. van Leeuwen, *Chem. Commun.*, 1999, 1119.
120. P. B. Rheiner and D. Seebach, *Chem. Eur. J.*, 1999, 3221.
121. M. E. Piotti, F. Rivera, R. Bond, C. J. Hawker and J. M. J. Fréchet, *J. Am. Chem. Soc.*, 1999, **121**, 9471.
122. C. Liang and J. M. J. Fréchet, *Prog. Polym. Sci.*, 2005, **30**, 385.
123. L. Liu and R. Breslow, *J. Am. Chem. Soc.*, 2003, **125**, 12110.
124. X. Zhang, H. Xu, Z. Dong, Y. Wang, J. Liu and J. Shen, *J. Am. Chem. Soc.*, 2004, **126**, 10556.
125. L. Balogh and D. A. Tomalia, *J. Am. Chem. Soc.*, 1998, **120**, 7355.
126. M. Zhao, L. Sun and R. M. Crooks, *J. Am. Chem. Soc.*, 1998, **120**, 4877.
127. K. Esumi, A. Susuki, N. Aihara, K. Usui and K. Torigoe, *Langmuir*, 1998, **14**, 3157.
128. J.-J. Lee, W. T. Ford, J. A. Moore and Y. Li, *Macromolecules*, 1994, **27**, 4632.
129. Y. Pan and W. T. Ford, *Macromolecules*, 2000, **33**, 3731.
130. J. W. J. Knapen, A. W. van der Made, J. C. de Wilde, P. W. N. M. van Leeuwen, P. Wijkens, D. M. Grove and G. van Koten, *Nature*, 1994, **372**, 659.
131. A. W. Kleij, R. A. Gossage, J. T. B. H. Jastrzebski, J. Boersma and G. van Koten, *Angew. Chem. Int. Ed.*, 2000, **39**, 176.
132. S. Gatard, S. Nlate, G. Bravic, J.-C. Blais and D. Astruc, *Angew. Chem. Int. Ed.*, 2003, **42**, 452.
133. S. Gatard, S. Kahlal, D. Mery, S. Nlate, E. Cloutet, J.-Y. Saillard and D. Astruc, *Organometallics*, 2004, **23**, 1313.
134. K. Heuze, D. Mery, D. Gauss, J.-C. Blais and D. Astruc, *Chem. Eur. J.*, 2004, **10**, 3936.
135. M. T. Reetz, G. Lohmer and R. Schwickardi, *Angew. Chem. Int. Ed.*, 1997, **36**, 1526.
136. V. Maraval, R. Laurent, A.-M. Caminade and J.-P. Majoral, *Organometallics*, 2000, **19**, 4025.
137. Y. Ribourdouille, G. Engel, M. Richard-Plouet and L. H. Gade, *Chem. Commun.*, 2003, 1228.
138. T. Mizugaki, M. Murata, M. Ooe, K. Ebitani and K. Kaneda, *Chem. Commun.*, 2002, 52.
139. M. D. Drake, F. V. Bright and M. R. Detty, *J. Am. Chem. Soc.*, 2003, **125**, 12558.

- 140. M. Mager, S. Becke, H. Windisch and U. Denninger, *Angew. Chem. Int. Ed.*, 2001, **40**, 1898.
- 141. R. Breinbauer and E. N. Jacobsen, *Angew. Chem. Int. Ed.*, 2000, **39**, 3604.
- 142. M. S. Sanford, M. Ulman and R. H. Grubbs, *J. Am. Chem. Soc.*, 2001, **123**, 749.
- 143. L. Ropartz, R. E. Morris, D. F. Foster and D. J. Cole-Hamilton, *Chem. Commun.*, 2001, 361.
- 144. K. J. Haxton, D. J. Cole-Hamilton and R. E. Morris, *Dalton Trans.*, 2004, 1665.
- 145. C. Claver and P. W. N. M. van Leeuwen, *Rhodium Catalyzed Hydroformylation*, Kluwer Academic Publishers edn., Dordrecht, 2000.
- 146. M. Kimura, M. Kato, T. Muto, K. Hanabusa and H. Shirai, *Macromolecules*, 2000, **33**, 1117.
- 147. R. van de Coevering, M. Kuil, R. J. M. K. Gebbink and G. van Koten, *Chem. Commun.*, 2002, 1636.
- 148. M. Ooe, M. Murata, A. Takahama, T. Mizugaki, K. Ebitani and K. Kaneda, *Chem. Lett.*, 2003, **32**, 692.
- 149. R. van de Coevering, R. J. M. Klein Gebbink and G. van Koten, *Prog. Polym. Sci.*, 2005, **30**, 474.

II. Diphenylphosphine based ligands in the palladium catalyzed ethene methoxycarbonylation

II. Diphenylphosphine based ligands in the palladium catalyzed ethene methoxycarbonylation

II. 1 Introduction

During a study of Polyhedral Oligomeric Silsesquioxane dendrimers with phosphine ligands attached to their periphery, Cole-Hamilton and co-workers discovered that a dendrimer with 16 terminal diphenylphosphines (Figure 2.1) gave much higher selectivity to the desired linear product (linear: branched ratio (l:b) = 13.9) in oct-1-ene hydroformylation reaction than any of its small molecule analogues (l:b typically 2-5).^{1, 2} This was one of the very first positive dendritic effects to be discovered and was very specific for a dendrimer in which the Ph_2P groups were separated by a $-(\text{CH}_2)_2\text{Si}(\text{CH}_2)_2-$ spacer. Shorter or longer chains, or replacing a C atom in the spacer by O were ineffective. Modelling studies using molecular mechanics suggest that the reason for the enhanced selectivity is that crowding on the dendrimer periphery forces the phosphines into a position that is ideal for coordination in two equatorial sites of trigonal bipyramidal intermediates in the catalytic cycle.³ It is known that such equatorial equatorial binding leads to increased linear selectivity for hydroformylation reactions.⁴

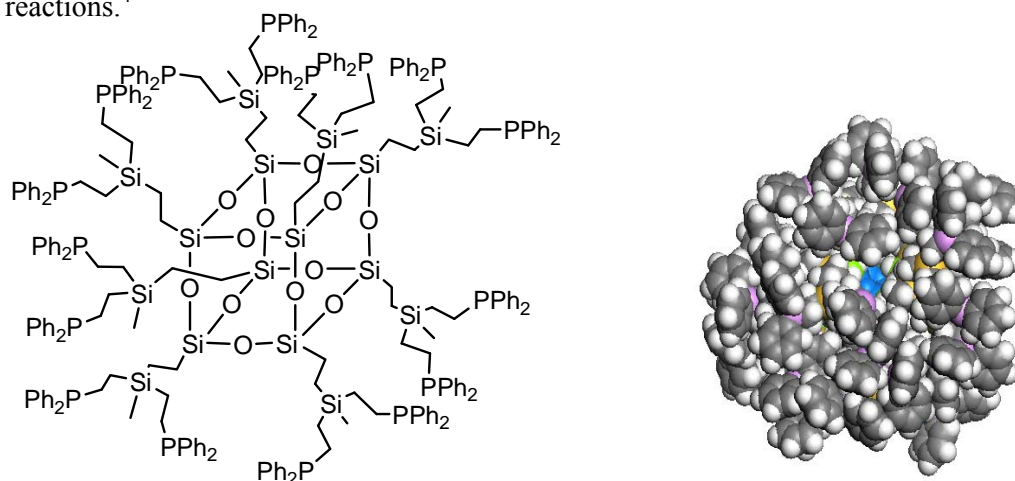
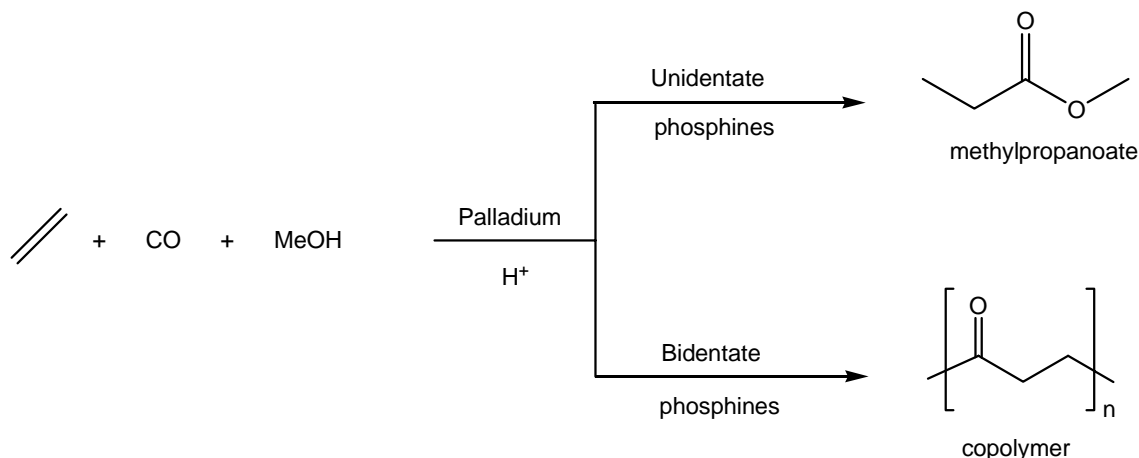


Figure 2.1 Chemdraw (left) and space filling (right) model of dendrimer used for selective hydroformylation reaction^{2, 3}

We now wish to explore further the exciting preliminary results described above in order to develop new highly selective catalysts for different reactions. Our strategy will be therefore to

design dendrimers with terminal groups that are not only able to bind metals but also to mimic monodentate ligands which are either ineffective in selective catalysis whilst bidentate analogues are effective, or which show a different selectivity from that shown by bidentate analogues. The rewards here may include easier synthesis than for bidentate ligands, possible enhanced selectivity as a result of the greater steric crowding at the periphery of the dendrimer and easier catalyst separation by ultra-filtration.

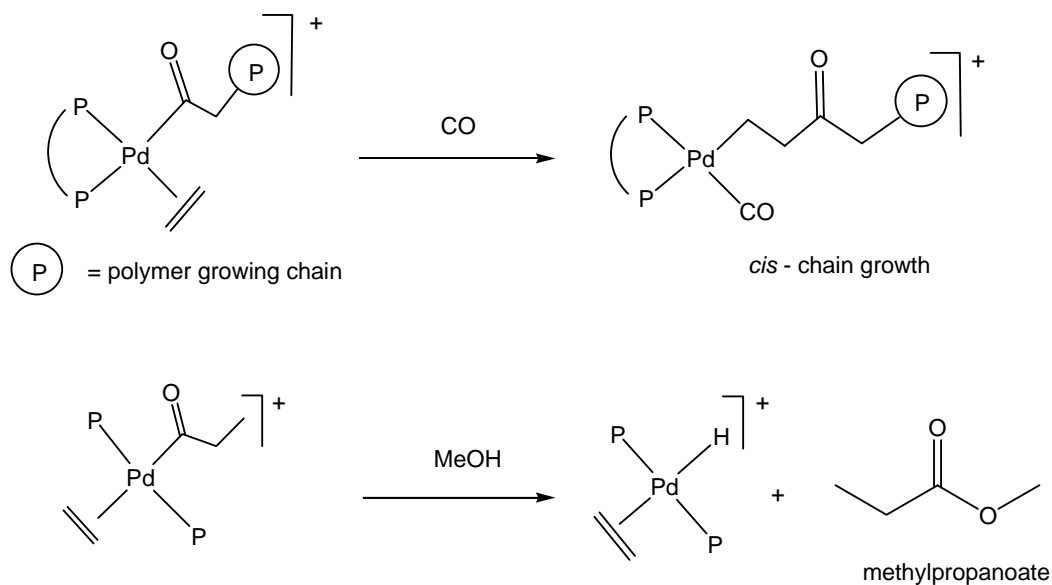
Among the numerous choices of terminal binding groups, we decided to develop the diphenylphosphines as similar studies and savoir-faire in the Cole-Hamilton group have been previously established in this field.⁵ Moreover, these phosphines are commonly used, in a variety of forms, in the methoxycarbonylation of ethene. In this reaction, carbon monoxide and ethene, two of the most readily available feedstocks in all of chemistry, react together in the presence of methanol and a suitable catalyst to give either methylpropanoate (MeP),⁶⁻⁸ a key intermediate in the production of methylmethacrylate, the monomer used for making Perspex, or a perfectly alternating copolymer (PK) which has excellent structural properties and is biodegradable.^{6, 9, 10} In some cases short chain oligomers can also be produced.⁸ The best catalysts for these reactions are cationic palladium complexes containing tertiary phosphines. Monodentate phosphines (e. g. PPh_3) generally give methylpropanoate, whilst bidentate phosphines (e.g. $\text{Ph}_2\text{P}(\text{CH}_2)_3\text{PPh}_2$) form copolymer (Scheme 2.1).



Scheme 2.1 Usual selectivity in the methoxycarbonylation of ethene catalysed by palladium phosphine complexes

This observation was originally ascribed^{6, 11} as arising due to the sites at which the catalytic reactions occur being stabilised in the mutually *cis* position when a bidentate ligand is present, so that migration of the growing chain onto ethene can readily occur. Monodentate ligands

prefer to adopt the thermodynamically more stable *trans* configuration, in which migration cannot occur and so rapid termination by reaction with methanol to give methylpropanoate occurs (Scheme 2.2).



Scheme 2.2 Rationale of the selectivity of CO-ethene reactions ($\text{P-P} = \text{Ph}_2\text{P}(\text{CH}_2)_3\text{PPh}_2$, $\text{P} = \text{PPh}_3$)^{6, 8}

In recent years however, a few bidentate ligands, mostly with bulky electron donating substituents, such as $\text{Bu}^t_2\text{P}(\text{CH}_2)_3\text{P}^t\text{Bu}_2$ ¹² and $1,2\text{-(Bu}^t_2\text{PCH}_2)_2\text{C}_6\text{H}_4$,^{13, 14} have been shown to be extremely effective for the selective formation of methylpropanoate. Indeed one is so effective that it is being commercialised. These ligands call into question the argument based on mutually *cis* or *trans* active sites as being responsible for the chemoselectivity of the reactions, although it is possible that these ligands give methylpropanoate because they become monodentate at some point in the cycle.⁸ The precise mechanistic reason for this unusual selectivity is the subject of continuing debate,^{8, 15-17} but an alternative explanation has been proposed¹⁵ on the basis of careful studies of the rate of methanolysis of model palladium acetyl cations. Complexes containing *trans* bidentate diphosphines either do not react with methanol under CO or react very slowly, whilst *cis* complexes react rapidly with larger ligands being generally more reactive. These observations have led to the proposal that the population of the *cis* isomer, at least in part determines the reactivity. The relative rate of acyl migration onto coordinated ethene and methanolysis determines the chemoselectivity between methyl propanoate and polyketone.

The conventional literature does not have extensive information on monodentate phosphines leading to polymer, because the majority give selective methylpropanoate formation. It has been shown that the selectivity can be tuned to polyketone formation by limiting termination by controlling the reaction conditions, for example by varying the solvent, increasing pressure or changing the anion, as was reported in early research.¹⁸ An intriguing instance of activity to polyketone being promoted by monodentate phosphines under different reaction conditions was reported by Drent.¹⁹ He observed that under low phosphine:palladium ratios, some activity to polyketone was afforded by triphenylphosphine (35 g PK (g Pd. h)⁻¹). This change in selectivity compared with the more usual methylpropanoate formation was explained by the suppression of the isomerism between the *cis/trans* species (this isomerisation is known to be catalysed by excess PPh₃) shown in Scheme 2.2, thus causing some *cis* intermediate to be present, and hence to polyketone. The only other system in the open literature reporting polyketone formation when using hemilabile phosphines is by Keim *et al.*,²⁰ using heteroatom containing phosphines which are themselves capable of bidentate coordination to palladium so giving the required *cis* geometry. The most significant and relevant consideration of monodentate phosphines, outwith the conventional literature, is work patented by Nozaki (Shell),²¹ where catalysts of general formula PR₁R₂R₃ are proposed to be active for the production of polyketone, where R₁ is an alkyl group and R₂, R₃ are aryl groups.

Before any further discussion of this reaction using POSS dendritic ligands and for clarity reasons, we will first report our investigation using non-dendritic monodentate phosphines trying to rationalize our results in terms of steric and electronic effects of the phosphines.

II. 2 Non dendritic monodentate ligands in the methoxycarbonylation of ethene²²

Triaryl-, dialkylphenyl-, alkylidiphenyl- and trialkylphosphines have been examined in this study. The same catalytic conditions, pressure, temperature, reaction time, catalyst concentration as well as the same acid promoter (MeSO₃H) were applied, for ease of comparison with previous studies. The palladium to phosphine ratio was varied from 1:4 to 1:30, along with the nature of the phosphine in order to focus on the steric and electronic effects of the ligands. The results obtained with triaryl phosphines are collected in Table 2.1.

II. 2. 1 Triaryl phosphines

Table 2.1 Rates of formation of methyl propanoate (MeP) and /or polyketone (PK) from the palladium catalysed methoxycarbonylation of ethene in the presence of aryl phosphines.^a Electronic parameters and cone angles of aryl phosphines.

Run	Phosphine	P: Pd ratio	Turnover frequency (TOF) , h ⁻¹		PK rate, g (g Pd. h) ⁻¹	Electronic Parameter, cm ⁻¹	Cone Angle, θ
			MeP	PK			
1	PPh ₃	4	4.5	-	<1	2069	145
2		10	10.5	0	0		
3		30	19.8	0	0		
4	P(4-C ₆ H ₄ F) ₃	4	5	0	0	2071.1	*
5		10	23.2	0	0		
6		30	67.8	0	0		
7	P(C ₆ F ₅) ₃	4	0	0	0	2089.7	184
8		30	0	0	0		
9	P(4-C ₆ H ₄ OMe) ₃	4	4.1	0	0	2066.3	*
10		10	5.4	0	0		
11		30	8.8	20.1	5		
12	P(2-C ₆ H ₄ OMe) ₃	4	0	0	0	2058.8	*
13		30	<1	0	0		

^a Reaction conditions: catalyst (0.02 mmol), MeSO₃H (0.4 mmol), MeOH (10 mL), p_{CO} = 30 bar, p_{Ethene} = 30 bar, temp = 85 °C, t = 2.5 h. TOF's are averaged over 2.5 h; * not determined

This related family of phosphines contains triphenylphosphine, which has historically been widely studied, particularly by early researchers such as Sen who showed that methyl propanoate was produced along with small amounts of short chain oligomer.^{18, 23} Thus, this gives a reference point from which we can rationalise the observed product selectivity of related triarylphosphine containing catalysts. When triphenylphosphine (Pd:P = 1:4) is used, both methylpropanoate and polyketone are formed, but at very low rates (Runs 1-3). This observation is entirely consistent with Drent's observations²⁴ that at low phosphine to palladium ratios, some activity to polyketone can be observed, because *cis-trans* isomerisation in the acyl intermediate is slower.

For triphenylphosphine (Runs 1-3), tris-(4-fluorophenyl)phosphine (Runs 4-6) and tris-(4-methoxyphenyl)phosphine (Runs 9-11) a general increase in the rate of formation of

methylpropanoate can be observed from the 1:4 to 1:30 ratio for each phosphine. This observation may also be related to the increase in the rate of *cis-trans* isomerisation. Tris-(2-methoxyphenyl)phosphine (Runs 12, 13) totally inhibits the reaction, presumably because the high degree of steric bulk directly around the phosphorus atom provided by the ortho substituents prevents any monomer molecules from coordinating to palladium in the catalytic complex or leads to complexes containing only one phosphine ligand. No activity is observed using the electron poor $\text{P}(\text{C}_6\text{F}_5)_3$ (Runs 7, 8).

In addition to this steric effect, we can also observe an electronic effect when the methylpropanoate rate is compared between the first four phosphines in Table 2.1 (Runs 1-11). A general increase in the rate of methylpropanoate formation moving from the electron donating 4-methoxy groups, through triphenylphosphine, to the electron withdrawing 4-fluoro groups is apparent at all ratios studied. However this rate increase is most pronounced when the P:Pd ratio is high (Runs 3, 6 and 11). This result is unsurprising, as it can be related to previous work on the electronic effect of substituents on product rate when using bidentate phosphines.²⁵ Electron donating bidentate phosphines increase the rate of polyketone formation through intermediate stabilisation, whilst electron withdrawing substituents are expected to increase the rate of termination by nucleophilic attack by methanol, thus affording the high rates of methylpropanoate observed. Methanolysis is believed to be rate determining in these reactions.²⁶

The only unexpected result is that some activity ($\text{TOF} = 20 \text{ h}^{-1}$) to polyketone is observed when using tris-(4-methoxyphenyl)phosphine under high phosphine:palladium ratios (Run 11). Even though this seems a moderate rate, the productivity in $\text{g PK (g Pd h)}^{-1}$ shows that the weight of polymer produced is small. This result is still surprising and may suggest that this phosphine in some way favours the *cis* isomer of the palladium complex.

II. 2. 2 Mixed alkyl aryl and trialkyl phosphines

Moving from aryl phosphines to alkyl phosphines, we will first focus our attention on alkyldiphenyl phosphines before investigating more closely dialkylphenyl phosphines and trialkyl phosphines (Table 2.2).

Table 2.2 Rates of formation of methyl propanoate (MeP) and /or polyketone (PK) from the palladium catalysed methoxycarbonylation of ethene in the presence of alkyl phosphines.^a Electronic parameters and cone angles of alkyl phosphines.

Run	Phosphine	P: Pd ratio	Turnover frequency (TOF) , h ⁻¹		PK rate, g (g Pd. h) ⁻¹	Electronic Parameter, cm ⁻¹	Cone Angle, θ
			MeP	PK			
14	PPh ₂ Me	4	0.6	289	72	2067.3	136
15		30	2.0	0	0		
16	PPh ₂ Et	4	1.0	5.2	1.3	2066.5	140
17		30	10.4	0	0		
18	PPh ₂ Pr	4	1.8	35	8.7	2066.3	141
19		30	20.4	0	0		
20	PPh ₂ Pr ⁱ	4	2.8	14.1	3.5	2065.7	150
21		30	62.4	0	0		
22	PPh ₂ Bu ^t	4	2.3	0	0	2064.7	157
23		30	140	0	0		
24	PPhMe ₂	4	0.5	409	101.8	2065.6	122
25		30	0.8	0	0		
26	PPhEt ₂	4	0.3	413	102.8	2064	136
27		30	0.7	0	0		
28	PMe ₃	4	0.8	220	54.8	2063.9	118
29		30	0.6	0	0		
30 ^b		30	0.5	39	9.8		
31	PEt ₃	4	0.3	165	41.1	2061.5	132
32		30	0.7	0	0		
33 ^b		30	0.6	111	27.6		
34	P ^t Bu ₃	4	0.7	0	0	2056.1	182
35		30	0	0	0		
36	P ⁱ Bu ₃	4	0.1	0	0	2059.7	143
37		30	0.4	0	0		
38	P ⁿ Bu ₃	4	0.3	365	90.9	2060.3	132
39		30	0.8	0	0		
40	P(oct) ₃	4	0.6	323	80.4	2057.9	132
41		30	0.6	0	0		

^a Reaction conditions: catalyst (0.02 mmol), MeSO₃H (0.4 mmol), MeOH (10 mL), p_{CO} = 30 bar, p_{Ethene} = 30 bar, temp = 85 °C, t = 2.5 h. TOF's are averaged over 2.5 h; ^b MeSO₃H (0.8 mmol); * not determined

Unusually for monodentate phosphines, all of the alkyldiphenylphosphines, except the very bulky $\text{Ph}_2\text{P}^t\text{Bu}$ (Run 22), give polyketone at low P:Pd ratios (Runs 14, 16, 18 and 20). Productivities of 1.3, 8.7 and 3.5 g PK (g Pd. h)⁻¹ for the ethyl, n-propyl and i-propyl are observed, corresponding to moderate TOFs. The rate of polyketone formation decreases when using Ph_2PR along the series $\text{Me} > \text{Pr} > \text{Pr}^i > \text{Et} > \text{Bu}^t$ (Runs 14, 18, 20, 16 and 22). Either steric or electronic effects (or both) could be responsible for this effect. Similarly, it is not possible to deconvolute steric and electronic effects upon the rate of formation of methyl propanoate when using alkyldiphenylphosphines, which increases along the series $\text{Me} > \text{Et} > \text{Pr} > \text{Pr}^i > \text{Bu}^t$, especially at high P:Pd ratios, where polyketone is not formed (Runs 15, 17, 19, 21 and 23).

None of the dialkylphenyl or trialkyl phosphines studied showed any significant activity for methyl propanoate formation, even at high (P:Pd) ratios, where no activity to any products was observed (Runs 25, 27, 29, 32, 35, 37, 39 and 41). These results are particularly surprising due to the significant rates achieved with their alkyldiphenylphosphine analogues. One possible reason for this lack of activity is that the highly basic phosphines may neutralise the acid and hence inhibit the formation of the catalytically active hydridopalladium species. We note, however, that diprotonated 1,2- $\text{C}_6\text{H}_4(\text{CH}_2\text{P}^t\text{Bu})_2$ is sufficiently acidic to protonate the related Pd complexes.²⁷ Support for the suggestion that excess phosphine does prevent protonation of the Pd centre is provided by the results obtained using PR_3 (R = Me or Et) with a Pd:P:H⁺ ratio of 1:30:40, where polyketone formation is again observed (Runs 30 and 33).

The excellent chemoselectivity to polyketone when using the dialkylphenyl and trialkylphosphines, with the exception of P^tBu_3 (Run 34) and P^iBu_3 (Run 36), at low phosphine ratios (Runs 24, 26, 28, 31, 33, 38 and 40) is unprecedented for monodentate phosphines apart from PPh_2Me (see above). We note also that small amounts of CO-ethene oligomers are formed when using these more basic phosphines. These are discussed in detail below.

In order to attempt to rationalise the differences in selectivity between these related alkyl phosphines in terms of the ligand structure, the productivity for polyketone formation has been plotted in a Tolman Map in Figure 2.2. Steric-electronic maps were devised by Tolman and were first described in his seminal paper of 1977.²⁸ They relate a parameter of interest, in

this case the polyketone productivity rate, to the steric and electronic parameters of the ligands, which may be calculated according to empirical rules.²⁸

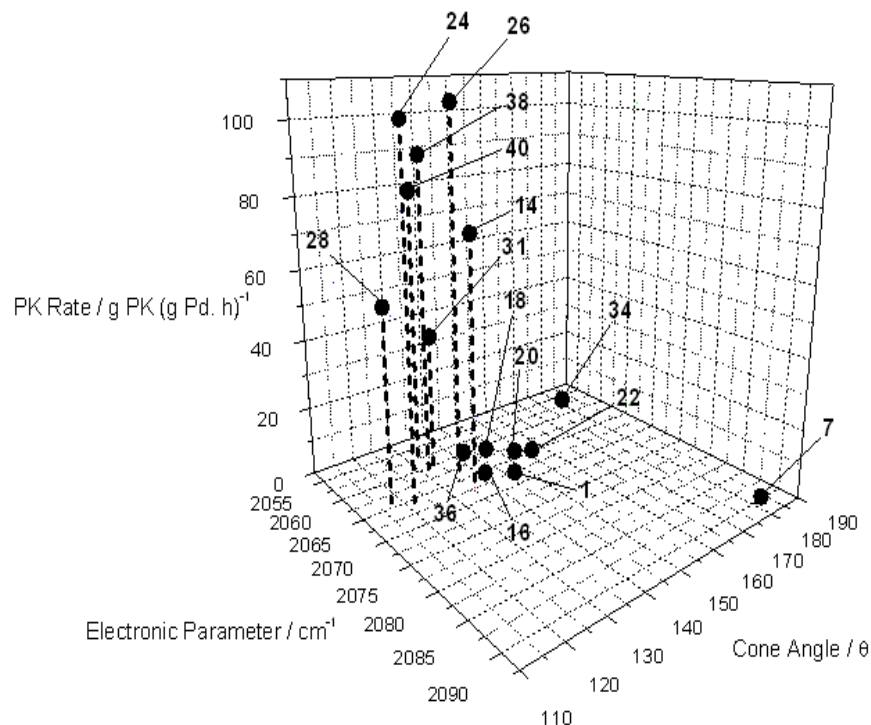


Figure 2.2 Tolman map of trialkyl, dialkylphenyl and alkylidiphenyl phosphines (1:4, Pd:P) in the palladium-catalyzed methoxycarbonylation of ethene. The parameters are defined in ref²⁸. **1** PPh₃, **7** P(C₆F₅)₃, **14** PPh₂Me, **16** PPh₂Et, **18** PPh₂Pr, **20** PPh₂Prⁱ, **22** PPh₂Bu^t, **24** PPhMe₂, **26** PPhEt₂, **28** PMe₃, **31** PEt₃, **34** PBu₃, **36** PBu₃ⁱ, **38** PBu₃ⁿ, **40** P(Oct)₃

By showing the relationships in three-dimensions, even if a parameter of interest is dependant on a mixture of steric and electronic properties, the qualitative deconvolution of both effects is possible. Figure 2.2 shows the averaged polyketone rates for all the phosphines studied. It shows that there is a well defined area in terms of steric and electronic parameters for active and selective polymer formation when using monodentate phosphines. The parameters required seem to be a combination of good electron donating ability and small size. How subtle this reliance is can be shown by the examples of methyl- and ethyldiphenylphosphine (Runs 14 and 16). The cone angles are 136 ° and 140 ° respectively for these phosphines, but one is active and the other has very low activity. Thus, an increase in steric bulk by 4 ° seems to cause an almost complete loss of activity to polyketone, which is a very surprising, but reproducible observation.

II. 2. 3 Oligoketone formation

Analysis of the distribution of soluble oligomers (containing 2-5 $-\text{CH}_2\text{CH}_2\text{C}(\text{O})-$ units) produced during co-polymerisation of CO and ethene in methanol can also help to give information on the origins of the selectivity of the reaction.¹⁶ As the bite angle of a bidentate phosphine increases, the pocket angle decreases and it has been argued that this favours termination¹⁶ so that the Flory-Schulz constant, α (rate of propagation / (rate of propagation + rate of termination)) will be lower. For monodentate ligands, the pocket angle is expected to be smaller for the larger cone-angle ligands, so they should favour termination over chain growth and hence should favour methyl propanoate production.

Under our conditions, negligible amounts of co-oligomers are obtained when using any of the triaryl phosphines, PBu^i_3 or PBu^t_3 (only methyl propanoate is formed) or when using PMePh_2 (only polyketone is formed). The amounts are extremely small for PR_2Ph ($\text{R} = \text{Me}$ or Et) and for PR_3 ($\text{R} = \text{Me}$, Et or Oct), all of which produce predominantly polyketone. Significant amounts of co-oligomers are observed only for the catalysts which produce smaller amounts of polyketone and significant amounts of methyl propanoate; those containing PRPh_2 ($\text{R} = \text{Et}$, Pr , Pr^i and Bu^t). In all cases the oligomers have one keto and one ester end group, although traces of 2-pentanone are also observed in some cases.

The end group analysis shows that only one mechanism (probably carried by Pd-H) operates.⁶ Quantitative analysis of the soluble co-oligomers formed for PRPh_2 ($\text{R} = \text{Et}$, Pr , Pr^i and Bu^t) shows a Flory-Schulz distribution with α (see Table 2.3) being 0.49 for $\text{R} = \text{Et}$ dropping to 0.41 ($\text{R} = \text{Bu}^t$) as the bulk of the ligand increases.

Table 2.3 Flory-Schulz constants (α) for soluble oligoketones formed using different ligands ($\text{Pd:P} = 1:4$)^a

Ligand	PEtPh_2	PPrPh_2	PPr^iPh_2	PBu^tPh_2
α	0.49	0.47	0.46	0.41

^a Calculated as described in refs ²⁹ and ³⁰

These results indicate that bulky ligands promote methyl propanoate formation, but that, as the bulk of the phosphine is reduced, the rate of chain growth increases relative to that of termination. Only the smallest ligands give polyketone. These results then reinforce the conclusions made on the basis of bidentate ligands that the reaction selectivity is

determined largely by the size of the pocket angle, with smaller pocket angles favouring termination.¹⁶

It is noteworthy that co-oligomers and polyketone are only ever observed when the P:Pd ratio is low. Most of the ligands promote methyl propanoate formation at higher phosphine loading. One possible explanation is that monophosphine complexes, which will have even wider pocket angles may promote polyketone formation at low P:Pd ratios. This observation does not appear to be consistent with the suggestion that the reduction of electron density on Pd caused by a bulky electron donating ligand becoming monodentate leads to faster attack by methanol and hence favours methyl propanoate formation.⁸

II. 2. 4 Studies of model complexes

In order to try to obtain more information about possible catalytic intermediates and their stereochemistry, [Pd(COD)MeCl] was treated with phosphines (2 equivalents) in order to synthesise [PdClMeP₂] (P = PMePh₂, PMe₃,³¹ PMe₂Ph³¹ and PPh₃³²), a model for the ethyl intermediate in the copolymerisation. Using PMe₂Ph, a singlet was observed at 26.6 ppm in the ³¹P{¹H} NMR spectrum suggesting that the phosphines must be coordinated *trans* about the metal centre (Figure 2.3).

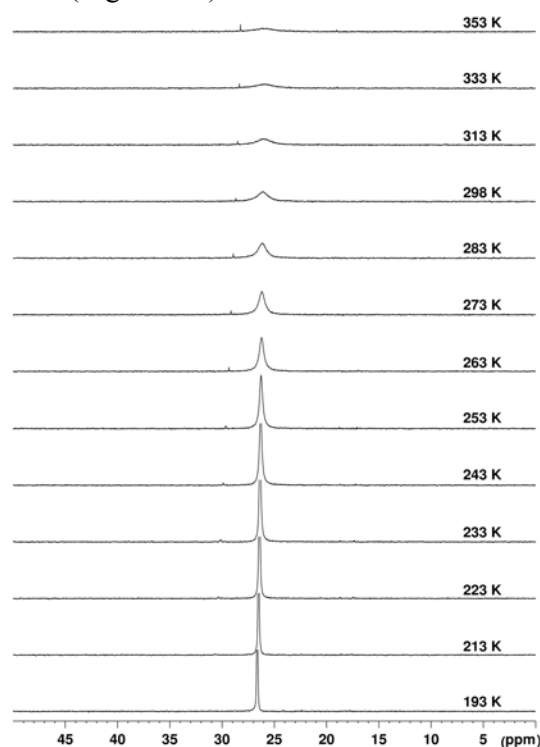


Figure 2.3 Variable temperatures ³¹P{¹H} NMR spectra of a d₈-toluene solution of [(COD)PdMeCl] with 2 equivalents of PPh₂Me

In addition, the triplet Pd-Me ($^3J_{\text{PH}} = 6 \text{ Hz}$) signal in the ^1H NMR spectrum confirms *trans* co-ordinating phosphines, at least in the methyl complex.³³ There is no evidence of any *cis*-species despite the selectivity towards polyketone formation when using this phosphine. On heating, the singlet broadens and shifts slightly to lower frequency, presumably because of exchange between free and bound phosphine. This has been confirmed by studying reactions in which the Pd:P ratio is 1:4. In this case singlets are observed at $\delta_{\text{P}} = 26.6$ and -16.5 ppm from the bound and the free phosphine respectively. On heating both broaden together with the coalescence temperature being $> 353 \text{ K}$. At any given temperature, the resonance from the phosphines attached to Pd are slightly broader when excess phosphine is present. An Eyring plot ($\text{P}:\text{Pd} = 4:1$) based upon simulation of the line shapes over the temperature range $223\text{-}293 \text{ K}$ gives activation parameters: $\Delta H^\ddagger = 19.9 \text{ kJ mol}^{-1}$ and $\Delta S^\ddagger = -119 \text{ J (mol K)}^{-1}$. The high negative entropy of activation confirms that the exchange is associative. Very similar behaviour is observed for PMe_3 ($\delta_{\text{P}} = -14.5 \text{ ppm}$), PMe_2Ph ($\delta_{\text{P}} = -1.9 \text{ ppm}$) and PPh_3 ($\delta_{\text{P}} = 30.5 \text{ ppm}$). The coalescence temperatures (Table 2.4) are in the order $\text{PPh}_3 > \text{PMePh}_2 > \text{PMe}_3 > \text{PMe}_2\text{Ph}$, suggesting that the exchange of free and bound phosphines is faster for the smaller more basic ligands, as expected for an associative process, with steric effects dominating. The position of PMe_3 is slightly anomalous, perhaps because its poor π -acceptor properties lead to a lower stability of the proposed 5-coordinate intermediate.³⁴

Finally, addition of excess COD to a solution containing $[\text{Pd}(\text{COD})\text{MeCl}]$ and 2 PMePh_2 leads to a sharpening of the ^{31}P NMR signal ($\delta_{\text{P}} = 26.0 \text{ ppm}$) at room temperature suggesting that exchange of free and bound P is accelerated by excess COD. In no case can signals from the *cis* isomer be observed.

Table 2.4 Coalescence temperatures (T) for exchange of free and bound phosphine in $[\text{PdMeCl}(\text{PR}_3)_2]$ as determined from variable temperature NMR studies of solutions containing $[\text{PdMeCl}(\text{COD})]$ and 2 PR_3 ^a

Ligand	PMe_3	PMe_2Ph	PMePh_2	PPh_3
T / K	300	250	340	>350

^a Traces of excess phosphine are present in all the solutions. The coalescence temperature is defined as the temperature at which the line width is highest

II. 2. 5 Conclusions

It has been shown that the copolymerisation of carbon monoxide and ethene is possible using a wide range of monodentate phosphines when the P:Pd ratio is low (4:1). This is an unexpected result, as most of the literature teaches that methyl propanoate should be selectively produced. Our results show that active, selective catalysts for polyketone formation can be generated from palladium complexes containing simple monodentate phosphines, although the rates are not very high compared with the best previously reported using e. g. $\text{Ph}_2\text{P}(\text{CH}_2)_3\text{PPh}_2$, which can be as high as $6,000 \text{ g PK (g Pd. h)}^{-1}$. Analysis of the results shows that monodentate phosphines must lie within a well defined area of steric and electronic properties to provide active catalysts for polyketone formation, with phosphines having low steric bulk and high electron density being most favoured. Analysis of the Flory-Schulz constants for the formation of co-oligomers, which are only significantly observed for alkyldiphenylphosphines, shows, as suggested previously,¹⁶ that steric bulk favours methyl propanoate formation. A P:Pd ratio of 4 allows polyketone formation when using smaller ligands, but higher phosphine ratios give methyl propanoate or inhibit the reaction. This would appear to indicate that monophosphine complexes, if they form, do not favour methyl propanoate formation.

After this investigation of non-dendritic monodentate ligands in the methoxycarbonylation of ethene, we will now turn our attention to POSS based dendritic diphenylphosphine ligands to observe the influence of the dendritic architecture on the outcome of the reaction.

II. 3 Polyhedral Oligomeric Silsesquioxane dendritic ligands in the methoxycarbonylation of ethene³⁵

Because it seemed possible that bidentate coordination might be forced on ligands, which act as monodentate ligands in their small molecule forms, by steric crowding at the periphery of a dendrimer, it appeared interesting to use dendrimers bearing diphenylphosphines at their periphery to probe the influence of the dendritic architecture on the chemoselectivity of the methoxycarbonylation of ethene. In addition, there may be significant advantages in terms of product separation in the instances where the product is methylpropanoate.

Very few examples of changes in chemoselectivity being brought about by dendritic effects are available in the literature, although a change from *di* to *mono* functionalisation of 1,4-

diiodobenzene was observed for Heck coupling with butyl acrylate catalyzed by a (poly(propyleneimine)) modified dendrimer-bound Pd- π -allyl complex.³⁶ The mono-Heck adduct was obtained in a 92/8 (*mono/di*) ratio upon using the G4 dendrimer whilst the parent model showed little selectivity 45/55 (*mono/di*).

II. 3. 1 Generation 0 Polyhedral Oligomeric Silsesquioxane decorated diphenylphosphines

Our initial studies centred on the macromolecule, **G0-8ethylPPh₂**, in which the eight PPh₂ groups are attached through an ethylidene spacer to the corners of a polyhedral oligomeric silsesquioxane (POSS) cube (Figure 2.4).

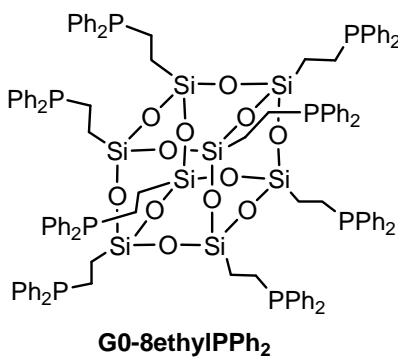


Figure 2.4 Structural formula of **G0-8ethylPPh₂**

In the presence of palladium, this ligand promoted the formation of methyl propanoate. There are three possible explanations for this chemoselectivity.

- 1) **G0-8ethylPPh₂** may simply act as a monodentate ligand to palladium, since monodentate ligands usually give methyl propanoate. However, the small molecule analogue, Ph₂PEt (**M2**), mainly promotes the formation of polyketone under similar reaction conditions, so this explanation in itself is inadequate.
- 2) Although Ph₂PEt (**M2**), mainly promotes the formation of polyketone, replacing the Et group with the bulkier Bu^t group²² changes the chemoselectivity so that small amounts of methyl propanoate and no polyketone are formed. The steric bulk of the POSS cube may, thus be responsible for the observed chemoselectivity, although the rate of formation of methyl propanoate is higher with the POSS based ligand than when using Ph₂PBu^t.

3) A third possible explanation, which may be related to the second one, above, is that the steric pressure applied by the peripheral POSS cube on the polymer chain may prevent its growth. Steric pressure has been invoked to explain the formation of lower molecular weight polymers in the copolymerisation of carbon monoxide with 4-tert-butylstyrene ³⁷ and in ethene polymerisation ³⁸ when using dendrimer based catalysts. A similar explanation has been used to rationalise the formation of methyl propanoate when using palladium complexes of bulky bidentate ligands for ethene carbonylation in methanol.¹⁶ It is proposed that the smaller pocket angle, the area where migratory insertion and reductive elimination reactions occur, encourages termination rather than chain growth.

In order to obtain more insight into the binding ability of **G0-8ethylPPh₂** and its related high activity in comparison with small models, we measured variable temperature ³¹P{¹H}NMR from -80 °C to +80 °C of **G0-8ethylPPh₂** together with [(COD)MeClPd] in toluene-d₈. Upon mixing the ligand and the metal together at a 1/5 (Pd/P) ratio, a precipitate instantaneously formed. This can be related to the formation of oligomeric dendritic species, bound to each other through a *trans* palladium metal complex. This observation clearly demonstrates monodentate binding of **G0-8ethylPPh₂** to Pd, which is consistent with the formation of methyl propanoate by this ligand. One single peak at -9.8 ppm, distinctive of the non palladium-bound **G0-8ethylPPh₂**, clearly dominates all spectra (Figure 2.5).

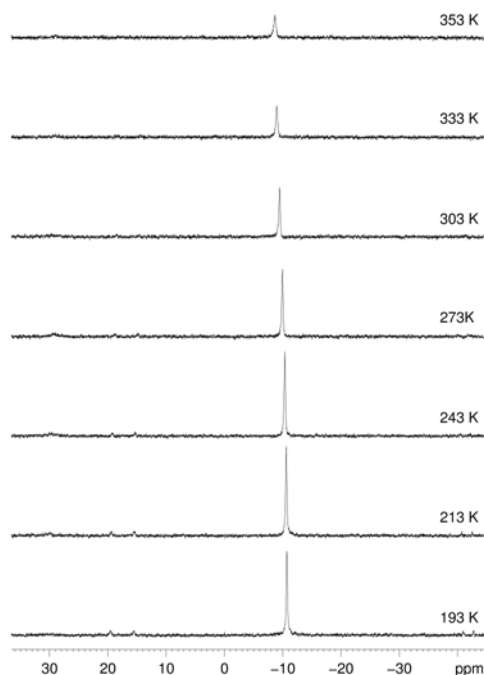


Figure 2.5 Variable temperatures ³¹P{¹H} NMR spectra of a d₈-toluene solution of [(COD)MePdCl] with **G0-8ethylPPh₂**

A small bump can be observed at +28.7 ppm which can be attributed to the small quantity of **G0-8ethylPPh₂** bound palladium complex soluble in toluene-d₈. Overall, mainly free phosphine is present in solution as the precipitate contains bound phosphine.

In order to try to distinguish between the 3 various aforementioned explanations concerning the chemoselectivity observed with **G0-8ethylPPh₂**, we have carried out ethene methoxycarbonylation using generation 1 POSS based molecules (Figure 2.6).

II. 3. 2 Generation 1 Polyhedral Oligomeric Silsesquioxane decorated diphenylphosphines

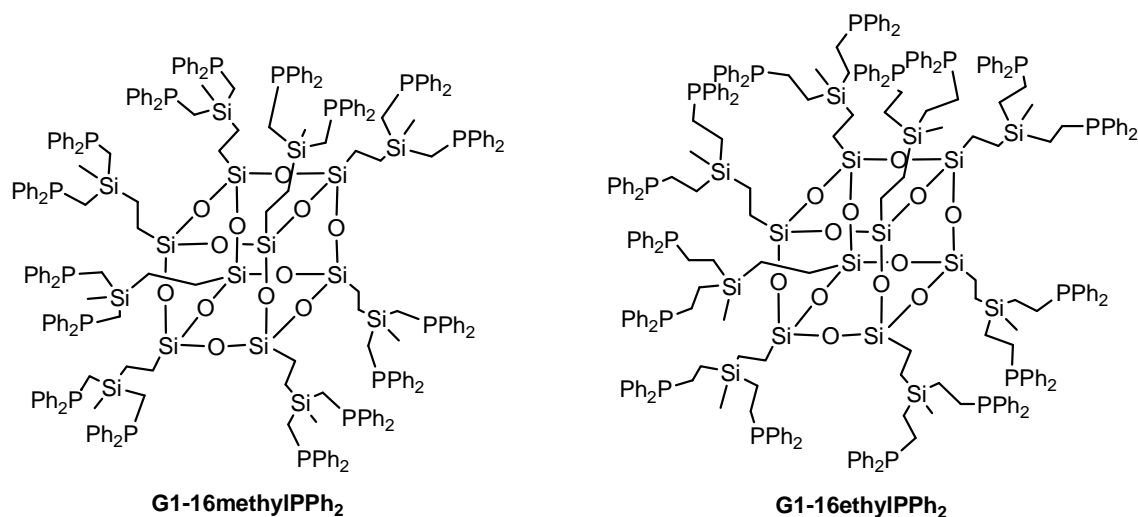


Figure 2.6 Structural formulas of **G1-16methylPPh₂** and **G1-16ethylPPh₂**

One, **G1-16ethylPPh₂**, has previously been shown to produce dendritic effects as a result of bidentate binding,² whilst the other, **G1-16methylPPh₂**, did not show the same effect.¹ We have also employed some more realistic small molecule models (Figure 2.7). MePPh₂ (**M1**) might be considered a good model for **G1-16methylPPh₂**, whilst EtPPh₂ (**M2**) might normally be seen a good model for **G0-8ethylPPh₂** and **G1-16ethylPPh₂**. However, we have shown that the chemoselectivity in ethene methoxycarbonylation when using monodentate ligands can vary depending upon small changes in cone angle and electronic parameters,²² so Ph₂P(CH₂)₂Si(OMe)₃ (**M3**) may be a better model for **G0-8ethylPPh₂**, Me₂Si(CH₂CH₂PPh₂)₂ (**M4**) for **G1-16ethylPPh₂** and Me₂Si(CH₂PPh₂)₂ (**M5**) for **G1-16methylPPh₂**.

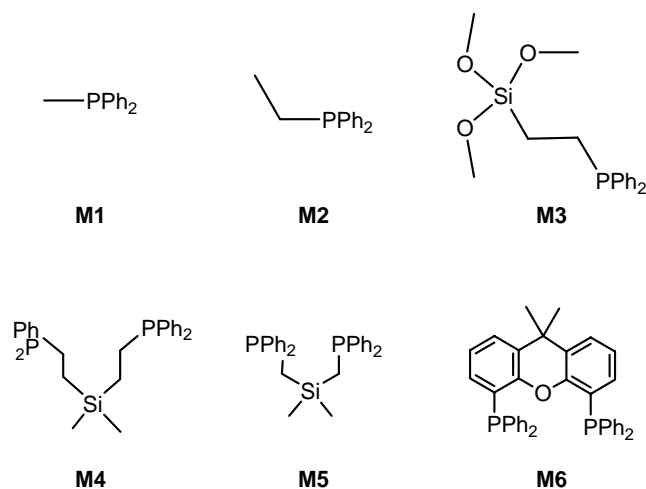


Figure 2.7 Structural formulas of molecular ligands **M1**, **M2**, **M3**, **M4**, **M5** and **M6**

Ethene carbonylation ($\text{CO}:\text{ethene}$, 1:1, 60 bar) reactions using all the macromolecular ligands and the small molecule analogues were carried out in a methanol/toluene mixture in the presence of catalysts prepared in situ from $[\text{Pd}(\text{OAc})_2]$, the ligand ($\text{Pd}:\text{P} = 1:4$ or $1:30$) and methanesulphonic acid (MSA) at 85°C . The results are summarised in Table 2.5.

A comparison between the results obtained using **G1-16methylPPh₂** with those from its closest analogues, **M1** and **M5** ($\text{P}:\text{Pd} = 4:1$) shows that they all produce polyketone as the major product. Although this is somewhat unexpected for **M1**, we have shown above that this arises because of the relatively small size and electron donating capability of this phosphine.²² **M5** is a bidentate phosphine with the three atom bridge between the P atoms leading to a small bite angle, so is expected, like $\text{Ph}_2(\text{CH}_2)_3\text{PPh}_2$ to be active for polyketone formation.¹¹ **G1-16methylPPh₂** gives a very similar rate of formation of polyketone to that for **M5**, suggesting that the macromolecular architecture does not interfere with bidentate binding of the ligand, nor significantly alter the bite angle. Similar behaviour between the dendritic complex and the monomer complex has been reported by Van Leeuwen and co workers where similar activity and selectivity were observed between phosphine functionalized urea adamantyl poly(propylene imine) dendrimers and bare phosphines in palladium-catalyzed allylic amination.³⁹

Table 2.5 Results of ethene carbonylation in methanol catalysed by Pd complexes of various ligands in the presence of MSA^a

Run	Ligand	P:Pd	Methyl Propanoate ^b / mol (mol Pd h) ⁻¹	Polyketone / g (g Pd h) ⁻¹
1	G0-8ethylPPh₂	4	47.3	<1
2	G1-16ethylPPh₂	4	3.0	<1
3	G1-16methylPPh₂	4	<1	369
4	M1	4	<1	72
5	M2	4	1.0	1.3
6	M3	4	2.8	<1
8	M4	4	36.7	<1
9	M5	4	<1	304
10	M6	4	66.5	<1
11	G0-8ethylPPh₂	30	4.3	<1
12	G1-16ethylPPh₂	30	1.6	<1
13	M1	30	2.0	<1
14	M2	30	10.4	<1
15	M3	30	29.6	<1
16	M4	30	109.2	<1

^a Conditions: [Pd(OAc)₂] (2.4 x 10⁻⁵ mol), MeSO₃H (4.8 x 10⁻⁴ mol), ligand, MeSO₃H/Pd = 20/1, methanol (8 cm³), toluene (4 cm³), 85 °C, 2.5 h., CO 30 bar, C₂H₄ 30 bar. ^bGC yields determined with external standard and expressed as average turnover number over 2.5 h

Comparing **G0-8ethylPPh₂** with **M2** and **M3** shows that the macromolecule promotes rates of formation of methyl propanoate an order of magnitude higher than either of the two small molecule analogues which appears to represent a positive dendritic effect. Forcing bidentate coordination might be expected to encourage polyketone formation as for Ph₂P(CH₂)_nPPh₂ it has been shown that these ligands tend to give polyketone with both the chain length and the reaction rate increasing from n = 1 – 3 and decreasing again for n = 3 – 6.¹¹ On the other hand, wider bite angle ligands have been shown to give methyl propanoate, especially if the P atoms can be mutually *cis*.¹⁵

The alternative explanation for the formation of methyl propanoate when using larger ligands is that the pocket angle is smaller and that increases the rate of termination.¹⁵ We have shown above that the selectivity of methoxycarbonylation reactions of ethene when using palladium complexes of monodentate phosphines at low P:Pd (1:4) can also be explained largely on steric grounds, with larger ligands giving higher rates of formation of methyl propanoate and less polyketone.²²

Analysis of the cooligomers is also instructive with the Flory-Schulz constant, α (rate of propagation)/(rate of propagation + rate of termination), being lower for larger ligands.¹⁶ For the model compound, **M3**, all of the soluble cooligomers $\text{H}(\text{C}_2\text{H}_4\text{C}(\text{O}))_n\text{CO}_2\text{Me}$ ($n = 1-6$) are observed. Quantitative analysis shows that the value of α is 0.43, between those of PPh_2Pr (0.47) and PPh_2Pr^i (0.46) and of PPh_2Bu^t (0.41),²² as would be expected for the extra bulk on the alkyl substituent.

The lack of observable polyketone when using **M3** makes it more like PPh_2Bu^t . In the case of **G0-8ethylPPh₂** very little co-oligomer production is observed and the rate of methyl propanoate formation is higher. Thus, the positive dendritic effect can be attributed to the increased bulk afforded by the POSS substituent leading to a smaller pocket angle and higher rate of methanolysis.

G1-16ethylPPh₂ provides another somewhat surprising result. Methyl propanoate is formed at a rate an order of magnitude lower than that of its closest analogue, **M4** indicating a negative dendritic effect. **G1-16ethylPPh₂** is the molecule that shows very high linear selectivity in rhodium catalysed alkene hydroformylation,² much higher linear:branched ratio (l:b) (13.9) than is observed for **M4** (l:b = 3.8). This high selectivity has been attributed to the ability of this ligand to bind two equatorial sites in a key trigonal bipyramidal intermediate and hence to have at least some of the phosphines constrained to have a bite angle close to 120 °C.³

In a seminal paper, it has been shown that wide bite angle ligands including xantphos (**M6**), which also binds to two equatorial sites in 5 coordinate rhodium complexes, binds with the two P atoms mutually *trans* in the model Pd acyl complex, $[\text{Pd}(\text{M6})(\text{C}(\text{O})\text{Me})][\text{CF}_3\text{SO}_3]$ and with the fourth coordination site occupied by the O of the central ring in **M6**.¹⁵ The rate of methanolysis of the Pd-C bond, which is assumed to model the rate determining step in the

methoxycarbonylation of ethene, is low compared with that in more active complexes. This suggests that wide bite angle ligands of this type might give low rates of formation of methyl propanoate. Of course, being bidentate, they might also give polyketone. Methoxycarbonylation of ethene using xantphos as a ligand to palladium does not appear to have been reported, although it has been reported that the related ligand $O(2-C_6H_4PPh_2)_2$ (DPEphos) gives high rates of co-oligomerisation ($2,500 \text{ mol (mol Pd h)}^{-1}$, $\alpha = 0.1$).¹⁵ DPEphos also binds to palladium in the acyl cation with P,O,P binding and mutually *trans* phosphines. This structure is maintained in the presence of CO or acetonitrile, but $[Pd(DPEphos)(C(O)Me)PPh_3][CF_3SO_3]$ with the DPEphos occupying *cis* sites is formed on reaction with PPh_3 showing that DPEphos can have the P atoms coordinated mutually *cis* or *trans*. *Cis* coordination is also observed in $[Pd_2(\mu-H)(\mu-CO)(DPEphos)_2][CF_3SO_3]$, which is formed on reaction of the acyl complex with CO and methanol. The *trans* form is expected to be inactive in co-oligomerisation, so the *cis* form must have very high activity. In contrast with $[Pd(\mathbf{M6})(C(O)Me)]^+$, which gives a slow reaction ($t_{1/2} = 3 \text{ h}$ at 12°C) with methanol, the rate of methanolysis of $[Pd(DPEphos)(C(O)Me)]^+$ was too fast to measure by ^1H NMR spectroscopy at room temperature. All of this suggests that **M6** should give a low rate of formation of methyl propanoate compared with that using DPEphos. We, therefore, tested **M6** as a ligand under our reaction conditions for the methoxycarbonylation of ethene. Indeed the rate ($66.5 \text{ mol (mol Pd h)}^{-1}$) is much lower than that reported for DPEphos, but high compared with that observed with **G1-16ethylPPh₂**. No co-oligomers were observed in this case.

Since for bidentate ligands, larger bite angles (smaller pocket angles) increase the rate of termination and hence methyl propanoate formation, we conclude that the bite angle for **G1-16ethylPPh₂** must be less than that of **M4** or of **M6**, hence accounting for the lower rate of methyl propanoate formation. It must, however, not be so low that chain growth to give polyketones competes with termination. This conclusion is consistent with our earlier observations based on rhodium catalysed hydroformylation reactions and modelling studies that **G1-16ethylPPh₂** affords diequatorial binding (bite angle $\sim 120^\circ$) to rhodium and that interactions at the periphery of the macromolecule constrain some phosphorus atoms to be closer to one another than those in the small molecule analogue, **M4**.^{3, 40}

It appears that very subtle changes in the bite angle of the ligand can have dramatic effects upon the rates of methoxycarbonylation reactions, with ligands favouring mutually *trans* coordination of the P atoms being essentially inactive.¹⁵ Where *trans* coordination is

favoured, the rate of isomerisation to the *cis* isomer as well as the equilibrium position will determine the overall rate of methoxycarbonylation of ethene in otherwise similar ligands. In order to try to determine the stereochemistry of a related palladium complex attached to **G1-16ethylPPh₂**, we have studied the ³¹P NMR spectrum of the complex formed between [PdClMe(COD)] (COD = 1,5-cylooctadiene) and **G1-16ethylPPh₂** at a 1/5 (Pd/P) ratio in toluene-d₈ (Figure 2.8) at different temperatures.

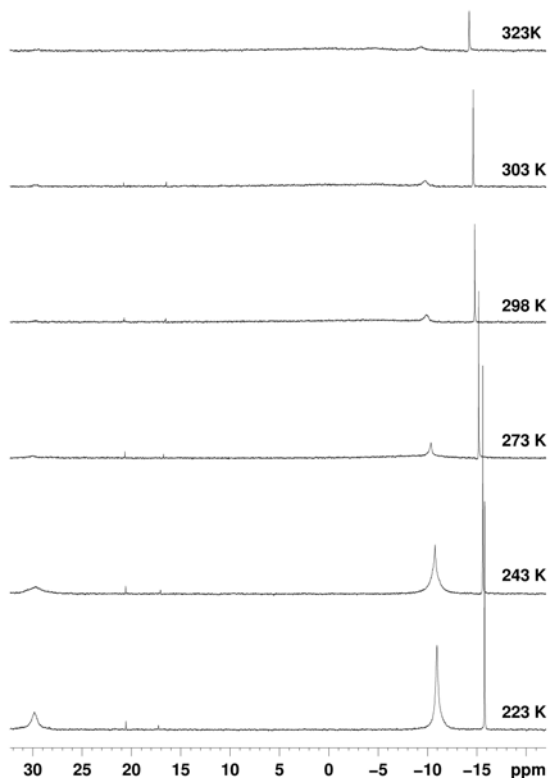


Figure 2.8 Variable temperatures ³¹P{¹H} NMR spectra of a d₈-toluene solution of [(COD)MePdCl] with **G1-16ethylPPh₂**

At 193 K three signals are observed. Two of these ($\delta = -15.8$ ppm (sharp) and -11.2 ppm (broad)) arise from the macromolecule bound phosphine, with the sharp resonance having been attributed to phosphorus atoms that are backfolded (buried in the macromolecule).¹ This phenomenon might mirror the poor activity of this ligand in the production of methyl propanoate in comparison with **G0-8ethylPPh₂**: fewer phosphines are accessible at the edge of the dendrimer to form the active catalytic complex, which results in an important decrease in activity. The third resonance is a broad singlet at $\delta = 29.8$ ppm in the region expected for Pd bound phosphines. On warming, this signal broadens and disappears, but the signals from

the free phosphine are not affected. Unfortunately, the data are not good enough to propose a stereochemistry for the complex formed.

II. 3. 3 Conclusions

The methoxycarbonylation of ethene using palladium complexes of macromolecules in which 8 or more equivalent phosphines are placed on the surface gives either methyl propanoate or polyketone. In the case where the groups on the surface are $-\text{Si}(\text{Me})(\text{CH}_2\text{PPh}_2)_2$, the macromolecule and the small molecule analogue, $\text{Me}_2\text{Si}(\text{CH}_2\text{PPh}_2)_2$ behave very similarly to produce comparable amounts of polyketone. This is as expected for a ligand of this type that can bind, like $\text{Ph}_2\text{P}(\text{CH}_2)_3\text{PPh}_2$, in a bidentate fashion with a relatively small bite angle and low steric hindrance. For ligands containing P atoms that are separated by longer spacers, the product is methyl propanoate with very little chain growth. This is expected for monodentate binding or for ligands which have wide bite angles. In one case, that using **G0-8ethylPPh₂**, the rate using the macromolecule is significantly enhanced in comparison to that obtained with the small molecule as a result of the extra steric bulk associated with the presence of the POSS core and its other arms. For **G1-16ethylPPh₂**, the rate is reduced compared with its small molecule analogue. This is probably because interactions on the periphery reduce the effective bite angle of the bidentate ligand, hence increasing the pocket angle and reducing the rate of termination. The rate of termination is not reduced enough, however for chain growth and polyketone formation to become competitive. These effects are only observed at low P-Pd ratios (4:1). At a higher ratio (30:1), all the ligands promote methyl propanoate formation, with the macromolecules generally being less efficient than their small molecule analogues (Table 2.5, Runs 11-16). Perhaps monodentate binding is preferred in all these cases and the ligand bulk determines the reaction rates.

II. 4 References

1. L. Ropartz, K. J. Haxton, D. F. Foster, R. E. Morris, A. M. Z. Slawin and D. J. Cole-Hamilton, *J. Chem. Soc., Dalton Trans.*, 2002, 4323.
2. L. Ropartz, R. E. Morris, D. F. Foster and D. J. Cole-Hamilton, *Chem. Commun.*, 2001, 361.
3. K. J. Haxton, D. J. Cole-Hamilton and R. E. Morris, *Dalton Trans.*, 2004, 1665.
4. C. Claver and P. W. N. M. van Leeuwen, *Rhodium Catalyzed Hydroformylation*, Kluwer Academic Publishers edn., Dordrecht, 2000.
5. L. Ropartz, PhD in St-Andrews, 2001.
6. E. Drent and P. H. M. Budzelaar, *Chem. Rev.*, 1996, **96**, 663.
7. R. A. M. Robertson and D. J. Cole-Hamilton, *Coord. Chem. Rev.*, 2002, **225**, 67.
8. R. A. M. Robertson and D. J. Cole-Hamilton, in *Catalytic Synthesis of Alkene-Carbon Monoxide Copolymers and Cooligomers*, ed. A. Sen, Dordrecht, The Netherlands, Kluwer Academic Publishers edn., 2003.
9. A. Sen, *Adv. Polym. Sci.*, 1986, **73**, 125.
10. A. Sen, *Acc. Chem. Res.*, 1993, **26**, 303.
11. E. Drent, J. A. M. van Broekhoven and M. J. Doyle, *J. Organomet. Chem.*, 1991, **417**, 235.
12. E. Drent and E. Kragtwijk, *EP Pat.*, 495 548, 1992.
13. G. R. Eastham, R. P. Tooze, X. L. Wang and K. Whiston, *Int. Pat.*, 9 619 434, 1996.
14. W. Clegg, G. R. Eastham, M. R. J. Elsegood, R. P. Tooze, X. L. Wang and K. Whiston, *Chem. Commun.*, 1999, 1877.
15. P. W. N. M. van Leeuwen, M. A. Zuideveld, B. H. G. Swennenhuis, Z. Freixa, P. C. J. Kamer, K. Goubitz, J. Fraanje, M. Lutz and A. S. Spek, *J. Am. Chem. Soc.*, 2003, **125**, 5523.
16. E. Zuidema, C. Bo and P. W. N. M. van Leeuwen, *J. Am. Chem. Soc.*, 2007, **129**, 3989.
17. S. M. A. Donald, S. A. Macgregor, V. Settels, D. J. Cole-Hamilton and G. R. Eastham, *Chem. Commun.*, 2007, 562.
18. A. Sen and T. W. Lai, *J. Am. Chem. Soc.*, 1982, **104**, 3520.
19. E. Drent, *US Pat.*, 4 835 250, 1989.
20. W. Keim, H. Mass and S. Z. Mecking, *Naturforsch (B)*, 1995, 50.
21. K. Nozaki, *US Pat.*, 3 694 412, 1972.

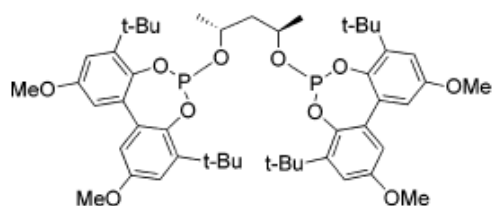
22. G. Smith, N. R. Vautravers and D. J. Cole-Hamilton, *Dalton Trans.*, 2008, Accepted.
23. A. Sen, J. T. Chen, W. M. Vetter and R. R. Whittle, *J. Am. Chem. Soc.*, 1987, **109**, 148.
24. E. Drent, *Chem. Abstr.*, 1985, **102**, 46423.
25. *Catalytic Synthesis of Alkene-Carbon Monoxide Copolymers and Cooligomers*, Sen, A. edn., Dordrecht, The Netherlands, 2003.
26. G. R. Eastham, R. P. Tooze, M. Kilner, D. F. Foster and D. J. Cole-Hamilton, *J. Chem. Soc., Dalton Trans.*, 2002, 1613.
27. A. J. Rucklidge, G. E. Morris, A. M. Z. Slawin and D. J. Cole-Hamilton, *Helv. Chim. Acta*, 2006, **89**, 1783.
28. C. A. Tolman, *Chem. Rev.*, 1977, **77**, 313.
29. T. W. Lai and A. Sen, *Organometallics*, 1984, **3**, 866.
30. G. Henrici-Olivé and S. Olivé, *Angew. Chem. Int. Ed. Engl.*, 1976, **15**, 138.
31. Y. Kayaki, I. Shimizu and A. Yamamoto, *Bull. Chem. Soc. Jpn.*, 1997, **70**, 917.
32. B. Bacchi, M. Carcelli, C. Pelizzi, G. Pelizzi, P. Pelagetti and S. Ugoletti, *Eur. J. Inorg. Chem.*, 2002, 2179.
33. L. K. Knight, Z. Freixa, P. W. N. M. van Leeuwen and J. N. H. Reek, *Organometallics*, 2006, **25**, 954.
34. T. G. Appleton, H. C. Clark and L. E. Manzer, *Coord. Chem. Rev.*, 1975, **10**, 335.
35. N. R. Vautravers and D. J. Cole-Hamilton, *Dalton Trans.*, 2008, Submitted.
36. M. Ooe, M. Murata, T. Mizugaki, K. Ebitani and K. Kaneda, *J. Am. Chem. Soc.*, 2004, **126**, 1604.
37. J. M. Benito, E. De Jesus, F. J. De la Mata, J. C. Flores and R. Gomez, *Organometallics*, 2006, **25**, 3045.
38. J. M. Benito, E. De Jesus, F. J. De la Mata, J. C. Flores and R. Gomez, *Chem. Commun.*, 2005, 5217.
39. D. de Groot, B. F. M. de Waal, J. N. H. Reek, A. P. H. J. Schenning, P. C. J. Kamer, E. W. Meijer and P. W. N. M. van Leeuwen, *J. Am. Chem. Soc.*, 2001, **123**, 8453.
40. K. J. Haxton, D. J. Cole-Hamilton and R. E. Morris, *Dalton Trans.*, 2007, 3415.

**III. Diazaphospholidine terminated
Polyhedral Oligomeric Silsesquioxanes
cored dendrimers in asymmetric
hydroformylation**

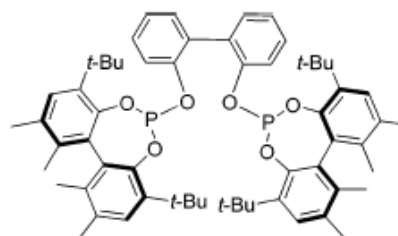
III. Diazaphospholidine terminated Polyhedral Oligomeric Silsesquioxanes cored dendrimers in asymmetric hydroformylation

III. 1 Introduction

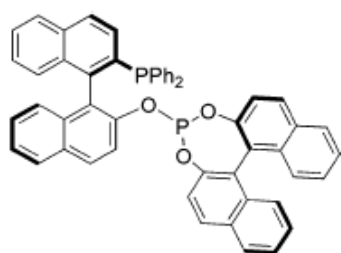
Asymmetric hydroformylation has attracted significant attention in the last decades as a powerful tool to the production of enantiomerically pure aldehydes from readily available cheap feedstocks.¹ Considerable effort has been made to identify effective chiral ligands for this reaction but only a few of them, including the bisphosphites Chiraphite² and Kelliphite,³ the phosphine-phosphite Binaphos⁴ and some bis-phosphacycles such as bis-phospholanes⁵ or bis-diazaphospholanes⁶ have been effective (Figure 3.1).



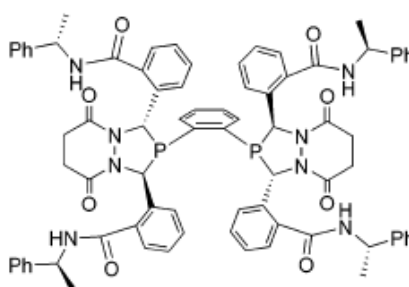
(2R, 4R)-Chiraphite



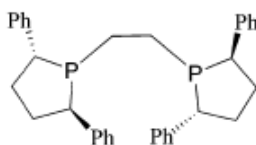
(S,S)-Kelliphite



(R,S)-Binaphos



bis-diazaphospholane



bis-phospholane

Figure 3.1 Efficient ligands for asymmetric hydroformylation⁷

Among the numerous papers about dendrimers in catalysis,⁸ few of them really focused on asymmetric catalysis. Relevant examples include the application of the Ti-TADDOL system in the addition of diethylzinc to benzaldehyde,^{9, 10} chiral Salen complexes in the hydrolytic resolution of terminal epoxides,¹¹ bis(diphenylphosphino)pyrrolidine functionalized poly(propyleneimine) PPI dendrimers in allylic amination,¹² dendritic BINAP,^{13, 14} biphenyl phosphines¹⁵ and phosphoramidate dendritic ligands^{16, 17} as well as various types of chiral ferrocenyldiphosphine¹⁸ and iminophosphine ligands¹⁹ in asymmetric hydrogenation (Figure 3.2). Moreover, other miscellaneous enantioselective reactions such as hydrosilylation,^{20, 21} allylation,¹⁸ hydroboration¹⁸ or hydrovinylation^{22, 23} have been studied but in general similar activity and enantioselectivity were obtained for the monomeric and dendritic catalysts.

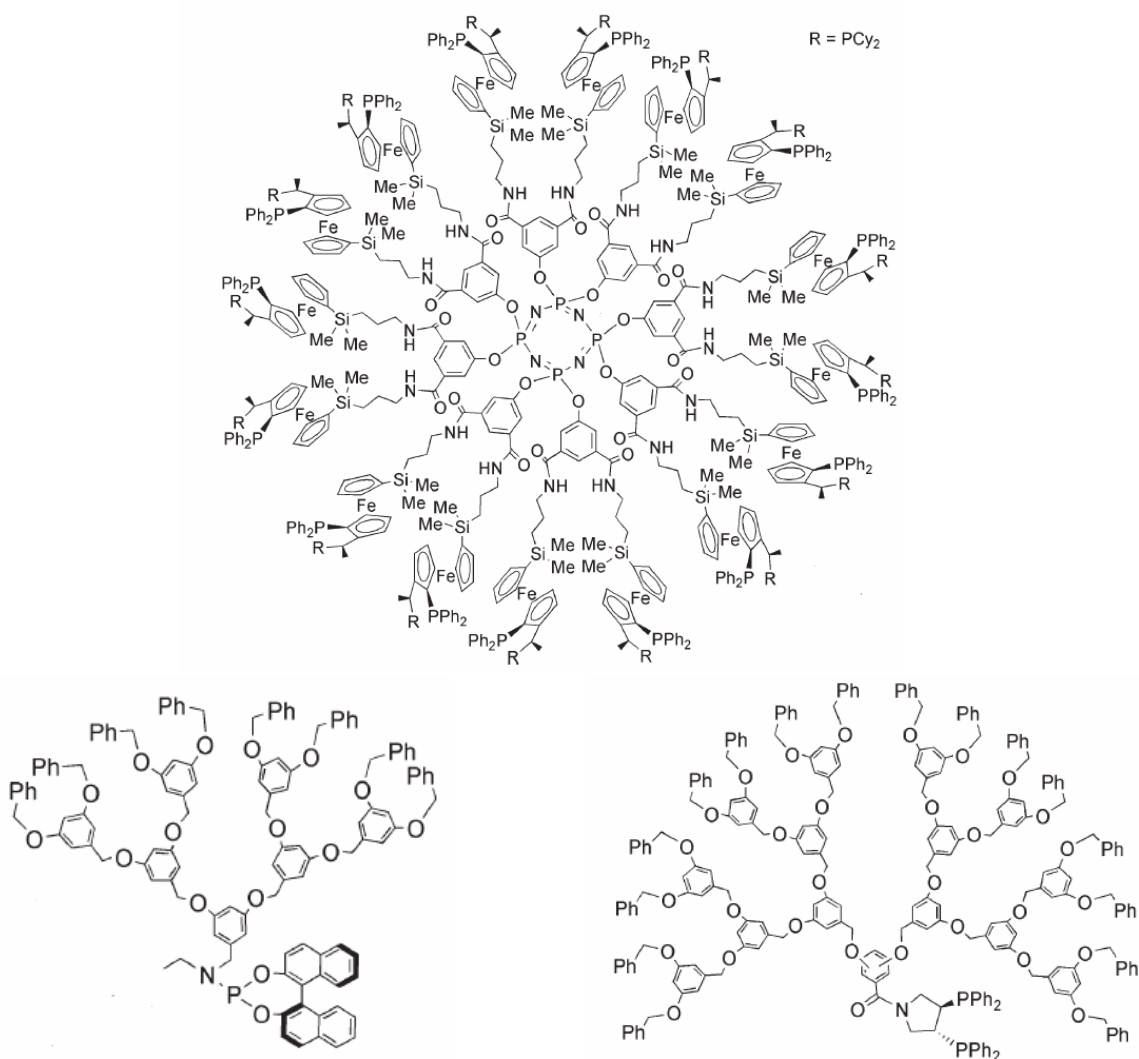


Figure 3.2 Top: Dendritic ferrocenyldiphosphine ligands; Bottom left: Dendritic phosphoramidate ligand; Bottom right: Dendritic bis(diphenylphosphino)pyrrolidine (reproduced from ²⁴)

These interesting features are well summarized by Majoral and co-workers in a review on dendrimeric phosphines in asymmetric catalysis.²⁴ Surprisingly, no example of asymmetric hydroformylation using dendritic ligands has been reported so far, although Alper and co-workers reported the use of diphenylphosphine terminated PAMAM silica supported dendrimers in the achiral version of this reaction.²⁵ In addition, the group of Rodriguez *et al.* has developed chiral dendrimers with the chirality directly situated on the phosphorus atom.²²

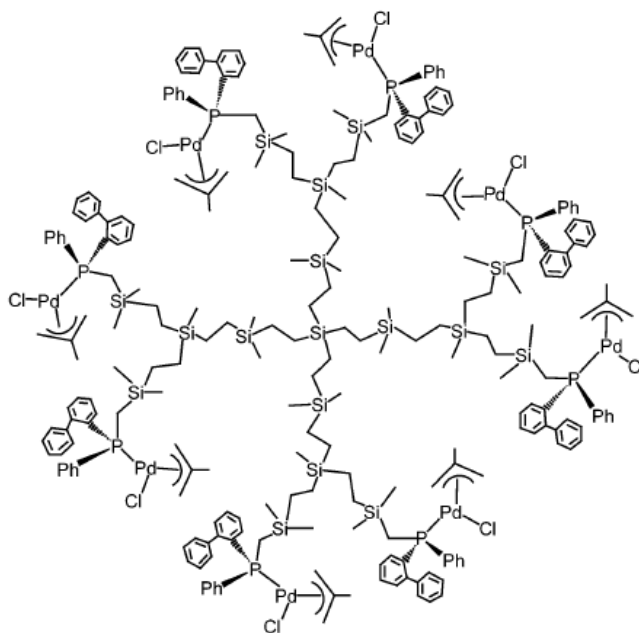
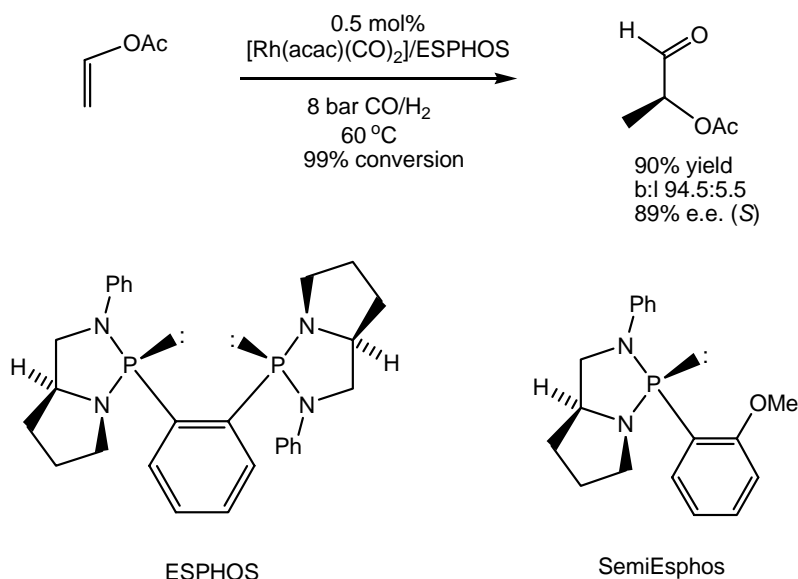


Figure 3.3 Grafting of chiral phosphines to carbosilane dendrimers²²

The intrinsic ability of dendrimers to outperform their parent models,²⁶ which is more commonly called “positive dendritic effect”, has been previously discussed (Chapter 1) and observed in oct-1-ene hydroformylation with Polyhedral Oligomeric Silsesquioxane (POSS) terminated by 16 terminal diphenylphosphines.²⁷ Bearing in mind that these peripheral constraints can change the selectivity of catalytic reactions so that the selectivities normally associated with bidentate ligands can be obtained with monodentate analogues, we postulated that an inactive monodentate ligand might be turned into an active bidentate upon attachment to the periphery of POSS cored dendrimers.

The bis(diazaphospholidine) ligand, ESPHOS, is a bidentate C_2 symmetric ligand, capable of acting as a ligand to rhodium for the asymmetric hydroformylation of vinyl acetate with regio- and stereo-selectivities that are amongst the highest yet reported (Scheme 3.1).²⁸ The monodentate analogue, SemiEsphos, is a very poor ligand for this

reaction giving very low conversions (Scheme 3.1).²⁸



Scheme 3.1 Asymmetric hydroformylation of vinyl acetate catalysed by rhodium complexes of ESPHOS. SemiEsphos gives very poor results (yield < 15 %, b:l 70:30, e.e < 2 %) even under forcing conditions (120 °C, 100 bar)²⁸

We thus investigated the attachment of the inactive monodentate SemiEsphos ligand onto the periphery of a POSS cored dendrimer,²⁹ anticipating that two or more of the SemiEsphos moieties might be held in such a way that they effectively promote bidentate binding and give good selectivity, possibly even better than ESPHOS itself (Figure 3.4).

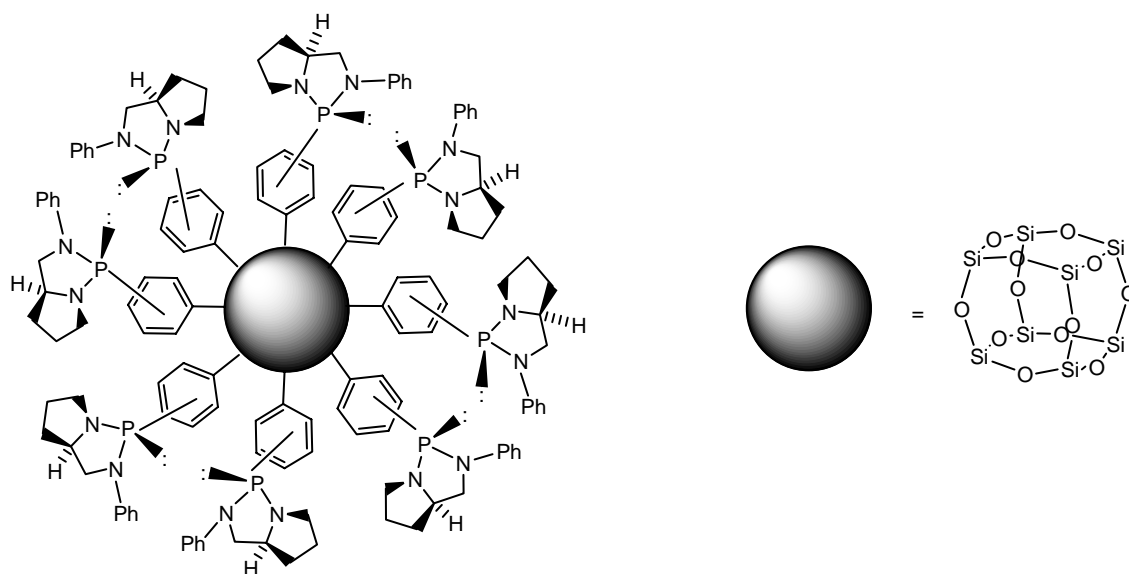
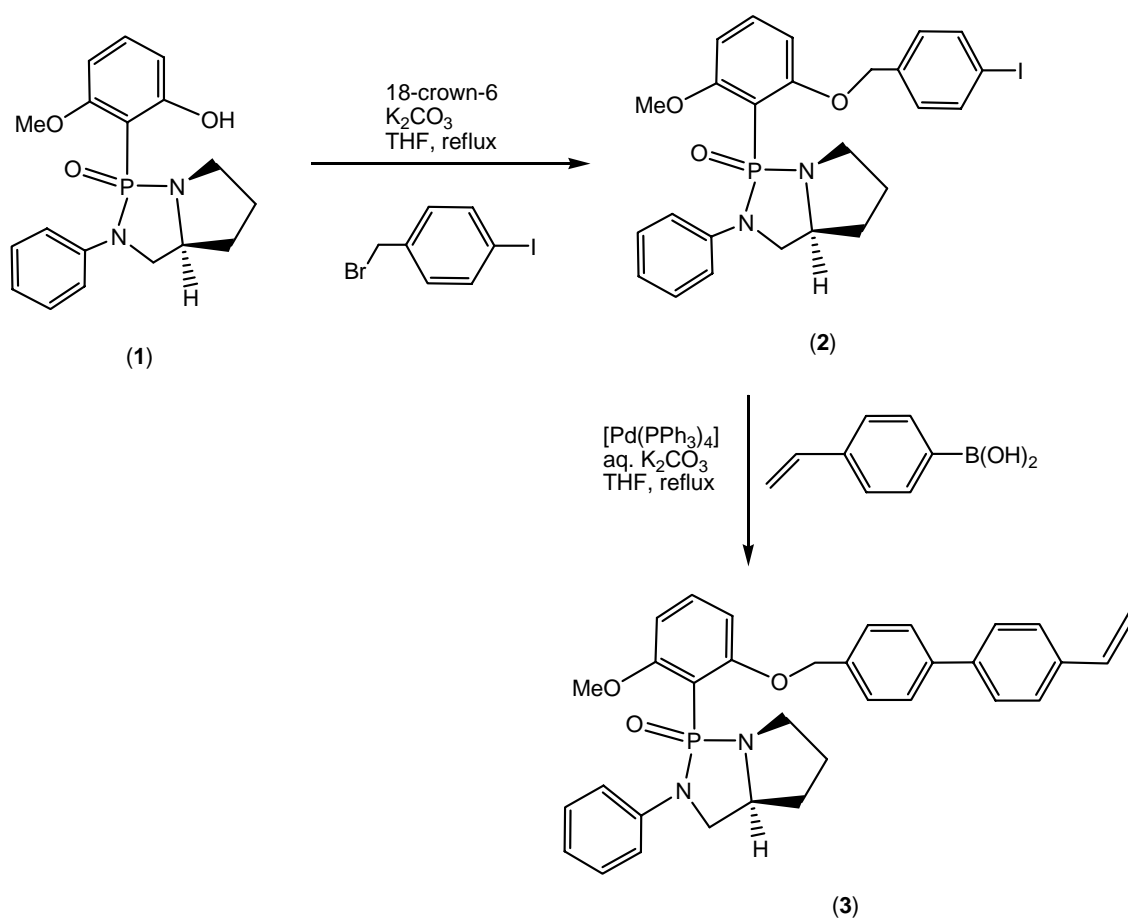


Figure 3.4 Mimicry of bidentate ESPHOS through monodentate SemiEsphos at the periphery of a POSS cube

III. 2 Synthetic approaches to the binding of SemiEsphos onto Polyhedral Oligomeric Silsesquioxane cored dendrimers

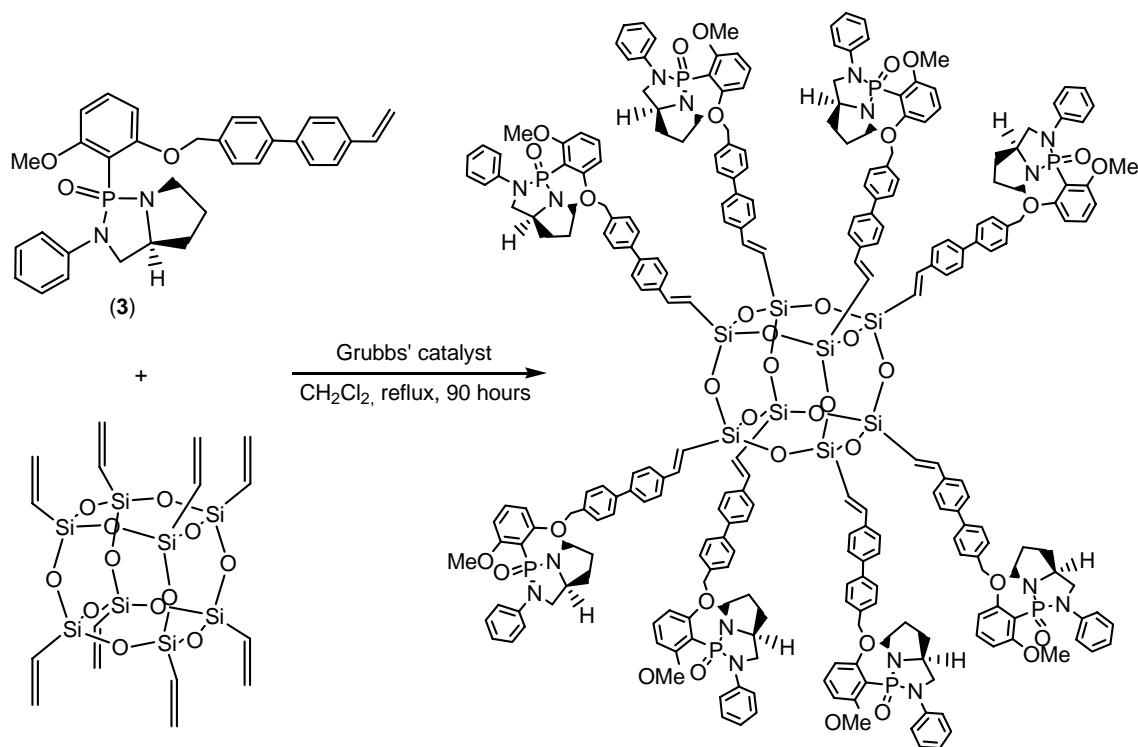
III. 2. 1 The SemiEsphos oxide route

One synthetic appealing pathway to attach SemiEsphos onto the POSS cube, recently developed in our group,³⁰ was the functionalization of the phosphine oxide ligand (**1**), synthesized according to literature procedures,³¹ with a terminal vinyl biphenyl tail (Scheme 3.2). O-alkylation of (**1**) with 4-iodobenzyl bromide in the presence of K₂CO₃ and 18-crown-6 as phase transfer agent afforded iodinated SemiEsphos oxide (**2**) in 80 % yield. Suzuki coupling reaction between (**2**) and commercially available styrylboronic acid produced the desired vinylbiphenyl modified SemiEsphos oxide (**3**) in good yield (90 %).



Scheme 3.2 Derivatization of SemiEsphos oxide ligand (**1**) with a vinyl biphenyl tail ³⁰

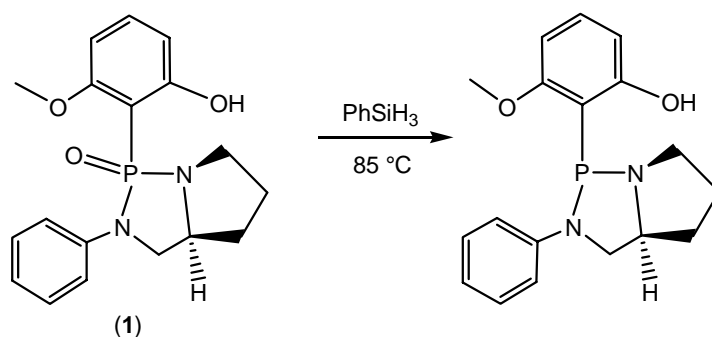
The POSS cored dendrimer decorated with eight SemiEsphos oxide moieties has been obtained through Grubbs cross-metathesis between octavinylsilsesquioxane and (3), after precipitation in hexane (Scheme 3.3).



Scheme 3.3 Grubbs metathesis between **G0-8vinyl** and modified SemiEsphos oxide ligand ³⁰

Several attempts at reducing this dendrimer with phenylsilane or trichlorosilane failed and the systematic presence at the end of the reaction of (1) (detected by ³¹P{¹H} NMR spectroscopy) revealed a cleavage of the dendrimer at the benzylic position. Similar observations have been made by Feher *et al.* as they never managed to reduce properly peripheral benzylic diphenylphosphine oxides on the POSS cube.³²

Indeed, the reduction of the non-dendritic phosphine oxide (1) with phenylsilane (Scheme 3.4) did provide the expected free phosphine as attested by the main peak observed by ³¹P{¹H} NMR spectroscopy at $\delta_P = 100.6$ ppm but its purification *via* silica gel column chromatography turned out to be very difficult.



Scheme 3.4 Reduction of phosphine oxide (**1**) with phenylsilane

The X-Ray crystal structure of (**1**) (Annexe I) clearly shows the preferential orientation of the hydroxyl group towards the oxygen of the phosphine oxide, *via* hydrogen bonding, to adopt the thermodynamically favored 6-membered ring conformation (Figure 3.5) ($d(\text{H}10)\dots\text{O}(1) = 1.609 \text{ \AA}$). This may explain the difficulties encountered during the purification of the free phosphine as the inherently stable chelate present in (**1**) through to the phosphine oxide disappears after reduction.

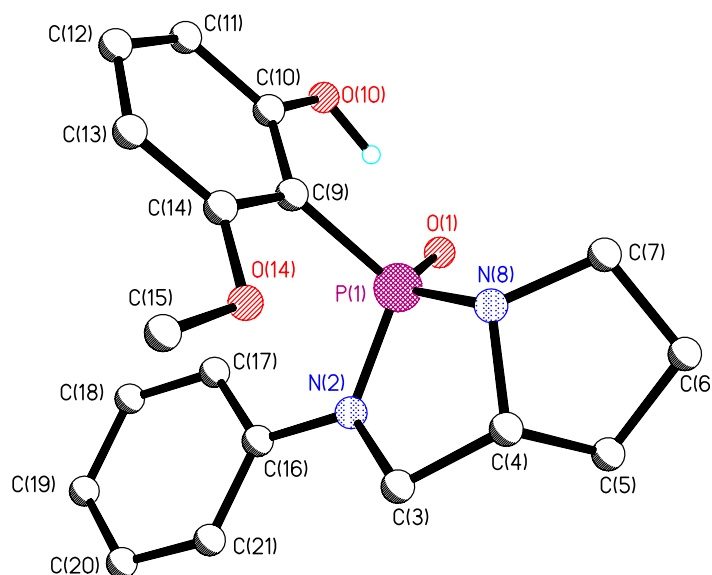
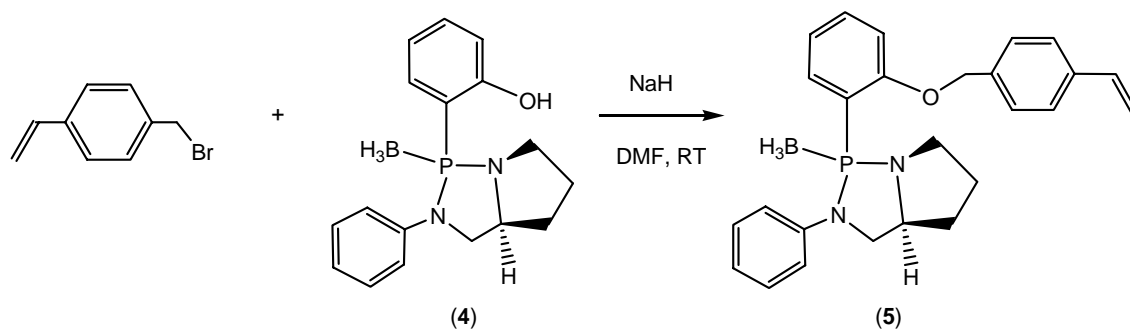


Figure 3.5 X Ray crystal structure of (**1**) (Annexe I)

This failure to reduce non-dendritic and dendritic SemiEsphos phosphine oxides prompted us to investigate the SemiEsphos phosphine with borane protection, using a similar methodology as above, as the tolerance of Grubbs' catalyst towards borane is well established.³³

III. 2. 2 The SemiEsphos borane protected route

O-alkylation of the borane protected SemiEsphos (**4**), synthesized according to literature methods,³⁴ with the readily available 4-vinylbenzylbromide³⁵ in DMF at room temperature with NaH afforded compound (**5**) in low yield (34 %) (Scheme 3.5).



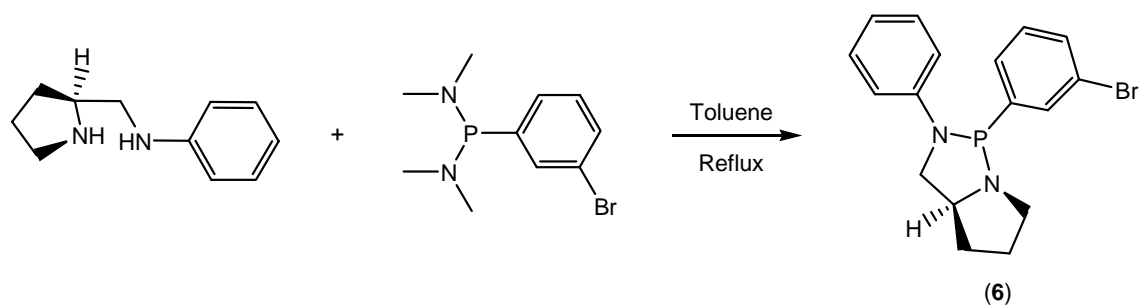
Scheme 3.5 O-alkylation of the SemiEsphos protected borane (**4**) with 4-vinylbenzylbromide

The unexpected failure of the Grubbs cross-metathesis between octavinylsilsesquioxane and the borane protected phosphine (**5**) with both 1st and 2nd generation Grubbs' catalyst remained unclear. The formation of a gel-like solution upon mixing the two starting materials in CH₂Cl₂, their presence at the end of the reaction (96 hours) confirmed by ¹H NMR spectroscopy together with the absence of the two doublets at 6.49 and 7.51 ppm in ¹H NMR spectrum characteristic of the internal double bond attached to the inorganic core reveal the failure of the reaction.

The two preceding unsuccessful synthetic pathways to attach SemiEsphos to the periphery of the POSS cube, employing oxide or borane protected modified ligands, led us naturally to consider an approach where the unprotected SemiEsphos phosphine would be directly attached onto the POSS macromolecule.

III. 2. 3 The unprotected SemiEsphos route

The first synthetic route we considered started with the formation of the bromobenzene modified diazaphospholidine (**6**), thermodynamically driven by the displacement of gaseous dimethylamine (Scheme 3.6).



Scheme 3.6 Formation of the bromobenzene modified diazaphospholidine (**6**)

Attachment of (**6**) onto a POSS cube terminated by Si-Cl groups (**G0-ethyl-8Cl**, Figure 3.6)³⁶ was then envisaged using several different methods.

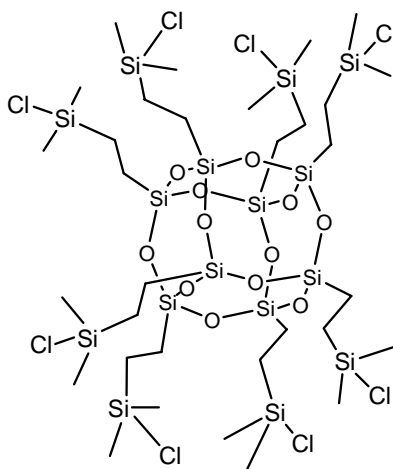
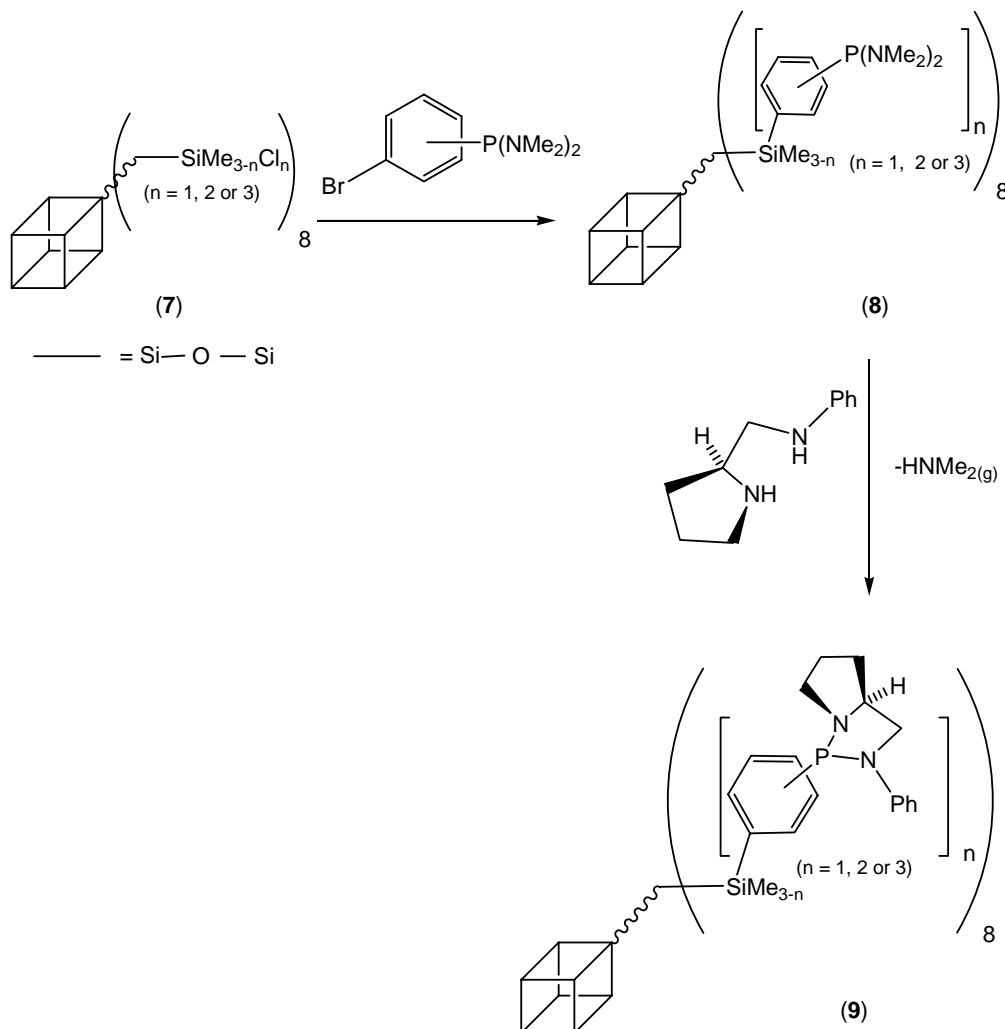


Figure 3.6 **G0-ethyl-8Cl**

First, ⁿBuLi was used to promote a lithium-halogen exchange with the bromine atom of (**6**), followed by a nucleophilic attack onto the electrophilic silicon atoms located at the periphery of the cube. However, the high nucleophilicity of the organolithium reagent opened the diazaphospholidine ring resulting in a variety of side products, whose purification was not attempted. The more bulky and less nucleophilic ^tBuLi did not seem to open the ring but a wide range of products was present in solution as assessed by ³¹P NMR spectroscopy, even when the reaction was carried out at -120 °C.

Then, the Grignard derivative of (**6**) was successfully made following the method conceived by Knochel and co-workers,³⁷ using a mixture of isopropylmagnesium chloride, lithium chloride solution in THF. Unfortunately, the resulting compound was not nucleophilic enough to displace the peripheral silicon atoms of **G0-ethyl-8Cl**.

Eventually, we investigated the strategy depicted in Scheme 3.7, to attach the unprotected SemiEsphos at the periphery of the POSS cube. Lithiation of 3-bis(dimethylamino)phosphinobromobenzene, prepared by a literature method,³⁸ followed by reaction with readily available chlorosilane terminated POSS (7)³⁶ led to bis(dimethylamino)phosphine terminated dendrimer (8). The synthesis was completed by amine exchange with (*S*)-2-(phenylaminomethyl)pyrrolidine³⁹ to form the desired cube (9) driven by the thermodynamic displacement of gaseous dimethylamine.



Scheme 3.7 Synthetic strategy for the preparation of SemiEsphos decorated POSS cored dendrimers

Following this method, four first generation SemiEsphos decorated POSS cored dendrimers – **G1-8SemiEsphos**, **G1-16SemiEsphos**, **G1-24SemiEsphos** and **G1-24SemiEsphos(ext)** and two second generation dendrimers **G2-16SemiEsphos** and **G2-32SemiEsphos** have been designed and successfully elaborated (Figure 3.7).^{29, 40} The first generation dendrimer **G1-**

24SemiEsphos(ext) represents an extended version of **G1-24SemiEsphos** in which an extra -Si(CH₂)₂- unit has been placed in the dendron arm.

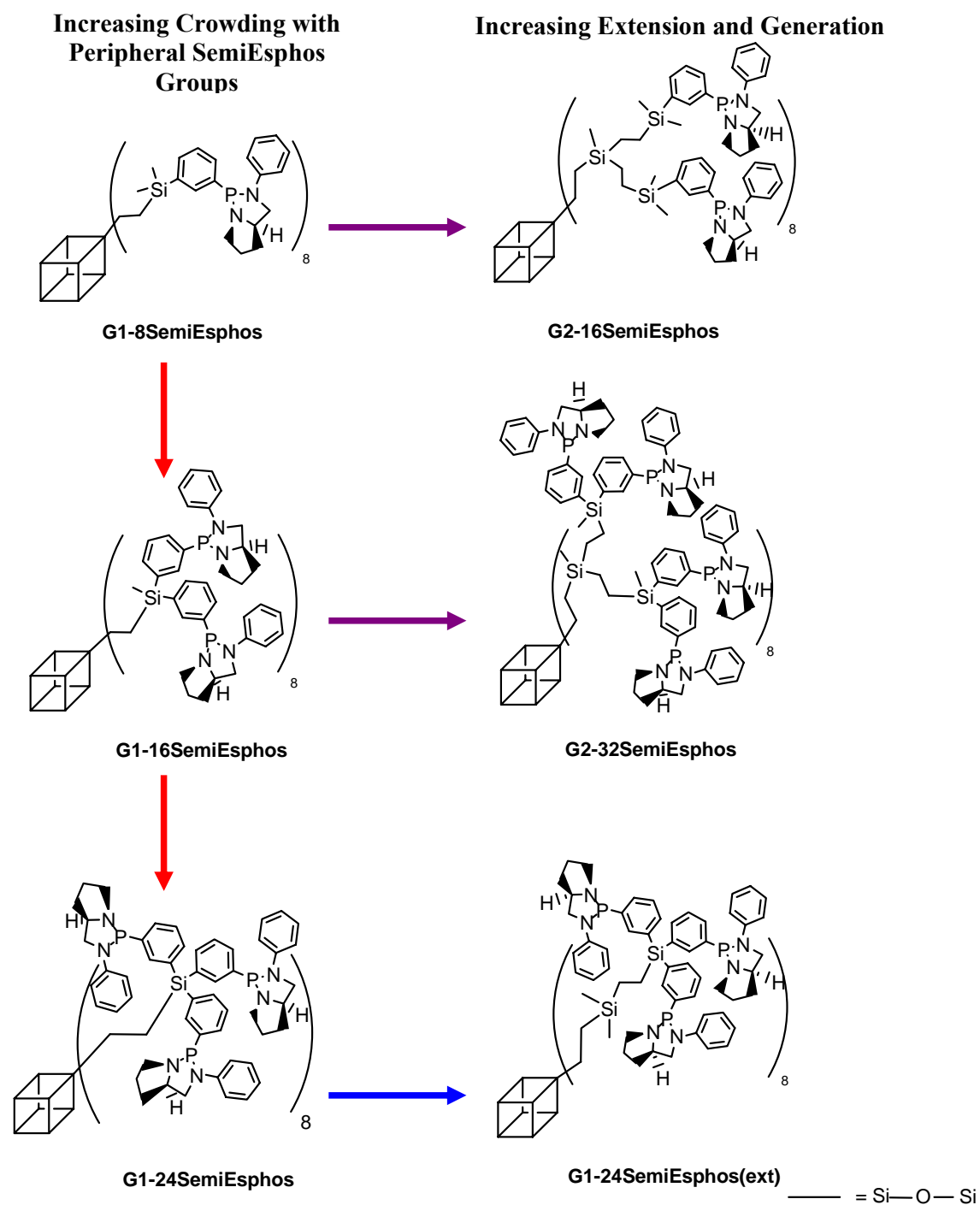
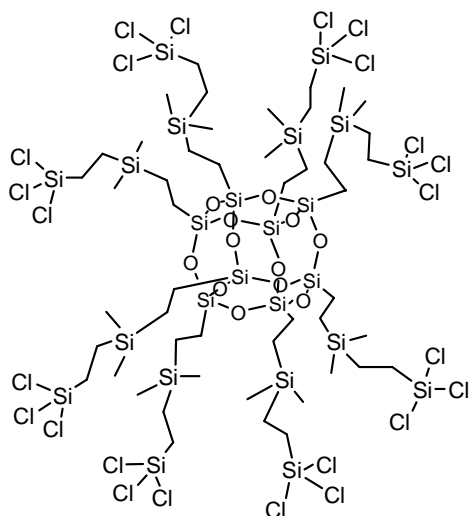


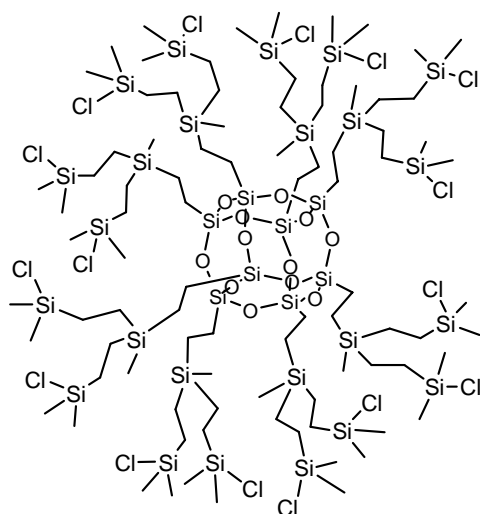
Figure 3. 7 Generation 1 and 2 SemiEsphos terminated POSS cored dendrimers

The red arrows highlight an increase in the steric crowding at the periphery of the dendrimer *via* an increase in the number of functional groups linked to one single silicon atom upon moving from **G1-8SemiEsphos** to **G1-16SemiEsphos** and **G1-24SemiEsphos**, whilst the blue arrow shows a reduction of steric crowding and enhancement of the branch flexibility between **G1-24SemiEsphos** and **G1-24SemiEsphos(ext)** but operating via the branch extension (two silicon atoms are now present on each branch in contrast of one and three silicon atoms per branch for G1 and G2, respectively). The purple arrows present the relation between generation 1 and generation 2 POSS, **G1-8SemiEsphos** vs **G1-16SemiEsphos** and **G2-16SemiEsphos** vs **G2-32SemiEsphos**, where the number of silicon atoms per branch is now equal to three. The formation of a generation 2 POSS surrounded by 48 peripheral SemiEsphos was not attempted as it was expected that steric hindrance at the periphery of the cube would have led to incomplete functionalisation.⁴¹

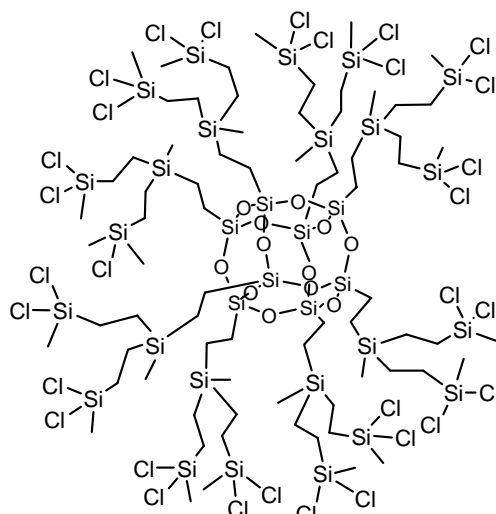
While already known chlorosilane terminated POSS³⁶ were employed in the synthesis of **G1-8SemiEsphos**, **G1-16SemiEsphos** and **G1-24SemiEsphos**, new precursors (7) –**G1-ethyl-24Cl(ext)**, **G2-ethyl-16Cl** and **G2-ethyl-32Cl**– were prepared following the literature method developed by Morris and co-workers³⁶ to produce **G1-24SemiEsphos(ext)**, **G2-16SemiEsphos** and **G2-32SemiEsphos** (Figure 3.8). Alkenylation of chlorosilane-terminated dendrimers with homemade vinylmagnesium bromide and hydrosilylation of vinyl terminated POSS led to the formation of 3 new chlorosilane terminated POSS molecules, which have all been characterized by multinuclear (¹³C, ¹H and ²⁹Si) NMR spectroscopy and microanalyses.



G1-ethyl-24Cl(ext)



G2-ethyl-16Cl



G2-ethyl-32Cl

Figure 3.8 Representation of **G1-ethyl-24Cl(ext)**, **G2-ethyl-16Cl** and **G2-ethyl-32Cl**

–PNMe₂ terminated compounds (**8**) were only worked up with basic water to destroy any traces of remaining *n*-butyllithium and used in the next step without any further purification. SemiEsphos terminated POSS were precipitated in hexane to wash away the excess of small molecules (3-bis(dimethylamino)phosphinobromobenzene and (*S*)-2-(phenylaminomethyl)pyrrolidine) until no phosphorus signal attributed to the small molecules could be detected by ³¹P NMR spectroscopy. Routine multinuclear NMR techniques (³¹P and ²⁹Si) were used to assess the completeness of the syntheses. The final ³¹P NMR spectrum

contained only one signal from each of the desired SemiEsphos terminated POSS cored macromolecules. ^{29}Si NMR was also very useful in monitoring this synthesis as 3 different signals –Si(T) (Silicon on the vertex of the cube), Si-Cl and Si-Phenyl are present in the final product. The purity of the final product was shown by the presence of a single ^{29}Si NMR signal at -67 ppm from the Si atoms in the cube. This resonance shows that the cube remains intact and that each corner has been substituted by the same group showing the presence of only one cube. Moreover, the nucleophilic substitution of the chlorine atoms on (7) by the lithium aryl entity, was confirmed by the observation in the ^{29}Si NMR spectrum of downfield signals characteristic of the Si-Phenyl bond at -1.3 ppm, -1.6 ppm, -6.0 ppm, -6.3 ppm, -9.4 ppm and -10.1 ppm (respectively for **G1-8SemiEsphos**, **G2-16SemiEsphos**, **G2-32SemiEsphos**, **G1-16SemiEsphos**, **G1-24SemiEsphos(ext)** and **G1-24SemiEsphos**). In addition microanalysis was also carried out and testified to the high degree of purity of these compounds.

III. 3 SemiEsphos decorated Polyhedral Oligomeric Silsesquioxane cored dendrimers in vinyl acetate and styrene hydroformylation^{29, 40}

III. 3. 1 Vinyl acetate hydroformylation

All the dendritic SemiEsphos species were investigated in rhodium catalysed hydroformylation of vinyl acetate to see whether crowding at the periphery might encourage bidentate binding and induce activity. Catalytic solutions were prepared in toluene by mixing the dendritic ligand with $[\text{Rh}(\text{acac})(\text{CO})_2]$ at the desired rhodium to phosphine ratio, before being transferred to a batch Hastelloy autoclave via canula. The conditions and results are summarized in Table 3.1.

Table 3.1 Hydroformylation of vinyl acetate with catalysis by rhodium complexes ^[a]

Entry	Ligand	P:Rh	Concentration [Mol/L]	Conversion [%]	Aldehyde yield [%] ^[b]	Aldehyde b:l ^[c]	Aldehyde ee [%]	Alcohol yield [%] ^[d]	Alcohol ee [%]
1	SemiEsphos	3.0	0.010	10.2	2.5	0.3	0.0	0.0	0.0
2		6.0	0.010	12.9	2.3	0.4			
3	Esphos	1.5 ^[f] , [g]	0.010	100.0	34.9	15.9	76.0 (S)	58.8	84.0 (S)
4		6.0 ⁴²	0.010	-ppt	–	–	–	–	–
5	G1-8SemiEsphos	3.0	0.010	-ppt	–	–	–	–	–
6		6.0	0.010						
7		6.0	0.001						
8	G1-16SemiEsphos	3.0	0.010	-ppt	–	–	–	–	–
9		6.0	0.010						
10		6.0	0.005		6.7	1.5	0.0	0.0	0.0
11	G1-24SemiEsphos	6.0 ^[f]	0.010	60.2	42.0	11.6	0.0	5.9	0.0
12		3.0	0.010	51.5	48.4	15.5	0.0	0.0	0.0
13		6.0	0.005	13.6	9.2	2.1	0.0	0.0	0.0
14	G1-24SemiEsphos(ext)	3.0	0.010	-ppt	–	–	–	–	–
15		6.0	0.010						
16		6.0	0.001						
17	G2-16SemiEsphos	3.0	0.010	-ppt	–	–	–	–	–
18		6.0	0.010						
19		6.0	0.001						
20	G2-32SemiEsphos	3.0	0.010	-ppt	–	–	–	–	–
21		6.0	0.010						
22		6.0	0.001						

[a] Catalyst prepared in situ from [Rh(acac)(CO)₂] and the phosphine in toluene (4 mL) containing vinyl acetate (1 mL). P_{CO/H₂} (1/1) = 40 bar. Temp = 80 °C, t = 20 hours. [b] Yield refers to 2-acetoxypropanal (1-acetoxypropanal decomposes under the reaction conditions to acetic acid and propenal). [c] Refers to aldehyde formation before decomposition/hydrogenation. Determined from the ratio of branched chain product (aldehyde+alcohol) to acetic acid. [d] This refers to 2-acetoxy-1-propanol plus 1-acetoxy-2-propanol. [e] Acetoxyacetone (0.3-1.3 %) is also a product. [f] t = 3 hours

Entries 1 and 2 show the low activity of monomeric SemiEsphos at different phosphine to metal ratio (around 11.5 % conversion, low b:l ratio (0.5) and no *ee*) whilst entry 3 emphasizes the very good behavior of ESPHOS in this reaction as total conversion is reached after 3 hours.²⁸ Entry 4 shows an interesting fact, namely the complete absence of activity of ESPHOS when a 6 to 1 phosphine to rhodium ratio is employed. This can be rationalized by the formation of an inactive complex containing two bidentate ESPHOS ligands which appears as a precipitate after opening the autoclave.⁴²

Upon mixing **G1-8SemiEsphos** or **G1-24SemiEsphos(ext)** and the rhodium precursor in a 3 to 1 phosphine to metal ratio (entries 5 and 14), a white precipitate instantaneously appeared. For both **G1-8SemiEsphos** and **G1-24SemiEsphos(ext)**, increasing the ratio to 6/1 (entries 6 and 15) or decreasing the precursor concentration (entries 7 and 16) did not

prevent the formation of such insoluble material. The same conclusions can be drawn about **G1-16SemiEsphos** (entries 8 and 9) except that no precipitate was present when the rhodium concentration was reduced to $0.005 \text{ mol dm}^{-3}$ (entry 10). Activity in vinyl acetate hydroformylation was observed, but the conversion and branched selectivity were poor (11 % and b:l = 1.5). However, when changing from **G1-16SemiEsphos** to **G1-24SemiEsphos** at 0.01 mol dm^{-3} of $[\text{Rh}(\text{acac})(\text{CO})_2]$, no precipitate was visible after mixing and significant activity in the hydroformylation of vinyl acetate was observed (60 % of vinyl acetate was converted with a branched to linear ratio of 11.6, entry 11). None of the **G2** ligands could be tested in this reaction as again a white precipitate instantaneously appeared upon mixing with the rhodium precursor (entries 17-22). The lack of rigidity inside their dendritic architecture is presumably the cause of the formation of these insoluble materials but it is still surprising as precipitation occurs even at high phosphine to metal ratio (6/1) where a better stabilisation of the rhodium would be expected as a result of the higher number of phosphines involved. The formation of these insoluble 'oligomeric' species results presumably from the rhodium bridging between two dendritic ligands. This precipitate could not be dissolved again even at higher temperature or on addition of excess ligands. A similar phenomenon of precipitation has been observed in the case of diphenylphosphine terminated dendrimers bound to $[\text{Rh}(\text{acac})(\text{CO})_2]$, although at lower phosphine/rhodium ratios (below 3/1),⁴³ and was also attributed to rhodium cross-linking between two dendrimers, i.e two phosphine groups of two different dendritic ligands bind to the same rhodium atom, leading to insoluble oligomeric species.⁴³ Steric hindrance within such complexes presumably prevents the complexation of any excess ligand.

For the dendritic SemiEsphos ligands, the compact and rigid macrostructure of **G1-24SemiEsphos** displays enough crowding at its periphery to constrain the SemiEsphos groups to allow bidentate binding to a single rhodium so that partial emulation of the active ESPHOS can be observed, whilst the more flexible arms of **G1-8SemiEsphos**, **G1-16SemiEsphos**, **G1-24SemiEsphos(ext)** and **G2** ligands allow the formation of oligomeric species, which precipitate. However, in order to ascertain that the whole POSS molecule is needed for this effect, it would have been better to compare **G1-24SemiEsphos** with the small molecule analogue where the Si of the tris(SemiEsphos) substituent is bound to a methyl group rather than *via* the ethylidene group to the POSS core. Unfortunately, despite many attempts, we were unable to prepare this compound.

A slight diminution in the yield (51.5 %) together with an increase in the branched to linear ratio to 15.5, comparable to that obtained with ESPHOS, was observed upon decreasing the ligand to metal ratio to 3/1 (entry 12). Although **G1-24SemiEsphos** does give conversion and branched selectivity in the hydroformylation of vinyl acetate, no *ee* was obtained. So this ligand does not behave exactly like ESPHOS, although it is known that asymmetric catalysis using dendritic ligands can sometimes be unsuccessful.^{44,20} The bridge between the two SemiEsphos portions is quite different in **G1-24SemiEsphos** from that in ESPHOS, so, although bidentate coordination may occur and allow reactivity, the chiral environment may be very different.

The positive role in both conversion and especially branched selectivity (entry 11) conferred by the dendritic architecture compared with SemiEsphos is even more apparent when comparing **G1-24SemiEsphos** and ESPHOS at different phosphine to metal ratios. Upon increasing this ratio from 3/1 to 6/1, the ESPHOS gives a dramatic drop of activity whilst its dendritic counterpart shows an increase in activity. This is believed to be due to the increased stabilization of the rhodium complex in the case of the dendritic ligand, which, unlike ESPHOS, cannot form a bis bidentate complex for steric reasons.

The performances of **G1-16SemiEsphos** and **G1-24SemiEsphos** (entry 13), under the only catalytic conditions where **G1-16SemiEsphos** is active (entry 10), are very similar suggesting that at low rhodium concentration and high SemiEsphos:Rh ratio, bidentate binding might also occur for **G1-16SemiEsphos**.

III. 3. 2 Styrene hydroformylation

G1-16SemiEsphos and **G1-24SemiEsphos** were also tested in the hydroformylation of styrene to observe whether or not any chiral induction could be achieved as neither SemiEsphos nor ESPHOS are enantioselective in that reaction (Table 3.2, entries 23-29).

Table 3.2 Asymmetric hydroformylation of styrene with catalysis by rhodium complexes ^[a]

Entry	Ligand	P:Rh	Concentration [Mol/L]	Conversion [%]	Aldehyde yield [%] ^[b]	Aldehyde b:1 ^[c]	Aldehyde ee [%]	Alcohol yield [%] ^[d]	Alcohol ee [%]
23	SemiEsphos	2 ^[i]	0.010	91.3	85.0	1.5	0.0	1.1	0.0
24		6 ^[i]		91.0	86.0	1.6	0.0	0.9	0.0
25	Esphos	1,5	0.010	99.6	98.9	3.5	0.0	0.0	0.0
26		6 ^[i]		-ppt	—	—	—	—	—
27	G1-16SemiEsphos	6	0.005	17.8	17.8	2.4	0.0	0.0	0.0
28	G1-24SemiEsphos	6 ^[i]	0.005	70.5	69.0	2.8	3.0	0.0	0.0
29		6	0.010	72.2	70.9	1.2	3.7	1.4	0.0

[a] Catalyst prepared in situ from [Rh(acac)(CO)₂] and the phosphine in toluene (4 mL) containing styrene (1 mL). 10 bar CO/H₂ (1/1). Temp = 80 °C, 2 hours. [b] Yield refers to 2-phenylpropanal + 3-phenylpropanal. [c] Refers to aldehyde formation before aldehyde decomposition/hydrogenation. Determined from the ratio of branched chain product (aldehyde + alcohol) to straight chain product (aldehyde + alcohol). [d] This refers to 2-phenyl-1-propanol plus 3-phenyl-1-propanol. [e] Acetophenone (<2 %) is also a product

Once again, **G1-24SemiEsphos** shows significant activity (70.5 % conversion, [Rh(acac)(CO)₂] = 0.005 mol dm⁻³, entry 28). At higher metal concentration (0.01 mol dm⁻³) the conversion is slightly higher (72.2 %, entry 29). **G1-16SemiEsphos** is also weakly active (entry 27) but very little or no chiral induction was observed for any of these catalysts. It may be that the excess of ligand may partly be responsible for the low enantioselectivity observed since it has been shown with other ligands that excess ligand can lead to a sharp decrease of enantioselectivity in hydroformylation reactions.⁷

G1-16SemiEsphos and **G1-24SemiEsphos** are the only POSS based ligands to show activity in vinyl acetate or styrene hydroformylation. The four other dendritic ligands precipitate upon mixing with the rhodium precursor leading to insoluble oligomeric species.

In order to try to understand the different behaviours of the various ligands, we have carried out molecular dynamics calculations.

III. 3. 3 Molecular Dynamics Studies

Molecular dynamics studies of SemiEsphos terminated POSS macromolecules were performed by Dr. Pascal André, in order to gain insight into the role of the dendritic architecture and identify the most probable conformations accessible to the macromolecules for the control of the outcome of alkene hydroformylation reactions. All the molecular dynamics calculations were completed in vacuum at 580 K following the

protocol detailed in the experimental section (Chapter 5). Their main outcomes are summarized in Table 3.3 and detailed in the associated figures.

Table 3.3 Molecular Dynamics results. Average radius of gyration (R_g) and distance between phosphorus atoms and the silicon atom connecting arm and POSS core (d_{Si-P} : average, minimum and maximum), intra-dendron distances between phosphorus atoms ($d_{PP-intra}$: average, minimum and maximum) and inter-dendron distances between phosphorus atoms ($d_{PP-inter}$: average, minimum and maximum). Molecular Dynamics calculations were completed in vacuum at 580 K

Ligand	$R_g / \text{\AA}$ ($\sigma_{st dev}$)	$d_{Si-P} / \text{\AA}$			$d_{PP-intra} / \text{\AA}$			$d_{PP-inter} / \text{\AA}$		
		avg	min	Max	avg	min	Max	avg	min	Max
G1-8SemiEsphos	8.74 (0.23)	7.7 (1.0)	4.7	10.3	NA	NA	NA	11.3 (3.7)	3.3	22.2
G1-16SemiEsphos	9.92 (0.15)	8.2 (1.3)	4.9	10.4	8.5 (1.5)	4.8	11.4	12.3 (3.3)	3.4	22.3
G1-24SemiEsphos	10.65 (0.07)	8.4 (1.3)	5.1	10.4	8.7 (1.5)	4.5	11.6	12.6 (4.1)	3.1	22.5
G1-24SemiEsphos(ext)	11.73 (0.16)	10.4 (1.8)	3.8	14.7	8.6 (1.6)	4.4	11.6	15.5 (4.7)	3.4	30.3
G2-16SemiEsphos	11.03 (0.17)	9.9 (2.0)	3.4	14.5	11.9 (3.4)	3.4	19.8	14.8 (5.1)	3.2	29.3
G2-32SemiEsphos	12.57 (0.08)	11.2 (1.8)	4.7	14.7	10.6 (3.5)	3.1	20.2	16.2 (5.2)	3.5	28.9

All the dendrimers regardless of their complexity have a spherical shape as illustrated by the small values of the asphericity of the moment of inertia in Figure 3.9A and 3.9B.

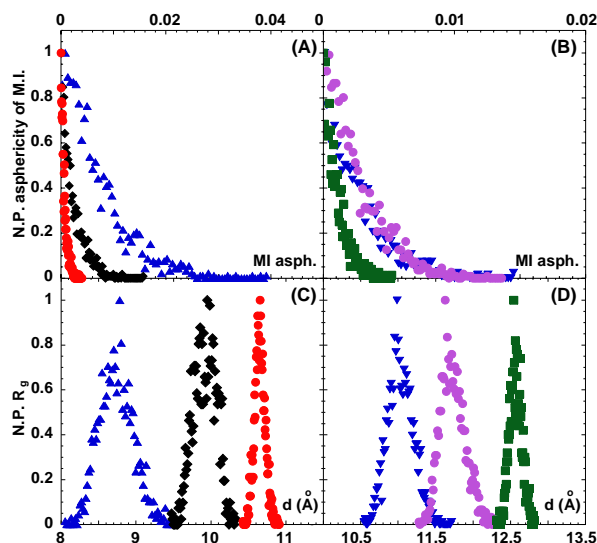


Figure 3. 9 Normalized population of the asphericity of the moment of inertia (A, B) and radius of gyration (C, D) of G1-8SemiEsphos (\blacktriangle), G1-16SemiEsphos (\blacklozenge), G1-24SemiEsphos (\bullet), G1-24SemiEsphos(ext) (\blacklozenge), G2-16SemiEsphos (\blacktriangledown) and G2-32SemiEsphos (\blacksquare). Molecular Dynamics calculations were completed in vacuum at 580 K

As expected, the radius of gyration is increased with the macromolecule complexity and generation from 8.7 \AA to 12.6 \AA , see Table 3.3 and Figure 3.9C and 3.9D. In addition a direct observation of Figure 3.9C and 3.9D shows that as the complexity of the macromolecules is increased, the curves of the radius of gyration populations become narrower consistent with an increase in the steric hindrance of phosphine groups at the periphery, see Figure 3.7 and $\sigma_{st dev}$ in Table 3.3, to compare **G1-8SemiEsphos** to **G1-**

24SemiEsphos (0.23 vs 0.15, respectively), **G1-24SemiEsphos(ext)** and **G1-24SemiEsphos** (0.16 vs 0.07, respectively), **G2-16SemiEsphos** to **G2-32SemiEsphos** (0.17 vs 0.08, respectively) as well as the comparison between the 1st and 2nd generations **G1-8SemiEsphos** to **G2-16SemiEsphos** (0.23 vs 0.17, respectively) and **G1-16SemiEsphos** to **G2-32SemiEsphos** (0.15 vs 0.08, respectively).

III. 3. 3. 1 “Branch extensions”

Figure 3.10 describes the normalised population of the arm extension defined as the distance between the phosphorus atoms and the associated silicon corner of the POSS cored dendrimers. In an attempt to find a compromise between averaging and blurring the range of conformations accessible to the arms of the dendrimers, when the macromolecule contains several phosphine groups, see Figure 3.7, then each of them was discriminated, averaged and plotted individually to obtain Figure 3.10 displaying up to three curves per graph.

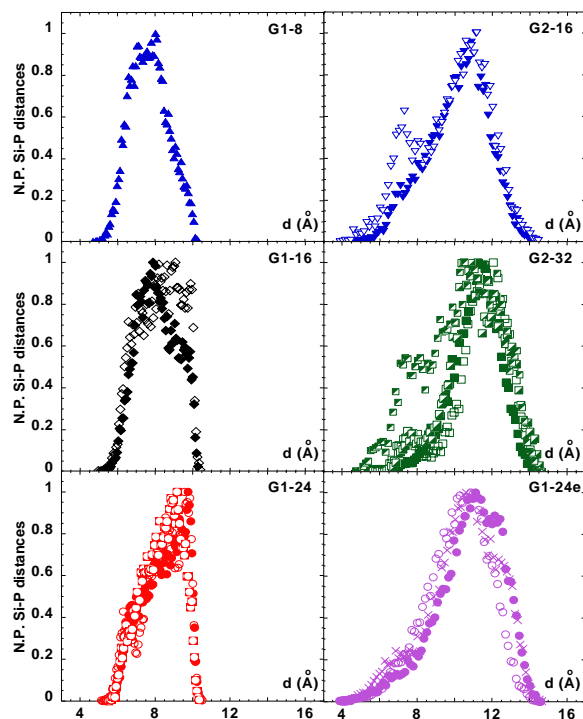


Figure 3.10 Normalized population of the extension of the arms calculated as the Si-P distances along the each arm. Molecular Dynamics calculations were completed in vacuum at 580 K. To find a compromise between averaging and blurring the range of conformations accessible to the arms of the dendrimers, when the macromolecule contains several phosphine groups each of them were discriminated, averaged and plotted individually leading to full, empty and half empty symbols, see text for details

For instance, **G1-8SemiEsphos** contains a single phosphorus atom per branch leading to a single curve, **G1-16SemiEsphos** and **G2-16SemiEsphos** contain two phosphorus atoms per branch leading to two curves, **G1-24SemiEsphos** and **G1-24SemiEsphos(ext)** contain three phosphorus atoms per branch leading to three curves, and **G2-32SemiEsphos** contains four phosphorus atoms per branch leading to four possible combinations. As for Figure 3.9, the distribution of conformations which can be seen in Figure 3.10, results from thermal agitation. Consistent with the radius of gyration behaviour, see Table 3.3, the average distance between the silicon corners of the POSS core to phosphorus atoms on the same arm shows a progressive increase from 7.7 Å to 10.4 Å for the generation 1 macromolecules and from 9.9 Å to 11.2 Å for the 2nd and extended 1st generation macromolecules, see Table 3.3. The arm extension of all the 1st generation macromolecules covers the same interval of distances, see min-max in Table 3.3, while as expected the 2nd and extended 1st generations of macromolecules cover a larger interval with a peak shifted towards longer distances, see Figure 3.10.

No strong back-folding is observed for any of the dendrimers probably because of the bulky structure of the phosphine groups. However; the 2nd and extended 1st generation macromolecules (right hand side of Figure 3.10) display a small peak at short distances, around 7 Å, indicative of some of the phosphorus atoms being embedded under the peripheral shell and consistent with the larger flexibility provided by the additional Si(CH₂)₂ group when compared with the 1st generation dendrimers, see Figure 3.7 and right hand side column of Figure 3.10. However, flexibility is not synonymous with free space. Indeed the more free space there is between peripheral groups, the more Gaussian-like the extension distribution is expected to be. However **G2-16SemiEsphos** and **G2-32SemiEsphos** display peaks on the lower side of the arm extension indicative of crowding confinement, space restriction or attractive interactions, whereas **G1-24SemiEsphos(ext)** only displays a shoulder indicative as expected of a lower degree of crowding. For hydroformylation to occur with the poorly active SemiEsphos, the formation of a complex between one rhodium and two phosphorus atoms is thought to be required so as partially to emulate the active ESPHOS. This can only happen when the phosphorus to phosphorus distance is in the order of 4 to 7 Å. The PP distances were numerically probed both within a single arm (intradendron) and between adjacent arms (interdendron).

III. 3. 3. 2 “Intradendron PP distances”

Figure 3.11 displays the normalized population of the PP distances within the same arms for all dendrimers except **G1-8SemiEsphos**, for which there is only one P atom per arm. For instance, **G1-16SemiEsphos** and **G2-16SemiEsphos** contain two phosphorus atoms per branch leading to a single curve, **G1-24SemiEsphos** and **G1-24SemiEsphos(ext)** contain three phosphorus atoms per branch leading to three possible combinations, and **G2-32SemiEsphos** contains four phosphorus atoms per branch leading to six possible combinations and curves.

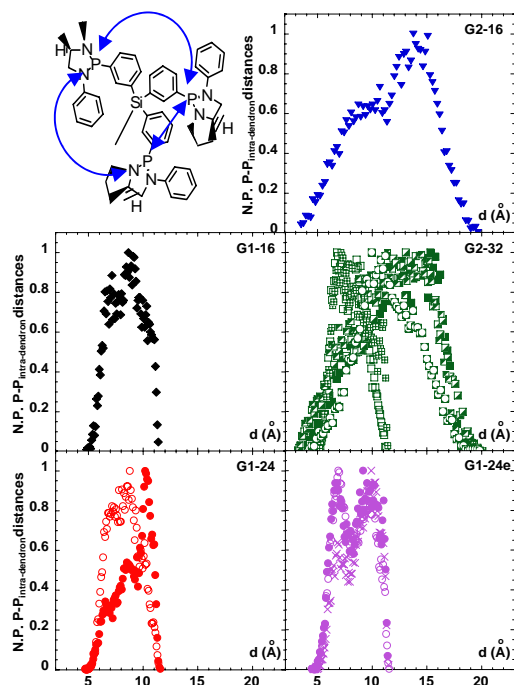


Figure 3.11 Illustration of intradendron PP distances (Top left hand side) and normalized population of the intradendrons PP distances within the same arms for each dendrimer (rest of the figure as labelled). Molecular Dynamics calculations were completed in vacuum at 580 K, see text for details

In all cases, most of these distances are in the region of 6-7 Å, even though they differ by double and triple end group functionalisations. **G1-16SemiEsphos** and **G1-24SemiEsphos** exhibit the same range of distances, 4.5 to 11.5 Å see Table 3.3, indicating similar packing of the intradendron terminal groups at the periphery of the macromolecules. The $\text{Si}(\text{CH}_2)_2$ group extension does not impact significantly on the intra dendron PP distances. Indeed **G1-24SemiEsphos** and **G1-24SemiEsphos(ext)** both cover the same range of intradendron PP distances. This is not very surprising, see Figure 3.7, as the external Si atom is fully substituted by three diazaphospholidine groups. This also indicates that any

variation of the intradendron PP distances with the generation would result from a dendritic effect and not an extension effect.

It is clear from Figure 3.11 that both **G2-16SemiEsphos** and **G2-32SemiEsphos** have intradendron PP distances spreading over a much wider interval than the 1st generation dendrimers. A direct comparison can be made between **G1-16SemiEsphos** and **G2-32SemiEsphos** with the latter extending toward longer distances even though still covering the short distances between 4 and 11 Å characteristic of the 1st generation. This is consistent with the double substitution of the external silicon atom by diazaphospholidine groups as well as the presence of two of such external substituted silicon atoms on a single arm. However spreading over such a wide range of PP distances also implies that the probability of finding the PP distance suitable for the formation of a complex with rhodium is actually lower than for materials displaying narrow PP distance intervals and this favours the first generation dendrimers to form bidentate coordination with the catalyst instead of forming insoluble polymer like materials, see Table 3.3.

Indeed **G1-16SemiEsphos** and **G1-24SemiEsphos** as well as **G1-24SemiEsphos(ext)** show most of their intradendron PP distances below 10 Å which is favourable for bidentate coordination. In addition, it has been shown previously that **G1-24SemiEsphos(ext)** has a more flexible structure than generation 1 species (see Figure 3.10), which favours the two first ligands for possible reactivity as space constraints associated with the 4 to 7 Å PP distance will increase the probability of bidentate complex formation. As a direct consequence it also reinforces the idea of the flexible dendritic structure to be more prone to form oligomeric species in contrast to the compact and rigid 1st generation dendritic structure able to promote bidentate coordination and hence activity.

III. 3. 3. 3 “Interdendron PP distances”

Interdendron bidentate binding could also occur, so these were numerically probed, see Figure 3.12. Again each phosphorous atom on each dendron was discriminated, distances with each phosphorus atoms on neighbouring dendrons were averaged to be plotted with Figure 3.12 displaying up to four curves per graph. In this context, **G1-8SemiEsphos** contains a single phosphorus atoms per branch leading to a single curve, **G1-**

16SemiEsphos and **G2-16SemiEsphos** contain two phosphorus atoms per branch leading to two curves, **G1-24SemiEsphos** and **G1-24SemiEsphos(ext)** contain three phosphorus atoms per branch leading to three curves and **G2-32SemiEsphos** contains four phosphorus atoms per branch leading to four curves.

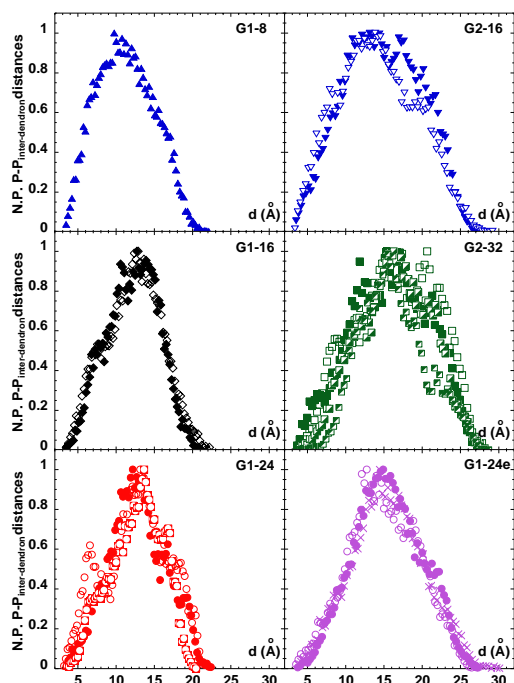


Figure 3.12 Normalized population of the interdendron PP distances. Molecular Dynamics calculations were completed in vacuum at 580 K, see text for details

All the first generation dendrimers cover an interdendron PP distance interval between 3 and 22 Å. Table 3.3 illustrate that average interdendron PP distances are of the order of 12 Å which seems less favorable to bidentate coordination when compared with the intradendron PP average distances of about 8.6 Å.

As opposed to **G1-8SemiEsphos**, both **G1-16SemiEsphos** and **G1-24SemiEsphos** show a shoulder around 6-7 Å which is also favourable to promote bidentate coordination. This shoulder is more pronounced for the more active **G1-24SemiEsphos** and the same statistical argument developed for intradendron PP distances can be used here to make **G1-16SemiEsphos** and **G1-24SemiEsphos** distinct from the other dendrimers.

Compared with the 1st generation, the 2nd generation species cover a wider range of interdendron PP distances, with an interval between 4 and 29 Å, see Table 3.3 and Figure 3.12, indicative of an even lower probability of finding two phosphorus atoms at the

appropriate distance for bidentate coordination. The same rationale applies to **G1-24SemiEsphos(ext)** for which the average interdendron PP distances is around 15.5 Å.

To summarize, we assume that bidentate coordination will be favoured for dendrimers for which PP distances of 4 to 7 Å are available, but otherwise monodentate binding occurs to give insoluble oligomers. More free space (**G1-8SemiEsphos** and **G1-24SemiEsphos(ext)**) and the larger the range of accessible conformation (**G2-16SemiEsphos** and **G2-32SemiEsphos**) reduce the probability of bidentate coordination thus favouring cross-linking and precipitation, as is observed. Only **G1-16SemiEsphos** and **G1-24SemiEsphos** combine the desired balance of crowding. The external silicon atoms of each dendron bare two or three bulky phosphine groups, which confine the intradendron PP distances in the appropriate regime for bidentate binding. Being 1st generation, the two dendrimers are fairly crowded and compact at the periphery which reduces the mobility of the phosphorus atoms.

G1-8SemiEsphos and **G1-24SemiEsphos(ext)** are not crowded enough to force bidentate binding, leaving more opportunities to oligomeric species. **G2-16SemiEsphos** and **G2-32SemiEsphos**, are less crowded at the periphery than **G1-16SemiEsphos** and **G1-24SemiEsphos** because the surface area is higher for the second generation dendrimers. They thus offer too large a range of accessible conformations, reducing the probability of bidentate binding and hence favouring the observed oligomerisation and precipitation. Even though the average intradendron PP distances in **G1-16SemiEsphos** and **G1-24SemiEsphos** are very close to the 4 to 7 Å needed for bidentate coordination, it is hard to discriminate the exact contributions and roles of both intra- and interdendron bidentate binding.

III. 3. 4 Conclusions

New diazaphospholidine terminated Polyhedral Oligomeric Silsesquioxane (POSS) molecules have been synthesized and tested in styrene and vinyl acetate hydroformylation. Some of them have been shown to precipitate upon mixing with rhodium precursors, whilst others remain in solution and show activity. These latter are more compact and rigid in comparison to the former, which are more flexible and hence more prone to monodentate binding to rhodium and cross-linking. Molecular dynamics investigation has

been able to rationalise these observations. PP distance calculations show that the ligands, for which precipitation occurs upon mixing with the rhodium precursor, have PP distances too big to promote bidentate coordination, whereas the two active ligands display more rigid and compact structures with PP distance falling in the range of possible bidentate coordination. We have, therefore succeeded in using macromolecular design to induce a dendritic effect by sufficiently crowding SemiEsphos units at the periphery of a dendrimer like molecule that the properties of ESPHOS (a bidentate analogue of monodentate SemiEsphos) are at least partially reproduced. The activity, branched selectivity and even the activity for subsequent aldehyde hydrogenation to alcohol of ESPHOS are reproduced, but not the enantioselectivity. This suggests that despite the crowding initiating bidentate binding, the exact chiral environment provided by ESPHOS has not been achieved.

III. 4 REFERENCES

1. C. Claver and P. W. N. M. van Leeuwen, *Rhodium Catalyzed Hydroformylation*, Kluwer Academic Publishers edn., Dordrecht, 2000.
2. J. E. Babin and G. T. Whiteker, *WO Pat.* 9 303 839, 1993.
3. C. J. Cobley, K. Gardner, J. Klosin, C. Praquin, C. Hill, G. T. Whiteker, A. Zanolli-Gerosa, J. L. Petersen and K. A. Abboud, *J. Org. Chem.*, 2004, **69**, 4031.
4. N. Sakai, S. Mano, K. Nozaki and H. Takaya, *J. Am. Chem. Soc.*, 1993, **115**, 7033.
5. C. J. Pilkington and A. Zanolli-Gerosa, *Org. Lett.*, 2003, **5**, 1273.
6. T. P. Clark, C. R. Landis, S. L. Freed, J. Klosin and K. A. Abboud, *J. Am. Chem. Soc.*, 2005, **127**, 5040.
7. A. T. Axtell, J. Klosin and K. A. Abboud, *Organometallics*, 2006, **25**, 5003.
8. L. H. Gade, *Dendrimer Catalysis*, Springer GmbH edn., Berlin, Germany, 2006.
9. P. B. Rheiner and D. Seebach, *Chem. Eur. J.*, 1999, 3221.
10. A. A. El-Shehawy, K. Sugiyama and A. Hirao, *Tetrahedron: Asymmetry*, 2008, **19**, 425.
11. R. Breinbauer and E. N. Jacobsen, *Angew. Chem. Int. Ed.*, 2000, **39**, 3604.
12. Y. Ribourdouille, G. Engel, M. Richard-Plouet and L. H. Gade, *Chem. Commun.*, 2003, 1228.
13. G. J. Deng, Q. H. Fan, X. M. Chen, D. S. Liu and A. S. C. Chan, *Chem. Commun.*, 2002, 1570.
14. Z. J. Wang, G. J. Deng, Y. M. Li, Y. M. He, W. J. Tang and Q. H. Fan, *Org. Lett.*, 2007, **9**, 1243.
15. G. J. Deng, G. R. Li, L. Y. Zhu, H. F. Zhou, Y. M. He, Q. H. Fan and Z. G. Shuai, *J. Mol. Catal. A: Chem.*, 2006, **244**, 118.
16. W. J. Tang, Y. Y. Huang, Y. M. He and Q. H. Fan, *Tetrahedron: Asymmetry*, 2006, **17**, 536.
17. P. N. M. Botman, A. Amore, R. van Heerbeek, J. W. Back, H. Hiemstra, J. N. H. Reek and J. H. van Maarseveen, *Tetrahedron Lett.*, 2004, **45**, 5999.
18. C. Kollner and A. Togni, *Can. J. Chem.*, 2001, **79**, 1762.
19. R. Laurent, A.-M. Caminade and J.-P. Majoral, *Tetrahedron Lett.*, 2005, **46**, 6503.
20. L. I. Rodriguez, O. Rossell, M. Seco and G. Muller, *J. Organomet. Chem.*, 2007, **692**, 851.
21. J. K. Kassube, H. Wadepohl and L. H. Gade, *Adv. Synth. Catal.*, 2008, **350**, 1155.

22. L. I. Rodriguez, O. Rossell, M. Seco, A. Grabulosa, G. Muller and M. Rocamora, *Organometallics*, 2006, **25**, 1368.
23. L. I. Rodriguez, O. Rossell, M. Seco, A. Orejon and A. M. Masdeu-Bulto, *J. Organomet. Chem.*, 2008, **693**, 1857.
24. A.-M. Caminade, P. Servin, R. Laurent and J.-P. Majoral, *Chem. Soc. Rev.*, 2008, **37**, 56.
25. S. C. Bourque and H. Alper, *J. Am. Chem. Soc.*, 2000, **122**, 956.
26. B. Helms and J. M. J. Fréchet, *Adv. Synth. Catal.*, 2006, **348**, 1125.
27. L. Ropartz, R. E. Morris, D. F. Foster and D. J. Cole-Hamilton, *Chem. Commun.*, 2001, 361.
28. S. Breeden, D. J. Cole-Hamilton, D. F. Foster, G. J. Schwarz and M. Wills, *Angew. Chem. Int. Ed.*, 2000, **39**, 4106.
29. N. R. Vautravers and D. J. Cole-Hamilton, *Chem. Commun.*, 2008, DOI:10.1039/B814582B.
30. P. André, G. Cheng, A. Ruseckas, T. van Mourik, H. Früchtel, J. A. Crayston, R. E. Morris, D. Cole-Hamilton and I. D. W. Samuel, *J. Phys. Chem. B*, 2008, Accepted.
31. O. Legrand, J.-M. Brunel and G. Buono, *Eur. J. Org. Chem.*, 1999, 1099.
32. F. J. Feher, J. J. Schwab, S. H. Phillips, A. Eklund and E. Martinez, *Organometallics*, 1995, **14**, 4452.
33. F. D. Toste, A. K. Chatterjee and R. H. Grubbs, *Pure Appl. Chem.*, 2002, **74**, 7.
34. C. J. Ngono, T. Constantieux and G. Buono, *Eur. J. Org. Chem.*, 2006, 1499.
35. O. Shimomura, B. S. Lee, S. Meth, H. Suzuki, S. Mahajan, R. Nomura and K. D. Janda, *Tetrahedron*, 2005, **61**, 12160.
36. P.-A. Jaffres and R. E. Morris, *J. Chem. Soc., Dalton Trans.*, 1998, 2767.
37. A. Krasovskiy and P. Knochel, *Angew. Chem. Int. Ed.*, 2004, **43**, 3333.
38. K. Drewelies and H. P. Latscha, *Angew. Chem.*, 1982, **94**, 642.
39. C. W. Edwards, M. R. Shipton, N. W. Alcock, H. Clase and M. Wills, *Tetrahedron* 2003, **59**, 6473.
40. N. R. Vautravers, P. André and D. J. Cole-Hamilton, *Dalton Trans.*, 2008, Submitted.
41. L. Ropartz, R. E. Morris, G. J. Schwarz, D. F. Foster and D. J. Cole-Hamilton, *Inorg. Chem. Commun.*, 2000, **3**, 714.
42. D. F. Foster, *Unpublished results*.
43. L. Ropartz, D. F. Foster, R. E. Morris, A. M. Z. Slawin and D. J. Cole-Hamilton, *J. Chem. Soc., Dalton Trans.*, 2002, 1997.

44. J. Brunner, *J. Organomet. Chem.*, 1995, **500**, 39.

**IV. Polyhedral Oligomeric
Silsesquioxanes cored dendrimers in
photoluminescence applications**

IV. Polyhedral Oligomeric Silsesquioxane cored dendrimers in photoluminescence applications

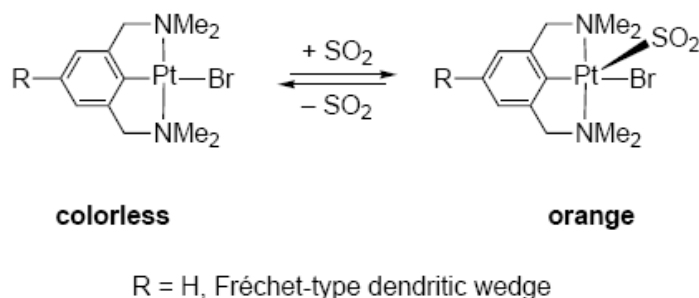
IV. 1 Introduction

The relative simplicity of the iterative synthesis of dendrimers allows the very precise location of functional groups throughout the macromolecule. The dendritic structure, including a central core from which radiates dendrons of controlled complexity, each being terminated by peripheral end groups, enables the incorporation of luminescent units all over the dendritic architecture. These luminescent fragments can display features including energy or electron transfer in light harvesting systems (“antenna effect”),^{1, 2} conversion of UV light into visible or infrared emission^{3, 4} or sensing molecules with signal amplification properties.⁵ In the latter case, gas,⁶ ions⁷⁻¹⁰ or organic compounds^{11, 12} have been found to induce significant and quantitative changes in physical, electrochemical or optical properties of the resultant dendritic-analyte complexes. Some selected examples of dendrimers as molecular sensors are reported below, highlighting the host-guest chemistry rather than providing comparisons between the dendrimer and its small molecule analogue. The field of biology makes extensive use of dendrimers as sensors for bacteria,¹³ DNA,¹⁴ and glucose^{15, 16} for instance but these applications will not be discussed further.

IV. 1. 1 Dendrimers as gas sensors

Detection of gases remains a current challenge in materials science even though important gases such as oxygen or carbon dioxide are now routinely detected.¹⁷ Sensors should possess high selectivity and sensitivity to be efficient, properties that can be displayed by specially designed dendrimers.

Platinum(II) pincer ligand decorated dendrimers synthesised by Van Koten and co-workers can reversibly absorb sulphur dioxide (SO₂) to yield macromolecules with enhanced solubility characteristics and drastic colour changes (Scheme 4.1).⁶



Scheme 4.1 Reversible bonding of SO₂ on platinum(II) pincer decorated dendrimers ¹⁸

The metal-to-ligand charge transfer complex, which turns the solution orange, can detect SO₂ concentrations as low as 10 mg dm⁻³, which makes these compounds highly active sensors for toxic SO₂ gas.

Another toxic gas, carbon monoxide, was successfully detected by measuring conductance variations of dendritic carbosilane thin films peripherally decorated with ferrocenyl groups.¹⁹ This sensor has been found to be very sensitive and selective to CO as the conductance linearly increased by an order of magnitude up to 40%, where it saturated. Following the same principle, Sulu *et al.* resorted to the high electrical conductivity of phthalocyanine compounds to produce dendritic carbon dioxide sensors that were sensitive to a large range of concentrations (from 500 to 8000 ppm).²⁰

A remarkable example of gas sensing was reported by Vinogradov and co-workers who designed metalloporphyrin cored dendritic complexes, for which the strong phosphorescence is totally quenched in the presence of oxygen (Figure 4.1).²¹

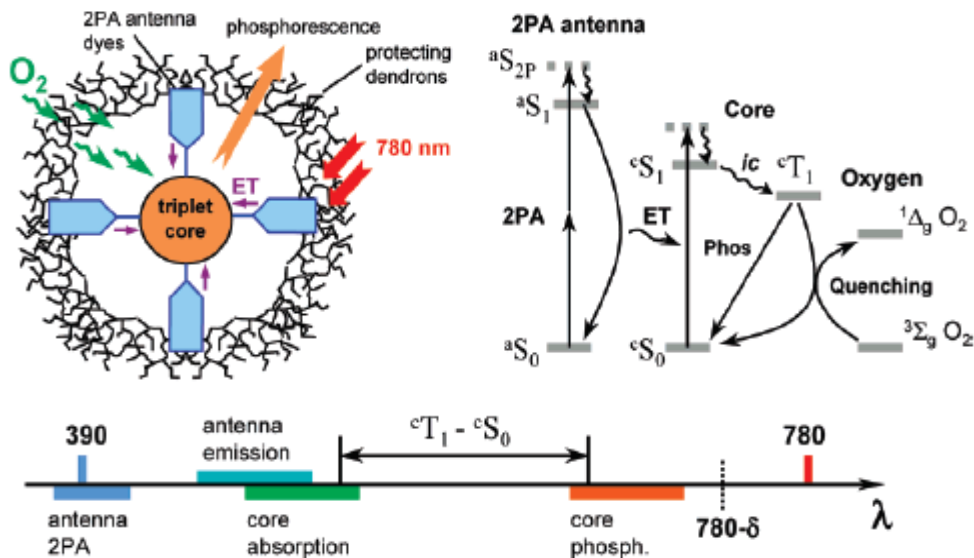


Figure 4.1 Scheme of the phosphorescence sensor, its Jablonski diagram and related wavelength scale ²¹

The chromophores embedded in the dendrimeric matrix and located at the periphery of the metallophorphyrin core, absorb radiation that is then transferred to the emissive core (antenna effect). The emissive core can release its energy by either emitting fluorescence or passing it onto a quencher molecule, e.g. oxygen. The dendrimer shown in Figure 4.1 is not only required to protect the core from oxygen but also to provide a matrix in which the active sites of the device (antenna and core) are positioned at the appropriate distance to facilitate energy exchange.

IV. 1. 2 Dendrimers as ion sensors

Numerous efforts have been devoted to the design and construction of sensors capable of detecting ions.²²⁻²⁵ Dendritic supports represent ideal candidates because of their ability to coordinate a large number of ions throughout their scaffold by electrostatic interactions. Many research groups have exploited the flexible luminescence property of dendrimers to detect ions, mainly by quenching or enhancing fluorescence after ionic interaction between the detected ion and the dendrimer.²⁶⁻²⁸

An elegant example was reported by the group of Balzani and Vögtle in 2000 for the detection of Co²⁺ ions with poly(propyleneimine) dendrimers (Figure 4.2).⁵

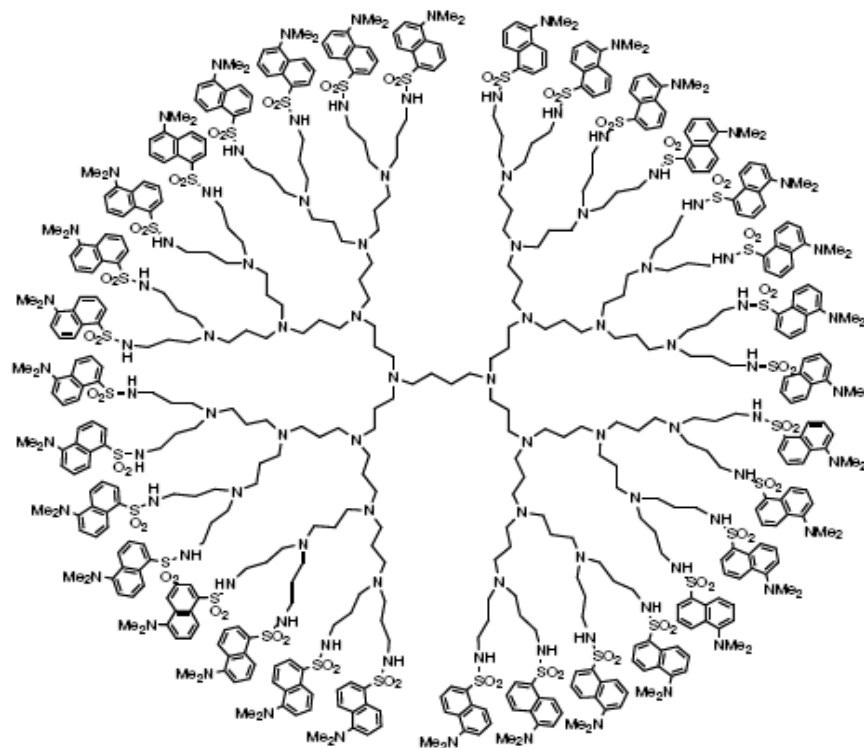


Figure 4.2 Poly(propyleneimine) dendrimer terminated with 32 dansyl units ⁵

It was demonstrated that complete quenching of fluorescent dansyl units, present at the periphery, occurs upon coordination of cobalt ions to the tertiary amines of these dendrimers. The true mechanism (electron or energy transfer) could not be revealed, since the excited state of the dansyl units is both a good energy- and electron donor, while Co(II) amine complexes have several low-energy excited states making it susceptible to oxidation. In addition, a strong amplification of this signal is observed with increasing dendrimer generation (Figure 4.3).

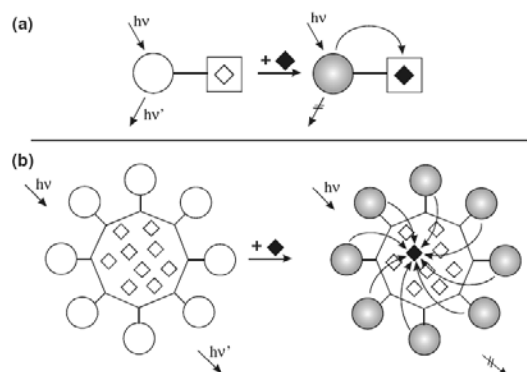


Figure 4.3 Schematic representation of (a) a conventional fluorescent sensor and (b) a fluorescent sensor with signal amplification ⁵

One cobalt ion is able to quench 32 dansyl units and this is the origin of amplified sensitivity compared to a monodansyl compound.

Conversely, Grabchev *et al.* showed a large fluorescent enhancement of 1,8-naphthalimide, grafted at the periphery of a PAMAM dendrimer, in the presence of protons or Cu^{2+} .²⁹ By interacting with amines, these ions quench the photo-induced electron transfer from the amino groups of the core to the peripheral chromophores, which produce a strong emissive signal.

The same idea was developed by Vögtle and co-workers where the coordination of Zn^{2+} to the lone pairs of nitrogen atoms in their cyclam cored dendrimer resulted in an intense naphthyl fluorescence.³⁰

Another powerful tool to sense inorganic ions has originated in the field of electrochemistry and has been thoroughly developed by Astruc and co-workers.^{7, 31, 32} They designed redox-active metallodendrimers capable of electrostatically binding oxo-anions, including adenosine-5'-triphosphate, H_2PO_4^- or halogens and followed their concentration through variations in cyclic voltammetry of ferrocenyl decorated dendrimers (Figure 4.4).

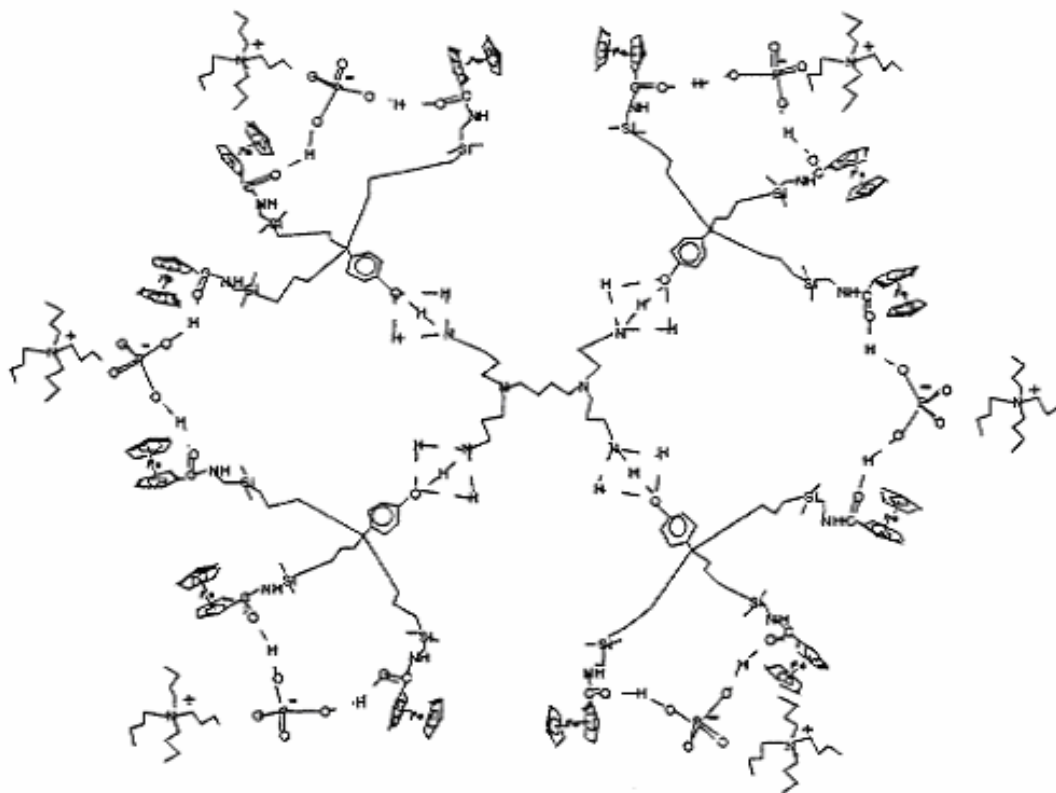


Figure 4.4 Example of electrostatic coordination of H_2PO_4^- at the periphery of supramolecular dendrimer decorated with termini ferrocenyl moieties³²

IV. 1. 3 Dendrimers as organic compound sensors

Sensing methods based on the variations of optical properties of the dendrimer upon binding the analyte are also common and useful in the detection of organic molecules. Others, more physical, are also successfully applied as reported below.

During the past few years, growing interest in the detection of Volatile Organic Compounds has led many research groups to study the application of dendrimers immobilized on surfaces for this purpose. Different physical detection methods were used such as mass balance measurements,^{11, 33-35} cyclic voltammetry³⁶ or electric conductivity measurements.^{37, 38} As a general rule, two types of interaction enable sensing of two categories of solvents: $\pi-\pi$ interactions between planar cycles favour recognition of hydrophobic compounds with polyphenylene dendrimers whereas hydrophilic PAMAM dendrimers were highly sensitive to alcohols or water due to hydrogen bonding.

Many papers report colour or fluorescence changes that occur as consequence of hydrogen interactions between the host dendrimer and the detected guest molecules for the design of sensors,³⁹⁻⁴² some of which are highlighted below.

Pu and co-workers, for example, developed optically active dendrimers with a binaphthyl core and successfully used them as enantioselective fluorescent sensors for chiral aminoalcohols⁴³ and mandelic acid.⁴⁴ Through hydrogen bonding interactions, the acid can enhance the fluorescence of these dendrimers whereas the alcohols decrease it.

De Cola and co-workers exploited the multiple hydrogen-bonding ability of the Hamilton receptor to detect barbiturates.⁴⁵ Upon complexation of these molecules to the receptor site, a photo-induced energy transfer from the receptor to the bipyridylrhodium moiety of the probed molecules is easily monitored by fluorescence variations (Figure 4.5).

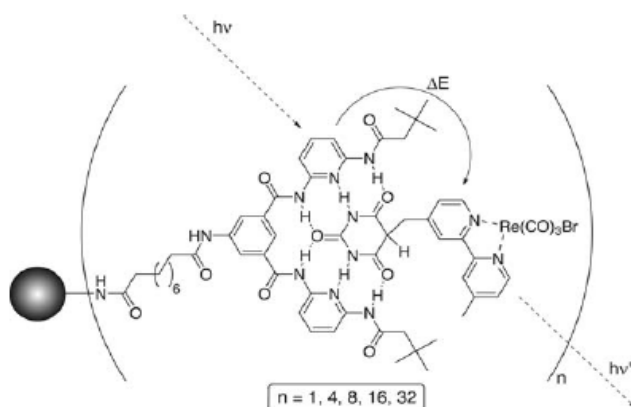


Figure 4.5 Hamilton receptor of barbiturates ⁴⁶

A more sophisticated means of exploiting dendrimers as sensors for organic molecules is to use them as a “cage” able to physically entrap target molecules. This idea of a “dendritic box” was pioneered by Meijer and co-workers in 1994.⁴⁷ They designed a polypropyleneimine dendrimer capable of physically encapsulating Rose Bengal and further releasing it after chemical reactions at the periphery of the macromolecule by breaking the outer shell (Figure 4.6).

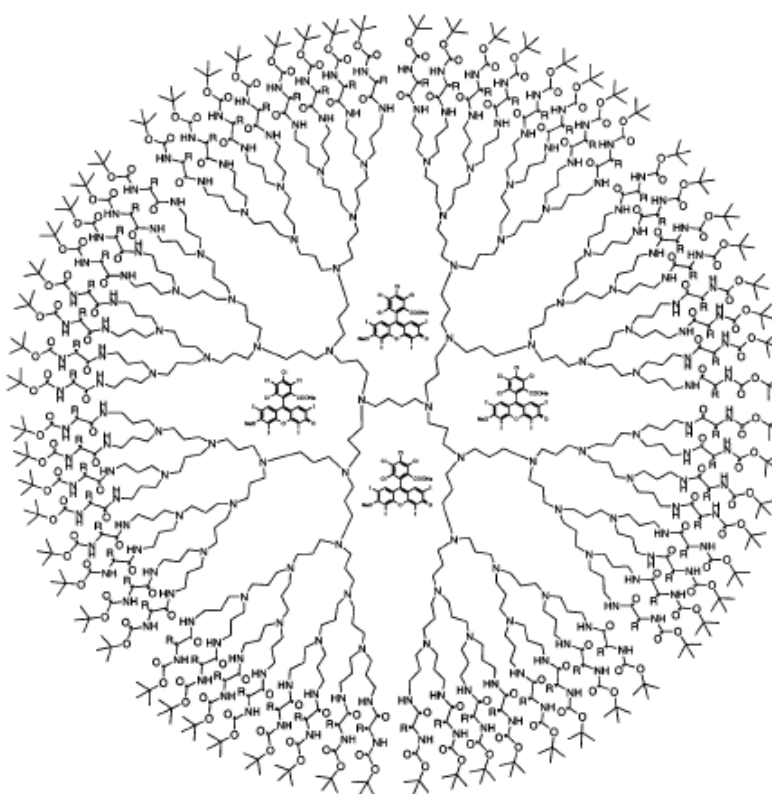
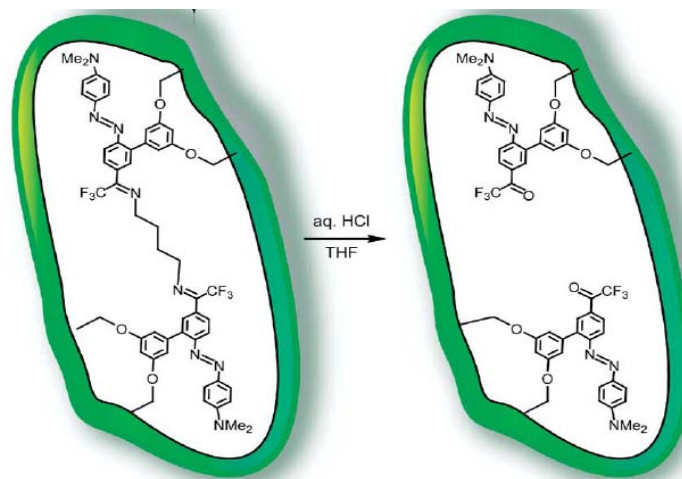


Figure 4.6 Meijer's dendritic box with Bengal Rose molecules inside (reproduced from ⁴⁸)

Following this principle, the research groups of Zimmerman⁴⁹ and Suslick⁵⁰ developed the concept of Molecular Imprinting inside Dendrimers. Cavities created inside dendrimers, following removal of templates, were able to host specific amines and alcohols via hydrogen bonding interactions. This chemical information was translated into optical signals by azo-dye chromogenic reporters, turning the system into highly selective sensors for amines and alcohols (Scheme 4.2).



Scheme 4.2 Creation of specific amines and alcohols sensors via Molecular Imprinting inside Dendrimers⁴⁹

In conclusion, it has been shown that dendrimers can be used as ideal candidates for recognition of gases, ions or molecules because they induce significant and quantitative changes in physical, electrochemical or optical properties of the resultant complexes with the analytes. In addition to their high sensitivity, they also present good selectivity, and their physical persistence and robustness give them a promising future as chemical sensors.

IV. 2 Sensing reducing agents through fluorescence activation of a Polyhedral Oligomeric Silsesquioxane⁵¹

Besides the abovementioned examples relying mainly on non-covalent interactions between the substrate and the dendritic receptor, the complete chemical transformation of the latter in the presence of the analyte has not been widely investigated. For instance, it has been shown that -OH terminated PAMAM dendrimers displayed stronger luminescence upon oxidation of hydroxyl groups,⁵² however the complete characterization of the luminescent centers was not reported.

We thus investigated the use of Polyhedral Oligomeric Silsesquioxanes decorated with vinyl biphenyl units to provide novel fluorescent chemosensors. The 4-vinyl biphenyl chromophore was chosen for its ability to be chemically modified, its relatively high Photoluminescence Quantum Yield (PLQY) and its weak oxygen quenching.⁵³

IV. 2. 1 Synthesis of a dialdehyde functionalized Polyhedral Oligomeric Silsesquioxane and its reduced alcoholic form

The macromolecule synthesis involves a Suzuki coupling reaction between styrene boronic acid and bromobenzenedicarbaldehyde⁵⁴ to give the dendron arm **M7** in good yield (82 %). Grubbs cross-metathesis between the readily available octavinylsilsesquioxane and **M7** allows the synthesis of the macromolecule **S1** in good yield (78 %), see Scheme 4.3. The side product resulting from the self metathesis of **M7** was separated chromatographically.

M7 and **S1** were characterized by Electrospray Ionisation (ESI) and Matrix Assisted Laser Desorption/Ionisation (MALDI) mass spectrometry, microanalysis and routine NMR techniques (¹H and ¹³C): the disappearance of the terminal vinyl of **M7** corresponds to the appearance of the internal double bond attached to the inorganic core (signals at 6.49 ppm and 7.51 ppm in the ¹H-¹H COSY 2D NMR spectrum), see Figure 4.7.

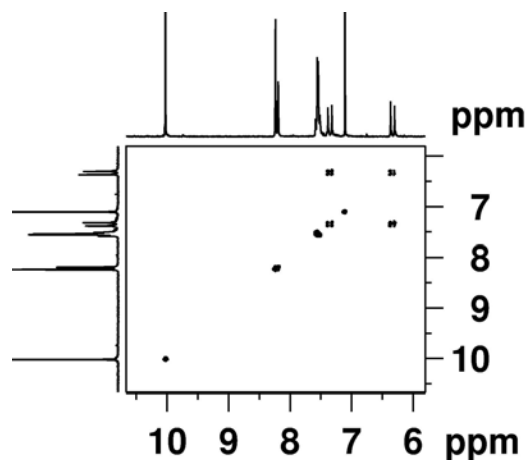
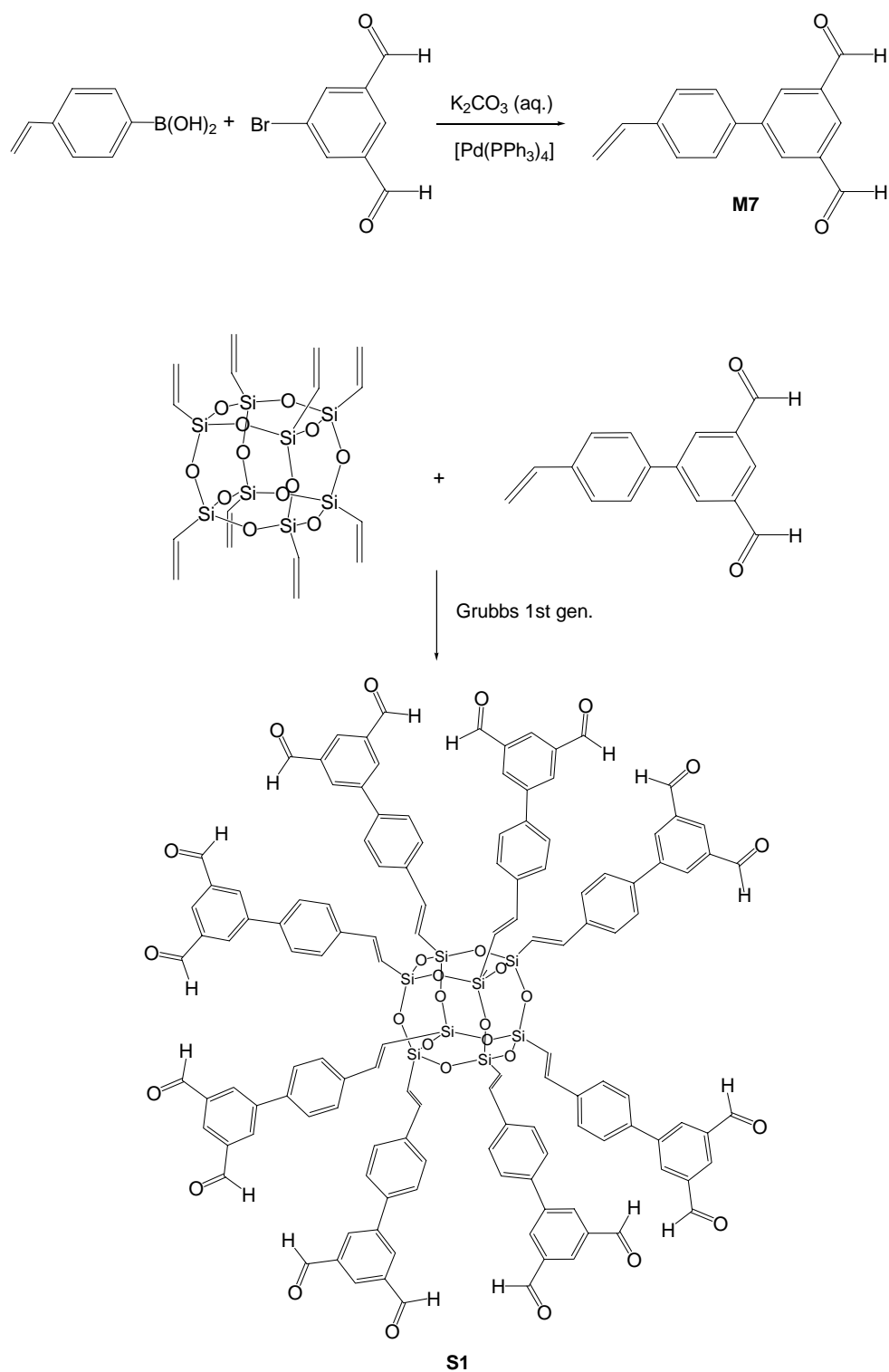
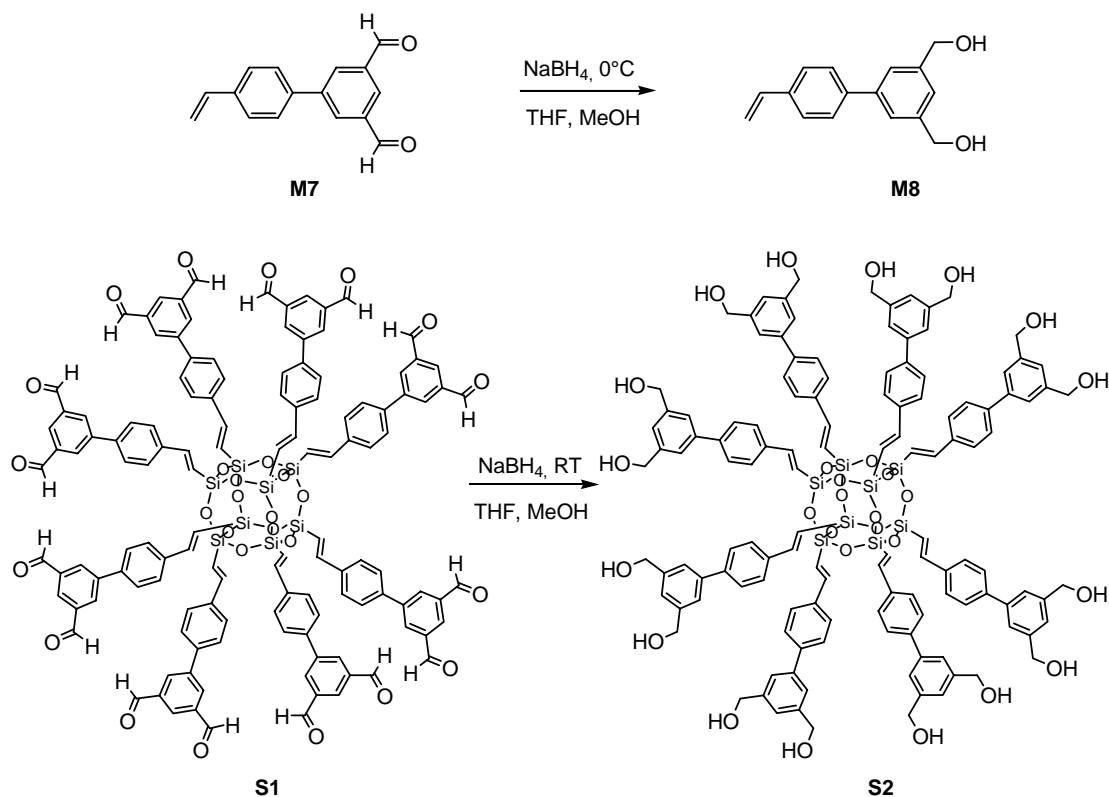


Figure 4.7 ¹H-¹H COSY 2D NMR of **S1**



Scheme 4.3 Synthesis of monomer **M7** and macromolecule **S1**

M7 and **S1** were next reduced with NaBH_4 to the primary alcohols, **M8** and **S2**, as illustrated in Scheme 4.4.



Scheme 4.4 Reduction of **M7** and **S1** with NaBH_4 affording **M8** and **S2**

IV. 2. 2 Molecular dynamics investigations of both macromolecules **S1** and **S2**

Numerical simulations at various levels of theory can be used to determine molecular conformations and to gain insight into electronic properties.⁵⁵⁻⁵⁷ In the context of dendritic molecules, hydrodynamic radii, extension and back-folding, crowding and arm flexibility have then been investigated as a function of dendrimer generation and solvent quality.⁵⁸⁻⁶² Assemblies of nanostructured POSS networks have been studied by lattice Monte-Carlo simulations in order to explore the effect of linker length on porosity and spatial distributions of the building blocks in 3D structures.⁶³ Other examples are based on numerical simulations compared with experimental data, to provide insight into the properties of single hybrid organic-inorganic nanomaterials.^{64, 65, 63, 66}

To gain insight into the molecular conformations of the two macromolecules **S1** and **S2**, molecular dynamics calculations were completed and the outcome is presented in Table 4.1 and Figure 4.8.

Table 4.1 For each macromolecule **S1** (■), **S2** (▲): Photoluminescent quantum yield (PLQY), Peak and standard deviation (δ) of the normalized populations of the radius of gyration, extension of the vinyl biphenyl branches from the Si atom of the POSS core to C₃ and C₁₀ and distance between C₁₀ atoms located on adjacent arms. Molecular Dynamics was completed in vacuum and at 400 K

	PLQY	Rg (δ) / Å	Si-C3 (δ) / Å	Si-C10 (δ) / Å	C10-C10 (δ) / Å
S1	0.00	10.17 (0.04)	4.12 (0.07)	11.12 (0.13)	15.8 (2.4)
S2	0.10	10.19 (0.05)	4.08 (0.07)	11.12 (0.14)	15.8 (2.8)

From this approach it is clear that all the parameters accessible by molecular dynamics indicate a similar structure and range of conformation for both **S1** and **S2**: a radius of gyration of ~ 10.2 Å, branch extension peaks of ~ 4.1 Å and ~ 11.1 Å for Si-C3 and Si-C10, as well as a distance between the tips of the vinyl biphenyl groups, C10, located on two adjacent arms, of ~ 15.8 Å. As the chemical grafting of the arms to the POSS core increases the degree of freedom (vibrational, translational, rotational) of the macromolecule relative to the free ungrafted chromophore,^{67, 68} the gaussian distributions in Figure 4.8 illustrates the large number of conformations accessible to the eight arms of the macromolecule.

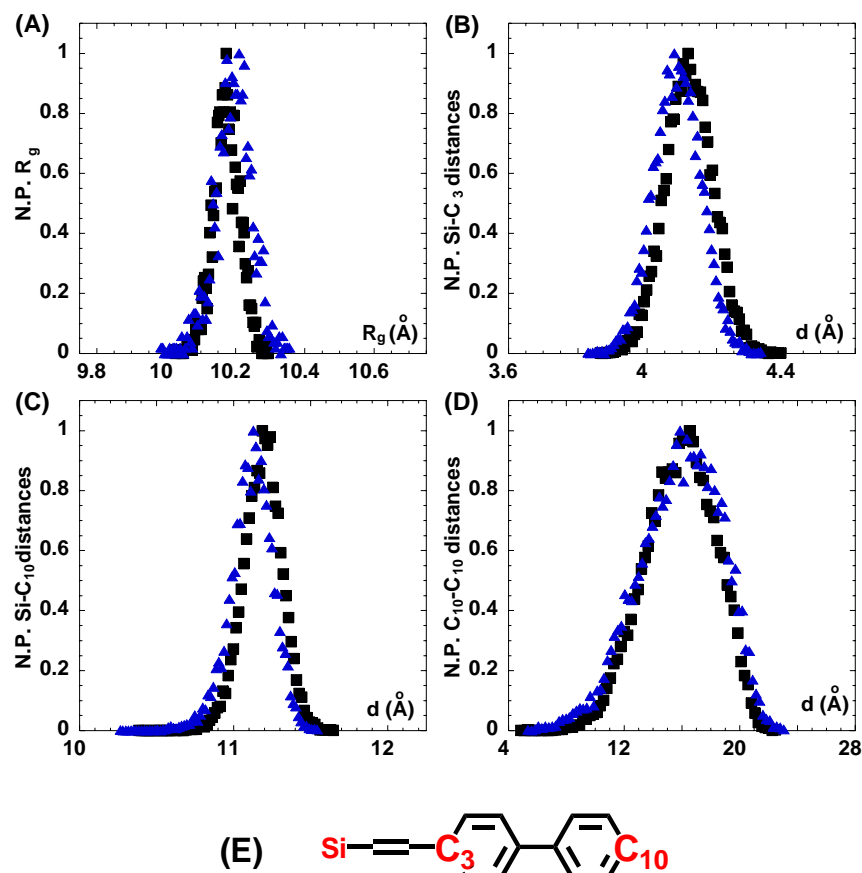


Figure 4.8 For each macromolecule S1 (■), S2 (▲): Normalized population of the radius of gyration (A) extension of the vinyl biphenyl branches for from the Si atom of the POSS core to C₃ (B) and C₁₀ (C), distance between C₁₀ atoms located on adjacent arms, and distance between the Si atom at the corner of the cube and C₁₀ (D), atom labeling (E). Molecular Dynamics was completed in vacuum and at 400 K

Figure 4.8B shows a single peak in the average distribution of the silicon to carbon distances along the eight branches. If two peaks were observed it would then indicate that the double bonds in some arms are *E* (~ 4.1 Å), i.e. more extended, while others are *Z*. For the *Z* configuration, C₃ would be (~ 3.2 Å according to molecular modelling) However the current results of the molecular dynamics simulations of both macromolecules illustrate the presence of a single (*E*) configuration for the olefinic bond as indicated by the C3 extension and consistent with the NMR data ($^3J_{HH} = 19.3$ Hz, SiCH=H). For the two macromolecules, the populations of the Si-C₁₀ distance show a narrow single peak, Figure 4.8C, indicating that the vinyl bridge is stiff enough to give the arms a fully extended conformation regardless of the thermal agitation. In addition, the structure of the macromolecules remained similar in both reduced and non reduced forms. The anisotropy of the moment of inertia remains very small, indicating an isotropic average branch distribution consistent with a spherical shape (Figure 4.9).

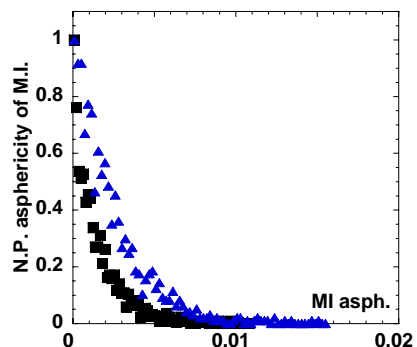


Figure 4.9 For each macromolecule S1 (■) and S2 (▲): Normalized population of the asphericity of the moment of inertia. All simulations were completed in vacuum at 400 K

All the modelling data demonstrate that from a molecular dynamics view point, there is little variation in the conformation of the arms between the two macromolecules S1 and S2 presented in this study regardless of their functional groups: all exhibit similar spherical shape, extension of the arms, angle between the centre of the POSS core, presence of a single *trans* configuration for the double bond, etc.

IV. 2. 3 Photoluminescence spectral characteristics of monomers M7 and M8 and macromolecules S1 and S2

The photophysical properties of these materials were investigated in a THF-methanol mixture (7:3 vol. ratio) at room temperature and the resulting absorbance (Abs) spectra are shown in Figure 4.10A.

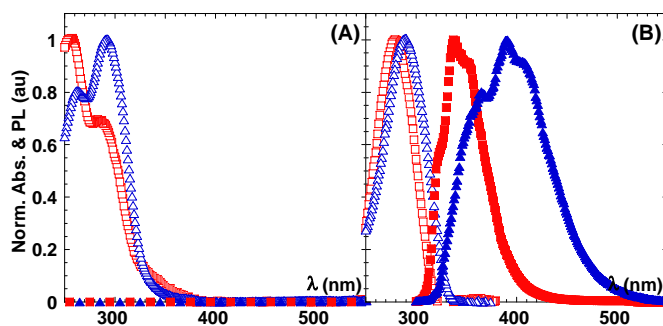


Figure 4.10 Normalized absorbance (Abs., empty symbols) and luminescence (PL, full symbols) spectra associated with the un-reduced (A) and reduced (B) compounds M (■) and S (▲). Measurements were completed at room temperature in THF-methanol solution

Not surprisingly, the grafting to the POSS core led to slight alterations in the absorption spectra of the vinyl biphenyl based chromophore, such as the change in relative intensity of the two absorption bands and a red shift (about 7 nm) of the lower energy absorption peak, which can be explained by a slight increase of the conjugation length or a slight inductive effect via the delocalization of the vinyl biphenyl electrons to the silicon atoms.^{67, 68} Although vinyl biphenyl itself is highly luminescent, photoluminescence (PL) measurements showed that the emission is completely quenched by the presence of the aldehyde functionalities.

As **M7** and **S1** were reduced with NaBH₄ to the primary alcohols, **M8** and **S2**, see Scheme 4.4, the appearance of the alcohol function on the macromolecule **S2** was confirmed by ¹H NMR spectroscopy. A doublet at 4.60 ppm (CH₂OH) and a triplet at 5.30 ppm (CH₂OH) replaced the former singlet at 10.20 ppm assigned to the aldehyde groups. The characteristic pattern of the internal double bond attached to the corner of the inorganic core previously observed in the ¹H-¹H COSY 2D NMR spectrum for **S1** (Figure 4.7) was still present in the case of **S2**. Monomer **M8** was fully analyzed by routine NMR techniques and microanalysis; For **M7** at room temperature, NaBH₄ not only reduced the aldehydic function but also the terminal double bond, whilst under the same conditions the internal double bond of the macromolecule **S1** was unaffected. This can be explained by the easier reduction of monosubstituted double bonds compared to disubstituted ones due to steric factors. Another contribution may be found in the macromolecule architecture for which the well buried olefin is protected by the peripheral groups preventing contact between the olefin and the reducing agents. The peripheral aldehydic groups create a polar shell whereas vinyl biphenyl groups provide the interior of the macromolecule with apolar properties possibly repelling polar molecules and reducing agents from the double bond.

The photophysical properties of **S2** and **M8** are presented in Figure 4.10B. The absorbance peaks are slightly altered when compared to the unreduced species. The environment and functional groups are known to influence the optical transition strength,⁶⁷ leading in the present case to the disappearance of the absorbance band located at high energy (~ 240-250 nm) and the relative strengthening of the transition at lower energy (~ 285 nm). The reduced macromolecule, **S2**, has absorbance features much more similar to that of its parent small molecule, **M8**, and to those of other vinyl biphenyl based compounds^{53, 67, 68} than does the aldehyde macromolecule, **S1**.

The main difference in the photophysical properties of the oxidised and reduced molecules is the recovery of the photoluminescence properties of the chromophores on reduction, confirming that the aldehyde molecules are responsible for the quenched emission. Indeed the reduced free chromophores **M8** and **S2** display emission with a substructure similar to vinyl biphenyl homologues.⁶⁸ The maximum values of their PLQY are respectively 13 % (**M8**) and 10 % (**S2**) at saturation. As expected, the POSS derivative with the reduced arms shows a red shift and broader spectral emission associated with a slight electronic delocalisation on the POSS core and a larger range of conformations accessible to the macromolecule compared with the free arm.

IV. 2. 4 Reducing agents titration with S1

The promotion of luminescence on reduction allows the use of the macromolecule to monitor the reducing properties of solution environments. This ability was confirmed by titrating **S1** with NaBH_4 in THF/MeOH (7/3) and with LiAlH_4 in THF, see Figure 4.11. A steady increase in the PLQY of the reduced macromolecular species is observed until a plateau at 16 equivalents is reached corresponding to the complete conversion of the aldehyde groups into primary alcohols to obtain **S2**, see Scheme 4.4. Within experimental error, NaBH_4 and LiAlH_4 both give the same saturation values of about 10 % PLQY, see Figure 4.11.

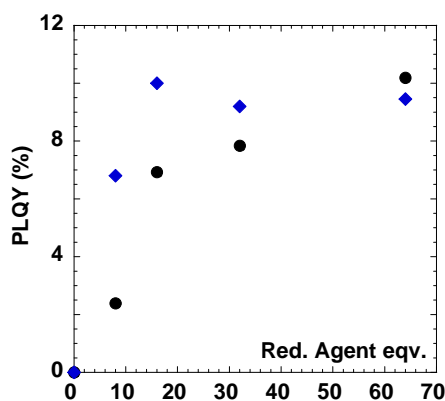


Figure 4.11 PL efficiency of the aldehyde based macromolecule in THF-methanol solution as a function of reducing agent equivalent, NaBH_4 (♦) and LiAlH_4 (●). Measurements were completed at room temperature with 290 nm as the excitation wavelength

PLQY and the amount of reducing agents have a “non-linear” but continuous relation. This behaviour is very common to many detectors or sensors and, combined with calibration curves, make **S1** a promising hybrid organic/inorganic photoluminescent

chemosensor.

While clear solutions were observed when adding NaBH_4 at any ratio, salts precipitated after the first addition of LiAlH_4 . This precipitation may explain the discrepancies noticed in Figure 4.11 between the PL efficiencies for the two reducing agents. In addition, similar switching on of the luminescence has been observed with excess BH_3 as a reducing agent.

IV. 2. 5 Conclusion

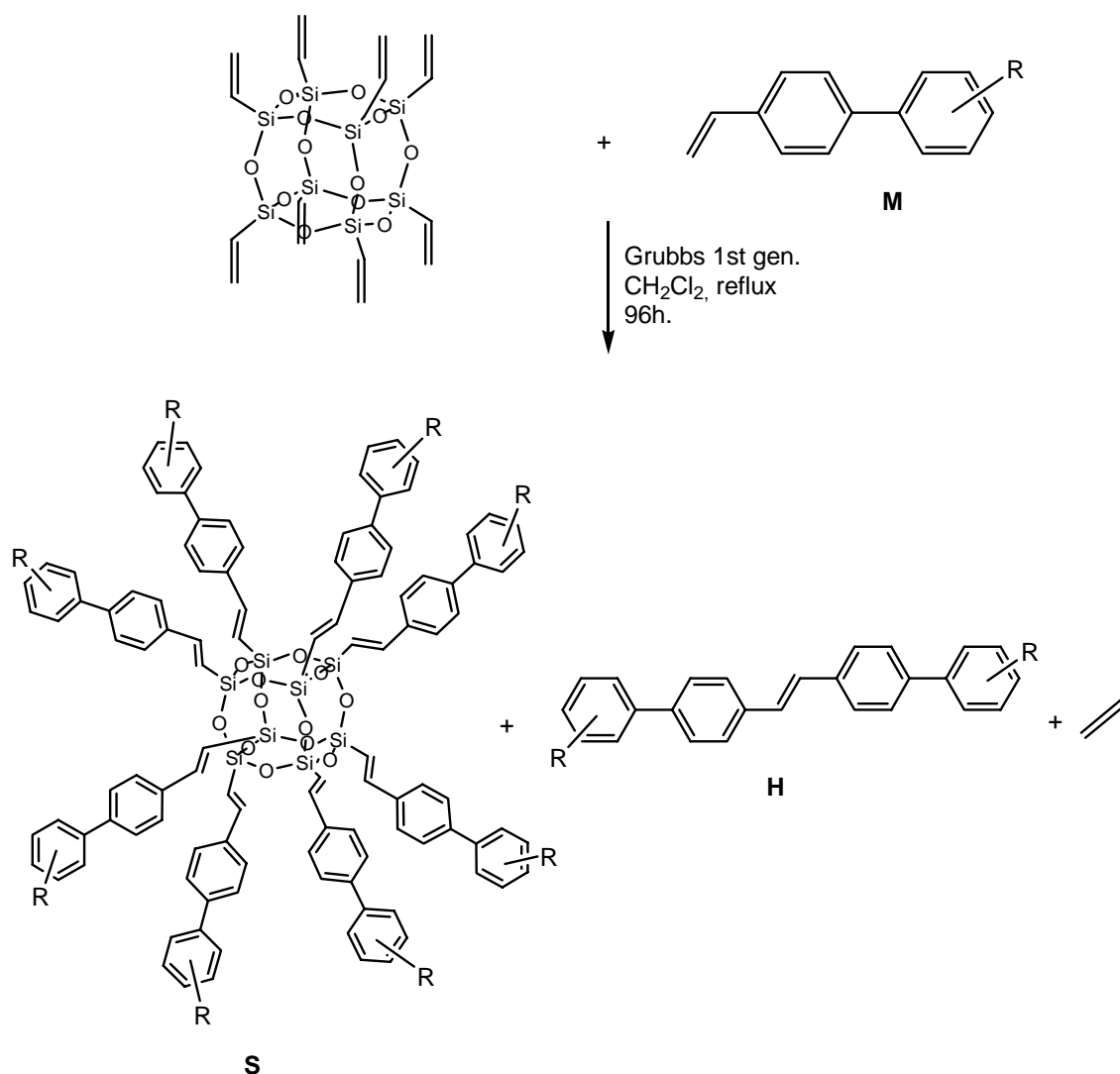
Complementing chemical sensor macromolecules based on non-covalent interactions between substrates and dendritic receptors, we have shown that a Polyhedral Oligomeric Silsesquioxane decorated with eight peripheral 4'-vinylbiphenyl-3,5-dicarbaldehyde groups displays the unusual ability to become luminescent when exposed to a reducing environment such as NaBH_4 , LiAlH_4 or BH_3 . We have, thus, demonstrated that the photoluminescence of POSS molecules can be used as a quantitative sensor for hydridic reducing agents.

In addition, a few drops of ethylenediamine added to **S1** also switch on the fluorescence of the macromolecule, whilst butanediol or TMEDA do not. Further studies would be required to understand this phenomenon, but it may be associated with Schiff base formation.

The synthesis of this dialdehyde functionalised POSS **S1** and its application in titrating reducing agents have not only proven to be successful but have also highlighted the potential of the vinylbiphenyl chromophore when anchored onto the cube. POSS-chromophore hybrid macromolecules have also attracted interest, among other reasons, because of their better casting and layer forming properties than those of pure chromophores, especially in the context of applications including organic semiconductors and solution processable light emitting diodes.⁶⁹⁻⁷¹ Additionally, the attachment of luminescent chromophores to the rigid POSS core is of scientific interest with regard to its effect on fluorescence quantum yield as well as for the design of multifunctional colloidal molecules.^{68, 72} We thus decided further to extend our studies by building a new family of photoluminescent vinylbiphenyl terminated POSS cored dendrimers and exploring their photoluminescent properties.

IV. 3 Synthesis and characterization of photoluminescent vinylbiphenyl decorated Polyhedral Oligomeric Silsesquioxanes ⁷³

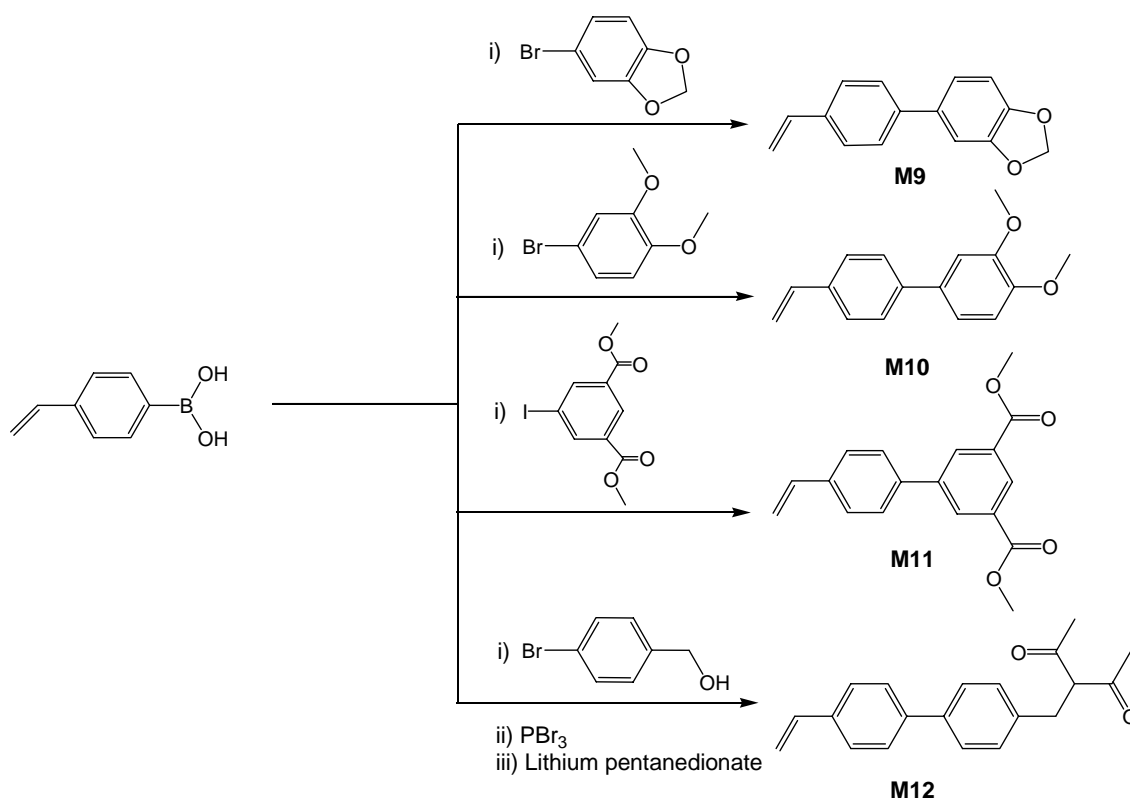
Four macromolecules (**S**) have been prepared via Grubbs metathesis between the readily available octavinylsilsesquioxane and vinylbiphenyl decorated monomers (**M**) (Scheme 4.5). During the Grubbs coupling, the homometathesis side product (**H**) from **M** was always produced together with the macromolecule and ethene. The reaction system is even more complex, as the alkene metathesis is reversible (equilibria); in the given case, the removal of ethene assures complete conversion from octavinylsilsesquioxane + (**M**) to (**S**) + (**H**). The cross-metathesis between two POSS species was never observed probably for steric reasons.



Scheme 4.5 Synthetic pathway of macromolecule (**S**) and homogrubbs (**H**) from vinylbiphenyl monomer (**M**) and octavinylsilsesquioxane

IV. 3. 1 Synthesis and photoluminescent properties of vinylbiphenyl monomers

The chemical functionalising groups R were chosen for their abilities to further elaborate on the resulting compound structure and properties by simple chemistry. In this context, four monomers (**M**) were synthesised via Suzuki coupling between styreneboronic acid and the desired haloaromatic compound. This yielded chromophores with a vinylbiphenyl backbone decorated with one methylenedioxy group **M9**, two methoxy groups **M10**, two methyl dicarboxylate groups **M11** and one acetylacetonate moiety **M12** (Scheme 4.6). The two first monomers **M9** and **M10** can lead, after deprotection, to diol decorated biphenyls which allow subsequent functionalization through a variety of reactions such as transesterification or nucleophilic substitution which could lead among other examples to novel polyester nanostructured materials for coating and fiber related applications.⁷⁴ Dimethyl ester groups present on **M11** are interesting candidates for polymerisation and the formation of porous hybrid materials as well as photoluminescent thin films whilst the acetylacetonate function of **M12** show great potential in the binding of molecules like metals including lanthanides for the purpose of sensing⁷⁵ and extraction applications.



Scheme 4.6 Formation of monomer (**M**) via Suzuki coupling between styreneboronic acid and the desired haloaromatic compound

The photophysical properties and mass characterisation of these four compounds were then investigated through a combination of absorbance (Abs), photoluminescence (PL), photoluminescence excitation (PLE) measurements and high resolution mass spectroscopy as reported in Figure 4.12 and Table 4.2.

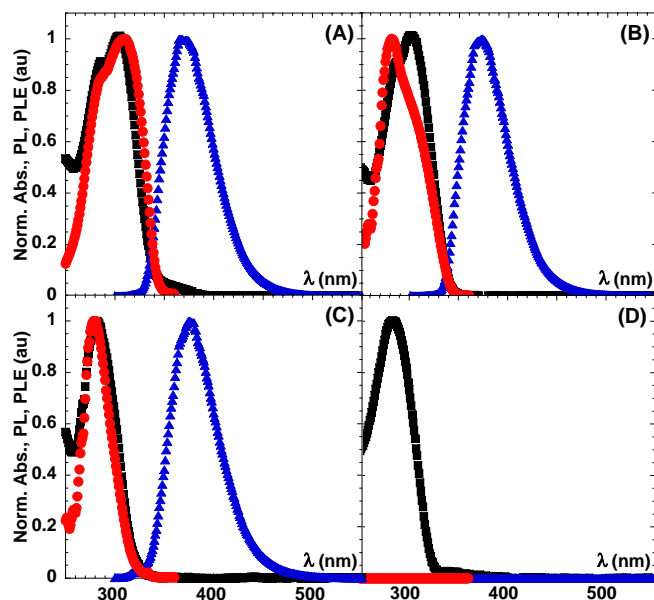


Figure 4.12 Normalized absorbance (Abs., ■), photoluminescence (PL, ▲, λ_{exc} : 290 nm) and photoluminescence excitation (PLE, ●, λ_{detec} : 340 nm) spectra associated with the monomers **M9** (A), **M10** (B), **M11** (C) and **M12** (D). Measurements were completed in THF and at room temperature

The photophysical properties of the four monomers are fairly consistent with those of vinylbiphenyl which is characterised in THF by absorption and photoluminescent peaks at 278 nm and 317 nm, respectively,^{53, 68} while the observed shifts result from the slight perturbation of the electronic properties induced by the functional groups, see Table 4.2. The variation in PLQY observed between the different monomers can be rationalised by the degree of freedom, i.e. rotational and vibrational, associated with the external functional groups as would be expected in rigidochromic systems.^{76, 77} For instance, the methoxy groups of **M10** induce an increase of the PLQY when compared to the pure vinylbiphenyl chromophore, 60 % and 45 % respectively, whereas the PLQY decreases dramatically passing from the rigid diol protected monomers **M9** and **M10** to the more flexible ester **M11**. The even lower PLQY of **M12** may be associated with the extra CH₂ providing further flexibility to the functional groups when compared to the other monomers. Because of the low signal to noise ratio the PL and PLE spectra of **M12** are not displayed in Figure 4.12. For each monomer, the close match between the PLE spectra

and the absorbance testifies to the high purity of the prepared compounds, further confirmed by High Resolution Mass spectroscopy (HRMS, Table 4.2)

Table 4.2 High Resolution Mass Spectroscopy (HRMS), Absorbance peak, position of the first photoluminescence peaks and photoluminescence quantum yield (PLQY) measured at the absorbance maximum

Structure	M9	M10	M11	M12
HRMS (g/mol)	225.0921 requires 225.0916	263.1046 requires 263.1048	297.1129 requires 297.1127	293.1541 requires 293.1542
Abs. Peak (nm)	301	300	280	292
1 st PL peak (nm)	374	374	355	340
PLQY (%)	40 @ 300 nm	60 @ 300 nm	14 @ 280	< 1 @ 285 nm

IV. 3. 2 Synthesis and photoluminescent properties of vinylbiphenyl functionalized Polyhedral Oligomeric Silsesquioxanes

Monomers (**M**) were then coupled to octavinylsilsesquioxane via a Grubbs type reaction affording the corresponding macromolecules (**S**), as illustrated in Figure 4.13. After precipitation in a mixture of ethyl acetate (120 mL) and petroleum ether (40-60) (500 mL), the four macromolecules were subjected to column chromatography, and their purity was attested on the one hand by both microanalysis and Matrix Assisted Laser Desorption/Ionization (MALDI) mass spectroscopy (Table 4.3) and on the other hand by the cross peaks which appear on their $^{29}\text{Si}^1\text{H}$ HMQC 2D NMR spectra, illustrated in Figure 4.14 for the macromolecule **S4**. The cross peaks correspond to the clean coupling between a corner silicon atom and the alkenyl protons at 6.49 ppm and 7.51 ppm. The sharp cross peaks indicate that the cube is intact and unique and that each corner is equivalent. Similar observations have been made for the other four macromolecules highlighting the uniqueness and full substitution of each cube.

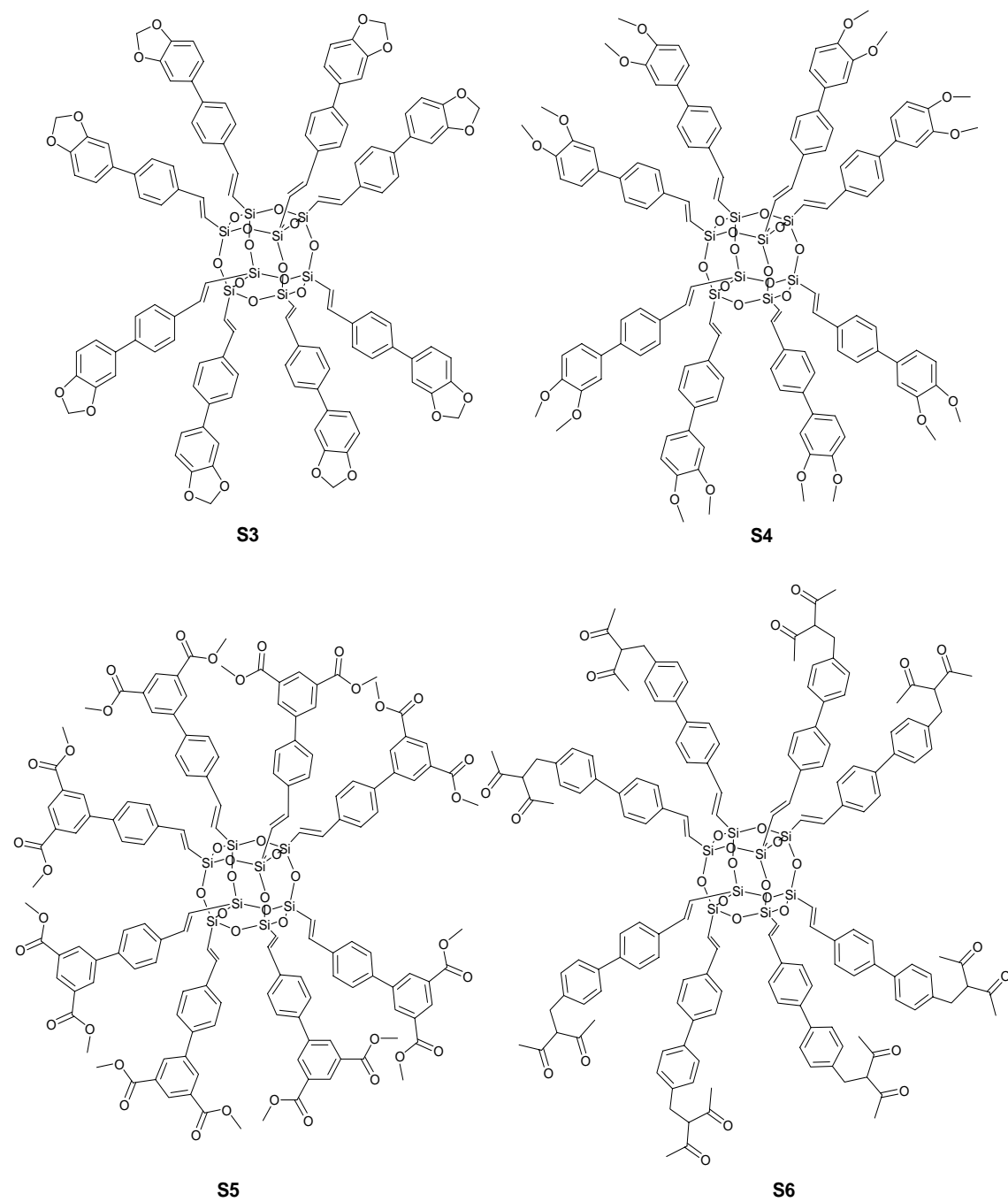


Figure 4.13 Representation of macromolecules, S3, S4, S5 and S6

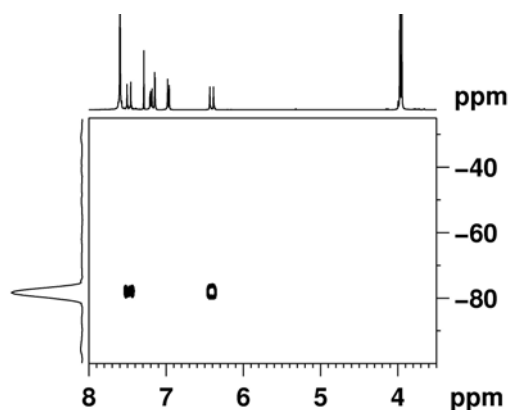


Figure 4.14 $^{29}\text{Si}^1\text{H}$ HMQC 2D NMR of S4

The optical characterisation and mass spectroscopic characterisation of the macromolecules are reported in Figure 4.15 and Table 4.3.

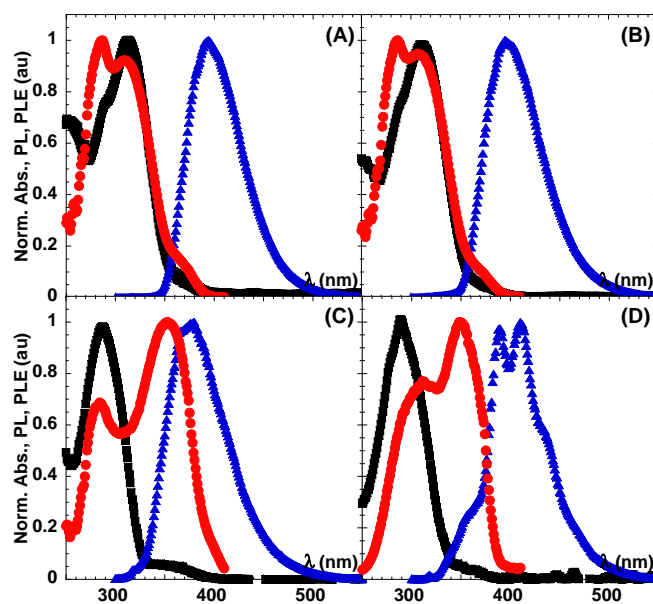


Figure 4.15 Normalized Abs. (■), PL (▲, λ_{exc} : 290 nm) and PLE (●, λ_{detec} : 420 nm) spectra associated with the macromolecules S3 (A), S4 (B), S5 (C) and S6 (D). Measurements were completed at room temperature

Due to a more extensive electron delocalisation into the POSS core, grafting **M** monomers onto the POSS cube leads to the expected slight red shift in the absorbance and PL spectra compared to the free dendrons.^{53, 68} Broader PL spectra are also observed for the four **S** macromolecules as more conformations become accessible to the chromophores.⁶⁷ The PLQY values seem to increase, but it is difficult to be certain as each macromolecule (especially **S4** and **S5**) is contaminated by a small amount of side product. The side products give rise to absorption features at *ca.* 345 nm, confirmed by extra peaks in this region in the PLE

spectrum. These photophysical methods seem to provide the only analytical technique that reveals the presence of this side product. In the case of **S3** and **S4**, the side-products precipitated as powders during the course of the Grubbs coupling and were isolated by filtration, whilst silica gel column chromatography was performed for **S5** and **S6** as both product and side product were soluble in the reaction mixture

Table 4.3 Matrix Assisted Laser Desorption/Ionization (MALDI) mass spectroscopy, absorbance peak, position of the first photoluminescence peaks and photoluminescence quantum yield (PLQY) measured at the absorbance maximum

Structure	S3	S4	S5	S6
MALDI (g/mol)	2202.44 requires 2201.84	2330.3 requires 2329.92	2802.41 requires 2801.08	2768.93 requires 2769.24
Abs. Peak (nm)	311	310	285	288
1 st PL peak (nm)	382	380	375	391
PLQY (%)	< 50 @ 300 nm	< 55 @ 300 nm	< 11 @ 290 nm	< 3 @ 290 nm

IV. 3. 3 Photoluminescent properties of homometathesis side products

The **H** side products were identified by HRMS as arising from self metathesis of the **M** monomers (Table 4.4 and Figure 4.16). In the mixtures **S3** + **H1** and **S4** + **H2**, the grafted **M** segments possess low solubility in apolar solvents, not much enhanced by the substituents R. In the POSS compounds **S**, the grafted **M** segments have worse possibilities for higher regular crystallization than in the **H** products, which are hence less soluble and precipitate more easily. In the case of **S5** and **S6**, this effect is cancelled by the high solubility of the **M** segments given by the ester groups on them. The chromatographic behavior of both mixtures **S5** + **H3** and **S6** + **H4** is thus dominated by mutual affinity and similar high solubility making their separation more complex.

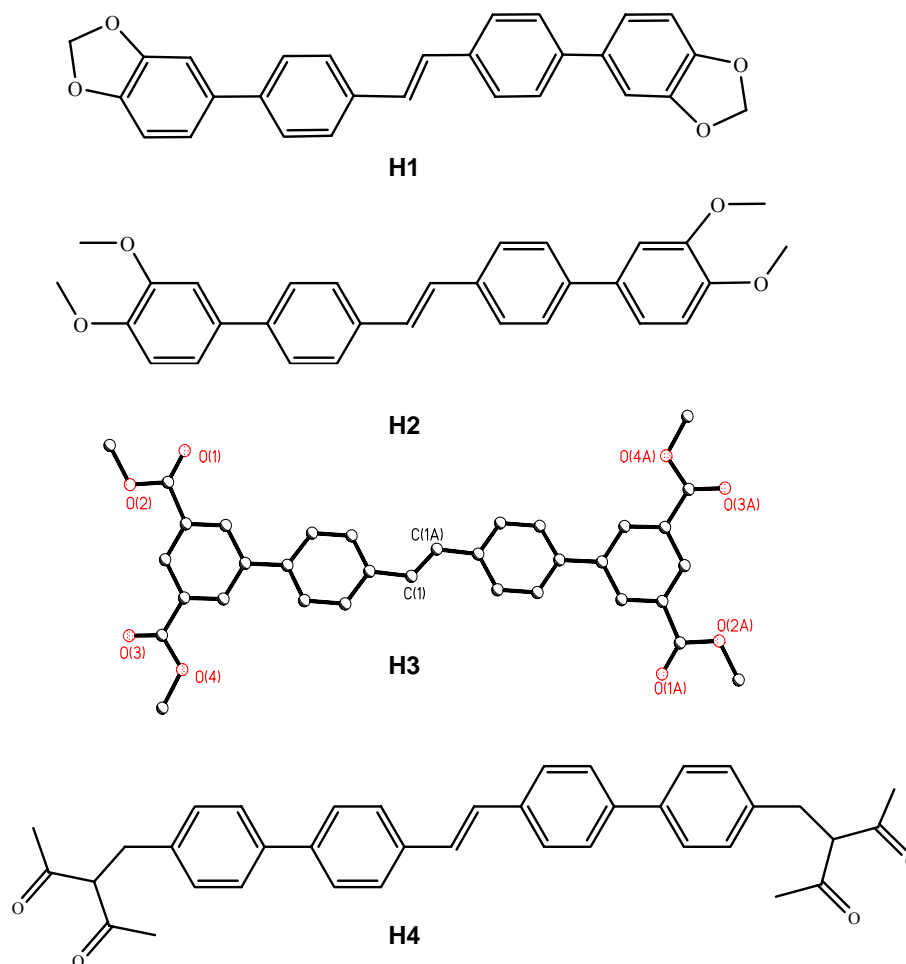


Figure 4.16 Representaion of homometathesis **H1**, **H2**, **H3** (X-Ray crystal structure, see Annexe II) and **H4**

H3 with substituent MeO_2C - groups was characterised crystallographically (see Annexe II for details). The X-ray structure of **H3** reveals that the molecule is planar, has an *E* double bond and is disposed about a centre of symmetry at the centre of the double bond. The central bond length is $1.330(3) \text{ \AA}$. The terminal aryl rings are inclined by 26° with respect to the central aryl rings whilst the ester substituents are essentially coplanar with the terminal aryl rings.

One discrepancy can be notice for **H4**, as a mass of 418.32 g/mol was found by both Electro-Spray Ionisation (ESI) and Chemical Ionisation (CI), whilst a mass of 556.38 g/mol would have been expected. The obtained mass 418.32 g/mol corresponds however to the dimer where the benzylic acetylacetonate functions are both oxidized to form carboxylic acid groups, such a process being likely to occur in the course of the mass spectroscopy measurement (Figure 4.17).

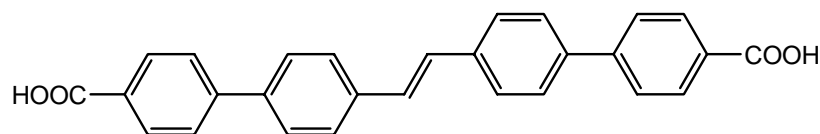


Figure 4.17 Carboxylic group terminated homomethathesis product

The photophysical properties of these homomethathesis products are shown in Figure 4.18 and Table 4.4.

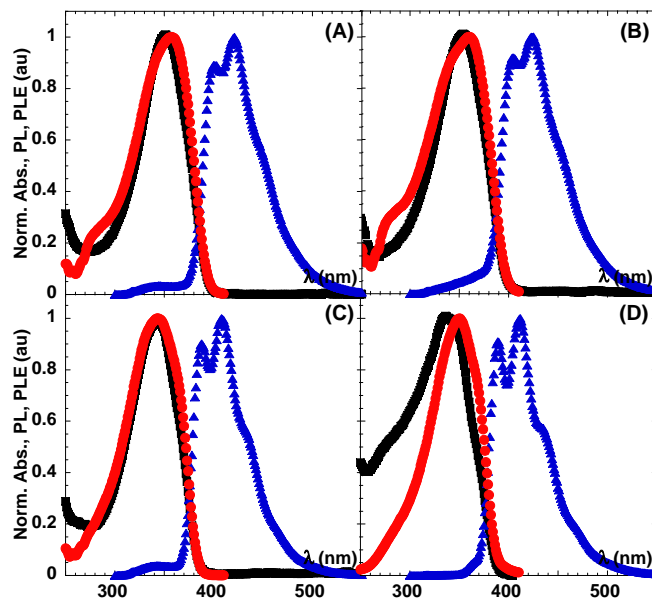


Figure 4.18 Normalized Abs. (■), PL, (▲, λ_{exc} : 290 nm) and PLE (●, λ_{detec} : 420 nm) spectra associated with the homogrubbs **H1** (A), **H2** (B), **H3** (C) and **H4** (D). Measurements were completed at room temperature

Table 4.4 High Resolution Mass Spectroscopy (HRMS), Absorbance peak, position of the first photoluminescence peaks and photoluminescence quantum yield (PLQY) measured at the absorbance maximum

Structure	H1	H2	H3	H4
HRMS (g/mol)	421.1436 requires 421.1440	453.2061 requires 453.2066	565.1864 requires 565.1860	*
Abs. Peak (nm)	350	350	345	335
1 st PL peak (nm)	402	400	390	390
PLQY (%)	66 @ 350 nm	80 @ 350 nm	70 @ 350 nm	30 @ 335 nm

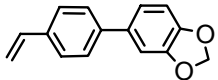
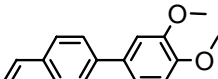
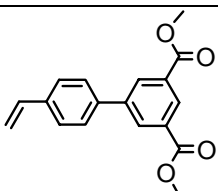
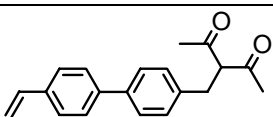
* acid group formation see text for details.

As a result of the increase in the conjugation length associated with the dimerisation, the expected red shift of both the absorption and PL features for the four homometathesis products compared with the free monomers is observed, see Table 4.2 and Table 4.4. The PL spectra of the homometathesis products display similar substructures, although they are shifted slightly because of the different effects of the aromatic substituents. For all four **H** chromophores, the PLQY is much higher than for **M** and **S** molecules, being up to 80 % for **H2** consistent with the rigidochromy already mentioned for the monomers. In addition, absorption and PLE spectra match one another and the maxima correspond exactly to the side products identified during the photophysical studies of the **S** macromolecules.

In this context, the high PLQYs of these dimers explain why the relatively small amount of homometathesis product remaining after purification of the macromolecules would lead to overestimation of the PLQY of the macromolecules. The higher intensity of the photoluminescence from the side products observed in the PLE for **S5** and **S6**, see Figures 4.15C and 4.15D, can now be explained: **H3** and **H4** have been isolated chromatographically but their similar polarity or intercalation within the macromolecule, make complete separation from the macromolecule difficult, even after several cycles. Conversely, the precipitation of **H1** and **H2** in the course of the Grubbs reaction followed by their filtration, allow for better purification.

The PLQY of all the compounds synthesized and characterised in the present section are compared in Table 4.5.

Table 4. 5 Comparison of the PLQY's of the four families

M	S	H	Molecular Structure of M
40 @ 300 nm	<50 @ 300 nm	66 @ 350 nm	
60 @ 300 nm	<55 @ 300 nm	80 @ 350 nm	
14 @ 280 nm	<11 @ 290 nm	70 @ 350 nm	
<1 @ 280 nm	<3 @ 290 nm	30 @ 350 nm	

On the basis of simple considerations of translational, vibrational and rotational degrees of freedom the “ester” and “acetylacetonate” families should, and do exhibit the lowest PLQYs. Rather unexpectedly, the PLQY's for the “methoxy” family are higher than those for the “methylenedioxy” family. The origin of this effect is not clear.

While targeting specific applications in the biomedical and material fields, it is crucial to select the appropriate synthetic pathways to control the exact composition of the final product without inducing side effects, nor altering thermal / mechanical / electrical material properties. In this context it is then worth noting that the presence of the homometathesis product within the final product has only been identified through its photophysical properties. None of NMR, MALDI-TOF nor microanalysis were able to distinguish between the small molecule and the macromolecule.

In conclusion, we have shown the synthesis and characterization of new macromolecules based on vinylbiphenyl decorated Polyhedral Oligomeric Silsesquioxane. The new molecules have been characterized by NMR, microanalysis and MALDI-TOF spectroscopy. Optical measurements were shown to be an interesting tool in analyzing the purity of these compounds. In the present study we have investigated different terminal functionalities, making the macromolecules good candidates for applications ranging from cross-linkable hybrid nano-structured polymers, to nano-probes, sensors and carriers. In the context of these

last applications, the fluorescent properties would allow monitoring or metal atom extraction from solution environments. Further investigations are needed to quantify the potential of these hybrids macromolecules for these applications. Some preliminary results aimed at exploring the properties of the macromolecules are presented below.

The conversion of methylenedioxy terminated POSS **S3** and dimethoxy peripherally modified cube **S4** to alcohols was attempted with BCl_3 and BBr_3 , leading in each case to powders which were barely soluble in common organic solvents. MALDI-TOF analyses of both compounds failed, giving no signal at all. Encouraging results were however, obtained by ^1H NMR in d_6 -DMSO. First, the usual sharp peak of water in neat d_6 -DMSO transforms into a broad peak, possibly because of exchange between the protons of water in d_6 -DMSO and the 16 hydroxyl groups. In addition, the complete disappearance of the methylene signal of **S3** and the methyl signal of **S4** after the reaction suggests successful deprotection. The only fear is that the POSS cube decomposes into insoluble powders, in the presence of BCl_3 or BBr_3 as previous studies have shown the cleavage of the Si-O-Si bond occurs when strong acids (HX) are present.⁷⁸

The attempted transesterification of **S5** with butanediol using different catalysts such as I_2 or H_2SO_4 also led to insoluble powders, showing no signal in the MALDI-TOF mass spectra. The binding of $\text{EuCl}_3 \cdot x\text{H}_2\text{O}$ or transition metals, such as $([\text{IrCl}(\text{ppy})_2]_2)$, $\text{RhCl}_3 \cdot x\text{H}_2\text{O}$, $[\text{Rh}(\text{acac})(\text{CO})_2]$, $\text{NiCl}_2 \cdot 6\text{H}_2\text{O}$ or V_2O_5 to the benzylic acetylacetonate moieties of **S6** failed in each case as indicated by the retention of the enolic proton of **S6** resonating at around 15 ppm in the ^1H NMR spectrum after reaction with the coordinating ions.

On the whole, even though functionalizations of the four macromolecules have not shown any promising results yet, more detailed investigations should be carried on to exploit the potential of these macromolecules.

IV. 4 References

1. A. Adronov and J. M. J. Fréchet, *Chem. Commun.*, 2000, 1701.
2. M. Kawa, *Top. Curr. Chem.*, 2003, **228**, 193.
3. D. W. Brousmiche, J. M. Serin, J. M. J. Fréchet, G. S. He, T. C. Lin, S. J. Chung and P. N. Prasad, *J. Am. Chem. Soc.*, 2003, **125**, 1448.
4. D. W. Brousmiche, J. M. Serin, J. M. J. Fréchet, G. S. He, T. C. Lin, S. J. Chung, P. N. Prasad, R. Kannan and L. S. Tan, *J. Phys. Chem. B*, 2004, **108**, 8592.
5. V. Balzani, P. Ceroni, S. Gestermann, C. Kauffmann, M. Gorka and F. Vogtle, *Chem. Commun.*, 2000, 853.
6. M. Albrecht, R. A. Gossage, A. L. Spek and G. van Koten, *Chem. Commun.*, 1998, 1003.
7. J. R. Aranzaes, C. Belin and D. Astruc, *Angew. Chem. Int. Ed.*, 2006, **45**, 132.
8. G. Bergamini, P. Ceroni, V. Balzani, L. Cornelissen, J. v. Heyst, S.-K. Lee and F. Vogtle, *J. Mater. Chem.*, 2005, **15**, 2959.
9. J. A. Lopez, J. Manriquez, S. Mendoza and L. A. Godinez, *Electrochem. Commun.*, 2007, **9**, 2133.
10. S. Berchmans, T. M. Vergheese, A. L. Kavitha, M. Veerakumar and V. Yegnaraman, *Anal. Bioanal. Chem.*, 2008, **390**, 939.
11. M. Schlupp, T. Weil, A. J. Berresheim, U. M. Wiesler, J. Bargon and K. Mullen, *Angew. Chem. Int. Ed.*, 2001, **40**, 4011.
12. A. Narayanan, O. Varnavski, O. Mongin, J.-P. Majoral, M. Blanchard-Desce and T. Goodson III, *Nanotechnology*, 2008, **19**, 115502.
13. A.-C. Chang, J. B. Gillepsie and M. B. Tabacco, *Anal. Chem.*, 2001, **73**, 467.
14. E. Kim, K. Kim, H. Yang, Y. T. Kim and J. Kwak, *Anal. Chem.*, 2003, **75**, 5665.
15. C. M. Casado, B. Gonzalez, I. Cuadrado, B. Alonso, M. Moran and J. Losada, *Angew. Chem. Int. Ed.*, 2000, **39**, 2135.
16. Y.-L. Zeng, Y.-F. Huang, J.-H. Jiang, X.-B. Zhang, C.-R. Tang, G.-L. Shen and R.-Q. Yu, *Electrochem. Commun.*, 2007, **9**, 185.
17. I. R. Lauks, *Acc. Chem. Res.*, 1998, **31**, 317.
18. M. Albrecht, N. J. Hovestad, J. Boersma and G. van Koten, *Chem. Eur. J.*, 2001, **7**, 1289.
19. C. Kim, E. park, C. K. Song and B. W. Koo, *Synth. Met.*, 2001, **123**, 493.

20. M. Sulu, A. Altindal and O. Bekaroglu, *Synth. Met.*, 2005, **155**, 211.
21. R. P. Brinas, T. Troxler, R. M. Hochstrasser and S. A. Vinogradov, *J. Am. Chem. Soc.*, 2005, **127**, 11851.
22. J.-M. Lehn, *Acc. Chem. Res.*, 1978, **11**, 49.
23. A. W. Czarnick, *Acc. Chem. Res.*, 1994, **27**, 302.
24. T. Saiji and I. Kinoshita, *J. Chem. Soc., Chem. Commun.*, 1986, 716.
25. M. Berger and F. P. Schmidtchen, *Chem. Rev.*, 1997, **97**, 1609.
26. S. Ghosh and A. K. Banthia, *Tetrahedron Lett.*, 2002, **43**, 6457.
27. S. A. Vinogradov and D. F. Wilson, *Chem. Eur. J.*, 2000, **6**, 2456.
28. J. Leclaire, R. Dagiral, S. Fery-Forgues, Y. Coppel, B. Donnadieu, A.-M. Caminade and J.-P. Majoral, *J. Am. Chem. Soc.*, 2005, **127**, 15762.
29. I. Grabchev, X. Qian, V. Bojinov, Y. Xiao and W. Zhang, *Polymer*, 2002, **43**, 5731.
30. G. Bergamini, P. Ceroni, V. Balzani, L. Cornelissen, J. v. Heyst, S.-K. Lee and F. Vogtle, *J. Mater. Chem.*, 2005, **15**, 2959.
31. C. Valerio, J.-L. Fillaut, J. Ruiz, J. Guittard, J.-C. Blais and D. Astruc, *J. Am. Chem. Soc.*, 1997, **119**, 2588.
32. D. Astruc, M.-C. Daniel and J. Ruiz, *Chem. Commun.*, 2004, 2637.
33. E. J. Houser, *US Pat.*, 0030168355, 2003.
34. M. Wells and R. M. Crooks, *J. Am. Chem. Soc.*, 1996, **118**, 3988.
35. R. M. Crooks and A. J. Ricco, *Acc. Chem. Res.*, 1998, **31**, 219.
36. D. C. Tully and J. M. J. Fréchet, *Chem. Commun.*, 2001, 1229.
37. T. Gao, E. S. Tillman and N. S. Lewis, *Chem. Mater.*, 2005, **17**, 2904.
38. N. Krasteva, I. Besnard, B. Guse, R. E. Bauer, K. Mullen, A. Yasuda and T. Vossmeier, *Nano Lett.*, 2002, **2**, 551.
39. M. Pittelkow, C. B. Nielsen, M. A. C. Broeren, J. L. J. van Dongenn, M. H. P. van Genderen, E. W. Meijer and J. B. Christensen, *Chem. Eur. J.*, 2005, **11**, 5126.
40. D. K. Smith and F. Diederich, *Chem. Commun.*, 1998, 2501.
41. W.-S. Li, D.-L. Jiang, Y. Suna and T. Aida, *J. Am. Chem. Soc.*, 2005, **127**, 7700.
42. R. van Heerbeek, P. C. J. Kamer, P. W. N. M. van Leeuwen and J. N. H. Reek, *Org. Biomol. Chem.*, 2006, **4**, 211.
43. L.-Z. Gong, Q.-S. Hu and L. Pu, *J. Org. Chem.*, 2001, **66**, 2358.
44. L. Pu, *J. Photochem. Photobiol. A*, 2003, **155**, 47.
45. A. Dirksen, U. Hahn, F. Schwanke, M. Nieger, J. N. H. Reek, F. Vogtle and L. D. Cola, *Chem. Eur. J.*, 2004, **10**, 2036.

46. A. Dirksen and L. De Cola, *C. R. Chimie* 2003, **6**, 873.
47. J. F. G. A. Jansen, E. M. M. de Brabander-van den Berg and E. W. Meijer, *Science*, 1994, **266**, 1226.
48. F. Zeng and S. C. Zimmerman, *Chem. Rev.*, 1997, **97**, 1681.
49. E. Mertz, S. L. Elmer, A. M. Balija and S. C. Zimmerman, *Tetrahedron*, 2004, **60**, 11191.
50. S. C. Zimmerman, I. Zharov, M. S. Wendland, N. A. Rakow and K. S. Suslick, *J. Am. Chem. Soc.*, 2003, **125**, 13504.
51. N. R. Vautravers, P. André and D. J. Cole-Hamilton, *J. Mater. Chem*, 2008, Submitted.
52. W. I. Lee, Y. Bae and A. J. Bard, *J. Am. Chem. Soc.*, 2004, **126**, 8358.
53. I. B. Berlman, *Handbook of fluorescence spectra of aromatic molecules*, 2d edn., Academic Press, New York, 1971.
54. K. Matsuda, N. Nakamura, K. Takahashi, K. Inoue, N. Koga and H. Iwamura, *J. Am. Chem. Soc.*, 1995, **117**, 5550.
55. G. D. Scholes, I. R. Gould, R. J. Cogdell and G. R. Fleming, *J. Phys. Chem. B*, 1999, **103**, 2543.
56. A. Myers Kelley, *J. Chem. Phys.*, 2003, **119**, 3320.
57. W. J. D. Beenken and H. Lischka, *J. Chem. Phys.*, 2005, **123**, 144311.
58. L. Cavallo and F. Fraternali, *Chem. Eur. J.*, 1998, **4**, 927.
59. C. B. Gorman and J. C. Smith, *Polymer*, 1999, **41**, 675.
60. R. Scherrenberg, B. Coussens, P. van Vliet, G. Edouard, J. Brackman, E. de Brabander and K. Mortensen, *Macromolecules*, 1998, **31**, 456.
61. N. Zacharopoulos and L. G. Economou, *Macromolecules*, 2002, **35**, 1814.
62. K. J. Haxton, D. J. Cole-Hamilton and R. E. Morris, *Dalton Trans.*, 2004, 1665.
63. M. H. Lamm, T. Chen and S. C. Glotzer, *Nano Lett.*, 2003, **3**, 989-994.
64. T. T. Lin, C. B. He and Y. Xiao, *J. Phys. Chem. B*, 2003, **107**, 13788, and references therein.
65. E. S. Baker, J. Gidden, S. E. Anderson, T. S. Haddad and M. T. Bowers, *Nano Lett.*, 2004, **4**, 779.
66. D. A. Wann, R. J. Less, F. Rataboul, P. D. McCaffrey, A. M. Reilly, H. E. Robertson, P. D. Lickiss and D. W. H. Rankin, *Organometallics*, 2008, **27**, 4183.
67. M. Pope and C. E. Swenberg, *Electronic processes in organic crystals and polymers*, 2nd edn., Oxford University Press, New York ; Oxford, 1999.

68. P. André, G. Cheng, A. Ruseckas, T. van Mourik, H. Früchtl, J. A. Crayston, R. E. Morris, D. Cole-Hamilton and I. D. W. Samuel, *J. Phys. Chem. B*, 2008, Accepted.
69. M. Y. Lo, C. Zhen, M. Lauters, G. E. Jabbour and A. Sellinger, *J. Am. Chem. Soc.*, 2007, **129**, 5808.
70. M. Y. Lo, K. Ueno, H. Tanabe and A. Sellinger, *Chem. Rec.*, 2006, **6**, 157.
71. S.-C. Lo and P. L. Burn, *Chem. Rev.*, 2007, **107**, 1097.
72. V. Balzani, P. Ceroni, S. Gestermann, C. Kauffmann, M. Gorka and F. Vogtle, *Chem. Commun.*, 2000, **10**, 853.
73. N. R. Vautravers, P. André and D. J. Cole-Hamilton, *Org. Biomol. Chem*, 2008, Accepted.
74. D. Satas and A. A. Tracton, *Coatings technology handbook*, 2nd edn., Marcel Dekker, New York, 2001.
75. J. Jiang, W. Liu, K.-L. Cheng, K.-W. Poon and D. K. P. Ng, *Eur. J. Inorg. Chem.*, 2001, 413.
76. J. McKiernan, J. C. Pouxviel, B. Dunn and J. I. Zink, *J. Phys. Chem.*, 1989, **93**, 2129.
77. M. van der Auweraer, M. van den Zegel, N. Boens, F. C. Deschryver and F. Willig, *J. Phys. Chem.*, 1986, **90**, 1169.
78. F. J. Feher, D. Soulivong and A. G. Eklund, *Chem. Commun.*, 1998, 399.

V. Experimental

V. Experimental

V. 1 General

All experiments were carried out in oven-dried glassware using standard Schlenk techniques under an atmosphere of nitrogen. Nitrogen was dried through a Cr(II)/silica packed glass column.

All chemicals were purchased from Sigma-Aldrich, Acros Organics or ABCR and used as received unless otherwise stated. Compounds **1**,¹ **2**,² **3**,² **4**,³ **M3**,⁴ **M4**,⁵ **M5**,⁵ octavinylsilsesquioxane,⁶ **G0-8ethylPPh₂**,⁷ **G1-16methylPPh₂**⁸ and **G1-16ethylPPh₂**⁸ were prepared according to literature methods. Chlorosilane compounds were distilled under inert atmosphere before used. All gases were purchased from BOC. Toluene, petroleum ether (40-60), diethyl ether and THF were purified using a solvent purification system from Innovative Technologies, UK. They were dried by passing through an activated alumina column and degassed in a second column containing copper catalyst, except in the case of THF where the second column also contained activated alumina. THF was degassed by repeated freeze-pump-thaw cycles. Dichloromethane was distilled over CaH₂ under nitrogen. Methanol was distilled over magnesium ethoxide under nitrogen. Cyclohexane and hexane were distilled over sodium under inert atmosphere. Water was distilled and stored under nitrogen. Deuteriated solvents (Cambridge Isotope Laboratories) were degassed by repeated freeze-pump-thaw cycles and stored under nitrogen over molecular sieves.

Proton, carbon and phosphorus NMR spectra were recorded on a Bruker AM 300 NMR spectrometer (¹H, 300.13 MHz; ¹³C, 75.5 MHz; ³¹P, 121.5 MHz) or Bruker Avance II 400 NMR spectrometer (¹H, 400.13 MHz; ¹³C, 100.6 MHz; ³¹P, 162.0 MHz, ²⁹Si, 79.5 MHz). Broad band decoupling was used for ¹³C and ³¹P NMR spectra. ¹H and ¹³C were referenced internally to deuteriated solvents: CDCl₃: ¹H, δ , 7.27 ppm, ¹³C, δ , 77.2 ppm; (CD₃)₂SO: ¹H, δ , 2.54 ppm, ¹³C, δ , 39.6 ppm and are reported relative to Me₄Si. ³¹P and ²⁹Si NMR spectra were referenced externally respectively to 85 % H₃PO₄ and Me₄Si.

Microanalyses were carried out by the University of St Andrews Microanalysis Service on a Carlo Erba 1110 CHNS analyser. A Micromass GCT provided Chemical Ionisation (CI) at

low and high resolution and a Micromass LCT provided a low and high resolution Electrospray Ionisation Service (ESI).

Matrix assisted laser desorption/ionization (MALDI) mass spectra were obtained using a Micromass TOF Spec 2E mass spectrometer system equipped with a 337 nm N2 laser operating in the positive ion detection mode. Samples were generated by addition to the matrix (α -cyano-4-hydroxycinnamic acid or 2,5-dihydroxybenzoic acid, with NaI as an ionization promoter) and dissolved in a suitable solvent (THF or CH₂Cl₂) before being transferred to the sample holder and dried. The spectra were calibrated using a tryptic digest of the beta-galactosidase protein.

Optical rotations were measured on a PERKIN ELMER (MODEL 341) polarimeter at $\lambda = 589$ nm.

V. 2 Photophysical measurements

Absorption spectra were recorded using a Cary 300 spectrophotometer, 10 mm optical path fluorescence cuvettes (Hellma) and the concentration was adjusted to reach an optical density of about 0.1. Photoluminescence (PL) spectra were recorded with a Jobin Yvon Horiba Fluoromax 2 fluorimeter. Spectra were corrected for grating and detector sensitivity variation with wavelength. Except when stated otherwise, all the photophysical properties were characterised at room temperature and in THF solution. The photoluminescence quantum yields (PLQY) were measured against quinine sulphate (Fluka) in 0.5 M sulphuric acid (Sigma-Aldrich) solution used as a standard because of its known quantum yield of 54.6 % as well as its very small sensitivity to oxygen quenching. The following equation was used to perform the appropriate corrections:⁹

$$\Phi_x = \Phi_r \left(\frac{A_r(\lambda_r)}{A_x(\lambda_x)} \right) \left(\frac{I(\lambda_r)}{I(\lambda_x)} \right) \left(\frac{n_x}{n_r} \right)^2 \left(\frac{D_x}{D_r} \right)$$

where Φ stands for PLQY, the subscripts x and r refer to the compound to be characterized and to the reference solutions, respectively. λ is the excitation wavelength, $A(\lambda)$ is the absorbance, $I(\lambda)$ is the relative intensity of the exciting light, n is the solvent refractive index, and D is the integrated area under the corrected emission spectrum.

V. 3 Molecular Dynamics: Protocole and Modelling Analysis

These studies were carried out by Dr. P. André. The geometries of the dendritic molecules were built using Hyperchem.¹⁰ All the relevant atoms were labeled in order to prepare the data analysis. After having optimized the structure of each dendritic molecule, MD was used to determine the average conformations.

The geometries of the molecules were optimized in vacuum using steepest descent / conjugate gradient methods until a minimum energy derivative of $\text{RMS} < 0.0001 \text{ kcal mol}^{-1} \text{ \AA}^{-1}$ was reached. The molecules were then subjected to a slow heating and annealing process at 1200 K designed to exclude high-lying energy minima. Next, the temperature was reduced to 400 K and the data were collected at constant temperature. In a typical simulation, the heating time was 200 ps, the step size was 0.0008 ps, the bath relaxation time was 0.1 ps and the data were collected every 350 time steps.

For every simulation, energies, temperatures and atom coordinates were monitored to allow the analysis of the trajectories. Atomic coordinates of the dendritic molecules were extracted from the snapshot files and used to calculate distances and angles over more than 1500 frames. For each dendritic molecule, snapshots were used to calculate average values and standard deviations of the radius of gyration, the angle between the branches and the POSS core centre and the branch extension from the silicon corners; the latter parameter being defined as the distance between a silicon corner of the POSS core and a given carbon atom located on grafted branch. These were subsequently averaged and analyzed to produce frequency histograms of parameters such as radii of gyration, moments of inertia, distances between atoms, backfolding and torsion angles.

Further insight was sought by analysis of the trajectories obtained by the molecular dynamics simulations. For each frame of the snapshots, the centre of mass (G_{cm}), radius of gyration (R_g), moment of inertia ($I_{x,y,z}$) and asphericity of the moment of inertia (δ) were calculated based on the following equations:

$$\vec{G}_{cm} = \sum_p m_p (x_p \vec{u}_x + y_p \vec{u}_y + z_p \vec{u}_z) / \sum_p m_p \quad (1)$$

$$R_g^2 = < \sum_p m_p r_p^2 > / \sum_p m_p \quad (2)$$

$$I_x = \sum_p m_p^2 [(y_p - Y_G)^2 + (z_p - Z_G)^2] \quad (3)$$

$$\delta = 1 - 3 \frac{< I_x I_y + I_y I_z + I_z I_x >}{< (I_x + I_y + I_z)^2 >} \quad (4)$$

where p is the atom index, m_p and x_p - y_p - z_p are the mass and Cartesian coordinates of the atom of index p , respectively. r_p is the distance to the centre of gravity for the atom of index p , I_x is the x-component of the moment of inertia, with Y_G and Z_G being the coordinates of the centre of mass along the y- and z-axes, respectively, and with δ being the asphericity of the moment of inertia.

V. 4 Procedure for alkene hydroformylation

A HastelloyTM autoclave of internal capacity 250 mL was used for vinylacetate and styrene hydroformylation. The reactor was purged three times with CO/H₂ (1/1); subsequently, the catalytic solution containing [Rh(acac)(CO)₂] (5.4 mg, 2.4 x 10⁻⁵ mol), toluene (4 mL), substrate (1 mL) and the SemiEsphos functionalised dendrimer was added *via* cannula. The autoclave was then pressurised with syngas and heated at the desired conditions. At the end of the reaction, the autoclave was rapidly cooled and the unreacted gases were vented. The liquids products were analyzed by GC with a flame ionization detector (quantitative) and GC-MS (qualitative). Both analysis methods employed a SupelcoTM beta-DEXTM [nonbonded phase with 25 % 2,3-di-O-acetyl-6-O-TBDMS- β -cyclodextrin in SPB-20 poly(20 % phenyl / 80 % dimethylsiloxane)] fused silica capillary column (60 m (2 x 30 m) x 0.25 mm x 0.25 μ m). The enantioselectivity of the reaction was determined by comparison with authentic product samples.

V. 5 Procedure for ethene methoxycarbonylation

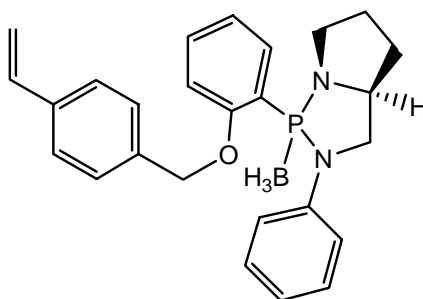
Catalytic reactions were carried out in identical 250 mL HastelloyTM autoclaves. The reactor was purged with CO prior to the catalytic solution containing palladium acetate (0.02 mmol), methanesulfonic acid (0.4 mmol) and the ligand, either in methanol (10 mL) for non-dendritic phosphines (work largely carried out by Mr. Graeme Smith) or in a mixture of methanol/toluene (8 mL/ 4 mL) for dendritic phosphines, being cannulated in under nitrogen. The autoclave was then pressurised to 60 bar using ethene and carbon monoxide (1:1) and heated at 85 °C for 2.5 hours. At the end of the reaction, the autoclave was rapidly cooled and the unreacted gases were vented. The reaction slurry was then collected by filtration, washed with fresh methanol and dried at 70 °C under vacuum. The solution was analysed by GC chromatography using a Hewlett-Packard 6890 series gas

chromatograph, fitted with a SupelcoTM Meridian MDN-35 (35 % phenyl / 65 % methylpolysiloxane) fused silica capillary column (30 m x 0.25 mm x 0.25 μ m) and equipped with an Agilent 6890 series injector. Both quantitative analysis by a flame ionisation detector (GC-FID) and qualitative analysis by a Hewlett-Packard 5973 series mass selective detector (GC-MS) were performed. A Hewlett-Packard Chemstation allowed the computerised integration of peak areas. The catalyst activity for polymer formation was determined both by the weight of the polymer produced (g PK (g Pd. h)⁻¹) and by average turnover frequency over 2.5 h (mol ethene introduced (mol Pd. h)⁻¹); the mass of the polymer was divided by 56 (CO + ethene) to give an approximation of the turnover number. This approximation is reasonable for longer chain polymers. This number is included in an attempt to obtain a comparison with the rates of formation of methyl propanoate). The activity for methyl propanoate and cooligomer formation was determined by gas chromatography.

V. 6 *SemiEsphos* terminated *Polyhedral* *Oligomeric Silsesquioxanes*

V. 6. 1 *SemiEsphos* modified dendrons

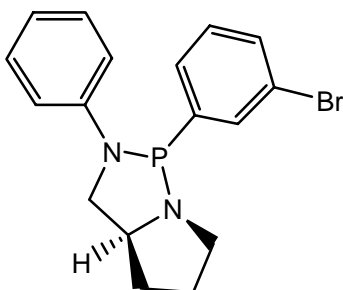
(*2R, 5S*)-2-[2-(4'-vinylbenzyloxy)phenyl]-3-phenyl-1,3-diaza-2-phosphabicyclo[3.3.0]^{1,5}]octane-Borane (**5**)



A solution of **4** (2.5 g, 8.01 mmol) ((*2R, 5S*)-2-(2-hydroxyphenyl)-3-phenyl-1,3-diaza-2-phosphabicyclo[3.3.0]^{1,5}]octane-Borane) in DMF (5 mL) was added dropwise to a suspension of NaH (288 mg, 12.0 mmol) in DMF (20 mL) cooled down at 0 °C. After 30 minutes, 4-vinylbenzyl bromide (1.57 g, 8.00 mmol) in DMF (5 mL) was added and the mixture stirred overnight at room temperature. The reaction was quenched with H₂O (50 mL) and the

aqueous layer was extracted with Et₂O (4 x 20 mL). The combined organic layers were dried with MgSO₄, filtered and concentrated in vacuo. The residue was precipitated by addition of petroleum ether (50 mL) affording a white powder (1.15g, 34 %); δ_{H} (400.13 MHz; CDCl₃; Me₄Si) 0.10-1.62 (3 H, m, BH₃), 1.65 (2 H, m, -CH₂-), 1.84-2.02 (2 H, m, -CH₂-), 3.00-3.19 (3 H, m, -CH₂-), 3.40 (1 H, m, NCH), 3.78-3.90 (1 H, m, -CH₂-), 4.93 (2 H, d, $^2J_{\text{HH}}$ 12.4, -OCH₂-), 5.01 (2 H, d, $^2J_{\text{HH}}$ 12.4, -OCH₂-), 5.27 (1 H, d, $^3J_{\text{HH}}$ 10.9, CH₂=CH), 5.78 (1 H, d, $^3J_{\text{HH}}$ 17.8, CH₂=CH), 6.71 (1 H, dd, $^3J_{\text{HH}}$ 17.8, $^3J_{\text{HH}}$ 10.9, CH₂=CH), 6.84 (2 H, m, ArH), 6.89 (2 H, d, $^3J_{\text{HH}}$ 9.2, ArH), 6.91 (2 H, d, J 7.5, ArH), 7.01 (1 H, td, J 1.6, J 7.6, ArH), 7.16 (2 H, m, ArH), 7.17 (2 H, d, $^3J_{\text{HH}}$ 9.2, ArH), 7.39 (1 H, t, J 7.6, ArH) and 7.99 (1 H, m, ArH); δ_{C} (100.6 MHz; CDCl₃; Me₄Si) 26.0 (-CH₂-), 32.0 (-CH₂-), 47.5 (-CH₂-), 53.8 (d, J_{CP} 5.3, -CH₂-), 61.7 (-CH₂-), 70.5 (OCH₂), 111.8, 113.5 (CH₂=CH), 116.2, 191.4, 120.6, 126.2, 128.6, 129.3, 130.1, 133.8, 135.6, 135.9, 136.3, 136.7, 145.6 (*ipso* NC) and 162.3 (*ipso* OC); δ_{P} (162.0 MHz; CDCl₃) 100.3 (br); m/z (CI) 437.1762 (M+Na-BH₃. C₂₆H₂₇N₂ONaP requires 437.1759).

(2R, 5S)-2-[3-bromophenyl]-3-phenyl-1,3-diaza-2-phospha-bicyclo[3.3.0]^{1,5}octane (6)

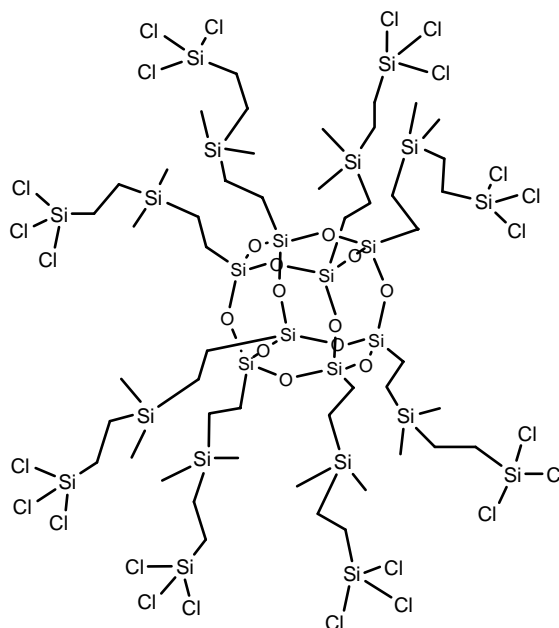


An oven-dried flask equipped with a condenser and a magnetic stirring bar was charged under nitrogen with 3-(bis(dimethylaminophosphine))bromobenzene ¹¹ (2.42 g, 8.8 mmol) and (*S*)-2-(Phenylaminomethyl)pyrrolidine ¹² (1.55 g, 8.8 mmol) in toluene (40 mL). The solution was refluxed for 5 days until no more release of HNMe₂ was detected as indicated by damp litmus paper. The solvent was then removed under *vacuo* leading to an oil which solidified upon cooling at -30 °C. A white powder was obtained in 73 % yield (2.32 g). δ_{H} (300.13 MHz; CDCl₃; Me₄Si) 1.79 (1 H, m, -CH₂-), 1.91 (2 H, m, -CH₂-), 2.08 (1 H, m, -CH₂-), 3.07 (1 H, m, -CH₂-), 3.27 (1 H, m, NCH), 3.38-3.52 (2 H, m, -CH₂-), 3.98 (1 H, m, -CH₂-), 6.81 (1 H, t, $^3J_{\text{HH}}$ 7.4, ArH), 6.90 (2 H, m, ArH), 7.11-7.33 (4 H, m, ArH), 7.41 (1 H, d, $^3J_{\text{HH}}$ 7.8, ArH) and 7.56 (1 H, d, $^3J_{\text{HH}}$ 5.5, ArH); δ_{C} (75.5 MHz; CDCl₃; Me₄Si) 26.6 (d, J_{CP} 5.7, -CH₂-), 31.7 (-

CH₂-), 52.9 (-CH₂-), 53.4 (d, J_{CP} 4.5, -CH₂-), 64.6 (d, J_{CP} 7.9, NCH₃), 114.7 (d, J_{CP} 12.8), 117.9, 122.9, 127.8, 129.3, 129.7, 131.6, 131.8, 146.3 and 146.6 (*ipso* NC); δ_P (162.0 MHz; CDCl₃) 98.6; m/z (ESI) 361.0460 (C₁₇H₁₈N₂PBr⁽⁷⁹⁾ requires 361.0469) and 363.0449 (C₁₇H₁₈N₂PBr⁽⁸¹⁾ requires 363.0434).

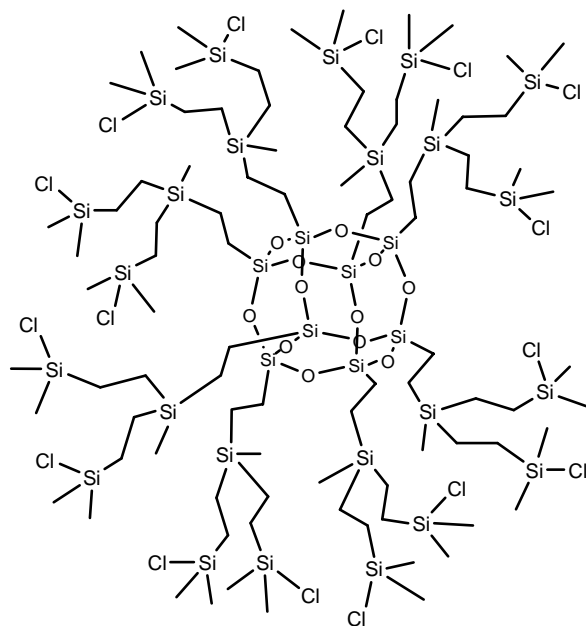
V. 6. 2 SemiEsphos terminated Polyhedral Oligomeric Silsesquioxane building blocks

G1-ethyl-24Cl(ext)



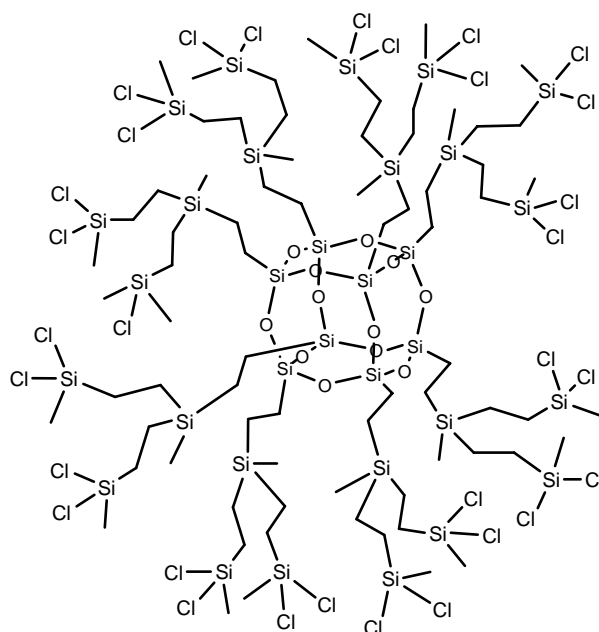
HSiCl₃ (0.94 mL, 9.29 mmol) was added to a solution of **G1-8vinyl**¹³ (548 mg, 0.42 mmol) in Et₂O (40 mL), followed by 10 drops of Karstedt catalyst (1,3-divinyl-1,1,3,3-tetramethyldisiloxaneplatinum(0) in xylene). The resulting solution was refluxed for 15 hours. The solvent was removed *in vacuo* to give **G1-ethyl-24Cl(ext)** as a waxy solid (910 mg, 91 %) (Found: C, 23.9; H, 3.8. Si₂₄O₁₂C₄₈H₁₁₂Cl₂₄ requires C, 24.0; H, 4.7%); δ_H (300.13 MHz; CDCl₃; Me₄Si) 0.02 (48 H, s, Si(CH₃)₂), 0.57 (32 H, m, O₃SiCH₂CH₂Si), 0.70 (16 H, m, SiCH₂CH₂SiCl₃) and 1.26 (m, 16H, SiCH₂CH₂SiCl₃); δ_C (75.5 MHz; CDCl₃; Me₄Si) -4.6 (Si(CH₃)₂), 4.4 (O₃SiCH₂CH₂Si), 5.7 (SiCH₂CH₂SiCl₃), 6.0 (O₃SiCH₂CH₂Si) and 17.6 (SiCH₂CH₂SiCl₃); δ_{Si} (79.5 MHz; CDCl₃; Me₄Si) -67.4 (SiO₃), 6.5 (Si(CH₃)₂) and 13.5 (SiCl₃).

G2-ethyl-16Cl



HSiMe₂Cl (1.63 mL, 14.67 mmol) was added to a solution of **G1-16vinyl**¹³ (520 mg, 0.37 mmol) in Et₂O (40 mL), followed by 10 drops of Karstedt catalyst (1,3-divinyl-1,1,3,3-tetramethyldisiloxaneplatinum(0) in xylene). The resulting solution was refluxed for 15 hours. The solvent was removed *in vacuo* to give **G2-ethyl-16Cl** as a waxy solid (946 mg, 88 %) (Found: C, 36.0; H, 7.5. Si₃₂O₁₂C₈₈H₂₁₆Cl₁₆ requires C, 36.1; H, 7.4%); δ_{H} (300.13 MHz; CDCl₃; Me₄Si) -0.02 (24 H, br, SiCH₃), 0.39 (96 H, m, Si(CH₃)₂Cl), 0.51 (32 H, m, SiCH₂CH₂SiCl), 0.55 (32 H, m, O₃SiCH₂CH₂Si) and 0.67 (32 H, m, SiCH₂CH₂SiCl); δ_{C} (75.5 MHz; CDCl₃; Me₄Si) -6.6 (SiCH₃), 1.1 (Si(CH₃)₂Cl), 3.9 (SiCH₂CH₂SiCl), 4.2 (O₃SiCH₂CH₂Si), 4.5 (O₃SiCH₂CH₂Si) and 11.4 (SiCH₂CH₂SiCl); δ_{Si} (79.5 MHz; CDCl₃; Me₄Si) -67.4 (SiO₃), 8.3 (SiCH₃) and 32.5 (SiCl).

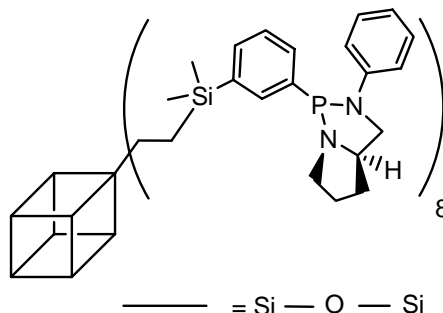
G2-ethyl-32Cl



HSiMeCl₂ (2.61 mL, 25.05 mmol) was added to a solution of **G1-16vinyl**¹³ (888 mg, 0.63 mmol) in Et₂O (50 mL), followed by 10 drops of Karstedt catalyst (1,3-divinyl-1,1,3,3-tetramethyldisiloxaneplatinum(0) in xylene). The resulting solution was refluxed for 30 hours. The solvent was removed *in vacuo* to give **G2-ethyl-32Cl** as a waxy solid (1.88 g, 92 %) (Found: C, 27.8; H, 4.9. Si₂₄O₁₂C₇₂H₁₆₈Cl₃₂ requires C, 28.5; H, 5.5%); δ_{H} (400.13 MHz; CDCl₃; Me₄Si) 0.00 (24 H, s, SiCH₃), 0.51-0.59 (32 H, m, O₃SiCH₂CH₂Si), 0.63 (32 H, m, SiCH₂CH₂SiCl₂), 0.75 (48 H, s, SiCl₂) and 0.95 (32 H, m, SiCH₂CH₂SiCl₂); δ_{C} (75.5 MHz; CDCl₃; Me₄Si) -6.7 (SiCH₃), 3.6 (SiCH₂CH₂SiCl₂), 3.9 (O₃SiCH₂CH₂Si), 4.2 (O₃SiCH₂CH₂Si), 4.5 (SiCH₃Cl₂) and 14.4 (SiCH₂CH₂SiCl₂); δ_{Si} (79.5 MHz; CDCl₃; Me₄Si) -66.7 (SiO₃), 8.8 (SiCH₃) and 33.3 (SiCl₂).

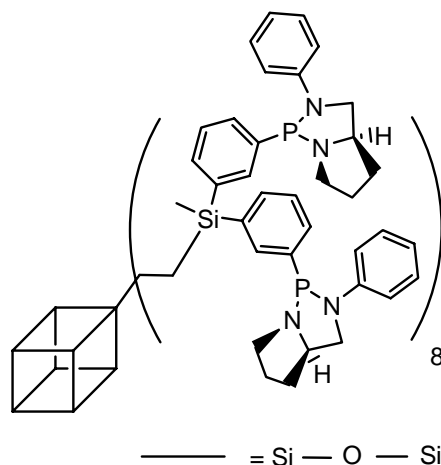
V. 6. 3 SemiEsphos terminated Polyhedral Oligomeric Silsesquioxanes

G1-8SemiEsphos



n-butyllithium (2.10 mL, 2.5 mol L⁻¹ in hexane, 5.25 mmol) was added dropwise to a stirred solution of 3-(bis(dimethylaminophosphine))bromobenzene ¹¹ (1.44 g, 5.25 mmol) in diethylether (30 mL) cooled at -78 °C. The reaction mixture was warmed gradually to -20 °C and maintained for 30 minutes at this temperature before being cooled to -78 °C. This solution was then slowly transferred via canula to a Schlenk flask containing **G1-8Cl** ¹³ (810 mg, 0.58 mmol) in THF (30 mL) and allowed to warm overnight with constant stirring. A saturated solution of NaHCO₃ was subsequently added to quench the reaction, followed by DCM (10 mL). The aqueous layer was extracted twice with DCM (2 x 20 mL) and the combined organic fractions washed with brine (30 mL), before being dried over MgSO₄. After filtration, the solvent was evaporated and the resulting yellow oil was used without any further purification in the next step. An oven-dried flask equipped with a condenser and a magnetic stirring bar was charged under nitrogen with the residue (1.29 g, 0.48 mmol) and (*S*)-2-(Phenylaminomethyl)pyrrolidine ¹² (923 mg, 5.25 mmol) in toluene (40 mL). The solution was refluxed for 5 days until no more release of HNMe₂ was detected as indicated by damp litmus paper. The solvent was then removed leading to a waxy solid, which was purified by precipitation in hexane (60 mL) after dissolution in toluene (3 mL). This procedure was repeated twice affording the desired compound as a white powder (1.23 g, 63 %); [α]_D = -0.5 (c = 1.0, CHCl₃); (Found: C, 59.7; H, 7.3; N, 6.9. Si₁₆O₁₂N₁₆P₈C₁₆₈H₂₂₄ requires C, 60.1; H, 6.7; N, 6.7%); δ_H (300.13 MHz; CDCl₃; Me₄Si) 0.16 (48 H, br, Si(CH₃)₂), 0.51 (16 H, m, O₃SiCH₂CH₂Si), 0.73 (16 H, m, O₃SiCH₂CH₂Si) 1.69-2.06 (32 H, m, -CH₂-), 2.95-3.03 (8 H, m, -CH₂-), 3.27 (16 H, m, -CH₂-), 3.41 (8 H, m, -CH₂-), 3.97 (8 H, m, NCH), 6.73 (8 H, m, ArH), 6.85 (16 H, m, ArH), 7.07-7.20 (32 H, m, ArH), 7.33 (8 H, m, ArH) and 7.56 (8 H, m, ArH); δ_C (75.5 MHz; CDCl₃; Me₄Si) -2.1 (Si(CH₃)₂), 4.9 (O₃SiCH₂CH₂Si), 7.5 (O₃SiCH₂CH₂Si), 26.3 (d, *J*_{CP} 6.3, -CH₂-), 31.3 (-CH₂-), 53.1 (-CH₂-), 53.5 (d, *J*_{CP} 4.7, -CH₂-), 64.8 (d, *J*_{CP} 8.5, NCH), 115.6 (d, *J*_{CP} 13.4), 118.3, 127.9, 129.5, 129.6, 129.7, 134.4, 139.0 (*ipso* SiC), 141.9 (d, *J*_{CP} 26.3, *ipso* PC) and 147.9 (d, *J*_{CP} 15.3, *ipso* NC); δ_P (162.0 MHz; CDCl₃) 100.6; δ_{Si} (79.5 MHz; CDCl₃; Me₄Si) -66.9 (SiO₃) and -1.3 (Si(CH₃)₂).

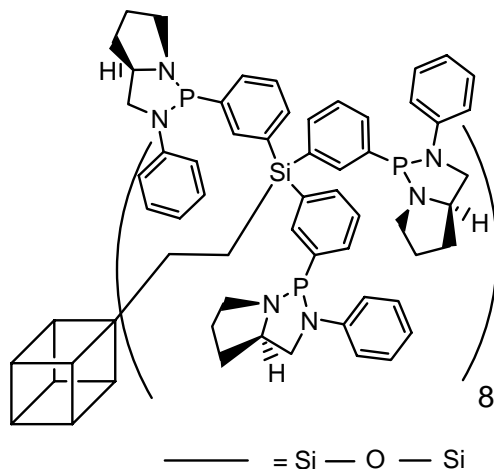
G1-16SemiEsphos



n-butyllithium (1.53 mL, 2.5 mol L⁻¹ in hexane, 3.82 mmol) was added dropwise to a stirred solution of 3-(bis(dimethylaminophosphine))bromobenzene ¹¹ (1.05 g, 3.82 mmol) in diethylether (20 mL) cooled at -78 °C. The reaction mixture was warmed gradually to -20 °C and maintained for 30 minutes at this temperature before being cooled to -78 °C. This solution was then slowly transferred via canula to a Schlenk flask containing **G1-16Cl** ¹³ (330 mg, 0.21 mmol) in THF (20 mL) and allowed to warm overnight with constant stirring. A saturated solution of NaHCO₃ was subsequently added to quench the reaction, followed by DCM (10 mL). The aqueous layer was extracted twice with DCM (2 x 10 mL) and the combined organic fractions washed with brine (30 mL), before being dried over MgSO₄. After filtration, the solvent was evaporated and the resulting yellow oil was used without any further purification in the next step. An oven-dried flask equipped with a condenser and a magnetic stirring bar was charged under nitrogen with the residue (737 mg, 0.18 mmol) and (*S*)-2-(Phenylaminomethyl)pyrrolidine ¹² (673 mg, 3.82 mmol) in toluene (30 mL). The solution was refluxed for 5 days until no more release of HNMe₂ was detected as indicated by damp litmus paper. The solvent was then removed leading to a waxy solid, which was purified by precipitation in hexane (60 mL) after dissolution in toluene (2 mL). This procedure was repeated twice affording the desired compound as a white powder (834 mg, 72 %); [α]_D = -0.8 (c = 1.0, CHCl₃); (Found: C, 64.9; H, 6.2; N, 8.2. Si₁₆O₁₂N₃₂P₁₆C₂₉₆H₃₄₄ requires C, 64.8; H, 6.3; N, 8.2%); δ_H (300.13 MHz; CDCl₃; Me₄Si) 0.08 (24 H, m, SiCH₃), β hydrosilylation (<25 %, m, 0.21-0.60), 0.62-0.74 (16 H, m, O₃SiCH₂CH₂Si), 1.01-1.16 (16 H, m, O₃SiCH₂CH₂Si), 1.46-2.06 (64 H, m, -CH₂-), 2.84-3.04 (16 H, m, -CH₂-), 3.11-3.41 (48 H, m, -CH₂-), 3.74-3.98 (16 H, m, NCH), 6.61-6.86 (48 H, m, ArH), 7.00-7.21 (64 H, m, ArH) and 7.31-7.66 (32 H, m, ArH); δ_C (75.5 MHz; CDCl₃; Me₄Si) -5.2 (SiCH₃), 4.6

(O₃SiCH₂CH₂Si), 5.5 (O₃SiCH₂CH₂Si), 25.8 (d, J_{CP} 5.3, -CH₂-), 31.4 (-CH₂), 52.6 (-CH₂-), 52.9 (d, J_{CP} 4.7, -CH₂-), 64.2 (d, J_{CP} 8.7, NCH), 115.1 (d, J_{CP} 13.5), 117.8, 127.7, 129.2, 129.3, 129.9, 135.1, 139.3 (*ipso* SiC), 141.1 (d, J_{CP} 26.6, *ipso* PC) and 146.8 (d, J_{CP} 15.3, *ipso* NC); δ_P (162.0 MHz; CDCl₃) 100.1; δ_{Si} (79.5 MHz; CDCl₃; Me₄Si) -66.1 (SiO₃) and -6.3 (SiCH₃).

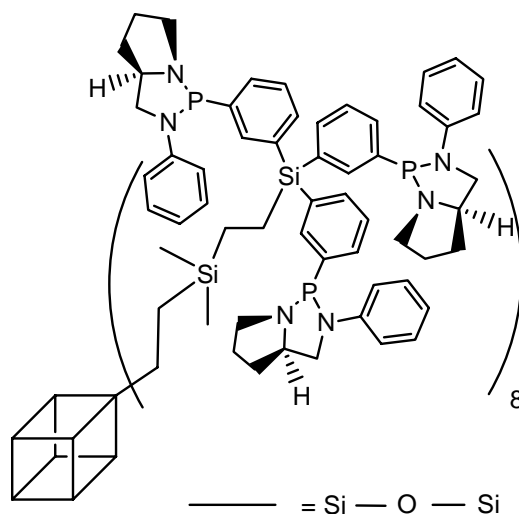
G1-24SemiEsphos



n-butyllithium (3.10 mL, 2.5 mol L⁻¹ in hexane, 7.75 mmol) was added dropwise to a stirred solution of 3-(bis(dimethylaminophosphine))bromobenzene ¹¹ (2.13 g, 7.75 mmol) in diethylether (35 mL) cooled at -78 °C. The reaction mixture was warmed gradually to -20 °C and maintained for 30 minutes at this temperature before being cooled to -78 °C. This solution was then slowly transferred via canula to a Schlenk flask containing **G1-24Cl** ¹³ (493 mg, 0.29 mmol) in THF (20 mL) and allowed to warm overnight with constant stirring. A saturated solution of NaHCO₃ was subsequently added to quench the reaction, followed by DCM (10 mL). The aqueous layer was extracted twice with DCM (2 x 20 mL) and the combined organic fractions washed with brine (30 mL), before being dried over MgSO₄. After filtration, the solvent was evaporated and the resulting yellow oil was used without any further purification in the next step. An oven-dried flask equipped with a condenser and a magnetic stirring bar was charged under nitrogen with the residue (1.26 g, 0.23 mmol) and (*S*)-2-(Phenylaminomethyl)pyrrolidine ¹² (1.36 g, 7.75 mmol) in toluene (40 mL). The solution was refluxed for 5 days until no more release of HNMe₂ was detected as indicated by damp litmus paper. The solvent was then removed leading to a waxy solid, which was purified by precipitation in hexane (60 mL) after dissolution in toluene (10 mL). This procedure was repeated twice affording the desired compound as a white powder (1.32 g, 60 %); $[\alpha]_D = -1.0$

($c = 1.01$, CHCl_3); (Found: C, 66.6; H, 6.7; N, 8.3. $\text{Si}_{16}\text{O}_{12}\text{N}_{48}\text{P}_{24}\text{C}_{424}\text{H}_{464}$ requires C, 66.9; H, 6.1; N, 8.8%); δ_{H} (300.13 MHz; CDCl_3 ; Me_4Si) 0.62 (16 H, m, $\text{O}_3\text{SiCH}_2\text{CH}_2\text{Si}$), 1.28 (16 H, m, $\text{O}_3\text{SiCH}_2\text{CH}_2\text{Si}$), 1.46-1.93 (96 H, m, $-\text{CH}_2-$), 2.74-2.93 (24 H, m, $-\text{CH}_2-$), 2.98-3.30 (72 H, m, $-\text{CH}_2-$), 3.68 (24 H, m, NCH), 6.51-6.82 (72 H, m, ArH), 6.92-7.21 (96 H, m, ArH) and 7.26-7.75 (48 H, m, ArH); δ_{C} (75.5 MHz; CDCl_3 ; Me_4Si) 4.2 ($\text{O}_3\text{SiCH}_2\text{CH}_2\text{Si}$), 5.1 ($\text{O}_3\text{SiCH}_2\text{CH}_2\text{Si}$), 25.8 (d, J_{CP} 5.3, $-\text{CH}_2-$), 31.3 ($-\text{CH}_2-$), 52.5 ($-\text{CH}_2-$), 52.9 (d, J_{CP} 4.7, $-\text{CH}_2-$), 64.3 (d, J_{CP} 8.7, NCH), 115.0 (d, J_{CP} 13.3), 117.7, 127.7, 129.1, 129.3, 130.2, 134.6, 139.2, 141.1(*ipso* SiC) (d, J_{CP} 26.9, *ipso* PC) and 146.8 (d, J_{CP} 15.3, *ipso* NC); δ_{P} (162.0 MHz; CDCl_3) 99.1; δ_{Si} (79.5 MHz; CDCl_3 ; Me_4Si) -66.7 (SiO_3) and -10.1 (SiAr).

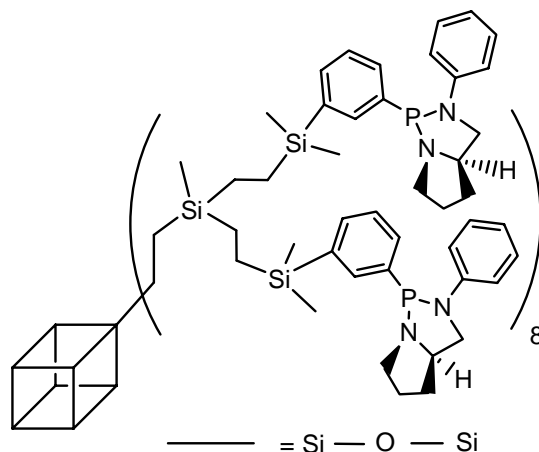
G1-24SemiEsphos(ext)



n-butyllithium (4.24 mL, 2.5 mol L⁻¹ in hexane, 10.6 mmol) was added dropwise to a stirred solution of 3-(bis(dimethylaminophosphine))bromobenzene¹¹ (2.91 g, 10.6 mmol) in diethylether (40 mL) cooled at -78 °C. The reaction mixture was warmed gradually to -20 °C and maintained for 30 minutes at this temperature before being cooled to -78 °C. This solution was then slowly transferred via canula to a Schlenk flask containing **G1-ethyl-24Cl(ext)** (910 mg, 0.38 mmol) in THF (35 mL) and allowed to warm overnight with constant stirring. A saturated solution of NaHCO_3 was subsequently added to quench the reaction, followed by DCM (10 mL). The aqueous layer was extracted twice with DCM (2 x 10 mL) and the combined organic fractions washed with brine (30 mL), before being dried over MgSO_4 . After filtration, the solvent was evaporated and the resulting yellow oil was used without any further purification in the next step. An oven-dried flask equipped with a condenser and a magnetic stirring bar was charged under nitrogen with the residue (2.23 g, 0.36 mmol) and

(*S*)-2-(Phenylaminomethyl)pyrrolidine ¹² (1.86 g, 10.6 mmol) in toluene (40 mL). The solution was refluxed for 5 days until no more release of HNMe₂ was detected as indicated by damp litmus paper. The solvent was then removed leading to a waxy solid, which was purified by precipitation in hexane (60 mL) after dissolution in toluene (5 mL). This procedure was repeated twice affording the desired compound as a white powder (1.64 g, 52 %); [α]_D = -1.2 (*c* = 1.04, CHCl₃); (Found: C, 65.5; H, 6.6; N, 8.6. Si₂₄O₁₂N₄₈P₂₄C₄₅₆H₅₄₄ requires C, 65.9; H, 6.6; N, 8.1%); δ_{H} (300.13 MHz; CDCl₃; Me₄Si) -0.16 (48 H, br, Si(CH₃)₂), 0.23-0.60 (32 H, m, O₃SiCH₂CH₂Si), 0.64-0.91 (16 H, m, SiCH₂CH₂Si), 0.98-1.33 (m, 16H, SiCH₂CH₂Si), 1.50-2.07 (96 H, m, -CH₂-), 2.83-3.05 (24 H, m, -CH₂-), 3.10-3.39 (72 H, m, -CH₂-), 3.83 (24 H, m, NCH), 6.62-6.86 (72 H, m, ArH), 6.92-7.21 (96 H, m, ArH) and 7.26-7.75 (48 H, m, ArH); δ_{C} (75.5 MHz; CDCl₃; Me₄Si) -4.4 (Si(CH₃)₂), 4.3, 5.0, 6.2, 7.0, 25.7 (d, *J*_{CP} 5.3, -CH₂-), 31.3 (-CH₂-), 52.5 (-CH₂-), 53.1 (d, *J*_{CP} 4.6, -CH₂-), 64.3 (d, *J*_{CP} 8.8, NCH), 115.1 (d, *J*_{CP} 13.3), 117.8, 127.6, 129.2, 129.5, 129.7, 134.6, 139.2 (*ipso* SiC), 140.1 (d, *J*_{CP} 27.4, *ipso* PC) and 146.8 (d, *J*_{CP} 15.3, *ipso* NC); δ_{P} (162.0 MHz; CDCl₃) 99.8; δ_{Si} (79.5 MHz; CDCl₃; Me₄Si) -66.1 (SiO₃), -9.4 (SiAr) and 6.3 (Si(CH₃)₂).

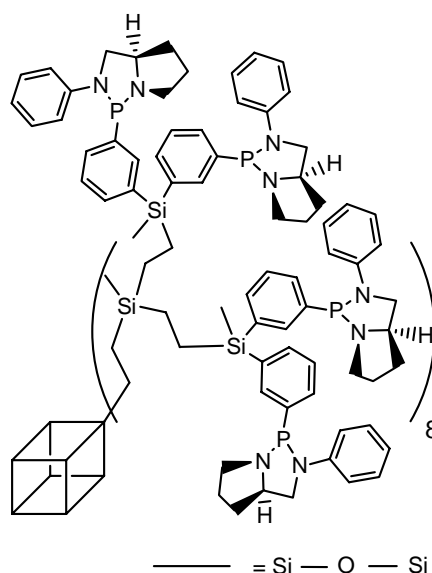
G2-16SemiEsphos



n-butyllithium (5.25 mL, 2.5 mol L⁻¹ in hexane, 13.13 mmol) was added dropwise to a stirred solution of 3-(bis(dimethylaminophosphine))bromobenzene ¹¹ (3.61 g, 13.13 mmol) in diethylether (40 mL) cooled at -78 °C. The reaction mixture was warmed gradually to -20 °C and maintained for 30 minutes at this temperature before being cooled to -78 °C. This solution was then slowly transferred via canula to a Schlenk flask containing **G2-ethyl-16Cl** (2.14 g, 0.73 mmol) in THF (40 mL) and allowed to warm overnight with constant stirring. A saturated solution of NaHCO₃ was subsequently added to quench the reaction, followed by

DCM (30 mL). The aqueous layer was extracted twice with DCM (2 x 40 mL) and the combined organic fractions washed with brine (40 mL), before being dried over MgSO₄. After filtration, the solvent was evaporated and the resulting yellow oil was used without any further purification in the next step. An oven-dried flask equipped with a condenser and a magnetic stirring bar was charged under nitrogen with the residue (3.45 g, 0.63 mmol) and (*S*)-2-(Phenylaminomethyl)pyrrolidine¹² (2.31 g, 13.13 mmol) in toluene (40 mL). The solution was refluxed for 5 days until no more release of HNMe₂ was detected as indicated by damp litmus paper. The solvent was then removed leading to a waxy solid, which was purified by precipitation in hexane (60 mL) after dissolution in toluene (5 mL). This procedure was repeated twice affording the desired compound as a white powder (2.83, 56 %); [α]_D = -1.3 (c = 1.0, CHCl₃); (Found: C, 62.8; H, 8.3; N, 6.4. Si₃₂O₁₂N₃₂P₁₆C₃₆₀H₅₀₄ requires C, 63.0; H, 7.4; N, 6.5%); δ_{H} (400.13 MHz; CDCl₃; Me₄Si) -0.15 (24 H, br, SiCH₃), 0.13, (br, 96H, Si(CH₃)₂), 0.24-0.65 (96 H, m, O₃SiCH₂CH₂Si(CH₂CH₂Si)₂), 1.60-2.05 (64 H, m, -CH₂-), 2.95-3.08 (16 H, m, -CH₂-), 3.10-3.45 (48 H, m, -CH₂-), 3.94 (16 H, m, NCH), 6.70 (16 H, m, ArH), 6.85 (32 H, m, ArH), 7.01-7.23 (64 H, m, ArH), 7.33 (16 H, m, ArH) and 7.54 (16 H, m, ArH); δ_{C} (100.6 MHz; CDCl₃; Me₄Si) -6.4 (SiCH₃), -3.4 (Si(CH₃)₂), 4.3, 4.6, 4.8, 7.9, 25.7 (d, *J*_{CP} 5.8, -CH₂-), 30.7 (-CH₂-), 52.7 (-CH₂-), 53.8 (d, *J*_{CP} 4.7, -CH₂-), 64.3 (d, *J*_{CP} 8.5, NCH), 115.8 (d, *J*_{CP} 12.3), 117.6, 127.5, 129.4, 129.5, 129.7, 134.8, 139.0 (*ipso* SiC), 140.3 (d, *J*_{CP} 27.1, *ipso* PC) and 147.9 (d, *J*_{CP} 15.3, *ipso* NC); δ_{P} (162.0 MHz; CDCl₃) 100.5; δ_{Si} (79.5 MHz; CDCl₃; Me₄Si) -66.8 (SiO₃), -1.6 (Si(CH₃)₂) and 8.3 (SiCH₃).

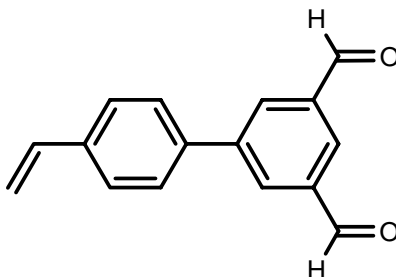
G2-32SemiEsphos



n-butyllithium (2.97 mL, 2.5 mol L⁻¹ in hexane, 7.44 mmol) was added dropwise to a stirred solution of 3-(bis(dimethylaminophosphine))bromobenzene ¹¹ (2.04 g, 7.44 mmol) in diethylether (30 mL) cooled at -78 °C. The reaction mixture was warmed gradually to -20 °C and maintained for 30 minutes at this temperature before being cooled to -78 °C. This solution was then slowly transferred via canula to a Schlenk flask containing **G2-ethyl-32Cl** (655 mg, 0.20 mmol) in THF (30 mL) and allowed to warm overnight with constant stirring. A saturated solution of NaHCO₃ was subsequently added to quench the reaction, followed by DCM (10 mL). The aqueous layer was extracted twice with DCM (2 x 20 mL) and the combined organic fractions washed with brine (30 mL), before being dried over MgSO₄. After filtration, the solvent was evaporated and the resulting yellow oil was used without any further purification in the next step. An oven-dried flask equipped with a condenser and a magnetic stirring bar was charged under nitrogen with the residue (1.43 g, 0.17 mmol) and (*S*)-2-(Phenylaminomethyl)pyrrolidine ¹² (1.31 g, 7.44 mmol) in toluene (50 mL). The solution was refluxed for 5 days until no more release of HNMe₂ was detected as indicated by damp litmus paper. The solvent was then removed leading to a waxy solid, which was purified by precipitation in hexane (60 mL) after dissolution in toluene (4 mL). This procedure was repeated twice affording the desired compound as a white powder (1.45 g, 65 %); [α]_D = -0.9 (c = 1.0, CHCl₃); (Found: C, 65.7; H, 7.3; N, 7.6. Si₃₂O₁₂N₆₄P₃₂C₆₁₆H₇₄₄ requires C, 66.5; H, 6.8; N, 8.1%); δ_{H} (300.13 MHz; CDCl₃; Me₄Si) -0.19 (24 H, br, SiCH₃), 0.18, (br, 48H, SiCH₃(Ar)₂), 0.25-0.80 (m, 96H, O₃SiCH₂CH₂Si(CH₂CH₂Si)₂), β hydrosilylation (<22 %, m, 1.15), 1.55-1.98 (128 H, m, -CH₂-), 2.83-3.39 (128 H, m, -CH₂-), 3.83 (32 H, m, NCH), 6.55-6.82 (96 H, m, ArH), 6.95-7.22 (128 H, m, ArH) and 7.32-7.79 (64 H, m, ArH); δ_{C} (100.6 MHz; CDCl₃; Me₄Si) -6.3 (SiCH₃), -5.2 (SiCH₃(Ar)₂), 4.3, 4.6, 4.8, 6.0, 25.8 (d, *J*_{CP} 5.8, -CH₂-), 31.2 (-CH₂-), 52.8 (-CH₂-), 53.8 (d, *J*_{CP} 5.3, -CH₂-), 64.4 (d, *J*_{CP} 8.5, NCH) 115.2 (d, *J*_{CP} 12.2), 117.8, 127.5, 129.1, 129.2, 129.9, 134.8, 139.1 (*ipso* SiC), 140.7 (d, *J*_{CP} 26.8, *ipso* PC) and 147.8 (d, *J*_{CP} 15.3, *ipso* NC); δ_{P} (162.0 MHz; CDCl₃) 100.1; δ_{Si} (79.5 MHz; CDCl₃; Me₄Si) -66.8 (SiO₃), -6.0 (SiAr) and 8.3 (SiCH₃).

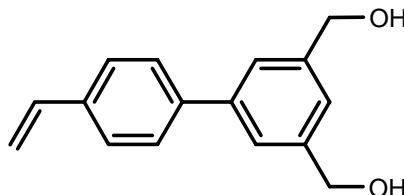
V. 7 Photoluminescent Polyhedral Oligomeric Silsesquioxane cored dendrimers and associated dendrons

4'-vinylbiphenyl-3,5-dicarbaldehyde (**M7**)



A mixture of 5-bromoisophthalaldehyde ¹⁴ (2.77 g, 13.01 mmol), 4-styrene boronic acid (2.41 g, 16.29 mmol), [Pd(PPh₃)₄] (374.8 mg, 0.32 mmol), K₂CO₃ (2M, 22.8 mL, 45.51 mmol) and THF (70 mL) was heated at 75 °C for 48 hours. After cooling to room temperature, CH₂Cl₂ (50 mL) and water (20 mL) were added and the layers were separated. The aqueous layer was extracted with CH₂Cl₂ (2 x 30 mL). The combined organic layers were washed with water (20 mL) and dried over MgSO₄. After evaporation of the solvents, the residue was loaded onto a silica gel column and eluted with CH₂Cl₂ affording **M7** as a white powder (2.51 g, 82 %) (Found: C, 81.30; H, 5.12. C₁₆H₁₂O₂ requires C, 81.36; H 5.08%); δ_{H} (400.13 MHz; CDCl₃; Me₄Si) 5.35 (1 H, d, ³J_{HH} 11.2, CH₂=CH), 5.85 (1 H, d, ³J_{HH} 17.6, CH₂=CH), 6.78 (1 H, dd, ³J_{HH} 11.2, ³J_{HH} 17.6, CH₂=CH), 7.55 (2 H, d, ³J_{HH} 8.4), 7.65 (2 H, d, ³J_{HH} 8.4), 8.33 (1 H, t, ⁴J_{HH} 1.5), 8.37 (2 H, d, ⁴J_{HH} 1.5) and 10.18 (2 H, s, CHO); δ_{C} (100.6 MHz; CDCl₃; Me₄Si) 115.2 (CH₂=CH), 127.2, 127.4, 129.9, 133.2, 136.6, 137.6, 137.7, 138.2, 143.0 and 191.3 (CHO); m/z (CI) 237.0913 (M+1. C₁₆H₁₃O₂ requires 237.0916).

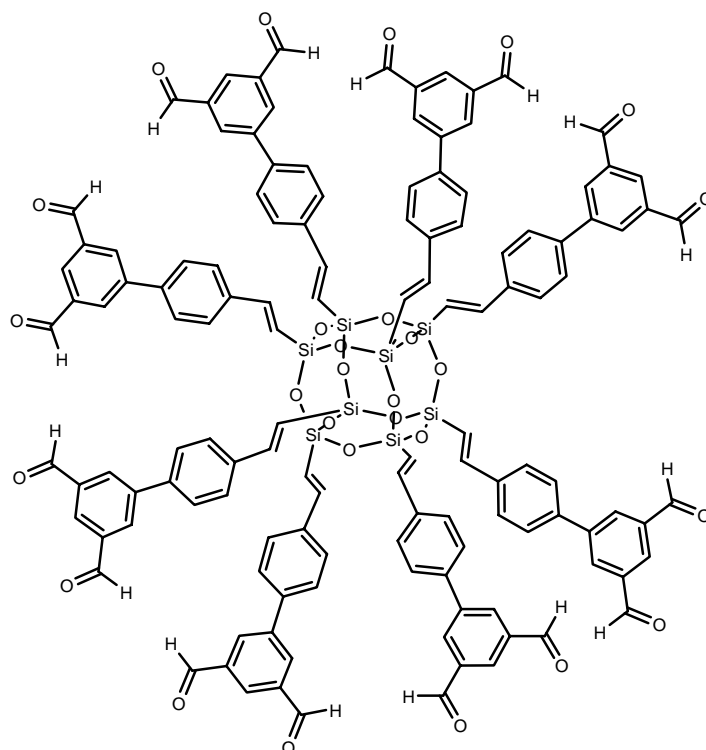
4'-vinylbiphenyl-3,5-dimethanol (**M8**)



4'-vinylbiphenyl-3,5-dicarbaldehyde **M7** (50 mg, 0.21 mmol) was dissolved in THF/MeOH (5 mL, 4/1) and cooled to 0 °C. NaBH₄ (32 mg, 0.85 mmol) was added and the solution stirred at 0°C for 30 min. After addition of water (1 mL), the aqueous layer was extracted with EtOAc (2 x 10 mL). The organic layer was washed with brine (10 mL) and dried over MgSO₄. After evaporation of the solvents, **M8** was obtained as a white powder (40 mg, 78 %)

(Found: C, 80.0; H, 6.6. C₁₆H₁₆O₂ requires C, 80.0; H, 6.7%); δ_{H} (400.13 MHz; (CD₃)₂SO; Me₄Si) 4.58 (4 H, d, $^3J_{\text{HH}}$ 5.7, CH₂OH), 5.25 (2 H, t, $^3J_{\text{HH}}$ 5.7, CH₂OH), 5.31 (1 H, d, $^3J_{\text{HH}}$ 11.1, CH₂=CH), 5.90 (1 H, d, $^3J_{\text{HH}}$ 17.9, CH₂=CH), 6.80 (1 H, dd, $^3J_{\text{HH}}$ 11.1, $^3J_{\text{HH}}$ 17.9, CH₂=CH), 7.30 (1 H, t, $^4J_{\text{HH}}$ 9.6), 7.48 (2 H, m), 7.58 (2 H, d, $^3J_{\text{HH}}$ 8.5) and 7.66 (2 H, d, $^3J_{\text{HH}}$ 8.5); δ_{C} (100.6 MHz; (CD₃)₂SO; Me₄Si) 63.7 (CH₂OH), 114.3 (CH₂=CH), 123.0, 124.4, 126.4, 126.5, 136.7, 137.8, 139.7, 142.9 and 143.0.

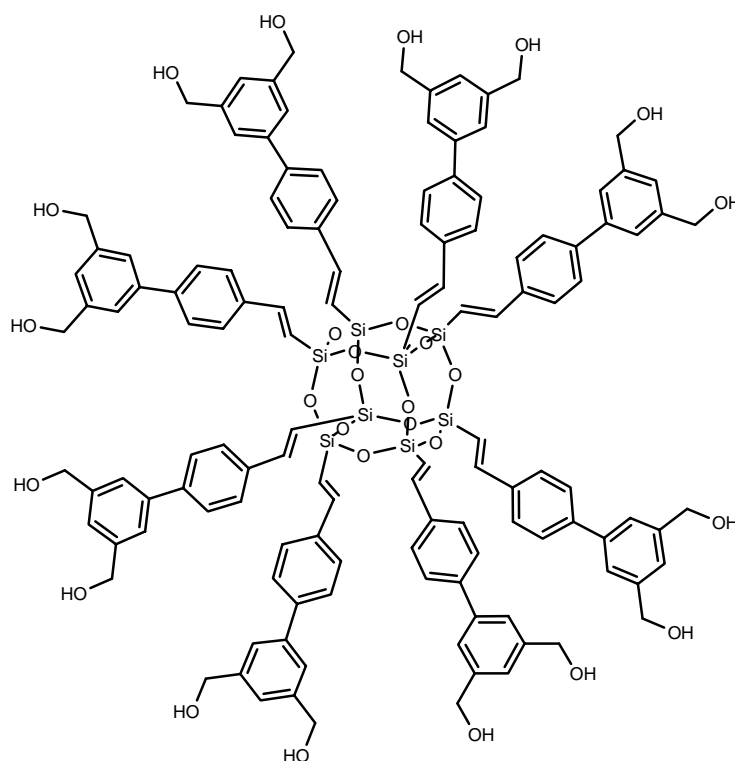
1,3,5,7,9,11,13,15-octakis[2-{4'-vinylbiphenyl-3,5-dicarbaldehyde}ethenyl]pentacyclo-[9.5.1.1^{3,9}.1^{5,15}.1^{7,13}]octasiloxane (S1)



An oven-dried flask equipped with a condenser and a magnetic stirring bar was charged under nitrogen with octavinylsilsesquioxane ⁶ (305 mg, 0.48 mmol) and 4'-vinylbiphenyl-3, 5 dicarbaldehyde **M7** (2 g, 8.47 mmol) in CH₂Cl₂ (10 mL). A solution of Grubbs' catalyst (16 mg, 0.019 mmol) in CH₂Cl₂ (3 mL) was injected into the mixture heated at 55 °C to maintain a gentle reflux. The reaction was stopped and cooled to room temperature after disappearance of the vinyl signals in ¹H NMR (90 hours). The mixture was filtered, concentrated and precipitated by adding the crude product in CH₂Cl₂ to a solution of ethyl acetate (120 mL) and petroleum ether (40-60) (500 mL). The residue was loaded onto a silica gel column and eluted with a gradient of CH₂Cl₂, EtOAc and (CH₃)₂CO (CH₂Cl₂/ EtOAc (10/1) → (CH₃)₂CO) affording **S1** as a white powder (0.865 mg, 78 %) (Found: C, 67.23; H, 3.86. C₁₂₈H₈₈O₂₈Si₈

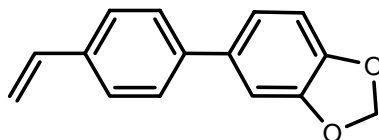
requires C, 66.89; H 3.83%); δ_{H} (400.13 MHz; CDCl_3 ; Me_4Si) 6.49 (8 H, d, $^3J_{\text{HH}}$ 19.3, $\text{SiCH}=\text{CH}$), 7.51 (8 H, d, $^3J_{\text{HH}}$ 19.3, $\text{SiCH}=\text{CH}$), 7.70 (32 H, m), 8.36 (8 H, m), 8.40 (16 H, m) and 10.18 (16 H, s, CHO); δ_{C} (100.6 MHz; CDCl_3 ; Me_4Si) 118.5 ($\text{SiCH}=\text{CH}$), 127.5, 127.7, 130.5, 132.7, 137.3, 137.9, 139.0, 142.7, 143.4, 148.6 ($\text{SiCH}=\text{CH}$) and 191.1 (CHO); m/z (MALDI) 2270.56 (M-CO. $\text{C}_{127}\text{H}_{88}\text{O}_{27}\text{Si}_8$ requires 2269.91).

1,3,5,7,9,11,13,15-octakis[2-{4'-vinylbiphenyl-3,5-dimethanol}ethenyl]pentacyclo-[9.5.1.1^{3,9}.1^{5,15}.1^{7,13}]octasiloxane (S2)



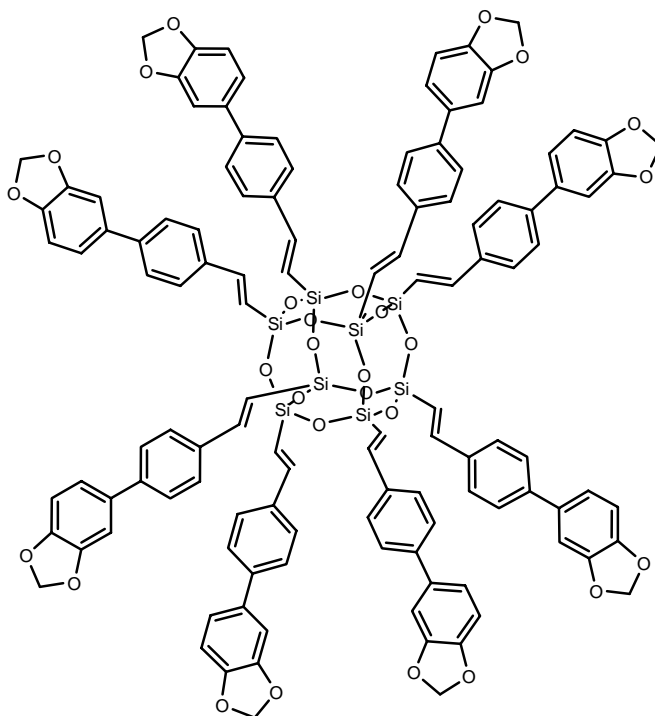
S1 (50 mg, 0.022 mmol) was dissolved in THF/MeOH (10 mL, 8/2) and cooled to 0 °C. NaBH_4 (26 mg, 0.70 mmol) was added and the solution stirred at 0 °C for 30 min. After addition of water (1 mL), the aqueous layer was extracted with EtOAc (20 mL). The organic layer was washed with brine (20 mL) and dried over MgSO_4 . After evaporation of the solvents, **S2** was obtained as a white powder (36 mg, 71 %). δ_{H} (400.13 MHz; $(\text{CD}_3)_2\text{SO}$; Me_4Si) 4.55 (32 H, d, $^3J_{\text{HH}}$ = 5.8, CH_2OH), 5.27 (16 H, t, $^3J_{\text{HH}}$ 5.8, CH_2OH), 6.57 (8 H, d, $^3J_{\text{HH}}$ 19.3, $\text{SiCH}=\text{CH}$), 7.24 (8 H, m), 7.47 (8 H, d, $^3J_{\text{HH}}$ 19.3, $\text{SiCH}=\text{CH}$), 7.50 (16 H, m) and 7.74 (32 H, m); δ_{C} (100.6 MHz; $(\text{CD}_3)_2\text{SO}$; Me_4Si) 63.6 (CH_2OH), 117.5 ($\text{SiCH}=\text{CH}$), 123.3, 124.6, 127.3, 127.9, 136.5, 137.3, 139.2, 143.1, 142.9 and 149.3 ($\text{SiCH}=\text{CH}$).

4-styryl-1,2-(methylenedioxy)benzene (**M9**)

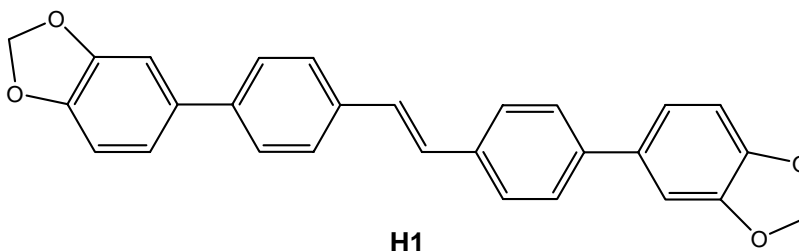


A mixture of 4-bromo-1,2-(methylenedioxy)benzene (1.3 mL, 10.8 mmol), 4-styrene boronic acid (2 g, 13.5 mmol), [Pd(PPh₃)₄] (374 mg, 0.32 mmol), K₂CO₃ (2M, 37.8 mmol) and THF (70 mL) was heated at 75 °C for 48 hours. After cooling to room temperature, CH₂Cl₂ (50 mL) and water (20 mL) were added and the layers were separated. The aqueous layer was extracted with CH₂Cl₂ (2 x 30 mL). The combined organic layers were washed with water (30 mL) and dried over MgSO₄. After evaporation of the solvents, flash column chromatography with CH₂Cl₂ afforded **M9** as a white luminescent powder (2.38 g, 98 %) (Found: C, 79.96; H, 5.16. C₁₅H₁₂O₂ requires C, 80.37; H 5.35%); δ_{H} (300.13 MHz; CDCl₃; Me₄Si) 5.27 (1 H, d, $^3J_{\text{HH}}$ 11.6, CH₂=CH), 5.79 (1 H, d, $^3J_{\text{HH}}$ 18.3, CH₂=CH), 6.01 (2 H, s, OCH₂O), 6.76 (1 H, dd, $^3J_{\text{HH}}$ 11.6 Hz, $^3J_{\text{HH}}$ 18.3, CH₂=CH), 6.90 (1 H, m), 7.09 (2 H, m) and 7.49 (4 H, m); δ_{C} (75.5 MHz; CDCl₃; Me₄Si) 101.6 (OCH₂O), 107.9, 109.0, 114.2 (CH₂=CH), 120.9, 127.3, 127.4, 135.5, 136.7, 136.8, 140.7, 147.5 and 148.8; m/z (CI) 225.0921 (M+1. C₁₅H₁₃O₂ requires 225.0916).

1,3,5,7,9,11,13,15-Octakis[2-{4-styryl-1,2-(methylenedioxy)benzene}ethenyl]pentacyclo[9.5.1.1^{3,9}.1^{5,15}.1^{7,13}]octasiloxane (**S3**)

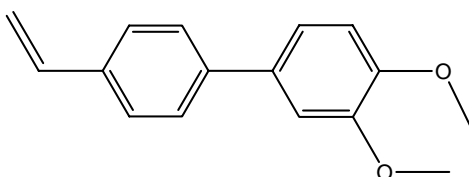


An oven-dried flask equipped with a condenser and a magnetic stirring bar was charged under nitrogen with octavinylsilsesquioxane ⁶ (100 mg, 0.16 mmol) and 4-styryl-1,2-(methylenedioxy)benzene **M9** (624 mg, 2.78 mmol) in CH₂Cl₂ (10 mL). A solution of Grubbs' catalyst (5 mg, 0.006 mmol) in CH₂Cl₂ (3 mL) was injected into the mixture heated at 55 °C to maintain a gentle reflux. The reaction was stopped and cooled to room temperature after disappearance of the vinyl signals in ¹H NMR (90 hours). The mixture was filtered, (isolation of **H1**), concentrated and precipitated by adding the crude product in CH₂Cl₂ to a solution of ethyl acetate (120 mL) and petroleum ether (40-60) (500 mL). The residue was loaded onto a silica gel column and eluted with CH₂Cl₂ affording **S3** as a white powder (231 mg, 67 %) (Found: C, 65.19; H, 4.02. C₁₂₀H₈₈O₂₈Si₈ requires C, 65.45; H, 4.00%); δ_H(300.13 MHz; CDCl₃; Me₄Si) 6.01 (16 H, s, OCH₂O), 6.37 (8 H, d, ³J_{HH} 18.6, SiCH=CH), 6.90 (8 H, m), 7.09 (16 H, m), 7.44 (8 H, d, ³J_{HH} 18.6, SiCH=CH) and 7.54 (32 H, m); δ_C(75.5 MHz; CDCl₃; Me₄Si) 101.6 (OCH₂O), 108.0, 109.0, 117.0 (SiCH=CH), 120.9, 127.3, 127.4, 135.5, 136.7, 140.7, 147.6, 148.5 (SiCH=CH) and 149.0; δ_{Si}(79.5 MHz; CDCl₃; Me₄Si) -77.6 (O₃Si); m/z (MALDI) 2202.44 (M. C₁₂₀H₈₈O₂₈Si₈ requires 2201.84).



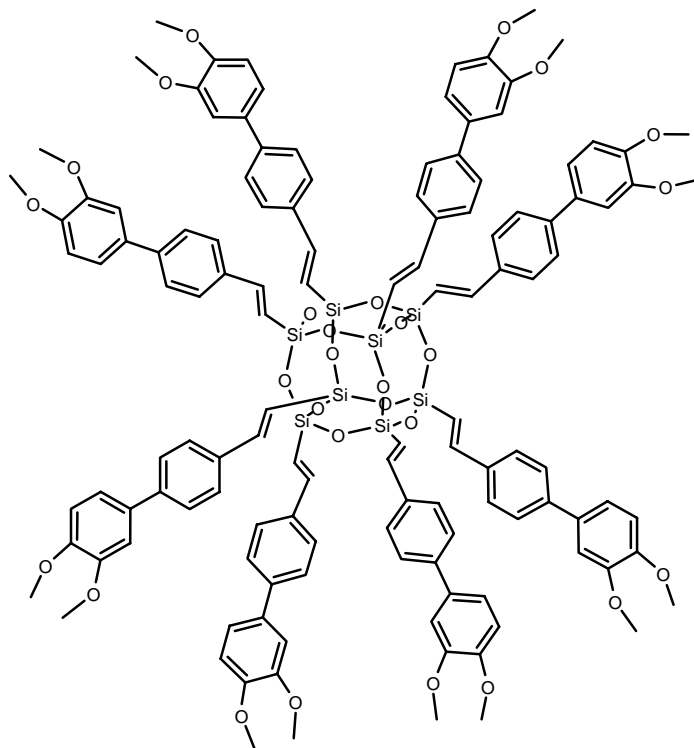
H1 (282 mg, 69 % based on unreacted **M9**) (Found: C, 79.93; H, 4.86. $C_{28}O_4H_{20}$ requires C, 79.98; H 4.79%); m/z (CI) 421.1436 ($M+1$. $C_{28}O_4H_{21}$ requires 421.1440)

3,4-dimethoxy-4'-vinylbiphenyl (**M10**)

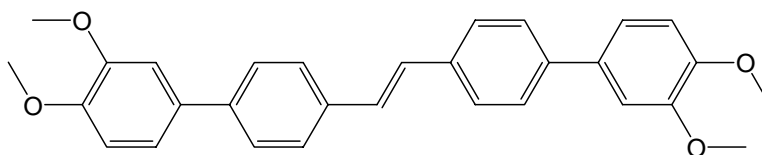


A mixture of 4-bromo-1,2-dimethoxybenzene (2.3 mL, 16.0 mmol), 4-styrene boronic acid (3 g, 20.3 mmol), $[Pd(PPh_3)_4]$ (562 mg, 0.48 mmol), K_2CO_3 (2M, 56.8 mmol) and THF (70 mL) was heated at 75 °C for 48 hours. After cooling to room temperature, CH_2Cl_2 (50 mL) and water (20 mL) were added and the layers were separated. The aqueous layer was extracted with CH_2Cl_2 (2 x 20 mL). The combined organic layers were washed with water (20 mL) and dried over $MgSO_4$. After evaporation of the solvents, flash column chromatography with CH_2Cl_2 afforded **M10** as a white luminescent powder (2.05 g, 53 %) (Found: C, 79.52; H, 6.90. $C_{16}H_{16}O_2$ requires C, 80.01; H, 6.66%); δ_H (300.13 MHz; $(CD_3)_2SO$; Me_4Si) 3.79 (3 H, s, OCH_3), 3.85 (3 H, s, OCH_3), 5.28 (1 H, d, $^3J_{HH}$ 11.1, $CH_2=CH$), 5.87 (1 H, d, $^3J_{HH}$ 17.8, $CH_2=CH$), 6.77 (1 H, dd, $^3J_{HH}$ 11.1, $^3J_{HH}$ 17.8, $CH_2=CH$), 7.03 (1 H, d, $^3J_{HH}$ 8.3), 7.22 (1 H, d, $^3J_{HH}$ 8.3), 7.23 (1 H, s), 7.53 (2 H, d, $^3J_{HH}$ 8.2) and 7.65 (2 H, d, $^3J_{HH}$ 8.2); δ_C (75.5 MHz; $(CD_3)_2SO$; Me_4Si) 55.5 (OCH_3), 110.2, 112.1, 114.0 ($CH_2=CH$), 118.7, 126.4, 126.6, 132.3, 135.6, 136.2, 139.5, 148.6 and 149.0 ; m/z (ESI) 263.1046 ($M+Na$. $C_{16}H_{16}O_2Na$ requires 263.1048).

**1,3,5,7,9,11,13,15-Octakis[2-{3,4-dimethoxy-4'-vinybiphenyl }ethenyl]pentacyclo
[9.5.1.1^{3,9}.1^{5,15}.1^{7,13}]octasiloxane (S4)**



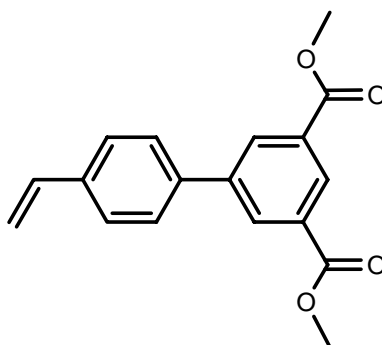
An oven-dried flask equipped with a condenser and a magnetic stirring bar was charged under nitrogen with octavinylsilsesquioxane ⁶ (100 mg, 0.16 mmol) and 3,4-dimethoxy-4'-vinylbiphenyl **M10** (662 mg, 2.76 mmol) in CH₂Cl₂ (10 mL). A solution of Grubbs' catalyst (5 mg, 0.006 mmol) in CH₂Cl₂ (3 mL) was injected into the mixture heated at 55 °C to maintain a gentle reflux. The reaction was stopped and cooled to room temperature after disappearance of the vinyl signals in ¹H NMR (90 hours). The mixture was filtered, (isolation of **H2**) concentrated and precipitated by adding the crude product in CH₂Cl₂ to a solution of ethyl acetate (120 mL) and petroleum ether (40-60) (500 mL). The residue was loaded onto a silica gel column and eluted with a gradient of CH₂Cl₂ and (CH₃)₂CO (CH₂Cl₂ → (CH₃)₂CO) affording **S4** as a white powder (252 mg, 69 %) (Found: C, 65.28; H, 4.75. C₁₂₈H₁₂₀Si₈O₂₈ requires C, 65.97; H, 5.15%); δ_H(300.13 MHz; CDCl₃; Me₄Si) 3.93 (24 H, s, OCH₃), 3.96 (24 H, s, OCH₃), 6.39 (8 H, d, ³J_{HH} = 19.2, SiCH=CH), 6.95 (8 H, d, ³J_{HH} 8.68), 7.16 (16 H, m), 7.46 (8 H, d, ³J_{HH} 19.2, SiCH=CH) and 7.58 (32 H, m); δ_C(75.5 MHz; CDCl₃; Me₄Si) 56.0 (OCH₃), 110.3, 111.5, 117.2 (SiCH=CH), 119.4, 127.0, 127.4, 133.5, 136.0, 141.6, 148.8 (SiCH=CH), 148.9 and 149.2; δ_{Si}(79.5 MHz; CDCl₃; Me₄Si) -78.3 (O₃Si); m/z (MALDI) 2330.30 (M. C₁₂₈H₁₂₀Si₈O₂₈ requires 2329.92).



H2

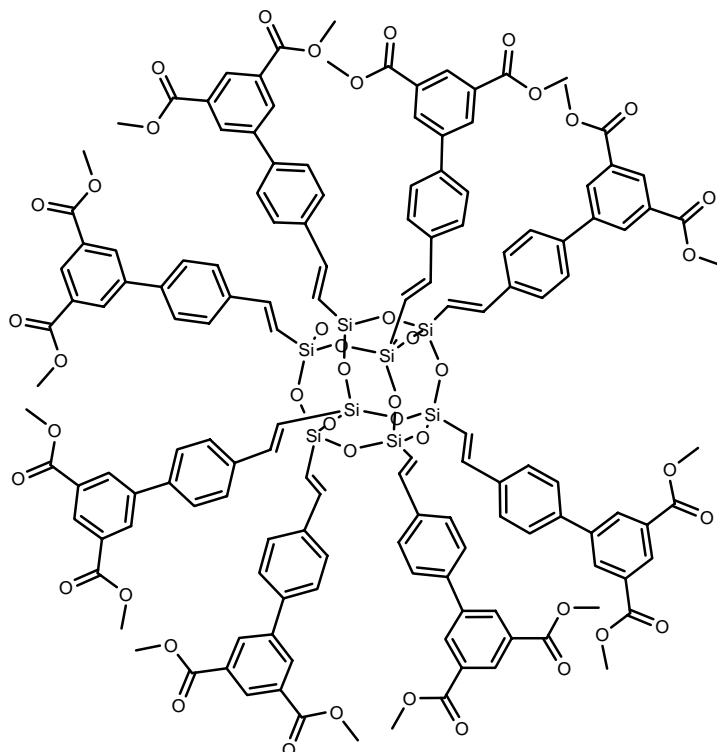
H2 (271 mg, 63 % based on unreacted **M10**) (Found: C, 79.6; H, 6.2 $C_{30}O_4H_{28}$ requires C, 80.1; H 6.3%); m/z (CI) 453.206 (M+1. $C_{30}O_4H_{29}$ requires 453.2066)

Dimethyl 4'-vinylbiphenyl-3,5-dicarboxylate (M11)

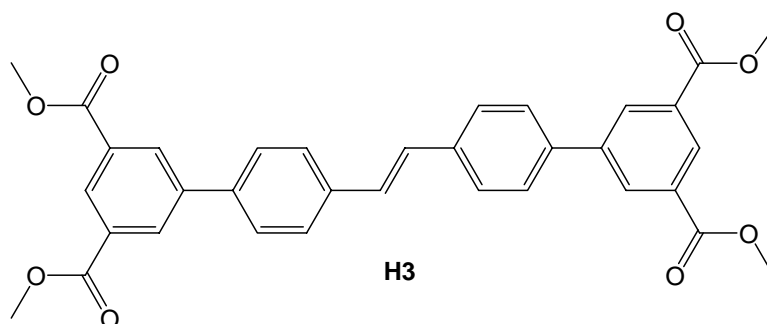


A mixture of dimethyl 5-iodobenzene-1,3-dicarboxylate ¹⁵ (755 mg, 2.36 mmol), 4-styrene boronic acid (436 mg, 2.95 mmol), $[Pd(PPh_3)_4]$ (82 mg, 0.071 mmol), K_2CO_3 (2M, 4.2 mL, 8.40 mmol) and THF (70 mL) was heated at 75 °C for 48 hours. After cooling to room temperature, CH_2Cl_2 (50 mL) and water (20 mL) were added and the layers were separated. The aqueous layer was extracted with CH_2Cl_2 (2 x 20 mL). The combined organic layers were washed with water (20 mL) and dried over $MgSO_4$. The residue was loaded onto a silica gel column and eluted with CH_2Cl_2 to afford **M11** as a white powder (531 mg, 76 %) (Found: C, 73.0; H, 4.6. $C_{18}H_{16}O_4$ requires C, 73.0, H 5.4%); δ_H (300.13 MHz; $CDCl_3$; Me_4Si) 3.99 (6 H, s, $OCOCH_3$), 5.33 (1 H, d, $^3J_{HH}$ 11.1, $CH_2=CH$), 5.83 (1 H, d, $^3J_{HH}$ 17.8, $CH_2=CH$), 6.78 (1 H, dd, $^3J_{HH}$ 11.1, $^3J_{HH}$ 17.8, $CH_2=CH$), 7.53 (2 H, d, $^3J_{HH}$ 8.3), 7.65 (2 H, d, $^3J_{HH}$ 8.3), 8.48 (2 H, d, $^4J_{HH}$ 1.6) and 8.65 (1 H, t, $^4J_{HH}$ 1.6); δ_C (75.5 MHz; $CDCl_3$; Me_4Si) 52.6 ($OCOCH_3$), 114.8 ($CH_2=CH$), 127.0, 127.5, 129.5, 131.3, 132.3, 136.3, 138.0, 138.4, 141.7 and 166.2 ($OCOCH_3$); m/z (CI) 297.1129 (M+1. $C_{18}H_{17}O_4$ requires 297.1127).

**1,3,5,7,9,11,13,15-octakis[2-{4 Dimethyl 4'-vinylbiphenyl-3,5-dicarboxylate
}ethenyl]pentacyclo-[9.5.1.1^{3,9}.1^{5,15}.1^{7,13}]octasiloxane (S5)**

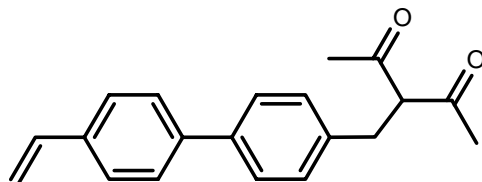


An oven-dried flask equipped with a condenser and a magnetic stirring bar was charged under nitrogen with octavinylsilsesquioxane ⁶ (20 mg, 0.032 mmol) and dimethyl 4'-vinylbiphenyl-3,5-dicarboxylate **M11** (164 mg, 0.55 mmol) in CH₂Cl₂ (10 mL). A solution of Grubbs' catalyst (1 mg, 0.001 mmol) in CH₂Cl₂ (3 mL) was injected into the mixture heated at 55 °C to maintain a gentle reflux. The reaction was stopped and cooled to room temperature after disappearance of the vinyl signals in ¹H NMR (90 hours). The mixture was filtered, concentrated and then precipitated by adding the crude product in CH₂Cl₂ to a solution of ethyl acetate (120 mL) and petroleum ether (40-60) (500 mL). The residue was loaded onto a silica gel column and eluted with a gradient of CH₂Cl₂ and EtOAc (CH₂Cl₂ → CH₂Cl₂/EtOAc (20/1) → EtOAc) affording **S5** as a white powder (54 mg, 61 %) (Found: C, 61.8; H, 3.6. C₁₂₀H₈₈O₄₄Si₈ requires C, 62.3; H 4.3%); δ_H(300.13 MHz; CDCl₃; Me₄Si) 3.99 (48 H, s, OCOCH₃), 6.47 (8 H, d, ³J_{HH} = 19.2, SiCH=CH), 7.50 (8 H, d, ³J_{HH} 19.2, SiCH=CH), 7.68 (32 H, m), 8.49 (16 H, d, ⁴J_{HH} 1.6) and 8.66 (8 H, t, ⁴J_{HH} 1.6); δ_C(75.5 MHz; CDCl₃; Me₄Si) 52.7 (OCOCH₃), 118.3 (SiCH=CH), 127.1, 127.4, 127.9, 131.3, 131.5, 137.8, 138.5, 141.3, 147.8 (SiCH=CH) and 166.4 (OCOCH₃); δ_{Si}(79.5 MHz; CDCl₃; Me₄Si) -78.5 (O₃Si); m/z (MALDI) 2802.41 (M+Na. C₁₂₀H₈₈O₄₄Si₈Na requires 2801.08).



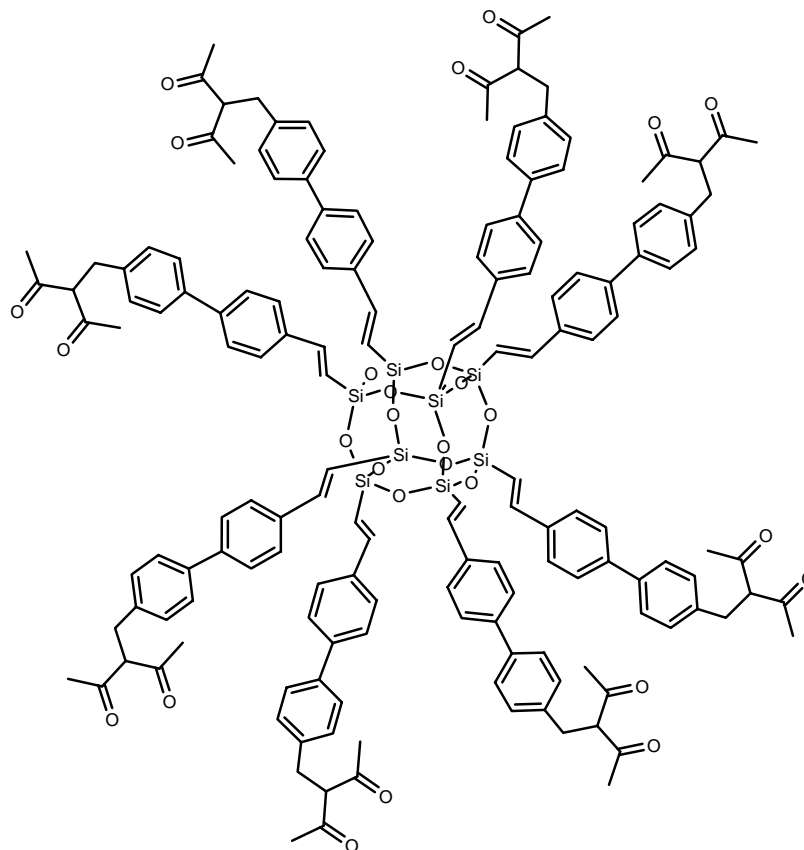
H3 (72 mg, 64 % based on unreacted **M11**) (Found: C, 72.3; H, 4.3. $C_{34}O_8H_{29}$ requires C, 71.7; H 4.6%); δ_H (400.13 MHz; $CDCl_3$; Me_4Si) 4.00 (12 H, s, $OCOCH_3$), 7.24 (2 H, s, $CH=CH$), 7.67 (4 H, d, $^3J_{HH}$ 8.5), 7.71 (4 H, d, $^3J_{HH}$ 8.5), 8.50 (4 H, d, $^4J_{HH}$ 1.7), 8.50 (4 H, d, $^4J_{HH}$ 1.7), 8.67 (2 H, d, $^4J_{HH}$ 1.7); δ_C (75.5 MHz; $CDCl_3$; Me_4Si) 52.6 ($OCOCH_3$), 127.3, 127.5, 128.6 ($CH=CH$), 129.4, 131.3, 132.0, 137.2, 138.2, 141.4, and 166.3 ($OCOCH_3$). m/z (CI) 565.1864 ($M+1$. $C_{34}O_8H_{29}$ requires 565.1860).

3-((4'-vinylbiphenyl-4-yl)methyl)pentane-2,4-dione (the mixture of enol and keto form, enol/keto = 3/1) (M12)



4-styryl-benzyl-bromide ¹⁶ (350 mg, 1.28 mmol) and lithium 2,4-pentanedioate (408 mg, 3.85 mmol) were dissolved in DMF (20 mL) and agitated overnight at room temperature. The mixture was then poured onto approximately 10 g of ice and stirred until all the ice had melted. Et_2O (30 mL) was added and the layers separated. The aqueous phase was extracted with Et_2O (4 x 20 mL). The combined organic layers were washed with brine (2 x 30 mL) and dried over $MgSO_4$. The residue was loaded onto a silica gel column and eluted with CH_2Cl_2 to afford **M12** as a white powder (177 mg, 47 %) (Found: C, 81.5; H, 6.9. $C_{20}H_{20}O_2$ requires C, 82.2; H, 6.9%); δ_H (400.13 MHz; $CDCl_3$; Me_4Si) 2.12 (6 H, s, enol CH_3), 2.20 (6 H, s, keto CH_3), 3.20 (2 H, d, $^3J_{HH}$ 7.5, keto CH_2), 3.71 (2 H, s, enol CH_2), 4.05 (1 H, t, $^3J_{HH}$ 7.5, keto CH), 5.28 (1 H, d, $^3J_{HH}$ 10.9, $CH_2=CH$), 5.80 (1 H, d, $^3J_{HH}$ 18.2, $CH_2=CH$), 6.76 (1 H, dd, $^3J_{HH} = 10.9$, $^3J_{HH}$ 18.2, $CH_2=CH$), 7.23 (2 H, m) and 7.53 (6 H, m); δ_C (75.5 MHz; $CDCl_3$; Me_4Si) 23.5, 29.9, 32.6, 32.8, 69.4 (keto CH), 108.4, 114.1 ($CH_2=CH$), 126.8, 127.2, 127.4, 128.1, 129.2, 136.5, 137.3, 138.2, 139.1, 140.2, 192.4, 203.5 (keto $C=O$) and 207.4; m/z (CI) 293.1541 ($M+1$. $C_{20}H_{21}O_2$ requires 293.1542).

1,3,5,7,9,11,13,15-octakis[2-{3-((4'-vinylbiphenyl-4-yl)methyl)pentane-2,4-dione}ethenyl]pentacyclo-[9.5.1.1^{3,9}.1^{5,15}.1^{7,13}]octasiloxane (the mixture of enol and keto form, enol/keto = 1/3) (S6)



An oven-dried flask equipped with a condenser and a magnetic stirring bar was charged under nitrogen with octavinylsilsesquioxane ⁶ (31 mg, 0.049 mmol) and 3-((4'-vinylbiphenyl-4-yl)methyl)pentane-2,4-dione **M12** (250 mg, 0.86 mmol) in CH₂Cl₂ (10 mL). A solution of Grubbs' catalyst (2 mg, 0.002 mmol) in CH₂Cl₂ (3 mL) was injected into the mixture heated at 55 °C to maintain a gentle reflux. The reaction was stopped and cooled to room temperature after disappearance of the vinyl signals in ¹H NMR (90 hours). The mixture was filtered, concentrated and precipitated by adding the crude product in CH₂Cl₂ to a solution of ethyl acetate (120 mL) and petroleum ether (40-60) (500 mL). The residue was loaded onto a silica gel column and eluted with a gradient of CH₂Cl₂, EtOAc and (CH₃)₂CO (CH₂Cl₂/EtOAc (10/1) → (CH₃)₂CO) affording **S6** as a white powder (102 mg, 76 %) (Found: C, 70.24; H, 4.97. C₁₆₀H₁₅₂O₂₈Si₈ requires C, 69.97; H, 5.53%); δ_H(400.13 MHz; CDCl₃; Me₄Si) 2.10 (48 H, s, enol CH₃), 2.15 (48 H, s, keto CH₃), 3.19 (16 H, m, keto CH₂), 3.70 (16 H, br s, enol CH₂), 4.04 (8 H, m, keto CH), 6.37 (8 H, d, ³J_{HH} 19.1, SiCH=CH), 7.21 (16 H, m), 7.43 (8 H, d, ³J_{HH} 19.1, SiCH=CH) and 7.57 (48 H, m); δ_C(75.5 MHz; CDCl₃; Me₄Si) 23.5, 29.9,

32.6, 33.9, 69.9 (keto CH), 108.4, 117.3 (SiCH=CH), 126.7, 127.0, 127.9, 128.1, 129.2, 136.4, 137.7, 138.5, 139.1, 140.2, 149.2 (SiCH=CH), 191.8, 203.5 (keto C=O) and 207.3; δ_{Si} (79.5 MHz; CDCl_3 ; Me_4Si) -78.5 (O_3Si); m/z (MALDI) 2768.93 ($\text{M}+\text{Na}$. $\text{C}_{160}\text{H}_{152}\text{O}_{28}\text{Si}_8\text{Na}$ requires 2769.24).

V. 8 References

1. O. Legrand, J.-M. Brunel and G. Buono, *Eur. J. Org. Chem.*, 1999, 1099.
2. P. André, G. Cheng, A. Ruseckas, T. van Mourik, H. Früchtl, J. A. Crayston, R. E. Morris, D. Cole-Hamilton and I. D. W. Samuel, *J. Phys. Chem. B*, 2008, Accepted.
3. C. J. Ngono, T. Constantieux and G. Buono, *Eur. J. Org. Chem.*, 2006, 1499.
4. D. K. Liu, M. S. Wrighton, D. R. McKay and G. E. Maciel, *Inorg. Chem.*, 1984, **23**, 212.
5. D. de Groot, J. N. H. Reek, P. C. J. Kamer and P. W. N. M. van Leeuwen, *Eur. J. Org. Chem.*, 2002, 1085.
6. M. Voronkov, T. N. Martynova, R. G. Mirskov and V. I. Bely, *J. Gen. Chem. USSR (Engl. Transl.)*, 1979, **49**, 1328.
7. B. Hong, T. P. S. Thoms, H. J. Murfee and M. J. Lebrun, *Inorg. Chem.*, 1997, **36**, 6146.
8. L. Ropartz, K. J. Haxton, D. F. Foster, R. E. Morris, A. M. Z. Slawin and D. J. Cole-Hamilton, *J. Chem. Soc., Dalton Trans.*, 2002, 4323.
9. J. N. Demas and G. A. Crosby, *J. Phys. Chem.*, 1971, **75**, 991-1024.
10. *Hyperchem*, Hypercube, Inc.
11. K. Drewelies and H. P. Latscha, *Angew. Chem.*, 1982, **94**, 642.
12. C. W. Edwards, M. R. Shipton, N. W. Alcock, H. Clase and M. Wills, *Tetrahedron* 2003, **59**, 6473.
13. P.-A. Jaffres and R. E. Morris, *J. Chem. Soc., Dalton Trans.*, 1998, 2767.
14. K. Matsuda, N. Nakamura, K. Takahashi, K. Inoue, N. Koga and H. Iwamura, *J. Am. Chem. Soc.*, 1995, **117**, 5550.
15. M. Mazik and A. König, *J. Org. Chem.*, 2006, **71**, 7854.
16. H. Sellner, C. Faber, P. B. Rheiner and D. Seebach, *Chem. Eur. J.*, 2000, **6**, 3692.

VI. Conclusions and future work

VI. Conclusions and future work

VI. 1 Conclusions

It has been shown that the copolymerisation of carbon monoxide and ethene is possible using a wide range of monodentate phosphines when the P:Pd ratio is low (4:1). This is an unexpected result, as most of the literature teaches that methyl propanoate should be selectively produced. Our results show that active, selective catalysts for polyketone formation can be generated from palladium complexes containing simple monodentate phosphines having low steric bulk and high electron density. Complexes of Polyhedral Oligomeric Silsesquioxane in which 8 or more equivalent phosphines are placed on the surface were also tested in this reaction and give either methyl propanoate or polyketone. In the case where the groups on the surface are $-\text{Si}(\text{Me})(\text{CH}_2\text{PPh}_2)_2$, the macromolecule and the small molecule analogue, $\text{Me}_2\text{Si}(\text{CH}_2\text{PPh}_2)_2$ behave very similarly to produce comparable amounts of polyketone. For ligands containing P atoms that are separated by longer spacers, the product is methyl propanoate with very little chain growth. In one case, that using **G0-8ethylPPh₂**, the rate using the macromolecule is significantly enhanced in comparison to that obtained with the small molecule as a result of the extra steric bulk associated with the presence of the POSS core and its other arms. In contrast, for **G1-16ethylPPh₂**, the rate is reduced compared with its small molecule analogue, probably because interactions on the periphery decrease the effective bite angle of the bidentate ligand, hence increasing the pocket angle and reducing the rate of termination.

New diazaphospholidine terminated Polyhedral Oligomeric Silsesquioxane (POSS) molecules have been synthesized and tested in styrene and vinyl acetate hydroformylation. Some of them have been shown to precipitate upon mixing with rhodium precursors, whilst others remain in solution and show activity. These latter are more compact and rigid in comparison to the former, which are more flexible and hence more prone to monodentate binding to rhodium and cross-linking. Modelling studies have been able to rationalise these observations. PP distance calculations show that the ligands, for which precipitation occurs upon mixing with the rhodium precursor, have PP distances too big to promote bidentate coordination, whereas the two active ligands display more rigid and compact structures with PP distance falling in the range of possible bidentate coordination. We have, therefore succeeded in using macromolecular design to induce a dendritic effect by sufficiently

crowding SemiEsphos units at the periphery of a dendrimer like molecule that the properties of ESPHOS (a bidentate analogue of monodentate SemiEsphos) are at least partially reproduced.

Novel photoluminescent vinylbiphenyl decorated Polyhedral Oligomeric Silsesquioxane cored dendrimers have been synthesised and characterized by NMR, microanalysis and MALDI-TOF spectroscopy. Optical measurements have proven in some cases to be an interesting tool in analyzing the purity of these compounds by showing the presence of light emitting side products not detected by NMR. In addition, dialdehyde modified vinylbiphenyl chromophores grafted at the periphery of the cube have displayed the unusual ability to become luminescent when exposed to reducing environments such as NaBH_4 , LiAlH_4 or BH_3 . The photoluminescence of this POSS molecule has been used as a quantitative hybrid organic/inorganic chemosensor for hydridic reducing agents.

VI. 2 Future work

VI. 2. 1 Catalysis

POSS decorated with $-\text{PBu}^t_2$ endgroups, synthesised by similar methodologies developed for $-\text{PPh}_2$ terminated dendrimers, could be investigated in the methoxycarbonylation of ethene to observe whether higher rates than $1,2-(\text{Bu}^t_2\text{PCH}_2)_2\text{C}_6\text{H}_4$ ¹ in methylpropanoate formation can be achieved, and how the selectivity varies with the dendritic architecture.

$1,2-(\text{Bu}^t_2\text{PCH}_2)_2\text{C}_6\text{H}_4$ is also the most selective ligand for the synthesis of linear esters by methoxycarbonylation reactions of internal or terminal alkenes^{2, 3} and for the synthesis of branched products from vinyl acetate carbonylation.^{4, 5} The use of $-\text{PBu}^t_2$ terminated dendrimers for these reactions would be interesting since here the product separation is a problem that has not so far been solved. Separation by ultrafiltration appears to be an exciting possibility. Similar recycling processes could be used with **G0-8ethylPPh₂**, bearing 8 diphenylphosphines at its periphery, as this dendrimer has been shown selectively to produce methylpropanoate (no copolymer or oligomers are formed).

The design of more rigid SEMI-ESPHOS terminated POSS should prevent any oligomerisation of dendrimers from occurring, giving rise to efficient catalysts in alkene

asymmetric hydroformylation. Enantiomeric excess (*ee*) may also be enhanced by those less flexible structures. The development of a suitable membrane and its application in a recycling process should be again the major target for future research as filtration of this nanometric ligand combining with its high reactivity may provide a separable asymmetric catalyst.

VI. 2. 2 Photoluminescence

Modified vinylbiphenyl chromophores have shown promising results when attached onto a POSS core so that widening the scope of their applications should open new exciting horizons.

For instance, chiral derivatisation of the reducing agents probe, POSS **S1**, would allow chiral amines to be quantified as amines have been shown to activate the fluorescence of the macromolecule. In addition, detailed investigations should be carried out to exploit the potential of these fluorescent macromolecules in applications ranging from cross-linkable hybrid nano-structured polymers, to nano-probes, sensors and carriers. The fluorescent properties of these systems may allow sensing or metal atom extraction from solution environments.

VI. 3 References

1. W. Clegg, G. R. Eastham, M. R. J. Elsegood, R. P. Tooze, X. L. Wang and K. Whiston, *Chem. Commun.*, 1999, 1877.
2. C. Jimenez, D. F. Foster, G. R. Eastham and D. J. Cole-Hamilton, *Chem. Commun.*, 2004, 1720-1721.
3. C. Jimenez-Rodriguez, G. R. Eastham and D. J. Cole-Hamilton, *Inorg. Chem. Commun.*, 2005, in press.
4. H. Ooka, T. Inoue, S. Itsuno and M. Tanaka, *Chem. Commun.*, 2005, 1173.
5. A. J. Rucklidge, G. E. Morris and D. J. Cole-Hamilton, *Chem. Commun.*, 2005, 1176.

Annexes

(2S,5S)-2-(2-Hydroxy-6-methoxyphenyl)-3-phenyl-1,3-diaza-2-phosphabicyclo[3.3.0]octane-2-one

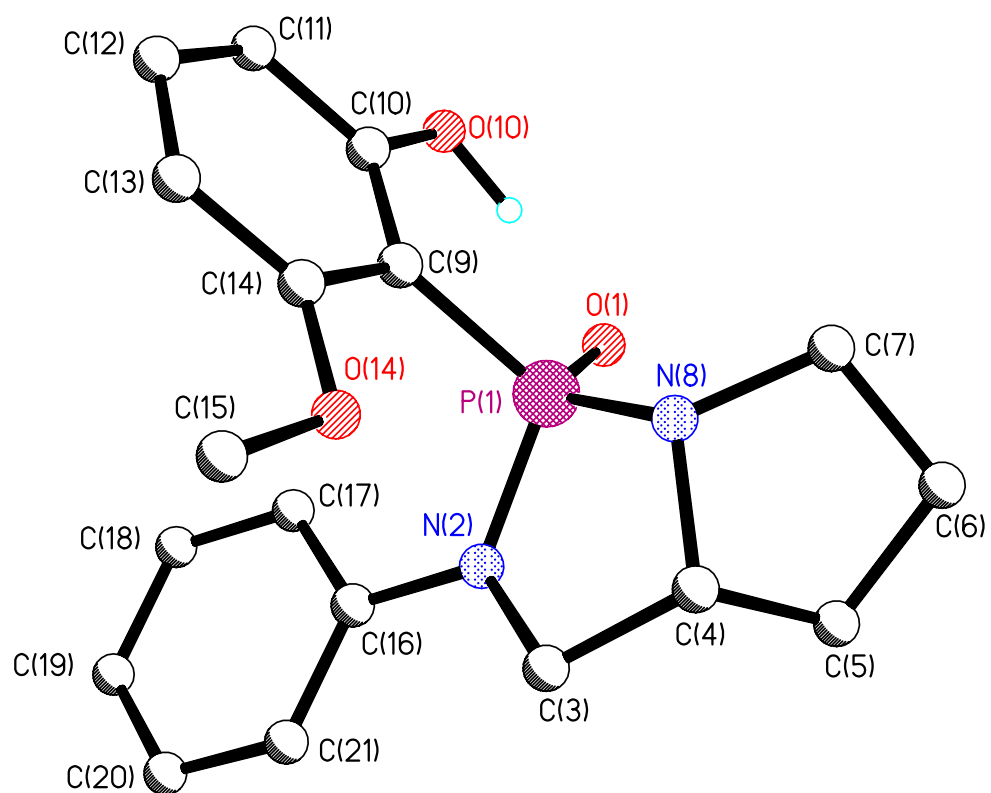


Table 1. Crystal data and structure refinement for C₁₈H₂₁N₂O₃P (1)

<i>Identification code</i>	nvdch3	
<i>Empirical formula</i>	C ₁₈ H ₂₁ N ₂ O ₃ P	
<i>Formula weight</i>	344.34	
<i>Temperature</i>	93(2) K	
<i>Wavelength</i>	0.71073 Å	
<i>Crystal system</i>	Monoclinic	
<i>Space group</i>	P2(1)/n	
<i>Unit cell dimensions</i>	a = 13.606(3) Å	alpha = 90°
	b = 8.4675(15) Å	beta = 100.050(5)°
	c = 14.752(3) Å	gamma = 90°
<i>Volume</i>	1673.4(6) Å ³	
<i>Z</i>	4	
<i>Density (calculated)</i>	1.367 Mg/m ³	
<i>Absorption coefficient</i>	0.183 mm ⁻¹	
<i>F(000)</i>	728	
<i>Crystal size</i>	0.1300 x 0.0800 x 0.0500 mm ³	
<i>Theta range for data collection</i>	1.88 to 25.36°	
<i>Index ranges</i>	-16<=h<=12, -10<=k<=7, -15<=l<=17	
<i>Reflections collected</i>	10737	
<i>Independent reflections</i>	3053 [R(int) = 0.0510]	
<i>Completeness to theta = 25.00°</i>	99.9 %	
<i>Absorption correction</i>	Multiscan	
<i>Max. and min. transmission</i>	1.0000 and 0.8877	
<i>Refinement method</i>	Full-matrix least-squares on F ²	
<i>Data / restraints / parameters</i>	3053 / 1 / 224	
<i>Goodness-of-fit on F²</i>	0.996	
<i>Final R indices [I>2sigma(I)]</i>	R1 = 0.0479, wR2 = 0.0976	
<i>R indices (all data)</i>	R1 = 0.0775, wR2 = 0.1109	
<i>Extinction coefficient</i>	0.0046(9)	
<i>Largest diff. peak and hole</i>	0.268 and -0.347 e.Å ⁻³	

Table 2. Atomic coordinates ($\times 10^4$) and equivalent isotropic displacement parameters ($\text{\AA}^2 \times 10^3$) for $\text{C}_{18}\text{H}_{21}\text{N}_2\text{O}_3\text{P}$. U(eq) is defined as one third of the trace of the orthogonalized U_{ij} tensor

	x	y	z	U(eq)
O(1)	6707(1)	4454(2)	5442(1)	24(1)
P(1)	6911(1)	2731(1)	5577(1)	21(1)
N(2)	7579(2)	2237(2)	6593(1)	20(1)
C(3)	7098(2)	1003(3)	7066(2)	24(1)
C(4)	6006(2)	1008(3)	6617(2)	22(1)
C(5)	5321(2)	2124(3)	7019(2)	27(1)
C(6)	4447(2)	2316(3)	6221(2)	33(1)
C(7)	4911(2)	2234(3)	5352(2)	26(1)
N(8)	5939(2)	1609(2)	5661(2)	21(1)
C(9)	7538(2)	2096(3)	4671(2)	18(1)
C(10)	7744(2)	3153(3)	3994(2)	21(1)
O(10)	7469(1)	4702(2)	3981(1)	27(1)
C(11)	8238(2)	2654(3)	3296(2)	24(1)
C(12)	8554(2)	1118(3)	3282(2)	29(1)
C(13)	8388(2)	49(3)	3948(2)	27(1)
C(14)	7888(2)	535(3)	4635(2)	22(1)
O(14)	7692(1)	-428(2)	5326(1)	28(1)
C(15)	8090(3)	-1996(3)	5366(2)	45(1)
C(16)	8610(2)	2528(3)	6852(2)	22(1)
C(17)	9094(2)	3585(3)	6345(2)	25(1)
C(18)	10110(2)	3845(3)	6589(2)	30(1)
C(19)	10658(2)	3106(3)	7346(2)	34(1)
C(20)	10190(2)	2087(3)	7858(2)	32(1)
C(21)	9170(2)	1774(3)	7614(2)	26(1)

Table 3. Bond lengths [\AA] and angles [$^\circ$] for $\text{C}_{18}\text{H}_{21}\text{N}_2\text{O}_3\text{P}$

Atoms	Length	Atoms	Length
O(1)-P(1)	1.4926(16)	C(15)-H(15C)	0.9800
P(1)-N(8)	1.650(2)	C(16)-C(21)	1.397(4)
P(1)-N(2)	1.664(2)	C(16)-C(17)	1.402(4)
P(1)-C(9)	1.789(3)	C(17)-C(18)	1.385(4)
N(2)-C(16)	1.410(3)	C(17)-H(17A)	0.9500
N(2)-C(3)	1.472(3)	C(18)-C(19)	1.379(4)
C(3)-C(4)	1.517(4)	C(18)-H(18A)	0.9500
C(3)-H(3A)	0.9900	C(19)-C(20)	1.374(4)
C(3)-H(3B)	0.9900	C(19)-H(19A)	0.9500
C(4)-N(8)	1.487(3)	C(20)-C(21)	1.398(4)
C(4)-C(5)	1.518(3)	C(20)-H(20A)	0.9500
C(4)-H(4A)	1.0000	C(21)-H(21A)	0.9500
C(5)-C(6)	1.530(4)		
C(5)-H(5A)	0.9900		
C(5)-H(5B)	0.9900		
C(6)-C(7)	1.528(4)		
C(6)-H(6A)	0.9900		
C(6)-H(6B)	0.9900		
C(7)-N(8)	1.490(3)		
C(7)-H(7A)	0.9900		
C(7)-H(7B)	0.9900		
C(9)-C(10)	1.406(3)		
C(9)-C(14)	1.409(3)		
C(10)-O(10)	1.363(3)		
C(10)-C(11)	1.390(4)		
O(10)-H(10O)	0.980(5)		
C(11)-C(12)	1.371(3)		
C(11)-H(11A)	0.9500		
C(12)-C(13)	1.383(4)		
C(12)-H(12A)	0.9500		
C(13)-C(14)	1.378(4)		
C(13)-H(13A)	0.9500		
C(14)-O(14)	1.368(3)		
O(14)-C(15)	1.431(3)		
C(15)-H(15A)	0.9800		
C(15)-H(15B)	0.9800		

Atoms	Angle	Atoms	Angle
O(1)-P(1)-N(8)	116.11(11)	C(6)-C(7)-H(7B)	110.7
O(1)-P(1)-N(2)	115.16(10)	H(7A)-C(7)-H(7B)	108.8
N(8)-P(1)-N(2)	96.14(11)	C(4)-N(8)-C(7)	108.1(2)
O(1)-P(1)-C(9)	107.21(10)	C(4)-N(8)-P(1)	110.55(17)
N(8)-P(1)-C(9)	112.11(11)	C(7)-N(8)-P(1)	119.61(15)
N(2)-P(1)-C(9)	109.87(11)	C(10)-C(9)-C(14)	117.4(2)
C(16)-N(2)-C(3)	120.0(2)	C(10)-C(9)-P(1)	121.30(17)
C(16)-N(2)-P(1)	124.18(18)	C(14)-C(9)-P(1)	121.26(19)
C(3)-N(2)-P(1)	112.73(17)	O(10)-C(10)-C(11)	116.7(2)
N(2)-C(3)-C(4)	105.9(2)	O(10)-C(10)-C(9)	122.3(2)
N(2)-C(3)-H(3A)	110.6	C(11)-C(10)-C(9)	121.0(2)
C(4)-C(3)-H(3A)	110.6	C(10)-O(10)-H(10O)	104.3(17)
N(2)-C(3)-H(3B)	110.6	C(12)-C(11)-C(10)	119.6(2)
C(4)-C(3)-H(3B)	110.6	C(12)-C(11)-H(11A)	120.2
H(3A)-C(3)-H(3B)	108.7	C(10)-C(11)-H(11A)	120.2
N(8)-C(4)-C(3)	107.9(2)	C(11)-C(12)-C(13)	121.3(3)
N(8)-C(4)-C(5)	102.55(19)	C(11)-C(12)-H(12A)	119.3
C(3)-C(4)-C(5)	116.9(2)	C(13)-C(12)-H(12A)	119.3
N(8)-C(4)-H(4A)	109.7	C(14)-C(13)-C(12)	119.3(2)
C(3)-C(4)-H(4A)	109.7	C(14)-C(13)-H(13A)	120.3
C(5)-C(4)-H(4A)	109.7	C(12)-C(13)-H(13A)	120.3
C(4)-C(5)-C(6)	102.3(2)	O(14)-C(14)-C(13)	123.8(2)
C(4)-C(5)-H(5A)	111.3	O(14)-C(14)-C(9)	114.8(2)
C(6)-C(5)-H(5A)	111.3	C(13)-C(14)-C(9)	121.5(2)
C(4)-C(5)-H(5B)	111.3	C(14)-O(14)-C(15)	117.6(2)
C(6)-C(5)-H(5B)	111.3	O(14)-C(15)-H(15A)	109.5
H(5A)-C(5)-H(5B)	109.2	O(14)-C(15)-H(15B)	109.5
C(7)-C(6)-C(5)	105.1(2)	H(15A)-C(15)-H(15B)	109.5
C(7)-C(6)-H(6A)	110.7	O(14)-C(15)-H(15C)	109.5
C(5)-C(6)-H(6A)	110.7	H(15A)-C(15)-H(15C)	109.5
C(7)-C(6)-H(6B)	110.7	H(15B)-C(15)-H(15C)	109.5
C(5)-C(6)-H(6B)	110.7	C(21)-C(16)-C(17)	118.8(3)
H(6A)-C(6)-H(6B)	108.8	C(21)-C(16)-N(2)	121.0(2)
N(8)-C(7)-C(6)	105.2(2)	C(17)-C(16)-N(2)	120.3(2)
N(8)-C(7)-H(7A)	110.7	C(18)-C(17)-C(16)	120.2(3)
C(6)-C(7)-H(7A)	110.7	C(18)-C(17)-H(17A)	119.9
N(8)-C(7)-H(7B)	110.7	C(16)-C(17)-H(17A)	119.9

Atoms	Angle
C(19)-C(18)-C(17)	120.8(3)
C(19)-C(18)-H(18A)	119.6
C(17)-C(18)-H(18A)	119.6
C(20)-C(19)-C(18)	119.6(3)
C(20)-C(19)-H(19A)	120.2
C(18)-C(19)-H(19A)	120.2
C(19)-C(20)-C(21)	120.8(3)
C(19)-C(20)-H(20A)	119.6
C(21)-C(20)-H(20A)	119.6
C(16)-C(21)-C(20)	119.9(3)
C(16)-C(21)-H(21A)	120.1
C(20)-C(21)-H(21A)	120.1

Table 4. Anisotropic displacement parameters ($\text{\AA}^2 \times 10^3$) for $\text{C}_{18}\text{H}_{21}\text{N}_2\text{O}_3\text{P}$. The anisotropic displacement factor exponent takes the form: $-2\pi^2 [h^2 a^{*2} U^{11} + \dots + 2 h k a^* b^* U^{12}]$

	U^{11}	U^{22}	U^{33}	U^{23}	U^{13}	U^{12}
O(1)	30(1)	18(1)	26(1)	0(1)	9(1)	3(1)
P(1)	22(1)	20(1)	21(1)	-1(1)	6(1)	0(1)
N(2)	17(2)	23(1)	21(1)	2(1)	4(1)	-1(1)
C(3)	26(2)	26(1)	20(2)	2(1)	7(1)	1(1)
C(4)	25(2)	20(1)	22(2)	1(1)	9(1)	-1(1)
C(5)	29(2)	30(1)	24(2)	2(1)	10(1)	2(1)
C(6)	31(2)	41(2)	27(2)	2(1)	10(2)	5(1)
C(7)	21(2)	31(2)	26(2)	-1(1)	4(1)	-1(1)
N(8)	19(2)	23(1)	22(1)	0(1)	5(1)	-1(1)
C(9)	17(2)	19(1)	18(1)	-1(1)	2(1)	-1(1)
C(10)	20(2)	20(1)	22(2)	-1(1)	1(1)	-2(1)
O(10)	34(1)	21(1)	28(1)	4(1)	10(1)	1(1)
C(11)	25(2)	27(1)	20(2)	1(1)	9(1)	-8(1)
C(12)	28(2)	33(2)	28(2)	-6(1)	12(1)	-4(1)
C(13)	29(2)	21(1)	30(2)	-3(1)	9(1)	2(1)
C(14)	24(2)	22(1)	22(2)	-1(1)	6(1)	-3(1)
O(14)	44(1)	18(1)	26(1)	3(1)	15(1)	3(1)
C(15)	80(3)	21(2)	40(2)	5(1)	24(2)	14(1)
C(16)	23(2)	20(1)	23(2)	-7(1)	6(1)	-1(1)
C(17)	25(2)	23(1)	26(2)	-7(1)	4(1)	-3(1)
C(18)	25(2)	31(2)	37(2)	-11(1)	10(2)	-7(1)
C(19)	21(2)	37(2)	42(2)	-11(1)	0(2)	3(1)
C(20)	31(2)	27(2)	34(2)	-8(1)	-2(2)	10(1)
C(21)	28(2)	20(1)	30(2)	-4(1)	2(1)	3(1)

Table 5. Hydrogen coordinates ($\times 10^4$) and isotropic displacement parameters ($\text{\AA}^2 \times 10^3$) for $\text{C}_{18}\text{H}_{21}\text{N}_2\text{O}_3\text{P}$

	x	y	z	U(eq)
H(3A)	7170	1240	7731	28
H(3B)	7403	-40	6991	28
H(4A)	5734	-90	6603	26
H(5A)	5652	3148	7192	32
H(5B)	5101	1656	7566	32
H(6A)	3953	1458	6227	39
H(6B)	4110	3343	6261	39
H(7A)	4523	1520	4892	31
H(7B)	4934	3295	5074	31
H(10O)	7180(20)	4830(30)	4539(13)	62(11)
H(11A)	8355	3371	2831	28
H(12A)	8895	782	2806	35
H(13A)	8615	-1010	3932	32
H(15A)	7872	-2524	4774	68
H(15B)	7849	-2588	5855	68
H(15C)	8820	-1948	5497	68
H(17A)	8723	4126	5832	30
H(18A)	10435	4540	6231	36
H(19A)	11353	3301	7513	41
H(20A)	10565	1588	8384	38
H(21A)	8857	1051	7965	32

Table 6. Torsion angles [°] for C₁₈H₂₁N₂O₃P.

Atoms	Angle
O(1)-P(1)-N(2)-C(16)	-72.9(2)
N(8)-P(1)-N(2)-C(16)	164.49(18)
C(9)-P(1)-N(2)-C(16)	48.3(2)
O(1)-P(1)-N(2)-C(3)	127.27(16)
N(8)-P(1)-N(2)-C(3)	4.61(18)
C(9)-P(1)-N(2)-C(3)	-111.58(17)
C(16)-N(2)-C(3)-C(4)	-179.8(2)
P(1)-N(2)-C(3)-C(4)	-19.0(2)
N(2)-C(3)-C(4)-N(8)	26.6(2)
N(2)-C(3)-C(4)-C(5)	-88.2(3)
N(8)-C(4)-C(5)-C(6)	40.7(2)
C(3)-C(4)-C(5)-C(6)	158.5(2)
C(4)-C(5)-C(6)-C(7)	-33.7(3)
C(5)-C(6)-C(7)-N(8)	13.8(3)
C(3)-C(4)-N(8)-C(7)	-157.26(19)
C(5)-C(4)-N(8)-C(7)	-33.3(2)
C(3)-C(4)-N(8)-P(1)	-24.6(2)
C(5)-C(4)-N(8)-P(1)	99.4(2)
C(6)-C(7)-N(8)-C(4)	12.1(2)
C(6)-C(7)-N(8)-P(1)	-115.6(2)
O(1)-P(1)-N(8)-C(4)	-109.89(16)
N(2)-P(1)-N(8)-C(4)	12.05(17)
C(9)-P(1)-N(8)-C(4)	126.42(16)
O(1)-P(1)-N(8)-C(7)	16.6(2)
N(2)-P(1)-N(8)-C(7)	138.58(19)
C(9)-P(1)-N(8)-C(7)	-107.0(2)
O(1)-P(1)-C(9)-C(10)	-0.7(2)
N(8)-P(1)-C(9)-C(10)	127.9(2)
N(2)-P(1)-C(9)-C(10)	-126.5(2)
O(1)-P(1)-C(9)-C(14)	176.2(2)
N(8)-P(1)-C(9)-C(14)	-55.2(2)
N(2)-P(1)-C(9)-C(14)	50.4(2)
C(14)-C(9)-C(10)-O(10)	-177.8(2)
P(1)-C(9)-C(10)-O(10)	-0.8(4)
C(14)-C(9)-C(10)-C(11)	2.5(4)

Atoms	Angle
P(1)-C(9)-C(10)-C(11)	179.5(2)
O(10)-C(10)-C(11)-C(12)	178.5(2)
C(9)-C(10)-C(11)-C(12)	-1.8(4)
C(10)-C(11)-C(12)-C(13)	0.3(4)
C(11)-C(12)-C(13)-C(14)	0.4(4)
C(12)-C(13)-C(14)-O(14)	-179.6(2)
C(12)-C(13)-C(14)-C(9)	0.4(4)
C(10)-C(9)-C(14)-O(14)	178.2(2)
P(1)-C(9)-C(14)-O(14)	1.2(3)
C(10)-C(9)-C(14)-C(13)	-1.8(4)
P(1)-C(9)-C(14)-C(13)	-178.8(2)
C(13)-C(14)-O(14)-C(15)	4.3(4)
C(9)-C(14)-O(14)-C(15)	-175.6(2)
C(3)-N(2)-C(16)-C(21)	-6.5(3)
P(1)-N(2)-C(16)-C(21)	-164.99(18)
C(3)-N(2)-C(16)-C(17)	173.5(2)
P(1)-N(2)-C(16)-C(17)	15.0(3)
C(21)-C(16)-C(17)-C(18)	1.3(3)
N(2)-C(16)-C(17)-C(18)	-178.7(2)
C(16)-C(17)-C(18)-C(19)	-1.8(4)
C(17)-C(18)-C(19)-C(20)	0.8(4)
C(18)-C(19)-C(20)-C(21)	0.8(4)
C(17)-C(16)-C(21)-C(20)	0.2(3)
N(2)-C(16)-C(21)-C(20)	-179.8(2)
C(19)-C(20)-C(21)-C(16)	-1.3(4)

Table 7. Hydrogen bonds for C₁₈H₂₁N₂O₃P [Å and °]

D-H...A	d(D-H)	d(H...A)	d(D...A)	<(DHA)
O(10)-H(10O)...O(1)	0.980(5)	1.609(10)	2.559(2)	162(3)

Annexe II: X-Ray Crystallographic Data for C₃₄H₂₈O₈ (H3)

1,2-ethene(bis(1,1'-biphenyl[3',5'-dimethylester]))

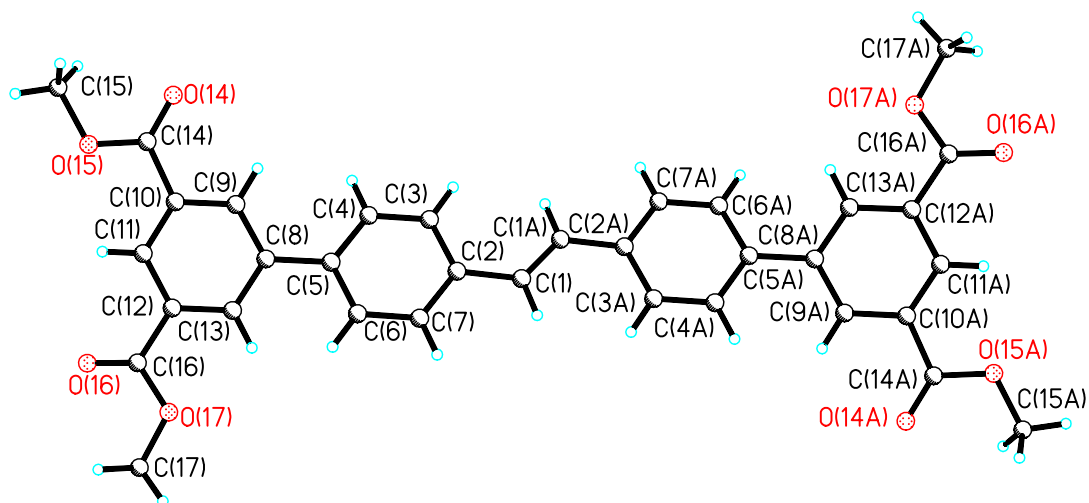


Table 1. Crystal data and structure refinement for C₃₄H₂₈O₈ (**H3**)

<i>Identification code</i>	nvdch5	
<i>Empirical formula</i>	C ₃₄ H ₂₈ O ₈	
<i>Formula weight</i>	564.56	
<i>Temperature</i>	93(2) K	
<i>Wavelength</i>	0.71073 Å	
<i>Crystal system</i>	Monoclinic	
<i>Space group</i>	P2(1)/c	
<i>Unit cell dimensions</i>	a = 4.7172(6) Å	alpha = 90°
	b = 14.805(2) Å	beta = 93.810(4)°
	c = 19.787(3) Å	gamma = 90°
<i>Volume</i>	1378.8(3) Å ³	
<i>Z</i>	2	
<i>Density (calculated)</i>	1.360 Mg/m ³	
<i>Absorption coefficient</i>	0.097 mm ⁻¹	
<i>F(000)</i>	592	
<i>Crystal size</i>	0.2000 x 0.0300 x 0.0300 mm ³	
<i>Theta range for data collection</i>	1.72 to 25.35°.	
<i>Index ranges</i>	-5<=h<=5, -17<=k<=17, -23<=l<=20	
<i>Reflections collected</i>	8788	
<i>Independent reflections</i>	2459 [R(int) = 0.0307]	
<i>Completeness to theta = 25.00°</i>	97.6 %	
<i>Absorption correction</i>	Multiscan	
<i>Max. and min. transmission</i>	1.0000 and 0.9330	
<i>Refinement method</i>	Full-matrix least-squares on F ²	
<i>Data / restraints / parameters</i>	2459 / 0 / 194	
<i>Goodness-of-fit on F²</i>	1.051	
<i>Final R indices [I>2sigma(I)]</i>	R1 = 0.0432, wR2 = 0.1124	
<i>R indices (all data)</i>	R1 = 0.0499, wR2 = 0.1201	
<i>Extinction coefficient</i>	0.010(3)	
<i>Largest diff. peak and hole</i>	0.203 and -0.196 e.Å ⁻³	

Table 2. Atomic coordinates ($\times 10^4$) and equivalent isotropic displacement parameters ($\text{\AA}^2 \times 10^3$) for $\text{C}_{34}\text{H}_{28}\text{O}_8$. $U(\text{eq})$ is defined as one third of the trace of the orthogonalized U_{ij} tensor

	x	y	z	$U(\text{eq})$
C(1)	14371(3)	5135(1)	274(1)	20(1)
C(2)	12309(3)	4613(1)	634(1)	20(1)
C(3)	11315(3)	3764(1)	416(1)	21(1)
C(4)	9457(3)	3278(1)	787(1)	20(1)
C(5)	8477(3)	3614(1)	1389(1)	19(1)
C(6)	9364(3)	4480(1)	1589(1)	21(1)
C(7)	11244(3)	4963(1)	1222(1)	21(1)
C(8)	6636(3)	3063(1)	1808(1)	20(1)
C(9)	4914(3)	2372(1)	1526(1)	20(1)
C(10)	3218(3)	1850(1)	1925(1)	20(1)
C(11)	3221(3)	2001(1)	2616(1)	22(1)
C(12)	4930(3)	2684(1)	2909(1)	23(1)
C(13)	6611(3)	3204(1)	2506(1)	21(1)
C(14)	1380(3)	1155(1)	1569(1)	22(1)
O(14)	1297(2)	1007(1)	968(1)	29(1)
O(15)	-205(2)	704(1)	1997(1)	27(1)
C(15)	-2090(3)	32(1)	1684(1)	30(1)
C(16)	4907(4)	2844(1)	3651(1)	29(1)
O(16)	3663(3)	2379(1)	4033(1)	55(1)
O(17)	6419(2)	3574(1)	3852(1)	29(1)
C(17)	6588(5)	3772(1)	4569(1)	46(1)

Table 3. Bond lengths [Å] and angles [°] for C₃₄H₂₈O₈

Atoms	Length
C(1)-C(1)#1	1.330(3)
C(1)-C(2)	1.4637(19)
C(1)-H(1A)	0.9500
C(2)-C(7)	1.3974(19)
C(2)-C(3)	1.400(2)
C(3)-C(4)	1.383(2)
C(3)-H(3A)	0.9500
C(4)-C(5)	1.3967(19)
C(4)-H(4A)	0.9500
C(5)-C(6)	1.397(2)
C(5)-C(8)	1.4853(19)
C(6)-C(7)	1.3828(19)
C(6)-H(6A)	0.9500
C(7)-H(7A)	0.9500
C(8)-C(13)	1.396(2)
C(8)-C(9)	1.399(2)
C(9)-C(10)	1.3948(19)
C(9)-H(9A)	0.9500
C(10)-C(11)	1.386(2)
C(10)-C(14)	1.492(2)
C(11)-C(12)	1.395(2)
C(11)-H(11A)	0.9500
C(12)-C(13)	1.3936(19)
C(12)-C(16)	1.489(2)
C(13)-H(13A)	0.9500
C(14)-O(14)	1.2077(17)
C(14)-O(15)	1.3450(17)
O(15)-C(15)	1.4467(18)
C(15)-H(15A)	0.9800
C(15)-H(15B)	0.9800
C(15)-H(15C)	0.9800
C(16)-O(16)	1.2030(18)
C(16)-O(17)	1.3412(19)
O(17)-C(17)	1.4466(18)

Atoms	Angle	Atoms	Angle
C(1)#1-C(1)-C(2)	125.81(16)	C(12)-C(11)-H(11A)	120.3
C(1)#1-C(1)-H(1A)	117.1	C(13)-C(12)-C(11)	119.86(13)
C(2)-C(1)-H(1A)	117.1	C(13)-C(12)-C(16)	121.24(14)
C(7)-C(2)-C(3)	117.26(12)	C(11)-C(12)-C(16)	118.90(12)
C(7)-C(2)-C(1)	119.80(13)	C(12)-C(13)-C(8)	121.72(14)
C(3)-C(2)-C(1)	122.93(12)	C(12)-C(13)-H(13A)	119.1
C(4)-C(3)-C(2)	120.95(12)	C(8)-C(13)-H(13A)	119.1
C(4)-C(3)-H(3A)	119.5	O(14)-C(14)-O(15)	123.20(14)
C(2)-C(3)-H(3A)	119.5	O(14)-C(14)-C(10)	124.81(13)
C(3)-C(4)-C(5)	121.66(13)	O(15)-C(14)-C(10)	111.99(12)
C(3)-C(4)-H(4A)	119.2	C(14)-O(15)-C(15)	115.02(12)
C(5)-C(4)-H(4A)	119.2	O(15)-C(15)-H(15A)	109.5
C(4)-C(5)-C(6)	117.34(12)	O(15)-C(15)-H(15B)	109.5
C(4)-C(5)-C(8)	121.27(12)	H(15A)-C(15)-H(15B)	109.5
C(6)-C(5)-C(8)	121.36(12)	O(15)-C(15)-H(15C)	109.5
C(7)-C(6)-C(5)	121.03(12)	H(15A)-C(15)-H(15C)	109.5
C(7)-C(6)-H(6A)	119.5	H(15B)-C(15)-H(15C)	109.5
C(5)-C(6)-H(6A)	119.5	O(16)-C(16)-O(17)	123.19(14)
C(6)-C(7)-C(2)	121.64(13)	O(16)-C(16)-C(12)	124.37(15)
C(6)-C(7)-H(7A)	119.2	O(17)-C(16)-C(12)	112.43(12)
C(2)-C(7)-H(7A)	119.2	C(16)-O(17)-C(17)	116.53(12)
C(13)-C(8)-C(9)	117.42(12)	O(17)-C(17)-H(17A)	109.5
C(13)-C(8)-C(5)	120.95(13)	O(17)-C(17)-H(17B)	109.5
C(9)-C(8)-C(5)	121.62(12)	H(17A)-C(17)-H(17B)	109.5
C(10)-C(9)-C(8)	121.32(13)	O(17)-C(17)-H(17C)	109.5
C(10)-C(9)-H(9A)	119.3	H(17A)-C(17)-H(17C)	109.5
C(8)-C(9)-H(9A)	119.3	H(17B)-C(17)-H(17C)	109.5
C(11)-C(10)-C(9)	120.35(13)		
C(11)-C(10)-C(14)	122.71(12)	Symmetry transformations used to generate equivalent atoms:	
C(9)-C(10)-C(14)	116.91(13)		
C(10)-C(11)-C(12)	119.33(12)	#1 -x+3,-y+1,-z	
C(10)-C(11)-H(11A)	120.3		

Table 4. Anisotropic displacement parameters ($\text{\AA}^2 \times 10^3$) for $\text{C}_{34}\text{H}_{28}\text{O}_8$. The anisotropic displacement factor exponent takes the form: $-2\pi^2 [h^2 a^{*2} U^{11} + \dots + 2 h k a^* b^* U^{12}]$

	U^{11}	U^{22}	U^{33}	U^{23}	U^{13}	U^{12}
C(1)	21(1)	18(1)	20(1)	2(1)	2(1)	0(1)
C(2)	18(1)	21(1)	20(1)	3(1)	2(1)	1(1)
C(3)	22(1)	22(1)	18(1)	-1(1)	4(1)	1(1)
C(4)	23(1)	17(1)	21(1)	-1(1)	2(1)	-1(1)
C(5)	18(1)	20(1)	18(1)	2(1)	1(1)	1(1)
C(6)	23(1)	23(1)	18(1)	-2(1)	5(1)	0(1)
C(7)	23(1)	19(1)	21(1)	-1(1)	2(1)	-1(1)
C(8)	20(1)	18(1)	21(1)	3(1)	4(1)	3(1)
C(9)	20(1)	20(1)	19(1)	2(1)	3(1)	3(1)
C(10)	20(1)	17(1)	25(1)	3(1)	2(1)	2(1)
C(11)	22(1)	20(1)	26(1)	6(1)	6(1)	1(1)
C(12)	27(1)	20(1)	22(1)	4(1)	6(1)	4(1)
C(13)	21(1)	18(1)	22(1)	1(1)	2(1)	1(1)
C(14)	21(1)	19(1)	26(1)	6(1)	2(1)	2(1)
O(14)	34(1)	28(1)	27(1)	-1(1)	2(1)	-7(1)
O(15)	26(1)	24(1)	31(1)	6(1)	1(1)	-9(1)
C(15)	26(1)	25(1)	38(1)	1(1)	-1(1)	-7(1)
C(16)	41(1)	24(1)	24(1)	4(1)	7(1)	0(1)
O(16)	99(1)	41(1)	28(1)	1(1)	24(1)	-28(1)
O(17)	41(1)	28(1)	17(1)	1(1)	1(1)	-3(1)
C(17)	81(2)	39(1)	17(1)	-1(1)	0(1)	-6(1)

Table 5. Hydrogen coordinates ($\times 10^4$) and isotropic displacement parameters ($\text{\AA}^2 \times 10^3$) for $\text{C}_{34}\text{H}_{28}\text{O}_8$

	x	y	z	U(eq)
H(1A)	14855	5717	447	24
H(3A)	11927	3518	7	25
H(4A)	8831	2701	630	25
H(6A)	8664	4740	1984	25
H(7A)	11827	5547	1373	25
H(9A)	4900	2257	1054	24
H(11A)	2070	1643	2888	27
H(13A)	7771	3666	2711	25
H(15A)	-3337	316	1329	45
H(15B)	-3244	-234	2026	45
H(15C)	-966	-443	1483	45
H(17A)	4677	3757	4736	69
H(17B)	7418	4372	4647	69
H(17C)	7783	3319	4811	69

Table 6. Torsion angles [°] for C₃₄H₂₈O₈

Atoms	Angle
C(1)#1-C(1)-C(2)-C(7)	177.18(18)
C(1)#1-C(1)-C(2)-C(3)	-2.9(3)
C(7)-C(2)-C(3)-C(4)	-2.9(2)
C(1)-C(2)-C(3)-C(4)	177.24(13)
C(2)-C(3)-C(4)-C(5)	0.6(2)
C(3)-C(4)-C(5)-C(6)	2.3(2)
C(3)-C(4)-C(5)-C(8)	-175.83(13)
C(4)-C(5)-C(6)-C(7)	-3.0(2)
C(8)-C(5)-C(6)-C(7)	175.18(13)
C(5)-C(6)-C(7)-C(2)	0.7(2)
C(3)-C(2)-C(7)-C(6)	2.2(2)
C(1)-C(2)-C(7)-C(6)	-177.89(13)
C(4)-C(5)-C(8)-C(13)	152.98(14)
C(6)-C(5)-C(8)-C(13)	-25.1(2)
C(4)-C(5)-C(8)-C(9)	-25.6(2)
C(6)-C(5)-C(8)-C(9)	156.30(14)
C(13)-C(8)-C(9)-C(10)	0.6(2)
C(5)-C(8)-C(9)-C(10)	179.20(12)
C(8)-C(9)-C(10)-C(11)	-0.5(2)
C(8)-C(9)-C(10)-C(14)	177.71(12)
C(9)-C(10)-C(11)-C(12)	0.2(2)
C(14)-C(10)-C(11)-C(12)	-177.87(13)
C(10)-C(11)-C(12)-C(13)	-0.1(2)
C(10)-C(11)-C(12)-C(16)	179.72(13)
C(11)-C(12)-C(13)-C(8)	0.1(2)
C(16)-C(12)-C(13)-C(8)	-179.62(13)
C(9)-C(8)-C(13)-C(12)	-0.4(2)
C(5)-C(8)-C(13)-C(12)	-179.03(13)
C(11)-C(10)-C(14)-O(14)	179.42(14)
C(9)-C(10)-C(14)-O(14)	1.3(2)
C(11)-C(10)-C(14)-O(15)	-0.56(19)
C(9)-C(10)-C(14)-O(15)	-178.72(11)
O(14)-C(14)-O(15)-C(15)	-1.3(2)
C(10)-C(14)-O(15)-C(15)	178.69(12)
C(13)-C(12)-C(16)-O(16)	-174.52(16)

Atoms	Angle
C(11)-C(12)-C(16)-O(16)	5.7(3)
C(13)-C(12)-C(16)-O(17)	6.0(2)
C(11)-C(12)-C(16)-O(17)	-173.72(13)
O(16)-C(16)-O(17)-C(17)	2.2(2)
C(12)-C(16)-O(17)-C(17)	-178.38(13)

Symmetry transformations used to generate equivalent atoms:

#1 -x+3,-y+1,-z